Florida International University

FIU Digital Commons

10-18-2021

Improving the Long-term Performance of Full-depth Precast Concrete (FDPC) Deck Panels Using Non-Proprietary UHPC

Esmail Shahrokhinasab
Esmail Shahrokhinasab, eshah004@fiu.edu

Follow this and additional works at: https://digitalcommons.fiu.edu/etd

Part of the Civil Engineering Commons, and the Structural Engineering Commons

Recommended Citation

FLORIDA INTERNATIONAL UNIVERSITY

Miami, Florida

IMPROVING THE LONG-TERM PERFORMANCE OF FULL-DEPTH PRECAST

CONCRETE (FDPC) DECK PANELS USING NON-PROPRIETARY ULTRA HIGH-

PERFORMANCE CONCRETE (UHPC)

A dissertation submitted in partial fulfillment of

the requirements for the degree of

DOCTOR OF PHILOSOPHY

in

CIVIL ENGINEERING

by

Esmail Shahrokhinasab

2021

To: Dean John L. Volakis
  College of Engineering and Computing

This dissertation, written by Esmail Shahrokhinasab, and entitled Improving the Long-Term Performance of Full-Depth Precast Concrete (FDPC) Deck Panels using Non-Proprietary Ultra High-Performance Concrete (UHPC), having been approved in respect to style and intellectual content, is referred to you for judgment.

We have read this dissertation and recommend that it be approved.

_____
Atorod Azizinamini

_____
Armin Mehrabi

_____
Wallied Orabi

_____
Kingsley Lau

_____
David Garber, Major Professor

Date of Defense: October 18, 2021

The dissertation of Esmail Shahrokhinasab is approved.

_____
Dean John L. Volakis
College of Engineering and Computing

_____
Andrés G. Gil
Vice President for Research and Economic Development
and Dean of the University Graduate School

Florida International University, 2021

DEDICATION

 I am extremely grateful to be able to finish this dissertation which is the result of

dedicating more than 20 years of my life to education. It is definitely one of the most

valuable achievements I have ever had, and I want to dedicate it to the most lovely and

respectful people.

I would like to dedicate this dissertation to my beloved wife for all her unconditional love

and support during this tough time and also our little man, Amirhosein who gave beauty,

love, patient and joy to our life. To my parents who taught me to be consistent and eager.

Last, but not least, I want to dedicate this dissertation to researchers who have worked on

my area of research, strut-and-tie method. Their studies took me to the edge of human

knowledge. I also dedicate this work to all scientists who put their time and effort to push

the boundaries of knowledge to make a safe and peaceful world for people. I hope this

research would be a small step toward this goal.

ACKNOWLEDGMENTS

First and foremost, I would like to express my deepest gratitude to my major professor, Dr. David Garber, who always stood by my side in this difficult path, and helped me with his well-thought-out advices. Without his support, valuable guidance, contribution, and patience, this dissertation would not have been possible.

Sincere thanks to the members of my doctoral committee, Dr. Atorod Azizinamini, Dr. Armin Mehrabi, Dr. Kingsley Lau, and Dr. Wallied Orabi for their input, valuable discussions, and accessibility.

I also want to acknowledge the help of graduate students at the Titan America Structures and Construction Testing Laboratory of the Florida International University, Amir Sadeghnejad, Sheharyar Rehmat and Francisco Chitty.

ABSTRACT OF THE DISSERTATION

IMPROVING THE LONG-TERM PERFORMANCE OF FULL-DEPTH PRECAST

CONCRETE (FDPC) DECK PANELS USING NON-PROPRIETARY ULTRA HIGH-

PERFORMANCE CONCRETE (UHPC)

by

Esmail Shahrokhinasab

Florida International University, 2021

Miami, Florida

Professor David Garber, Major Professor

Full-depth precast concrete (FDPC) deck panels are a type of prefabricated bridge element used in accelerated bridge construction (ABC) that have been used in bridge construction since the 1960's as an alternative to conventional CIP decks. The main purpose of using the prefabricated elements is to accelerate the construction and increase the long-term performance. FDPC deck panels itself offers superior durability and performance, but the connection between these elements still have shown some long-term issues like cracking. Ultra-high-performance concrete (UHPC) is an innovative and commercially available material that has been used to address concerns related to connection between precast elements. The high compressive strength and tensile strength alongside with superior durability of UHPC, has made it a solution for addressing the performance issue related to connection precast members, but its relatively high cost, has limited its widespread use. Hence, the non-proprietary UHPC was considered as an alternative of commercial UHPC

with significantly lower price. In this study, previous investigations on FDPC deck panels were reviewed and a database for bridges constructed with FDPC deck panels were created and their long-term performance were predicted and compared with bridges constructed with cast in place deck. Then, a comprehensive experimental work was conducted to develop the non-proprietary UHPC using locally-produced raw available material.

This research was expanded numerically then by studying the performance of non-proprietary UHPC in joint between FDPC deck panels. Finite element numerical analysis using ATENA was performed to compare the performance of developed non-proprietary UHPC with commercial UHPC in joint applications. Six different numerical specimens with different joint width were considered and the performance of different material under static loading were analyzed.

Results, revealed that the developed non-proprietary UHPC in this study, can perform similar to specimens with commercial UHPC joints. As it was expected, sensitivity analysis determined that tensile strength, tension function of UHPC and its bond behavior with precast elements, play the critical role and having a very high compressive strength and modulus of elasticity is not a big advantage when it is used to connect precast members under flexural load.

CONTENTS

LIST OF TABLES

LIST OF FIGURES

Chapter 1: **Introduction**

1.1. Overview

The use of full-depth precast concrete (FDPC) deck panels allows for accelerated construction and repair of bridge superstructures, and in some cases decreased overall project costs. These panels have been used for new construction and rehabilitation since 1965 [1]. There are several research projects that have been conducted looking into the behavior of different panel and joint details, but there is minimal published work on the performance of in-service FDPC deck panels. Although full-depth, precast decks have been used alongside conventional CIP decks in bridge construction since 1965, there has never been a formal study to determine if precast deck panels behave the same, better, or worse than CIP decks.

On the other hand, introducing the ultra-high performance concrete (UHPC) opened a new window of connecting precast members. UHPC is generally known for its high compressive and tensile strength, self-consolidation, exceptional durability, and significant post-cracking ductility. These exceptional performance characteristics have made UHPC an ideal option for different sectors of the construction industry including precast concrete fields. UHPC can be used to ease the design and improve the performance of joints between precast elements. UHPC also allows designers to utilize smaller cross-sections, reduce the conventional reinforcement, increase the prestressing force, and consequently produce longer-span elements. UHPC has made a significant improvement in accelerating the construction process through the use of UHPC in joints between conventional concrete precast elements and as the primary material for UHPC precast elements [2]. Despite all

these advantages, the use of UHPC in the United States remains limited. Proprietary UHPC mixtures can cost up to 20 to 30 times more than conventional concrete. Non-proprietary mixtures can decrease costs but often require much stricter quality control measures than conventional concrete. These enhanced quality control measures plus the high material cost for the material has limited the widespread use of UHPC in the U.S. infrastructure [3], [4].

This research was designed to develop a non-proprietary UHPC mix design, help to create guidance for others to use this mix and create their own, and evaluate the effect of non-proprietary UHPC on the performance of the connections between FDPC deck panels. The results of this research can lead to improved joint performance in future projects using FDPC deck panels.

1.2. Research Objective

The primary objectives of this research project are the following:

1- Compare the long-term performance of FDPC decks to CIP decks (with similar parameters: ADT, spans, location/climates, crossing, etc.)

2- Identify successful and unsuccessful details for FDPC deck panels and joints

3- Identify owner (state DOT) perceptions of FDPC decks and determine perceived successes and challenges

4- Develop non-proprietary UHPC concrete using locally-produced raw material (Aggregates, cement, and slag) and

5- Model FDPC deck panel joints and compare the performance of normal concrete, commercial UHPC and non-proprietary UHPC

1.3. Research Scope

These objectives were accomplished through the following research tasks.

- *Task 1 – FDPC deck panels*: A comprehensive study was conducted to gather available information related to performance of in-service bridge decks. The NBI and LTBP databases were used as a starting point to understand general national trends related to bridge deck performance.

- *Task 2 – Industry Survey of Owners*: A survey was developed and administered. The survey was sent to bridge owners (state DOTs).

- *Task 3 – Determine Comparison Projects*: The objective of this task was to select the projects to be included in the performance comparison and to begin to gather information on these bridges. The project selection process incorporated the bridge selection methodology and clusters and corridors approach adopted by the LTBP Program when possible.

- *Task 4 – Collect Required Inspection Information*: The objective of this task was to collect additional information for the bridges selected during Task 3. This was limited to currently available information. It is recommended that more detailed inspections be used in the future to expand on the results presented in this report.

- *Task 5 – Analysis of Inspection Information*: The objective of this task was to analyze the results gathered under Task 4 and both quantitatively and qualitatively compare the performance of full-depth, precast decks to the similar CIP decks.

Side-by-side performance comparisons with the selected comparison projects selected in Task 3 are included in this analysis.

- *Task 6 – Design Recommendations*: Details on panel and joint design were gathered during Task 2 and Task 4. The objective of this task was to suggest panel and joint details that are performing well and are easy to assemble.

- *Task 7 – Review of Non-Proprietary UHPC Mix Designs*: A comprehensive literature review was conducted on developing non-proprietary UHPC mix and the primary non-proprietary UHPC mix designs of previous researchers were considered as a start point.

- *Task 8 – Mechanical Testing and Customization of Non-Proprietary Mix*: Several different experimental tests were conducted on over 600 3″×6″ cylinder samples to find qualified mix designs with required mechanical properties. Recommended mix designs using locally-produced raw available material in Florida (Cement, slag, aggregates) determined.

- *Task 9 – Design Recommendations*: All observations including mix optimization, material characterization, test results, and performance of different fiber types were discussed.

- *Task 10-Numerical Analysis*: Modeling the full-scale joints connecting the deck panels with finite element base software (ATENA) and compare the performance of normal concrete, commercial UHPC and non-proprietary UHPC

- *Task 11-Cost analysis of material*: A brief cost comparison between three different concretes used in this study to evaluate the application of non-UHPC.

1.4. Thesis Organization

This dissertation is written based on the format of 'Thesis Containing Journal Papers'. The dissertation includes one manuscript for scholarly journals and magazine, of which is published. Two chapters are provided based on research conducted at FIU which is published. Additional chapters are provided to complete the dissertation and summarize work not adequately captured in published paper and ABC-UTC research project.

This dissertation is written according to following chapter:

Chapter 2 - "FDPC Deck Panels" (submitted to Engineering Structures Journal) [5]: This chapter summarizes a comprehensive literature review of FDPC deck panels, developing the database including all bridges made by FDPC deck panels and their performance compared to similar bridges constructed with cast in place (CIP) decks.

Chapter 3 – "Background on Non-Proprietary UHPC" (submitted to ABC-UTC research-Report) [6]: This chapter introduces the non-proprietary ultra-high-performance concrete (N-UHPC) and its influence on improving the performance of structures and decreasing the high costs due to use commercial UHPC.

Chapter 4 – "Experimental Study on Non-Proprietary UHPC" (submitted to ABC-UTC research-Report)[6]: This chapter describes the experimental works, laboratory tests which resulted in developing ABC-UTC non-proprietary UHPC concrete.

Chapter 5 – "Numerical Analysis of Joint Performance": This chapter contains the numerical modeling efforts to compare the performance of conventional concrete, N-UHPC and C-UHPC in connection joints between FDPC deck panels.

Chapter 6 – "Summary, Conclusions and Recommendations": This section concludes this dissertation by summarizing all the findings and presents conclusions.

Chapter 2: **FDPC Deck Panels**

2.1. Introduction

This chapter is taken from published paper which was published in "Engineering Structure Journal" [5] and is the summarized version of report. A significant portion of construction or rehabilitation time is used for forming, placement and tying of steel reinforcement, and placement and curing of concrete required for conventional cast-in-place (CIP) bridge decks. CIP decks are common because of their relatively low initial cost (without consideration for the cost of traffic delay) and because of their ability to accommodate larger differential cambers and other construction tolerances [1]. CIP decks also provide flexibility for bridges with complicated geometries (e.g., curved or heavily skewed bridges) and where tight tolerances may be a concern.

Full-depth precast concrete (FDPC) deck panels are a type of prefabricated bridge element used in accelerated bridge construction (ABC) that have been used in bridge construction since the 1960's as an alternative to conventional CIP decks [7]. FDPC deck panels can have several different types of joints, as highlighted in Figure 2.1: transverse joints and longitudinal joints to connect adjacent panels and shear pockets to create a composite connection between the panel and the girders. An overlay can be used to create the riding surface, or the deck panels and joints can be ground down to create the riding surface. FDPC deck panels have many benefits over conventional CIP deck systems [1], [8]–[10]. These benefits include: high-quality plant production under tight tolerances, low maintenance cost, lower permeability of the precast concrete (due to higher strength

concrete typically being used for FDPC deck panels), and reduced volume changes due to shrinkage and temperature effects during initial curing [1], [11], [12].
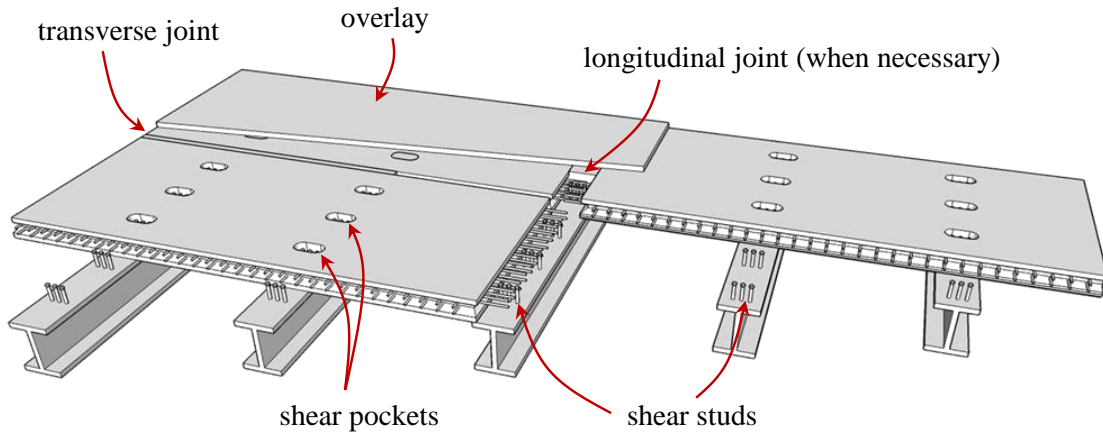
Figure 2.1: Components of FDPC deck panel deck system

There have been many previous studies on the mechanical performance of the joint detail between FDPC deck panels [13]–[18] and the materials used in the joint regions[16], [17], [19]–[22]. The results of these research projects led to the development of different recommended joint details [13], [15], [16], [19] and the use of some materials over other materials (e.g., ultra-high performance concrete over non-shrink grout) [21], [23]–[25]. These studies will not be mentioned in detail here, but more details on some of these studies are available in Graybeal et al. [13], [26].

Utah DOT has conducted a comprehensive study to monitor the performance of their bridges constructed with ABC methods and published findings in "lessons learned" reports between 2009 to 2016 [27]–[31]. Based on this study, the most prevalent issue is cracking accompanied by efflorescence and leakage in connections. Utah DOT has found their welded tie-back connections between FDPC deck panels to be their worst performing joint

detail. Utah has also found that the grouted dowel connection performed poorly. They built one bridge and widespread leaking started in the negative moment region within one year. This performance combined with the high initial cost of this connections has limited the use of this type of joint specially in negative moment regions [30]. Other joint types, including longitudinal post tensioning, conventional concrete, and UHPC, were found to be performing very well with no problems noted to date [27]–[31].

Beyond these efforts to investigate the mechanical (static and fatigue) response of the joints between panels and the recent performance evaluation of several ABC projects in Utah, there are no recent studies that have attempted to evaluate the long-term performance of bridges with FDPC deck panels that have been constructed over the past 60 years. The main objective of this study was to address this research gap and evaluate the long-term performance of bridges constructed with FDPC deck panels and determine successful and unsuccessful details of this system. A comprehensive survey of bridge owners was conducted to collect information on the performance of FDPC decks, owner experience, average construction cost, observed performance issues and general information such as location, traffic impact category (based on the length of time traffic was impacted by construction [32]), type of joints and other details to determine the most common joints used and their current performance. Survey results were used to create the FDPC Deck Panel Database. Additional variables thought to affect the long-term performance of FDPC deck panels (e.g. climate zone [33]) were also determined and included in the database. The information from the survey (specifically the most common joint details and most common issues reported) was used with the information gathered from the LTBP InfoBridge [34], to determine quantifiable assessment of the performance of decks

constructed with FDPC deck panels. This study has been conducted using available data from the National Bridge Inventory (NBI) [35] database including previous inspection data based on a visual inspection.

The NBI database has an overall deck rating for bridges which is based on the overall condition of decks; since joints typically control the overall performance of the deck system, it is reasonable to assume that the overall deck rating reflects the joint performance. Deck rating available in the NBI database is exclusively for deck condition and cannot be used as a performance criterion for joints or even the whole system. The overall performance of FDPC deck panel or cast in place deck panels system compiles of performance of deck and performance of all available connections including transverse and longitudinal joints and shear pockets. Results from this study can be used as a good starting point for more in-depth studies focusing on the joint performance (e.g., non-destructive testing and evaluation). Additional details on this study can be found in [10], [36].

2.2. Full-Depth Precast Concrete (FDPC) Deck Panel Use in the U.S.

The current NBI [35] and LTBP program [37] track the inventory and visual inspection performance of all federal, state, county, city, and privately-owned bridges over 20 feet in length. These databases contain information including identification information, bridge types and specifications, deck type, operational conditions, bridge data including geometric data and functional description, inspection data, and more [38]. While these databases do classify bridges based on deck type, the current classification system does not differentiate between full-depth and partial-depth precast panels. Due to this lack of information, a state

10

survey was developed to collect information from the State Departments of Transportation (DOTs) to create a database exclusively for bridges with FDPC deck panels. The goal of this survey was to determine:

1. Number of FDPC deck panel projects (including NBI information) and type of joint used

2. Reasons why FDPC deck panels are considered over CIP decks

3. Observed problems with deck systems (with panels or joints)

4. Repair techniques used for problematic decks

The results from this survey are presented in the following section.

2.2.1. Survey Results:

The survey was sent out to all the state DOTs, through the AASHTO T-4 Committee on Construction, and forty-three states responded. Of the 43 responding states, 31 states (72 percent) have previously used FDPC deck panels and currently allow their use, which shows that states in general are interested in using FDPC deck panels.

A total of 301 projects were reported from the survey to utilize FDPC deck panels. These projects are broken down by decade in Figure 2.2. States are becoming more comfortable with the use of FDPC deck panels, so over half of the total FDPC deck panel projects have been completed in the past decade.
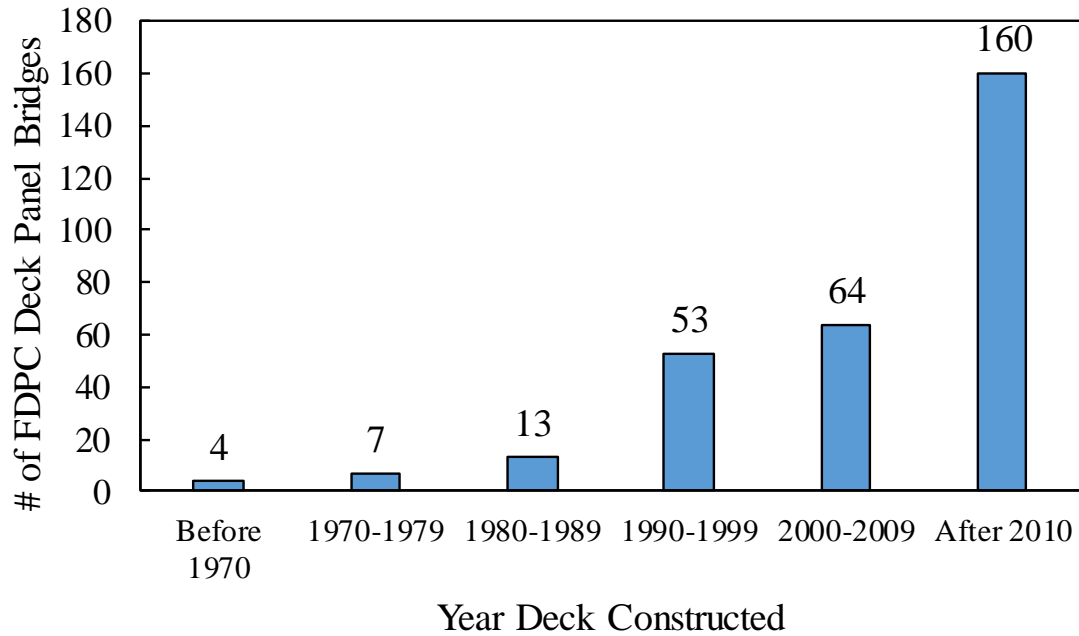
Figure 2.2: Number of bridges utilizing FDPC deck panels in each decade

The total number of bridge projects utilizing FDPC deck panels is also broken down by

state and presented in Figure 2.3. The largest number of bridges with FDPC deck panels

are found in New York, Alaska, Utah, Pennsylvania, and Tennessee.
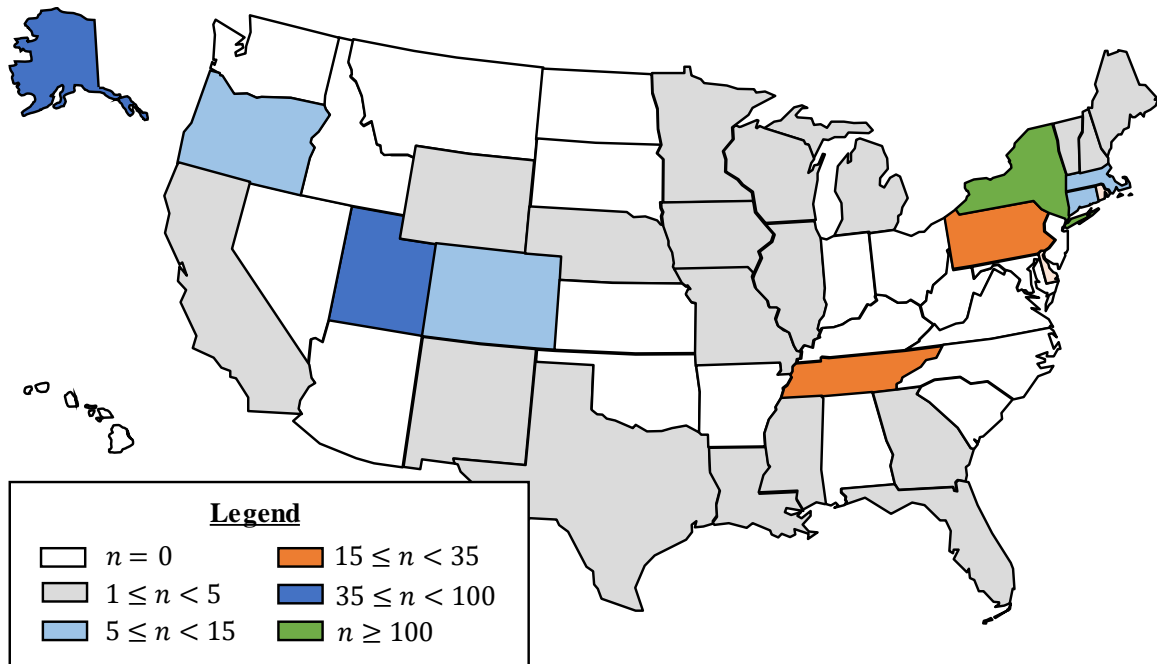
Figure 2.3: Number of bridges utilizing FDPC deck panels in each state

2.2.2. Reasons for using or not using FDPC

Based on the outcomes of survey, the primary reasons that states use and/or allow the use of FDPC deck panels are to:

- Decrease construction time

- Reduce traffic impact

- Provide better quality for finishing surface

- Increase long-term durability due to better quality

- Eliminates in-place curing time

The primary reasons states do not use or do not permit the use of FDPC deck panels are:

- CIP decks can cover up errors or differential cambers between members

- FDPC deck panels are not usually bid by contractors

- Lack of experienced local contractor

- FDPC require quality control and quality assurance program for preventing misalignment, which increases costs and decreases the number of qualified contractors

- The need for joints between panels (CIP allows for a jointless bridge)

- Higher cost of FDPC panels compared to CIP decks

- Uncertainty about connection details in FDPC

- Concerns about cracking, proper connections, and long-term performance

- Bridge geometry specially curved or heavily skewed bridges that requires very specific panels geometry

2.2.3. Cost Comparison

States also responded with the approximate costs associated with the FDPC deck panels compared to CIP decks (including the cost of the wearing surface). The ratio of deck costs for FDPC deck panel decks to CIP decks is presented in Figure 2.4.

The average reported cost of FDPC deck panel decks is 1.8 times the cost of CIP decks. However, decks constructed with FDPC deck panels are less expensive than CIP decks in Alaska, where there is a shorter construction window and a lot of experience in the construction method. Iowa, Massachusetts, Missouri, Nebraska, and Rhode Island reported FDPC decks costing between 0 and 40 percent more than CIP decks. Delaware and Pennsylvania are the states where FDPC decks cost the most compared to CIP decks.
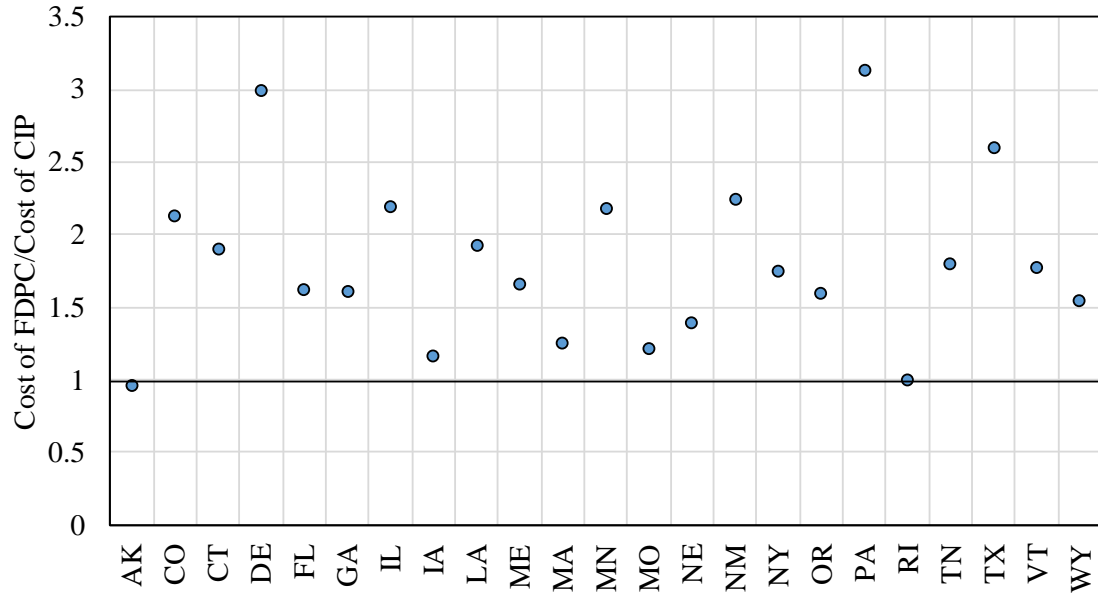
Figure 2.4: Relative cost of FDPC to CIP

2.2.4.   *Different Joint Types*

Several common joint details were found in the literature, shown in Figure 2.5. These joints were broken into four different categories: (1) post-tensioned, (2) mechanical, (3) made with ultra-high-performance concrete (UHPC), and (4) made with conventional concrete (CC). The UHPC and CC joint details included straight, headed, and hoop reinforcement splice details.
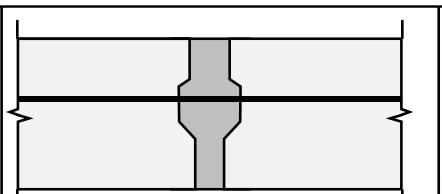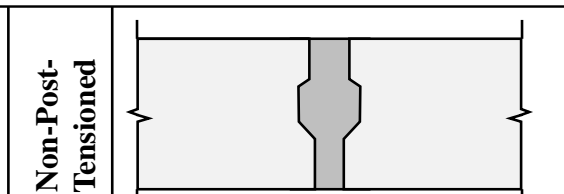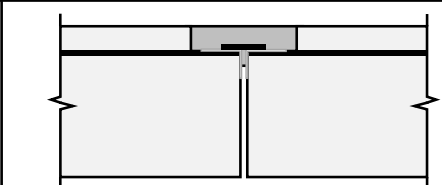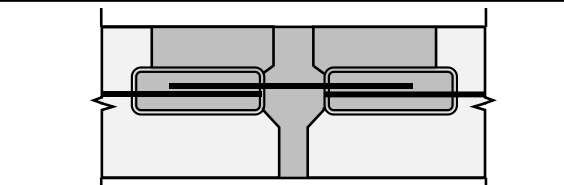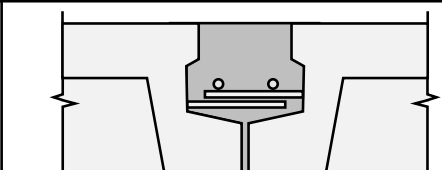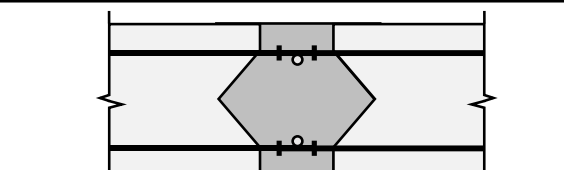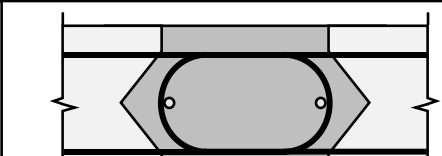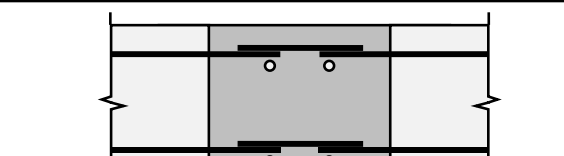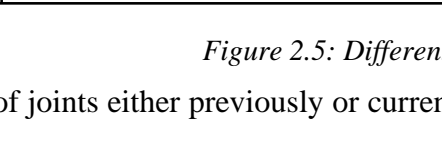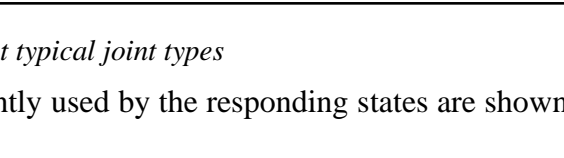
Post-Tensioned <3" (75mm) width	Long. PT - C1.a	**Non-Post-Tensioned** Non-PT - C1.a
Mechanical width varies	Welded - C1.b	Grouted Dowel - C1.c
Ultra-High Performance Concrete(UHPC) ~6-8" (150-200mm) width	Waffle Slab w/Straight Bars - C1.d / Straight Bar - C1.f	Headed Bar - C1.e / Hooped Bar - C1.g
Conventional Concrete (CC) >12" (300mm) width	Hooped Bar - C1.h / Headed Bar - C1.j	Straight Bar - C1.i / Hooked Bar - C1.k

Figure 2.5: Different typical joint types

The types of joints either previously or currently used by the responding states are shown

in Figure 2.6. The post-tensioned joint detail is the most used joint detail and the UHPC

joint with straight bars is the next most used.

The conventional concrete joint with hooped bars is the third most used joint. Also note that some states, like Alaska and Utah, have used welded connections in the past, but these are not commonly used anymore because of their poor long-term performance [31].
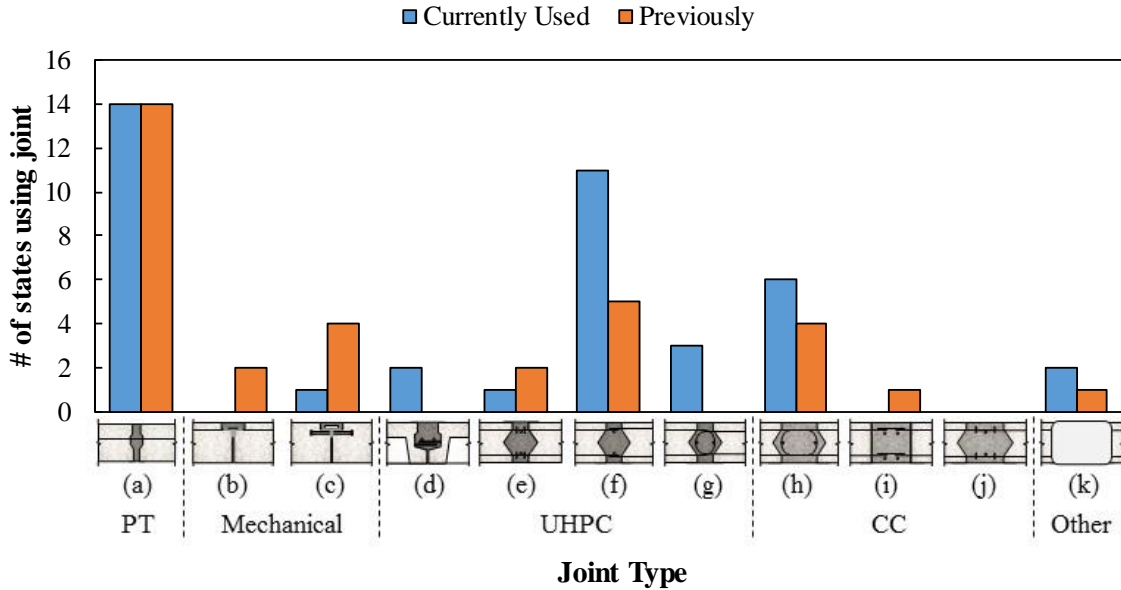
Figure 2.6: Types of joint details used by states

2.2.5. Performance of FDPC Deck Panels Based on Survey

Based on survey results, the most common issues reported are different types of cracking, efflorescence, and active leakage. Active leakage has been observed in several cases and is mainly located in the interface between the joints and the FDPC deck panels. The performance of bridges with FDPC deck panels was investigated further through the FDPC Deck Panel Database.

2.3. FDPC Deck Panel Database

The FDPC Deck Panel Database was developed based on the results of the survey discussed in this paper and information gathered from the ABC Project Database [7]. This database includes the NBI number, detailed project information, and available inspection data for 280 bridges with FDPC deck panels. The NBI includes a structural evaluation of the deck, superstructure, substructure and culvert on a 0 to 9 scale, which was included in the FDPC Deck Panel Database [37].

At the time of this study, 21 of the 301 bridges with FDPC deck panel decks mentioned above were not yet constructed and did not have an NBI number. The FDPC Deck Panel Database is a valuable resource as it only includes bridges constructed using FDPC deck panels compared to the NBI deck classification "Concrete Precast Panels" which includes both partial and full-depth panels. The FDPC Deck Panel Database is available from Garber and Shahrokhinasab [39].

The information gathered for the bridges in the FDPC Deck Panel Database from the LTBP InfoBridge included:

- State
- NBI number
- Bridge name
- Owner
- Latitude/Longitude
- Age / age of deck
- Number of main spans

- Length of largest span

- Total bridge length

- Year built

- Year of deck construction

- Average Daily Traffic (ADT)/ Average Daily Truck Traffic (ADTT)

- Main span material

- Main span design

- Wearing surface

- Deck rating the year of deck construction (from 0 to 9)

- Estimated service life using the LTBP Machine-Learning Model [34]

The type transverse and longitudinal joint and the impact category were gathered through the DOT survey. Information on the joint type was provided for 158 bridges. The impact category defines the total amount of time traffic flow is impacted due to the construction process. Impact categories were defined by AASHTO Committee on Bridges and Structures Technical Committee T-4 (Construction). The six impact category tiers are:

- Tier 1: traffic impacts within 1 day

- Tier 2: traffic impacts within 3 days

- Tier 3: traffic impacts within 2 weeks

- Tier 4: traffic impacts within 1 month

- Tier 5: traffic impacts within 3 months

- Tier 6: overall project schedule is significantly reduced by months to years

Current impact categories do not distinguish between full-day and night closures (e.g. 4 full-day and 4-night closures would both be considered Tier 3). Information on impact category was gathered for 70 of the 280 bridges in the FDPC Deck Panel Database. Many states did not have this information for older bridges.

The climate zone also was found for all bridges based on the latitude and longitude data from the NBI and the Department of Energy (DOE) climate zone map [33] shown in Figure 2.7.
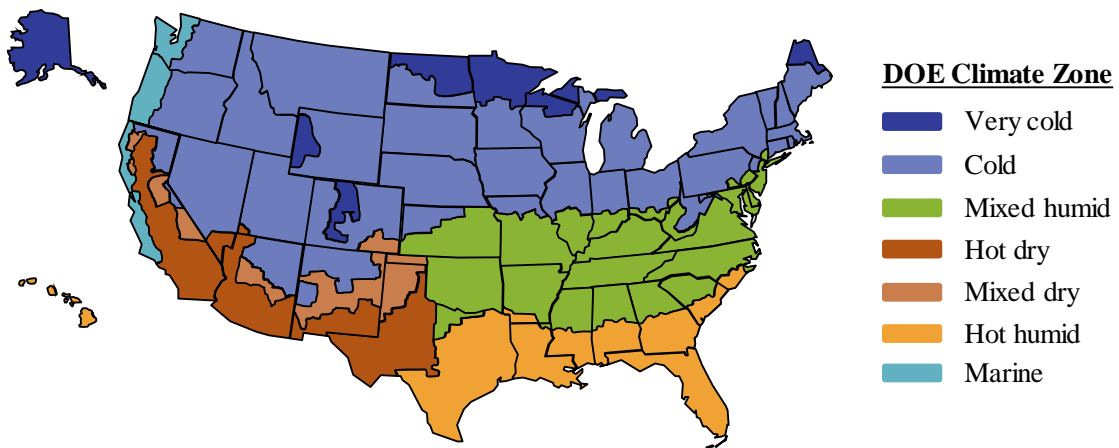
Figure 2.7: Department of Energy climate zones (based on [33])

The following analysis was conducted using the FDPC Deck Panel Database.

2.4. Data Analysis and Filtering

Two different approaches were used to conduct a performance comparison of FDPC deck panel bridges based on different variables, e.g., joint type, climate, traffic. The first approach was using the linear regression of previous deck ratings to estimate the remaining service life of the bridge. The second approach was based on developed forecast models by FHWA for the LTBP InfoBridge [40]. Two different bridge deck condition forecast

models have been developed by FHWA researchers include a machine learning model and survival model. These models are products of on-going research. Information related to the machine learning model was available for most of the bridges in the FDPC Deck Panel Database at the time of this study and was used as an alternative metric for long-term performance comparisons. Additional information related to the machine learning models can be found at the LTBP InfoBridge [34].

2.4.1. Linear regression for bridge degradation

In this procedure, two different factors were used for performance comparison purposes: (a) deterioration of deck and (b) estimated service life. The deterioration rate (*D*) was found as the slope of the deck rating numbers since the last rehabilitation or renovation of deck using a simple linear regression as shown in Equation 2-1.

$$D = \frac{\sum[(R_{d.i} - \bar{R}_d)(t_i - \bar{t})]}{\sum(t_i - \bar{t})^2} \qquad \text{Equation 2-1}$$

where:

D = deterioration rate for deck calculated based on NBI database

$R_{d,i}$ = deck rating obtained from NBI database for the *i*th inspection in years between the most recent deck construction and year of final inspection (latest data available from 2017)

$\bar{R}_d$ = average deck rating from NBI database for time between most recent deck construction and year of final inspection (latest data available from 2017)

21

$$t_i \quad = \quad \text{time in years between year of most recent deck construction and year of}$$

ith inspection (coincides with $R_{D,\,i}$)

$$\bar{t} \quad = \quad \text{average of } t_i \text{ between year of most recent deck construction and year of}$$

final inspection

The estimated service life (S) of the decks was calculated based on the number of years after the last rehabilitation for the deck rating to reach a value of 4 using the calculate deterioration rate, as shown in Equation 2-2.

$$S = \frac{R_{d,0} - 4}{D} \qquad\qquad \text{\textit{Equation 2-2}}$$

where:

$$S \quad = \quad \text{estimated service lift based on the deterioration rate calculated using}$$

Equation 2-2

$$R_{d,0} \quad = \quad \text{initial deck rating immediately after deck construction}$$

A deck rating of 4 was selected as the threshold for when reconstruction or repair is required. This value has been used previously by other researchers as the boundary between acceptable and unacceptable condition for bridge decks [41]. Additionally, an upper limit for the estimated service life was set at 50 years. This amount is equal to the average forecasted service life using the machine learning models for bridges with zero or positive deterioration rates.

Bridges with less than three inspection records were neglected as bridges with relatively new deck construction are unlikely to be representative of the true performance of the deck.

There were 206 (of the 280 total) bridges in the FDPC Deck Panel Database with at least three inspections; these were used for further evaluation.

2.4.2. Machine learning model for bridge degradation

The machine learning model [40] estimates the future condition of a bridge deck based on the available data for each bridge and is using deep learning algorithms [42]. The specific deep-learning algorithm employed for data analysis is the convolutional neural network (CNN). For avoiding significant uncertainty in CNN, the deterioration model utilizes a standard Markov chain [43] procedure that assumes the deterioration process complies with the Markov property [42]. This model considers 28 different variables affecting the deterioration process including traffic volumes, construction materials, geometry, protection system and climate factors (freeze-thaw cycles and snowfalls). The general procedure of this model involves data preparation (including changing the format of all historical record to data matrix format) followed by the prepared datasets being validated and tested in the trained CNN model. The model then computes forecasting results predicting the future deck ratings up to 2070. All plots include an upper and lower limit, which are defined by considering 25 percent uncertainty in predicted results.

A sample of the forecasted bridge deck performance for a bridge using the machine learning model is shown in Figure 2.8. A lower-bound, median, and upper-bound are provided for the estimated performance. The estimated service life for a deck was found as the time between the deck construction and when the median predicted performance from the forecasting model reached a rating of 4. For the example shown in Figure 2.8, there

were 64 years between the deck construction (1985) and when the bridge is forecasted to reach a deck rating of 4 (2049).

A deck rating of 4 was selected as the threshold for when reconstruction or repair is required for similar reasons as stated before. There were some cases where the median forecasted performance never reached a rating of 4 during the forecasting window (50 years). These bridges were not included in the analysis; several of these bridges also did not have the three inspection records that were required for the linear regression model.
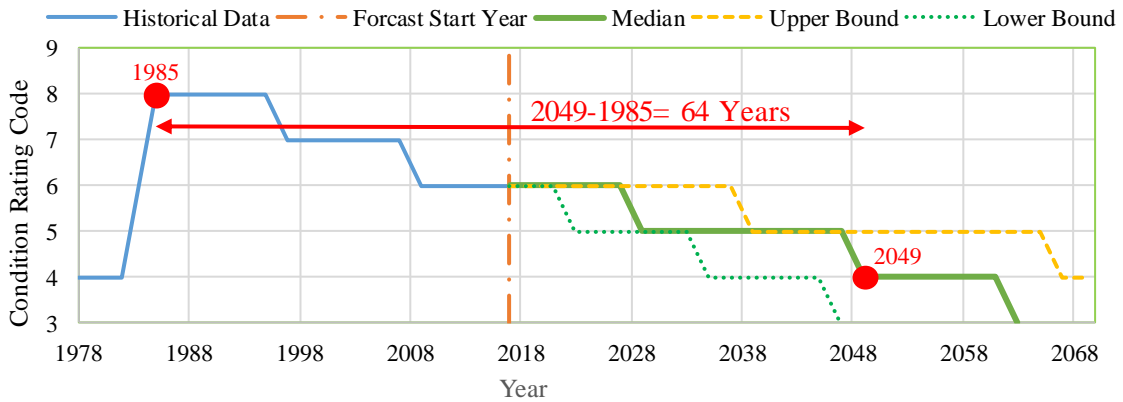
Figure 2.8: Sample of Deep Learning Models output from InfoBridge [34]

2.5. Performance comparison based on the classification of variables

The behavior of the bridges in the FDPC Deck Panel Database was analyzed based on the following classifications:

- Joint type

- Traffic impact category

- Climate zone

- Wearing surface

- Main span material type

- Average daily traffic (ADT) and average daily truck traffic (ADTT)

- Construction type (new versus rehabilitation)

2.5.1. Performance Based on Joint Type for FDPC Bridges

The performance of the bridges with FDPC deck panels was first evaluated based on joint type. The types of longitudinal and transverse joints for the bridges in the FDPC Deck Panel Database and their distribution are summarized in Figure 2.9. The grouted shear key (with and without post-tensioning) is the most commonly used joint in the transverse direction, and the conventional concrete with hooked and straight bars and UHPC with straight bar joints were the most commonly used joint in the longitudinal direction.
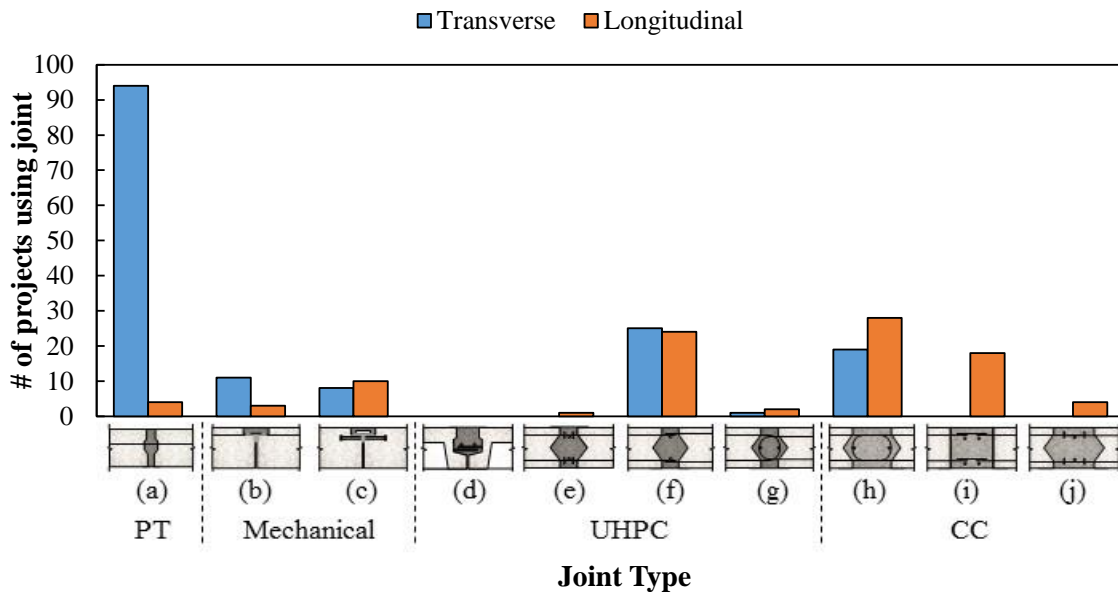
Figure 2.9: Distribution of transverse and longitudinal joint type

The performance of decks constructed with FDPC deck panels based on the transverse and longitudinal joint types are shown in Table 2-1 and Table 2-2, respectively. The average

behavior of joints that have been used on less bridges may be skewed by good or poor performance of one bridge; only joint categories with 10 or more bridges were compared in the following discussion. Another important factor that affects the joint performance is the joint width. This detail is not available in NBI or LTBP portal and was not gathered for all bridges through the survey, so it is not included here.

Of the four transverse joints with 10 bridges or more, the welded joint had the shortest average estimated service life based on both linear regression and machine learning model; this observation is consistent with findings from the detailed inspections conducted in Utah [27]–[31]. Difference between predicted service lives are more noticeable in the linear regression model than the deep learning model. There is not a significant difference in the estimated service life from the machine learning model between the long-term performance of the longitudinal post-tensioned joint, non-post-tensioned grouted joint, and UHPC with straight bar detail.

The non-post-tensioned grouted joint has been used longer (on average) than the other joint types. This joint was used in 36 bridges in Alaska (most low traffic volume) with 8 built in the 1990s, 24 built between 2000 and 2009, and 6 built since 2010. The low traffic volume on these bridges likely had a large impact on the average behavior of bridges with this joint type.

The UHPC with straight bar detail (UHPC-C1.f) had the next longest average estimated service life. All these bridges were built between 2012 and 2015 with only three of them having a decrease in deck rating after initial construction. The transverse joints with longitudinal post-tensioning (Long. PT-C1.a) joint has been used since 1995; the oldest

bridge using longitudinal post tensioning was constructed in Connecticut with a bituminous overlay and has not seen a drop in deck rating since construction.

Table 2-1: Average performance of bridges with FDPC deck panel based on transverse joint types

Joint Category		Long. PT - C1.a	Non-PT - C1.a	Welded - C1-b	Grouted Dowel - C1.c	UHPC - C1.f	UHPC - C1.g	CC - C1.h
Linear Regression Model	$n_{bridges}$	41	38	10	5	12	1	3
	Avg. $n_{inspections}$ per bridge	8	14.9	6.2	4.6	3.8	8.0	11.0
	Avg. Year of 1st Inspection	2009	2003	2008	2012	2014	2010	2006
	Deterioration Rate	-0.12	-0.07	-0.13	-0.07	-0.14	-0.24	-0.17
	Estimated Service Life (year)	35.5	43.0	33.3	43.2	39.9	21	33.7
Machine Learning Model	Estimated Service Life (year)	49.7	49.9	48.1	53.0	49.7	-	74

The performance was also evaluated based on the longitudinal joint type, as shown in Table 2-2. Bridges under the "None" category have no longitudinal joint, i.e. the FDPC deck panel extends the full width of the bridge. The bridges with no longitudinal joint would be expected to have the best performance, since the joint is typically the weak point of the deck. Of the joint categories with 10 or more bridges, three of them (UHPC with straight bar [C1.f], CC with hoop bar [C1.h], and CC with straight bar [C1.i]) had a similar performance to the bridges with no joints. This similar performance suggests that these three joint types lead to similar performance to decks without longitudinal joints.

The bridges with the grouted dowels (C1.c) longitudinal connection had shorter estimated service lives, which is consistent with the findings from the detailed inspections conducted in Utah [27]–[31]. The three bridges with the welded (C1.b) longitudinal connection had a

much longer average estimated service life, but there were not enough bridges in this category and the finding is inconsistent with previous observations the inspections conducted in Utah.

Table 2-2: Average performance of bridges with FDPC deck panels based on longitudinal joint types

Joint Category		Non-PT - C1.a	Welded - C1.b	Grouted Dowel - C1.c	UHPC - C1.f	UHPC - C1.g	CC - C1.h	CC - C1.i	CC - C1.j	None
Linear Regression Model	$n_{bridges}$	4	3	10	11	2	12	16	2	53
	Avg. $n_{inspections}$ per bridge	13.5	21.7	4.0	3.7	5.5	6.0	6.4	4.0	12.8
	Avg. Year of 1st Inspection	2005	1997	2011	2014	2013	2011	2008	2014	2005
	Deterioration Rate	-0.07	-0.07	-0.08	-0.16	-0.37	-0.09	-0.11	-0.40	-0.08
	Estimated Service Life (year)	40.3	47.0	33.1	39.0	15.5	41.5	35.8	11.3	41.0
Machine Learning Model	Estimated Service Life (year)	40.8	72.0	43.3	49.6	-	49.6	51.2	56.0	50.5

2.5.2. Performance Based on Impact Category

The average performance of bridges with FDPC deck panel decks grouped based on the impact categories are shown in Table 2-3. The impact category is still not collected for all ABC projects, so only a limited number of bridges (20%) in the FDPC Deck Panel Database had impact category data. Because of the limited data, no clear trends can be seen. The impact category should be collected for all future projects to help determine any correlation between speed of construction and bridge performance.

Table 2-3: Average performance of bridges with FDPC deck panels based on impact category

Impact Category		Tier 1	Tier 2	Tier 3	Tier 4	Tier 5	Tier 6
Linear Regression Model	$n_{bridges}$	3	4	3	3	16	12
	Avg. $n_{inspections}$ per bridge	4.0	12.0	19.0	3.0	8.9	8.6
	Avg. Year of 1st Inspection	2012	2006	2007	2014	2009	2009
	Deterioration Rate	0.0	-0.04	-0.09	-0.25	-0.16	-0.16
	Estimated Service Life (year)	50.0	43.5	38.7	25.3	33.9	36.3
Machine Learning Model	Estimated Service Life (year)	52.7	40.0	40.0	26.0	54.4	52.6

2.5.3. Performance Based on Climate Zone

The average performance of bridges with FDPC deck panel decks grouped based on the DOE climate zones are shown in Table 2-4. Most bridges with FDPC deck panels are found in very cold or cold climate zones, which is a result of most of the bridges being in New York, Alaska, and Utah. As expected, the bridges in cold climate zones had the highest deterioration rates and shortest average estimated service life (using both linear regression and machine learning models). These cold climate zones typically have the most freeze-thaw cycles, which combined with moisture and deicing salts are the primary cause of damage to concrete decks. Nearly all the bridges located in very cold climate zones are in Alaska (having less freeze-thaw cycles than the cold regions) and are on low volume roads; both facts would contribute to the better performance of these bridges.

Table 2-4: Comparison of average performance of bridges with FDPC deck panels based on climate zone

Climate Category		Very Cold	Cold	Mixed humid	Hot humid	Marine
Linear Regression Model	$n_{bridges}$	41	148	15	1	2
	Avg. $n_{inspections}$ per bridge	14.8	12.3	12.8	5.0	5.0
	Avg. Year of 1st Inspection	2003	2004	2004	2008	2013
	Deterioration Rate	-0.07	-0.14	-0.10	-0.10	-0.00
	Estimated Service Life (year)	43.8	36.3	40.6	50.0	50.0
Machine Learning Model	Estimated Service Life (year)	52.4	50.4	50.8	-	32.0

2.5.4. Performance Based on Wearing Surface

Several different wearing surfaces were used for the FDPC deck panel decks in the database, as shown in Table 2-5. The definitions for the wearing surfaces are found in Weseman [38], but are not entirely clear with respect to FDPC deck panel decks. "Monolithic Concrete" decks are defined as a wearing surface concurrently placed with the structural deck, while "Integral Concrete" decks are cast separate from and in addition to the structural deck. "None" refers to bridge decks with no additional concrete thickness or wearing surface. Additional details were available for several of the projects in the FDPC Deck Panel Database through the ABC Project Database [7]. Two projects in Alaska, one project in Iowa and one project in Oregon all coded "Monolithic Concrete" for FDPC deck panel decks were confirmed through the ABC Project Database to not have any overlay provided (i.e. the top of the FDPC deck panel is the riding surface). Grinding was typically done after casting of the joints to obtain the final riding surface for these projects. There was one project in New York found in the ABC Project Database that had a 2-inch thick CIP concrete riding surface cast after the placement of the FDPC deck panels and casting

of the joints that was coded as "Monolithic Concrete" in the NBI. Additional details were found for one project in Iowa with an NBI coding of "Integral Concrete" wearing surface; this bridge was confirmed through the ABC Project Database to have a 2-inch thick CIP concrete wearing surface also cast after the placement of the FDPC deck panels and casting of the joints. Additional details were found on one bridge in California with "None" as the riding surface in the NBI; this bridge has no additional overlay provided. Based on these additional details, the bridges with a "None" overlay in the NBI were revised to "Monolithic Concrete" in the FDPC Deck Panel Database. The one project in New York with a 2-inch concrete overlay was revised to "Integral Concrete". The authors recommend states use this coding basis for future project entries.

The bridges with "Other" wearing surface performed the best out of all the overlays. Additional information was obtained for three of these bridges; these bridges had the following overlays: 2.4-inch microsilica concrete, 0.75-inch polyester polymer, and 1.5-inch silica fume concrete.

The bridges without an overlay and with an integral concrete overlay had the next best performance for the overlay options (based on the linear regression and machine learning models). The performance of the group of bridges without an overlay was biased by the 35 bridges found in Alaska. The 11 bridges without an overlay outside of Alaska had almost a similar deterioration rate (-0.12) and average estimated service life (37 years) to bridges with integral concrete wearing surfaces. Bridges with epoxy overlays and bituminous overlays had the shortest estimated service lives.

Table 2-5: Comparison of average performance of bridges with FDPC deck panels based on wearing surface

Wearing Surface		Monolithic Concrete	Integral Concrete	Latex Concrete	Epoxy overlay	Bituminous	Other
Linear Regression Model	$n_{bridges}$	46	17	8	26	100	14
	Avg. $n_{inspections}$ per bridge	2004	2010	2008	2010	2001	2001
	Avg. Year of 1st Inspection	13.5	8.3	10.4	4.3	14.9	14.9
	Deterioration Rate	-0.09	-0.15	-0.25	-0.11	-0.11	-0.06
	Estimated Service Life (year)	43.0	39.4	27.1	34.2	37.3	45.1
Machine Learning Model	Estimated Service Life (year)	50.9	53.1	52.8	49.1	49.1	55.9

2.5.5. Performance Based on Main Span Material

The average performance of bridges with FDPC deck panel decks grouped based on the main span material are shown in Table 2-6. FDPC deck panels have been most often used with steel superstructures: 85 percent have been used with either steel single-span or continuous main spans. Most of the bridges with steel superstructures are in states with the most experience with FDPC deck panels: 90 percent of the bridges with steel superstructures are in Alaska, New York, or Utah. Additionally, the bridges with FDPC deck panels on steel superstructures have been on average in service for a longer period of time. These facts likely contributed to the improved behavior experienced by the bridges with FDPC deck panels on steel superstructures.

Table 2-6: Comparison of average performance of bridges with FDPC deck panels based on main span material

Main Span Material		Concrete continuous	Steel	Steel continuous	Prestressed concrete	Prestressed concrete continuous	Wood or timber
Linear Regression Model	$n_{bridges}$	1	144	31	26	2	1
	Avg. $n_{inspections}$ per bridge	7.0	14.4	11.7	6.0	5.0	24.0
	Avg. Year of 1st Inspection	2011	2003	2004	2009	2013	1994
	Deterioration Rate	0.000	-0.114	-0.09	-0.127	-0.200	-0.121
	Estimated Service Life (year)	50.0	39.6	37.8	33.6	30.0	24.7
Machine Learning Model	Estimated Service Life (year)	-	51.7	48.5	46.6	42.0	14.0

2.5.6. Performance Based on ADTT and ADT

Another factor that affects the performance of decks is average daily traffic (ADT) and average daily truck traffic (ADTT); higher ADT and ADTT will lead to higher deterioration rate. The performance of bridges in the FDPC Deck Panel Database is divided into low-volume (ADTT ≤ 6,000, ADT ≤ 30,000) and high-volume (ADTT > 6,000, ADT > 30,000) roads, shown in Table 2-7. High traffic volume and low traffic volume limits are usually defined based on the geographic area and functional classification. These definitions are different for highways, freeways, streets, or roads. The assumed limits here were assigned based on discussions with bridge engineers in several states to cover most road functions.

As expected, the bridges in the database with high traffic volumes on average have a higher deterioration rate and shorter estimated service live than those with low traffic volumes.

Table 2-7: Comparison of average performance of bridges with FDPC deck panels based on ADTT and ADT

Traffic Condition		ADTT		ADT	
		≤ 6000	> 6000	≤ 30000	> 30000
Linear Regression Model	$n_{bridges}$	184	27	181	30
	Avg. $n_{inspections}$ per bridge	13.7	4.9	13.8	5.5
	Avg. Year of 1st Inspection	2003	2011	2003	2011
	Deterioration Rate	-0.11	-0.16	-0.11	-0.15
	Estimated Service Life	39.2	33.1	39.0	34.8
Machine Learning Model	Estimated Service Life (year)	50.8	47.7	50.7	49.0

2.5.7. Performance Based on Construction Type

FDPC deck panels can be used on both new and rehabilitation projects. The performance of the bridge in the FDPC Deck Panel Database was broken down based on the construction type in Table 2-8. The type of construction was determined from the NBI data; new construction was assumed where the year of the bridge construction was equal to the year of the deck construction and rehabilitation assumed where the year of bridge construction was earlier than the date for the year of deck construction. Bridge with FDPC deck panels used for new construction performed similar to those where FDPC deck panels were used to rehabilitate the bridge.

Table 2-8: Comparison of average performance of bridges with FDPC deck panels based on type of construction (new or rehabilitation)

Construction Type		New	Rehab
Linear Regression Model	$n_{bridges}$	93	114
	Avg. $n_{inspections}$ per bridge	13.5	11.9
	Avg. Year of 1st Inspection	2003	2005
	Deterioration Rate	-0.12	-0.12
	Estimated Service Life	38.3	38.3
Machine Learning Model	Estimated Service Life (year)	49.6	51.8

2.5.8. Summary and Conclusions

A summary of inspection and survey results for the bridges with FDPC deck panels were presented in this paper. The FDPC Deck Panel Database was created based on the survey results and information obtained from the ABC Project Database. This database contained detailed information on 280 bridges throughout the U.S. specifically for those constructed with FDPC deck panels. Some of the detailed information includes joint types, impact category (describing the time traffic was impacted by construction), main span material and climate zones. The performance of the bridges in the FDPC Deck Panel Database was analyzed based on NBI inspection data and the influential variables according to linear regression and deep learning model. The following conclusions were made based on this analysis:

- **Joint Type**: The three joints with better performance in terms of higher estimated service life coming from estimation models, were the UHPC with straight bar (C1.f) (for transverse or longitudinal joints), longitudinal post-tensioned (C1.a) (for transverse joints), and conventional concrete with hooped bar details (C1.h) (for longitudinal joints). It also would be expected that bridges with no longitudinal joint should have the best performance as bridges without joints should perform the best, which is consistent with the study findings. The non-PT grouted joint (with a similar geometry to the PT joint-C1.a) showed good performance but was only used in low-volume roads in Alaska. Welded connections (C1.b) in transverse joints and grouted dowel connections (C1.c) in longitudinal joints were shown to have a shorter service life through the reported visual inspections and database analysis.

35

- **Climate Zone**: As expected, bridges with FDPC deck panels have the shortest average estimated service life in cold climate zones. More freeze-thaw cycles compare to very cold zones has made the most damages to bridges constructed in cold zones.

- **Wearing Surface**: FDPC deck panel bridges with monolithic concrete, integral concrete, epoxy overlay, and bituminous wearing surfaces have shown similar performance. Bridges with other wearing surfaces (including microsilica concrete, polyester polymer, and silica fume concrete) have longer estimated service lives. Anyway, using a proper protection layer prevent aggressive ions like chloride to reach the concrete surface and enhance the durability of protected elements

- **Traffic**: As expected, bridges with FDPC deck panels and high traffic volumes have a shorter average estimated service life than similar bridges with lower traffic volumes. A more detailed study is required to investigate the effect of passing traffic based on the bridge function.

- **Construction Type**: There was no difference in performance between bridges using FDPC deck panels for new construction compared with those using them for rehabilitation projects.

Chapter 3: **Background On Non-Proprietary UHPC**

3.1. Introduction

Ultra-high-performance concrete (UHPC) has recently become more popular between academia, engineers, and owners due to its unique properties. UHPC is generally known for its high compressive and tensile strength, self-consolidation, exceptional durability, and significant post-cracking ductility. Maximum water-to-binder ratios (w/b) of 0.24 in UHPC lead to compressive strengths of 22 ksi or more at 28-day age [44]. Low matrix porosity and high particle packing density result in higher durability for UHPC compared to conventional concrete [45]. UHPC has been shown to have a tenfold lower chloride diffusion rate and almost zero deterioration rate under freeze and thawing cycles[46], [47]. The use of steel fibers give UHPC the ability to resist direct tensile stresses of over 0.72 ksi, have a strain hardening response after initial cracking, and have limited crack width [4]. Using smooth fibers with high tensile strength in UHPC has created high tensile strength that enables material to undergo tension before pulling out the fibers in failure mechanism.

Large superplasticizer dosages allow for hydration of the cementitious materials in the mixture and give UHPC its self-consolidating properties.

These exceptional performance characteristics have made UHPC an ideal option for different sectors of the construction industry including precast concrete fields.

UHPC can be used to ease the design and improve the performance of joints between precast elements. UHPC also allows designers to utilize smaller cross-sections, reduce the

conventional reinforcement, increase the prestressing force, and consequently produce longer-span elements. UHPC has made a significant improvement in accelerating the construction process, through the use of UHPC in joints between conventional concrete precast elements and as the primary material for UHPC precast elements [2].

Despite all these advantages, the use of UHPC in the United States remains limited. Proprietary UHPC mixtures can cost up to 20 to 30 times more than conventional concrete. Non-propritary mixtures can decrease costs but often require much stricter quality control measures than conventional concrete. These enhanced quality control measures plus the high material cost for the material has limited the widespread use of UHPC in the U.S. infrastructure [3], [4].

For this reason, many research efforts have focused on the non-proprietary UHPC to make UHPC more accessible from locally-produced raw available materials and give guidance on how to mix and use the material. This study investigates the development of non-proprietary UHPC using locally-produced raw available material in Florida and gives details on how to mix and test the material.

3.2. Definition of UHPC and Typical Material Properties

Some of the typical material properties for UHPC are summarized in Table 3-1.

Table 3-1: Typical range of mechanical properties for UHPC [10], [48]

Property	Typical Range
7-day Compressive Strength	14.5 to 19.5 ksi
14-day Compressive Strength	18 to 22 ksi
Direct Tensile Cracking Strength	0.8 to 1.2 ksi
Direct Tension Bond Test	0.35 to 0.6 ksi
Modulus of Elasticity	4,250 to 8,000 ksi
Long-term Drying Shrinkage	300 to 1,200 $\mu\varepsilon$
Long-term Autogenous Shrinkage	200 to 900 $\mu\varepsilon$
Initial setting time	4 to 10 hours
Final setting time	7 to 24 hours
Static flow	7.5 to 10 inches

UHPC typically is defined by some combination of its mechanical properties, however, the actual material properties that are typically included in the definition vary based on the researchers or organization that is providing the definition and the application for the UHPC. A summary of some of the typical minimum definitions of UHPC are summarized in Table 3-2.

Table 3-2: Minimum definitions of UHPC (modified from [46])

Document	Ref.	Country	Min. f'_c (ksi)	Min. Tensile Strength (ksi)	Other Criteria
ACI 239R-18	[49]	USA	22.0	--	--
AFNOR NF P 18-470	[50]	France	18.8	0.87 (first crack, f_t)	Durability, ductility, and fire resistance
ASTM C1856-17	[51]	USA	17.0	--	--
CSA A23.1	[52]	Canada	17.4	0.58 (first crack, f_t)	Durability and ductility
FHWA	[13]	USA	21.7	0.72 (post crack, f_t)	w/b $\leq$ 0.25
PCI	[46]	USA	18.0	1.50 (first crack, f_r), 2.00 (peak, f_r)	Durability and ductility
SIA 2052	[53]	Switz.	17.4	1.00 (first crack, f_t)	Ductility

The compressive strength is typically specified to be greater than or equal to 18 ksi [46] or

21.7 ksi [13]. Lower strengths are sometimes allowed or specified for specific applications,

e.g., 14 ksi for the development length equations for the design of field-cast connections

from FHWA [48] and 10 ksi for release strength for precast, prestressed UHPC [46].

UHPC definitions also typically include some requirement for tensile strength and

sustained tensile or post-cracking strength. The definition is typically either measured

using direct tension tests or modulus of rupture tests. The tensile strength at first cracking,

the peak tensile strength, and some related deflections. Typical tensile strength curves are

shown in Figure 3.1 for the tensile strength based on flexural stress modulus of rupture

tests and direct tension.
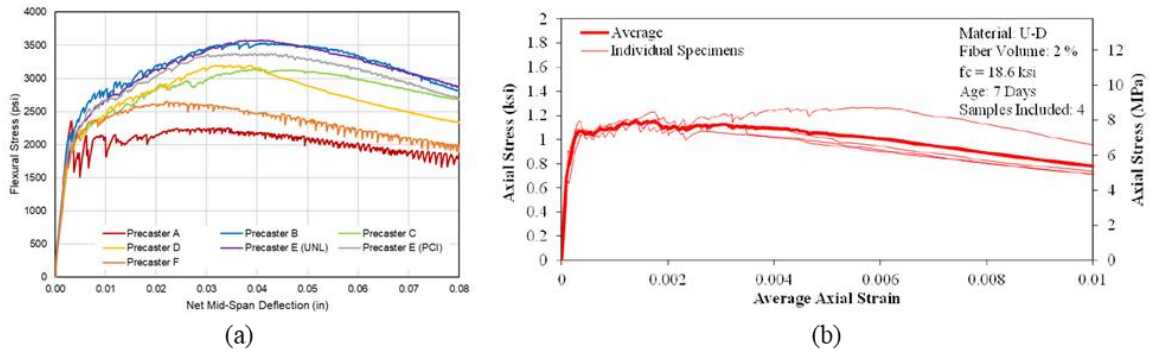
Figure 3.1: Tensile strength curves based on (a) flexural strength from modulus of rupture [46] and (b) direct tensile strength using prismatic samples [54]

The idealized stress-strain response of UHPC loaded under direct tension has a similar

shape to conventional steel reinforcement, as shown in Figure 3.2. This idealized response

illustrates four of the primary phases in the UHPC tensile response [3]:

1. *Elastic*: linear-elastic response, no crack formation

2. *First cracking*: beginning of the plastic response phase, multiple tightly spaced

   cracks form in the UHPC matrix

3. *Crack saturation*: start of the strain hardening response, larger cracks begin to

   develop in the UHPC matrix

4. *Localization*: sample reaches its ultimate tensile strength and begins to drop in

   strength, a single crack begins to open larger, fibers start to pull out of the UHPC

   matrix

The actual behavior of the UHPC in tension depends on many different factors, including

fiber type, content, and distribution.
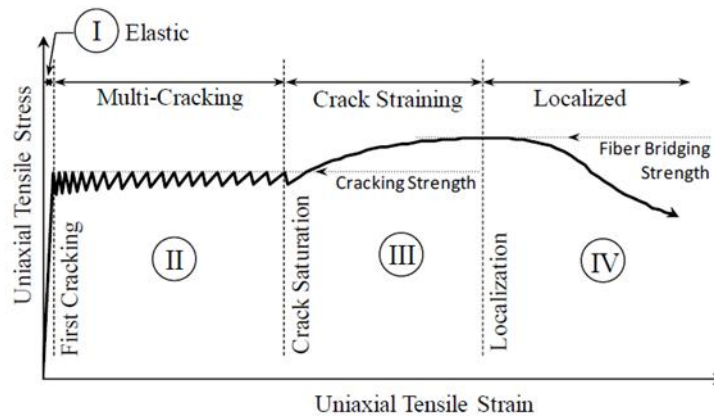
Figure 3.2: Idealized uniaxial tensile mechanical response of a UHPC [3]

3.3. UHPC Application

UHPC has been used in a wide variety of infrastructure applications including repair and

retrofit of existing structures and the construction of new structures. UHPC's high

compressive and tensile strength, self-consolidating nature, low permeability, long-term

durability, and high bonding properties have helped UHPC perform well in different repair

applications, such as thin-bonded overlay on deteriorated bridge decks, shown in Figure

3.3(a), or as a shell around a damaged region of a component [3], [55]. In a recent study, the use of UHPC encasements was shown to increase the load-carrying capacity of timber piles more than 100 percent based on the initial timber pile diameter and UHPC shell thickness [56]. UHPC has also been used as formwork for cap beams and other elements to eliminate the need for assembling or stripping formwork [57].

UHPC also has been used in new construction in several different ways: (1) in the joints between precast elements, (2) as the material for full precast elements, and (3) as material for parts of a precast or prefabricated element. The primary application of UHPC to date has been for the field-cast connection between prefabricated bridge components [3], [15], [58]. The properties of UHPC lead to much shorter required development and splice lengths for reinforcement extending from the precast elements, and the presence of the steel fibers allow for connections to be designed without any field-placed reinforcement. The UHPC has enhanced bonding properties between the UHPC joint and precast element. UHPC joints can be designed to minimize the amount of material required, which helps to mitigate the higher cost of the material. The use of UHPC in the joint between precast elements has been considered recently by many owners, designers, and contractors, especially for joints between precast deck panels [3], [13]. An example of a UHPC joint between precast deck panels is shown in Figure 3.3(b). UHPC has also been used to connect other prefabricated elements, such as precast barriers to decks or deck panels [59].

UHPC is also being used to produce full precast bridge elements, such as waffle deck panels, pile elements, and girders. The use of UHPC allows for optimized shapes for precast elements with decreased weights, less conventional reinforcement, increased span

lengths, and decreased section profiles. An example of a UHPC precast waffle deck panel is shown in Figure 3.3 (c).

UHPC has also been used in application other than bridges. Many precast tunnel segments are made of UHPC or using UHPC as a thin fire resistance overlay due to its fire resistance property [60]. The high compressive strength and tensile resistance of UHPC have broadened its use even in military and critical infrastructures for security and blast mitigation purposes [61]. UHPC has also been used in the energy industry to construct taller and more efficient wind turbine towers [62], as shown in Figure 3.3 (d).

(a)   (b)   (c)   (d)

Figure 3.3: Structural applications of UHPC; (a) overlay (UT) [10], (b) UHPC joints (OR) [10], (c) waffle deck panels (NE) [63], [64] and (d) wind turbine towers(IA) [62], [65]

UHPC has also been used for architectural elements like stairways, facades, street furniture, bus shelters, sun shades, and stuff like that for its high durability and resistance [66], [67]. Some architectural applications are shown in Figure 3.4.

(a)   (b)   (c)   (d)

Figure 3.4: Architectural applications of UHPC; (a) Staircases (DK), (b) Sunshade (CA), (c) Gateway Pavilion (US) and (d) Facade Cladding Panels (Fr) [68]

UHPC is applicable to any applications where conventional concrete cannot address the minimum required mechanical properties [13]. For example, several researchers reported poor performance of normal concrete in the joint between bridge deck panels [10], [31]. UHPC has been used in these applications to improve the behavior of the joint and system.

3.4. UHPC Constituent Materials

The performance of UHPC is based on the properties and proportions of the different material components making up the UHPC mixture. The primary components of UHPC include cement, silica fume, an additional supplementary cementitious material of intermediate sizes (e.g., fly ash, slag), and fine sand (usually finer than conventional concrete sand). The proportions of these components are chosen based on their particle size distributions and reactive properties. A high-range water-reducing admixture (HRWR) or superplasticizer is responsible for providing the desirable flowability while the water-to-binder ratio (w/b) is around 0.2. Steel fibers are usually added at a dosage of 1 to 6 percent by volume to the mixture and provide post-cracking ductility and tensile strength for the UHPC.

One of the most popular proprietary UHPC product in the US is Ductal®, produced by Lafarge-Holcim [68]. This product meets the typical requirements for UHPC materials [69], also described above. The typical composition of Ductal® is shown in Table 3-3.

Table 3-3: Typical Composition of Ductal® [3]

Material	lb/yd³	kg/m³	Percentage by Weight
Portland Cement	1200	712	28.5
Fine Sand	1720	1020	40.8
Silica Fume	390	231	9.3
Ground Quartz	355	211	8.4
HRWR	51.8	30.7	1.2
Accelerator	50.5	30	1.2
Steel Fibers	263	156	6.2
Water	184	109	4.4

Most proprietary and non-proprietary UHPC mixtures have a similar composition to what is shown in Table 3-3. A further explanation of each constituent material is provided in the following sections.

3.4.1. Aggregate

UHPC materials typically only include fine aggregates, although coarser aggregates can be used in lower strength mixtures. Aggregate sizes up to 0.25 inches have been used successfully in UHPC mixture designs [48]. For high strength concrete, the failure cracking in the concrete matrix will often go through the weaker coarse aggregate, which will limit the achievable compressive strength. There have been a few studies that went beyond a maximum aggregate size of 0.25 inches and reported a decrease in the mechanical properties of UHPC. One study used coarse basalt aggregates with a maximum size of 0.63 inches in the UHPC mixture; using the larger aggregate size decreased splitting tensile strength and compressive strength by approximately 8 and 19%, respectively [70].

Using only fine aggregates allows for mixtures where the compressive strength is controlled by the strength of the hydrated cementitious materials and not the aggregate. The use of fine aggregates also provides a gradation of dry materials that facilitates the flowability of UHPC and a denser concrete matrix. Decreasing the maximum aggregate size to 0.23 inches (6 mm) and combining it with finer aggregate categories with a maximum grain size of 0.19, 0.09, and 0.008 inches resulted in a minimum 18 ksi compressive strength at 28 days [71]. Using two different aggregate sizes (0.003 to 0.008 inches and 0.016 to 0.031 inches) and combining them could result in a denser matrix and increased particle packing, which consequently leads to higher mechanical properties (compressive strength of 28 ksi in 28 days) [72]. Using multiple aggregate sizes and combining them based on optimized packing models is a verified solution to get the highest possible density out of available dry constituents and has been used successfully in several studies [26], [70], [71], [73], [74]. Different aggregate sizes and types used in previous studies are shown in Figure 3.5.
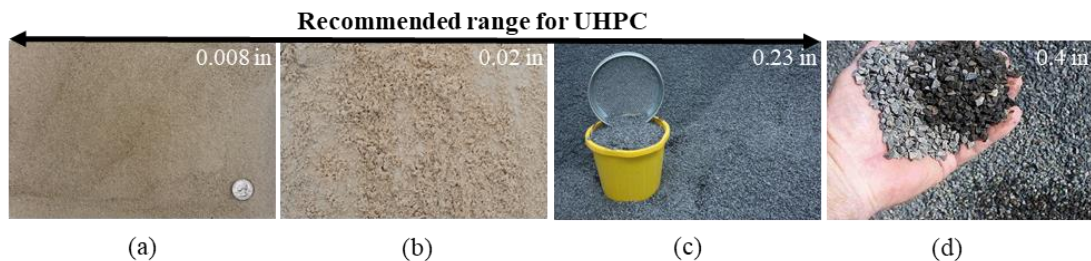
Figure 3.5:Range of the aggregate size used in UHPC; (a) Ultra fines recovery (UFR), (b) Fine sand- limestone, (c) limestone aggregates, (d) basalt aggregates

Different fine aggregate types, including limestone, basalt, and quartz, have also be used successfully in a UHPC mixtures [48], [75], [76]. Different types of aggregates have different properties. Quartz particles offer a higher strength than limestone particles.

46

Previous studies reported using fine quartz particles in the UHPC matrix [75] and getting higher compressive strengths [77].

Other aggregate types have been explored for additional benefits, e.g., internal curing. Previous researchers used an aluminosilicate material (ECat) for this reason [78]. ECat has a chemical composition that encourages pozzolanic activity and a high specific surface area with water affinity, which leads to significant water absorption. This aggregate type was used initially to provide internal curing action on UHPC mixture and improve the mechanical properties of the UHPC.

Quartz particles were not available locally for this study, so ultra-fine recovery (UFR) or limestone powder was used as intermediate aggregates to enhance the density of the final mixture. UFR solid parts are recoverable fine materials coming from wastewater streams of aggregate plant system. The fine size of UFR (less than 150µm) has made it a conveyable and stackable material ideal for several industries.

A maximum grain size of 0.02 inches was used for the fine aggregate in this research to be consistent with the materials used by the University of Oklahoma (OU), who was the lead university for this research project. Limestone aggregate was used as it was the most widely available in South Florida.

3.4.2. Cement

A wide variety of portland cements are used in the construction industry, each one designed for a specific purpose and required performance. Although several studies have reported UHPC mix designs made by different cement types, few have been done to investigate the effect of various cement types on the final properties of UHPC. The most commonly used

47

cement type in UHPC has been Type I/II cement which is a good candidate for UHPC mixtures due to its low cost and widespread availability [3], [4], [71], [72], [74], [79]–[82], [46]. There have been some studies that used Type I White, Type III and Type V cement successfully, but the final mixtures were produced at a higher cost than similar mixtures with Type I/II cement [72], [74], [80], [82]. Additionally, to minimize the workability challenges, it is recommended to use cement with a maximum C_3A content of 8 percent and a blain fineness of less than 281228 in^2/lb [83].

Five different cement types were investigated in this research to see their effect on the rheology and mechanical properties of the UHPC mixtures. Details on the five cement types investigated in this research are summarized in Table 3-4. The 28-day strength was reported by the manufacturer and found using ASTM C109 with a water-to-cement ratio of 0.485 [84].

Table 3-4: Manufacturer supplied properties of cements evaluated

Cement Type	Producer	28-day strength, ksi (MPa)	C_3S	C_2S	C_3A	C_4AF	Blaine Fineness in^2/lb (m^2/kg)	Air Content %	Setting Time (min)	
									Initial	Final
Masonry	Titan America	2.9 (20.2)	-	-	-	-	-	15	145	-
Type I-II	Titan America	6.8 (47.0)	63	9	6	11	279822 (398)	7	109	228
Type I-II	Ash Grove	4.7 (32.3)	59	19	6	10	-	6	115	115
Type III	Titan America	7.9 (54.7)	69	6	6	11	355050 (505)	6	75	155
Type I (white)	Lehigh	7.1 (49.1)	73	7	13	1	339583 (483)	6.7	100	200

3.4.3. Silica Fume

Silica fume plays an important role in UHPC mixtures due to its fine particle size and pozzolanic properties. These fine particles fill the gaps between coarser grains in the matrix and promote higher density. Besides its physical role, its pozzolanic activity provides additional strength and improved durability for the UHPC mixture. Typical UHPC mixtures have silica fume contents between 10 to 20 percent of cement weight [48].

A silica fume provided by BASF was used in this research at contents between 16 and 21 percent of the cement weight.

3.4.4. Supplemental Cementitious Materials (SCM)

Other supplemental cementitious materials are also used in UHPC mixtures. These materials typically are added to concrete to improve particle packing and make concrete mixtures more economical, sustainable, impermeable or improve mechanical properties [46], [48]. Fly ash, slag, and metakaolin are the most popular SCMs that have been used to date [85], [77].

Slag cement or blends of portland cement with ground-granulated blast-furnace slag (GGBS) has been used in several studies [72], [74], [80], [82]. Using GGBS typically helps to reduce the cost of the mixture and helps create a more sustainable cementitious material by using less ordinary portland cement. Using a 50:50 mix of Type I portland cement and GGBS as a binder not only offered a more reasonable cost but also satisfied typical requirements for UHPC mixtures in several studies [72], [74], [80], [82].

Fly ash has also been used in several studies but has generally shown less improvement in mechanical properties compared to UHPC mixtures made with GGBS [71], [74], [86].

Comparing the hydration process of mixes containing fly ash and slag revealed that fly ash requires more water to be actively involved in the hydration process compared to slag. Therefore, in UHPC and other special concretes with low w/b, the pozzolanic reaction of fly ash is significantly retarded [86]. Fly ash can still be used in the UHPC mixture based on its availability and price. Although fly ash can be obtained at a more reasonable price than other SCM's like silica powder, it may not be as effective as other SCMs due to its higher water demand [4].

Several additional SCMs have been investigated for use in UHPC. These include nano-silica, silica powder, metakaolin, and nano-metakaolin.

Several studies used nano-silica particles with an average diameter between 1 and 100 nanometers to improve the durability of different types of cementitious material. Most of these studies reported significant improvement in strength development, modulus of elasticity and durability [87], [88], [88], [89]. Also, few studies used nano silica fume to investigate the final mechanical properties of UHPC mixtures. Using nano silica fume (5 percent of the cement weight) with silica fume (30 percent of the cement weight) resulted in a 21 ksi compressive strength at 28 days [90]. Nano-silica can be used in UHPC mixtures based on the availability and price. In this study nano-silica particles were not used to be consistent with other university partners.

One study investigated the use of silica powder in UHPC. They suggested to remove the silica powder from the mixture due to its relatively high cost and delayed reaction compared to silica fume [74].

Metakaolin is another SCM that has been used to improve the mechanical properties and durability of UHPC mixtures in a similar way as silica fume. Metakaolin can be more accessible than silica fume and has a white color, which makes it more appropriate for architectural purposes [77]. Kaolinite, the source of metakaolin is available in most countries and locations with more reasonable price compared to nano silica and silica fume. Metakaolin has also been used in the nano scale in some past studies to improve the particle packing of the UHPC. While replacing up to 10 percent of cement weight with nano-metakaolin improved the compressive strength at older ages, it also significantly decreased the flowability, so more HRWR was required to get the necessary flowability [91], [92]. Metakaolin was not used in this study to be consistent with other partner universities.

In general, most SCMs can be used in UHPC mix design based on availability but should be tested in small trial batches to ensure adequate performance before being used in field applications.

3.4.5. Fibers

Fibers have been used in cementitious composites since 1980 [93], [94] and play an important role in UHPC. Fibers are added to the UHPC matrix to provide post-cracking ductility and increase the tensile strength [21]. A fiber content of 2 percent of total mixture volume is typically used in UHPC, but contents as high as 6 percent have been used to attempt to increase the tensile strength [48]. Although higher fiber contents generally result in higher tensile strength, a higher dosage of fibers may cause negative results due to improper fiber distribution and decreased workability. This issue can be even worse when fibers are relatively heavy, lengthy, and hooked. Dispersion of heavier fibers in the

concrete matrix is more challenging and requires special mixing consideration. Deformed fibers like hooked end fibers perform better in terms of pullout resistance but need special attention as they are more susceptible to clumping during batching.

Fibers used for UHPC are classified based on the material type: metallic fibers (commonly made of steel) and non-metallic fibers (made of organic polymers; synthetic fibers). Steel fibers have higher yield strength (up to 400 ksi) compared to synthetic fibers (less than 100 ksi), which leads to UHPC with steel fibers having a much higher post-cracking tensile strength. Although steel fibers provide superior after-cracking behavior for UHPC, synthetic fibers can lead to improved fire resistance and also a softer UHPC response.

The effect of fibers on the mechanical performance of UHPC will depend on geometry, anchorage type, material, coating, chemical composition, weight, yield strength, volume fraction, dispersion, and orientation of the fibers [46].

The most commonly used steel fiber in UHPC is a brass-coated, straight, steel fiber with 0.008-inch (0.2-mm) diameter and 0.5-inch (13-mm) length and a specified minimum tensile strength of 290 ksi (2,000 MPa) [48]. The tensile strength of these fibers is typically around 400 ksi (2,758 MPa).

Four different steel fibers from various manufacturers and one synthetic fiber were used in this research at several different fiber contents. The properties of the fibers used in this research are summarized in Table 3-5 and a photograph of the different fibers is shown in Figure 3.6. The Bekaert OL 13/.20 and Hiper Fiber Type A fibers had the same physical properties, and both were brass coated. Although the exact chemical composition of fibers was not obtained, the researchers were informed by the manufacturer that the Helix 5-13

fibers contained a higher zinc content. The manufacturer informed the researchers that the zinc content was decreased in the fibers, but new fibers were not obtained after this change had occurred.

The fiber types are given a short name in Table 3-5 for use in the mixture design tables.

Table 3-5: Fiber Properties

Name	Fiber	Length, in (mm)	Diameter, in (mm)	Aspect Ratio (l/d)	Tensile strength, ksi (MPa)
A	Dramix 4D 65/35BG	1.4 (35.6)	0.020 (0.51)	70	268.0 (1,850)
H	Helix 5-13 (uncoated)	0.5 (12.7)	0.020 (0.51)	25	246.5 (1,700)
OL	Dramix OL 13/.20	0.5 (12.7)	0.008 (0.20)	63	400.0 (2,758)
HF	Hiper Fiber Type A	0.5 (12.7)	0.008 (0.20)	63	400.0 (2,758)
Sy	STRUX® 90/40	1.55 (40)	0.017 (0.43)	92	90.0 (620)

(a)   (b)   (c)   (d)
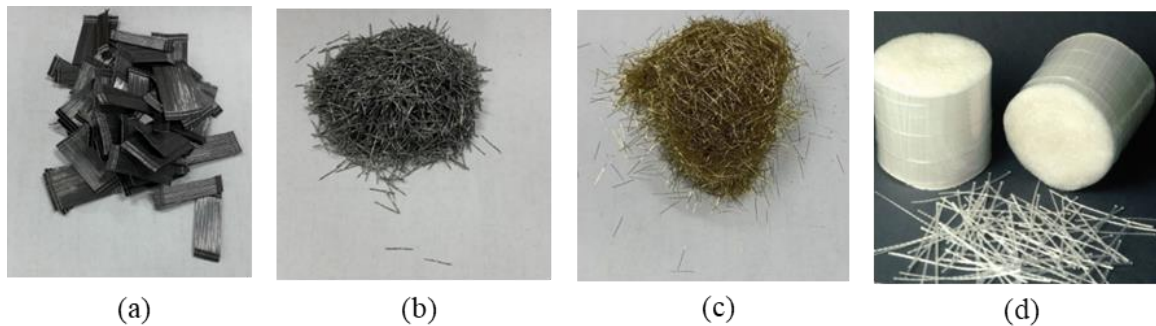
Figure 3.6: Different steel fibers (a) Bekaert 4D 65/35BG, (b) Helix 5-13, (c) BEKAERT OL 13/0.2 & Hiper Fiber and (d) STRUX® 90/40

3.4.6. Water

Like other cementitious composites, UHPC needs water to complete the hydration process. All water quality and control requirements relevant to conventional concrete are also applicable for UHPC mixtures [48]. Besides the role of water in the chemical reaction, its temperature during addition to the mixture plays a very important role in the final

properties of fresh concrete. A lower temperature reduces the heat of hydration and results in higher flowability [48]. For this reason, cold water or ice cubes were used in many studies and are recommended for casting in high-temperature climates [46]. Using ice particles not only improves the flowability by controlling the heat of hydration but also improves the mixing efficiency by gradually releasing water in the mixture and improving the mixing action [48].

3.4.7. Chemical Admixtures

The most common chemical admixtures in UHPC are high-range water reducers (HRWR) or superplasticizers. Both polycarboxylate-based superplasticizers and phosphonate-based superplasticizers have been used in UHPC mixtures to provide the required flowability for this concrete with low w/b. Other chemical admixtures like viscosity modifying admixtures (VMA) and corrosion inhibiter admixtures are also used in UHPC mixtures for specific actions [46].

VMA are water-soluble polymers that have been used in concrete technology to modify the viscosity of mixing water and increase the ability of cementitious paste to retain its constituents in suspension [95]. VMA have been widely used for self-compacting concrete (SCC) with slump flows ranging from 26 to 31 inches [95].

In this study, BASF Master Glenium 7920 was used as HRWR to provide required flowability. The BASF VMA 358 was also used for specific mix designs for uniform dispersion of heavier fibers and preventing fiber segregation.

3.5. Water-to-Binder Ratio

The water-to-binder ratio (w/b) is an important factor that affects the final mechanical properties of the cementitious composite. Lower w/b typically results in higher strength, but there are thresholds for high and low w/b defined based on the properties of the constituents in a mixture. In other words, decreasing the w/b will only increase strength to a certain point. After this point, further decreasing w/b will decrease the strength because there is not enough water to hydrate all the cementitious materials and be available for later pozzolanic reactions. Additionally, low w/b will decrease the workability of a mixture and require more HRWR.

There are several different ways to measure the proportion of water in a concrete mixture. The water-to-cement ratio (w/c) is the weight of the total water in the mixture divided by the weight of cement, as shown in Equation 3-1. The w/c was initially used for conventional concrete with one single cementitious material as the binder.

Since the water in a mixture is also used to hydrate some SCMs or in the pozzolanic reaction for others (depending on SCM composition), the w/b became became more representative of the proportion of water in a concrete mixture. The w/b may also be written the water-to-cementitious material ratio (w/cm). The w/b is defined as the weight of the free water (including the natural moisture in aggregates) divided by the weight of all cementitious material [83], as shown in Equation 3-2.

For concrete mixtures with low w/b like UHPC, the water contained in the added chemical admixtures will influence the hydration and mechanical properties of the mixture [46]. The most accurate way to calculate the total water in a mixture includes all water components,

including free water, moisture from aggregates, and the water content of chemical admixtures. This modified water-to-binder ratio (w^*/b) can be found as shown in Equation 3-3. Most past researchers have not considered the water content from the chemical admixtures when finding w/b.

Water-to-cement:
$$w/c = \frac{(W_1 + W_2)}{C_1}$$
Equation 3-1

Water-to-binder:
$$w/b = \frac{(W_1 + W_2)}{(C_1 + C_2)}$$
Equation 3-2

Modified water-to-binder:
$$w^*/b = \frac{(W_1 + W_2 + W_3)}{(C_1 + C_2)}$$
Equation 3-3

where:

W_1 =   weight of free water

W_2 =   weight of water available as moisture content in aggregates

W_3 =   weight of liquid portion of chemical admixtures (defined by manufacturer)

C_1 =   weight of cement

C_2 =   weight of SCMs

All three equations were used to report results in this research to make them more comparable with previous studies.

3.6. Previous Efforts on Developing Non-Proprietary UHPC Mixture.

There have been several previous research efforts for developing non-proprietary UHPC mixture made with locally-produced raw available materials in different regions of the U.S.

Most of the studies satisfied the typical minimum requirements for UHPC mixtures and in some cases ended up with much higher mechanical properties [4], [45], [72], [75], [78]–[81], [96]. A summary of previous studies on non-proprietary UHPC mixtures is shown in Table 3-6.

Table 3-6: Previous research projects for developing non-proprietary UHPC mixes.

Researcher	Year	Location	Selected-UHPC Mix Parameters						Performance	
			C: SF: SCM	Other SCMs Used	w/c	w/b	Agg.:b	Fiber vol. fraction (%)	Flow (in.)	f'$_c$ (ksi)
Tadros et al.[1]	2020	A	1.0: 0.25: 0.00	-	0.25	0.200	0.88	0 and 2	8-11	25.0
		B	1.0: 0.25: 0.11	LP	0.25	0.184	1.10	0 and 2	8.9, 9.2	23.4
		C	1.0: 0.25: 0.00	-	0.24	0.195	0.77	0 and 2	9.1	23.1
		D	1.0: 0.20: 0.18	LP	0.29	0.202	0.77	0 and 2	9.1	21.4
		E	1.0: 0.25: 0.00	-	0.23	0.188	1.10	0 and 2	8.9	23.6
Lawler et al.	2019	FL	1.0: 0.15: 0.15	FA (Class F)	0.23	0.170	1:0 to 2:0	1.5 and 2	8-10	18-19
Karim et al.[2]	2019	Iowa	1.0: 0.07: 0.00	-	0.20, 0.25	0.18, 0.2, 0.23	1.12, 1.3	2	8-9	10-17
Matos et al.	2019	Portugal	1.0: 0.54: 0.27	-	0.40	-	1.0	3	11.2-12.2	21-22
Looney et al.	2019	OK	1.0: 0.17: 0.50	S	0.18 to 0.22	0.18 to 0.23	0.75, 1.0	1 and 2	9-11	16-18.2
Berry et al.	2017	Montana	SF/FA = 0.75	FA	0.24	-	1.4 [3]	0 and 2	8-11	20-21
El-Tawil et al.	2016	Michigan	1.0: 0.25: 1.0	S	0.22	0.18	1.0	1.5	-	20.9-28.3
Graybeal	2013	WA, OR, ND, SD, NY, PA	1.0: 0.25: 0.25	FA	0.22 to 0.24	0.15 to 0.16	1.0	1 and 2	10.4-12.4	22.5-29
Tafraoui et al.	2009	France	1.0: 0.25: 0.25	Metakaolin	0.27	0.22	0.9, 1.18	0 and 2	-	15-27.5

c = cement; b = all cementitious materials; FA=fly ash; LP=limestone powder; S=slag or GGBS

[1]liquid portion of chemical admixtures was included in w:c and w:b calculations ,[2]compressive strength was measured at 7 days,[3] this is sand to cement ratio

3.7. Available Constituent Materials

The materials selected for this research were chosen based on their local availability in South Florida. Three different cement types (Masonry, Type I-II and Type III), slag, fine aggregates and UFR were produced locally; other material were purchased from local vendors while the source of material was not from Florida.

Five different types of cement and five different types of fibers were studied in this research. The amounts of the other SCMs, fine aggregate, and chemical admixtures were varied but the type was the same in all mixtures in this research. The material details, supplier information, and abbreviations used throughout this report are summarized in Table 3-7.

Table 3-7: Material detail, suppliers, and abbreviations

Material	Details	Sign	Supplier
Fibers	Dramix 4D 65/35BG	A	Bekaert
	Helix 5-13	H	HELIX
	Dramix OL 13/.20	OL	Bekaert
	Hiper Fiber	HF	Hiper Fiber
	STRUX® 90/40	Sy	GCP Applied Technology
Cement	Type M- Masonry Cement	C-M	Titan America
	Type I-II	C-T-I/II	
	Type III	C-T-III	
	Type I-II	C-A-I/II	Ash Grove
	Type I	C-W-I	Lehigh White Cement
Ground-Granulated Blast-Furnace Slag (GGBFS)	-	S	ARGOS USA Cement
Silica Fume	Master Life® SF 10	SF	BASF
Sand	Fine Masonry	FA	Titan America
UFR	-	UFR	Titan America
HRWR	Glenium 7920	HRWR	BASF
VMA	VMA 358	VMA	BASF

3.8. Base Mixture

The base mixture for this research was given by the lead university for the overall project, the University of Oklahoma (OU), and based on work done by Looney et al. [82]. The mixture design is shown in Table 3-8.

Table 3-8: Non-proprietary UHPC mix design initially proposed by OU

Type	Quantity
Type I Cement, lb/yd^3	1179.6
Slag, lb/yd^3	589.8
Silica Fume, lb/yd^3	196.6
w/b	0.20
Fine Masonry Sand, lb/yd^3	1966
Steel Fibers, lb/yd^3	255.2
Steel Fibers, %	2.0
Glenium 7920, oz./cwt	15.77

This mixture design was used as a starting point in this research and was modified to determine the effects of different materials and quantities on the mechanical properties.

UHPC Standard Tests

Most tests for conventional concrete can be used as is or with slight modifications for evaluating the performance of UHPC material. There are some additional tests that should be used to properly test the enhanced properties of UHPC. A summary of some of the most important tests used previously by other researchers that will be used in this study is shown in Table 3-9.

Table 3-9: Conducted tests for qualified UHPC mixtures [51], [97]–[104]

Property	Test Method	Specimen Geometry	Age for Testing (# specimens to test)
Flowability	ASTM C1437 ASTM C230	n/a	tested during casting
Compressive Strength	ASTM C39 ASTM C1856	3"x6" cylinders	3 days (3), 28 days (3)
Modulus of Elasticity	ASTM C469 ASTM C1856	3"x6" cylinders	28 days (3)
Splitting Tensile Strength	ASTM C496	3"x6" cylinders	28 days (3)
Flexural Strength	ASTM C78	3"x3"x11" prisms	28 days (3)
Total and Drying Shrinkage	Embedded VWGs ASTM C157	6"x12" cylinders	Begin measuring after casting (3)
Set Time	ASTM C403	6"x6" cylinder	at time of casting (3)
Bulk Resistivity Test	ASTM C1760	4"x8" cylinders	3,7,14,28,56 and 90 days (4)

More details on these tests will be provided in the following chapters when discussing experimental procedures.

3.9. Mixture Optimization

3.9.1. Particle Packing Theory

There are two dependent approaches for optimizing cementitious materials. The first approach, known as particle packing theory, is related to the physical characteristics of constituents and their proportions in the final mix. The second approach relates to the chemical composition of the constituents and the reaction between components; this approach focuses on choosing appropriate SCMs to expedite and improve cement hydration. This chapter will focus on particle packing theory and its application to this research.

Different models can be used for the particle packing of UHPC. The most-used particle

packing model was originally developed by Andreasen and Andreasen [105]. The model

provides an equation that represents the optimal partical size distribution based on the

physical characteristics of the constituents; the density and strength of a mixture will

theoretically be higher the closer the actual particle size distribution curve is the the optimal

curve. Andreasen and Andreasen's model was modified by Funk and Dinger [106] to

account for the smallest particle size; this model is shown in Equation 3-4.

$$D(P) = \frac{D^q - D^q_{min}}{D^q_{max} - D^q_{min}} \qquad \text{Equation 3-4}$$

where:

$D(P)$ =   percent passing for each diameter evaluated

D =   particle diameter being evaluated

D_{min} =   smallest particle diameter used in the mix design

D_{max} =   largest particle size used in the mix design

q =   distribution modulus

The distribution modulus (q) defines the coarseness of the final mixture: q closer to 1.0

produces a more coarsely graded mixture, while q closer to 0 produces a more finely graded

mixture. Typical q values used for UHPC mixtures are in the range of 0.19 to 0.37 [46],

[72], [74], [107].

Many previous studies have used the particle packing theory and tried to best match actual

particle size distributions to the optimal curves from Andreasen and Andreasen [105] and

Funk and Dinger [106]. A recent study by Tadros et al. [46] used particle packing optimization in five different locations across the U.S. to develop five different UHPC mixtures with 28-day compressive strengths greater than 22 ksi. Particle packing optimization has also been used to create sustainable concrete mixtures with reduced portland cement contents (50 percent reduction) while keeping similar mechanical properties [108]. It has also been used for developing special concretes like self-compacting concrete (SCC), high-performance concrete (HPC), recycled aggregate concrete, and 3D printable concretes [109]–[111].

3.9.2. Particle Packing Analysis

The first step in the particle packing optimization process is to determine the particle size distribution curves for each of the possible constituent materials. Samples of the different constituent materials were obtained from each of the producers for characterization and review.

Dry constituents in UHPC are very fine, so their full particle size distributions cannot typically be determined using a physical sieving process. Commercial laser diffraction devices can be used to determine the particle size distributions for very fine particles (4.0 x 10^{-6} in. to 4.0 x 10^{-2} in. [0.1 µm to 1000 µm]). The particle size distributions of the powder materials were determined by laser particle size analysis using a Malvern Mastersizer 2000 by Titan America in Miami.

The particle size distributions for the primary dry materials used in this study are shown in Figure 3.7 (a). The size of the smallest and largest particles is also determined using the laser particle size analysis. The largest particle size in this study was 2.0 x 10^{-5} in. (500

µm), measured in the fine sand aggregates. The smallest particle diameter was around 3.9

x 10^{-8} in. (1 µm), measured from the silica fume. The silica fume used in the testing was

coarser than expected, so the particle size analysis was performed on different samples to

verify the results. The silica fume contained some larger particles (by observation) than

would typically be expected from silica fume. The ideal curves found using Equation 3-4

with the measured minimum and maximum particle size is shown in Figure 3.7(b) for

different values for the distribution modulus (q). A distribution modulus q of 0.25 was

considered for the particle packing analysis in this study, based on previous researchers

[46], [74], [82].
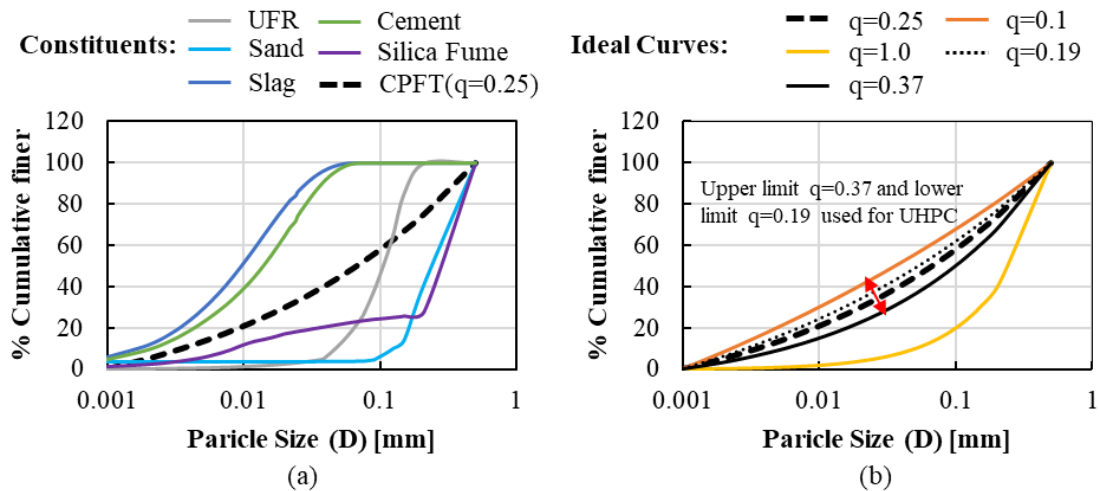
Figure 3.7: Particle packing analysis: (a) distribution curves of different constituents and (b) effect of varying "q" parameter in Modified Andreasen and Andersen model with D_{max} = 0.5 mm and D_{min} = 0.001 mm.

3.9.3. Qualified UHPC Mixtures

A spreadsheet tool was developed to evaluate different proportions of the constituent

materials and the resulting particle size distribution curves. The proportions of the

constituent materials were generally kept within the ranges typically used for UHPC

mixtures. Several different aggregate-to-cementitious material ratios (agg/cm) were investigated, including 0.8, 0.9, 1.0, 1.1, and 1.2. The trial-and-error process revealed an optimum agg/cm of 1.0. Several different proportions of cementitious materials were investigated to reveal the optimal cement to slag to silica fume ratio of 0.6 to 0.3 to 0.1.

Using agg/cm equal to 1.0 and the proportions of cementitious materials kept at 0.6:0.3:0.1, several mixture designs were evaluated with different proportions of aggregates. Five of these iterations with different proportions of sand and UFR are shown next to the optimal particle size distribution curve (with $q = 0.25$) in Figure 3.8. The closer the particle size distribution curve is to the optimal curve, the better the particle packing density for the mixture.
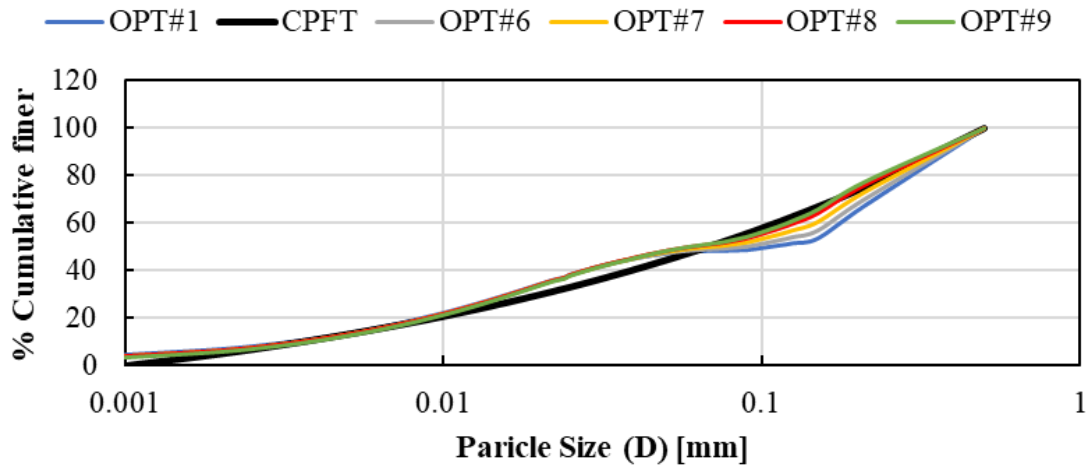
Figure 3.8: Particle size distributions for five mix design and the optimal particle size distribution curve with q = 0.25

A summary of the proportions of the constituent materials in these five mixtures developed based on the particle packing analysis is provided in Table 3-10. An ideal cement to the slag to silica fume ratio (0.6:0.3:0.1) was determined based on this analysis, OPT#1.

Modifying the sand to UFR ratio was found to improve the particle packing in the range where there was the largest difference between the mixture curves and idealized curves; four mixtures with UFR were designed as comparisons OPT#6 through OPT#9.

Table 3-10: Proportions of the initially qualified mixes

Mixes	Agg./C	Cement %	Slag %	Silica Fume %	Sand %	UFR %
		Cementitious Materials			Aggregate	
OPT#1	1.0	0.6	0.3	0.1	1.00	0.00
OPT#6	1.0	0.6	0.3	0.1	0.90	0.10
OPT#7	1.0	0.6	0.3	0.1	0.80	0.20
OPT#8	1.0	0.6	0.3	0.1	0.70	0.30
OPT#9	1.0	0.6	0.3	0.1	0.65	0.35

These proportions were used as the starting point for the experimental work.

Chapter 4: **Experimental Study on Non-Proprietary UHPC**

4.1. Small Scale batches

4.1.1. Introduction

For more efficient use of material, two different experimental steps were defined for developing the UHPC mixtures. The first series of experimental testing was conducted as a trial-and-error process using 0.15 ft^3 mixtures (small-scale batches) using only compressive strength and flow table testing. A total of 115 0.15-ft^3 batches and 690 3-in. by 6-in. cylinders were cast during this portion of the experimental program. Several of these mixtures were then selected for casting of larger volume mixtures (2.2 ft^3) for conducting a larger range of experimental tests.

Variables investigated in the small-scale batches included water-to-binder ratio (w/b), cement type, proportions of cementitious materials, aggregate type and proportions, aggregate preparation (wet versus dry), fiber type and fiber content, HRWR dosage, VMA dosage, and mixing time and procedure. Mixtures were developed in the small-scale batches with compressive strengths greater than 18 ksi and flowability between 8 and 10 inches.

4.1.2. Determining Amount of Material for Mixtures

The base proportions of the constituent materials were determined based on the particle packing analysis described in Chapter 3. The actual amount of material to include in each 0.15 ft^3 mixture was determined by first determining the amount of material per cubic foot and then multiplying these amounts by 0.15 ft^3, which was the desired volume.

An example for determining the amount for a specific mix is provided below. Some of the information that is needed for the base mixture is shown in Table 4.1 for the proportions. The proportions of cement, slag, and silica fume are based on only the cementitious materials. The proportion of fine sand and UFR are based on only the fine aggregate. The aggregate to cementitious materials ratio was 1.0 for most of the mixtures that were investigated. The total units equal 2.0 based on 1.0 unit for cementitious materials and 1.0 unit for aggregates.

Table 4-1: Example information needed to determine materials for small-scale batch mixture

Constituent	Proportion	Variable
agg/cm	1.0	
Cement	0.6	P_c
Slag	0.3	P_s
Silica Fume	0.1	P_{sf}
Fine Sand	0.9	P_{sand}
UFR	0.1	P_{UFR}
Total Units	2.0	P_{tot}

Additional information is needed on the desired fiber content, fiber density, desired water-to-binder ratio (w/b), HRWR content, VMA content, and the estimated density of the UHPC mixture without fibers. Values for this example are shown in Table 4.2. These HRWR content is typical for some of the mixtures. The density is the measured density from one of the base mixtures.

Table 4-2: Additional information needed for example to determine materials for small-scale batch mixture

Property	Value	Variable
Fiber Content [%]	2.0	FC
Fiber Density [lb/ft^3]	490	ρ_f
Water-to-binder ratio	0.2	w/b
HRWR [oz./cwt]	27.5	V_{HRWR}
VMA [oz./cwt]	0.0	V_{VMA}
Estimated Density [lb/ft^3]	148.6	ρ_c

The information from Table 4.1 and Table 4.2 can be used to determine the amount of material required per cubic foot of material. The amount of cement, slag, and silica fume can be found using Equation 4-1, Equation 4-2, and Equation 4-3, respectively. An example is provided for determining the amount of cement, slag, and silica fume in the example mixture.

Cement (lb/ft^3):
$$W_c = \frac{\rho_c P_c (1 - FC)}{P_{tot}}$$
Equation 4-1

$$W_c = \frac{\left(148.6 \; {}^{lb}/_{ft^3}\right)(0.6)(1 - 0.02)}{2.0}$$

$$= 43.7 \; {}^{lb}/_{ft^3}$$

Slag (lb/ft^3):
$$W_s = \frac{\rho_c P_s (1 - FC)}{P_{tot}}$$
Equation 4-2

$$W_s = \frac{\left(148.6 \ ^{lb}/_{ft^3}\right)(0.3)(1 - 0.02)}{2.0}$$

$$= 21.8 \ ^{lb}/_{ft^3}$$

Silica Fume (lb/ft³):

$$W_{sf} = \frac{\rho_c P_{sf}(1 - FC)}{P_{tot}}$$

Equation 4-3

$$W_{sf} = \frac{\left(148.6 \ ^{lb}/_{ft^3}\right)(0.1)(1 - 0.02)}{2.0}$$

$$= 7.3 \ ^{lb}/_{ft^3}$$

The amount of water can be found by summing the weight of the cementitious materials and multiplying by w/b, as shown in Equation 4-4. The weight of water per cubic foot for the example is also shown.

Water (lb/ft³):

$$W_w = \left(W_c + W_s + W_{sf}\right)\left(^w/_b\right)$$

Equation 4-4

$$W_w = \left(43.7 \ ^{lb}/_{ft^3} + 21.8 \ ^{lb}/_{ft^3} + 7.3 \ ^{lb}/_{ft^3}\right)(0.2) = 14.6 \ ^{lb}/_{ft^3}$$

The amount of fine sand and UFR can be found using a similar procedure as the cementitious materials, as shown in Equation 4-5 and Equation 4-6.

Fine Sand (lb/ft³):

$$W_{sand} = \frac{\rho_c P_{sand}(1 - FC)}{P_{tot}}$$

Equation 4-5

UFR (lb/ft³):

$$W_{UFR} = \frac{\rho_c P_{UFR}(1 - FC)}{P_{tot}}$$

Equation 4-6

The weight of fibers to include can be found just by taking the fiber density (ρ_f) times the fiber content (FC) as shown in Equation 4-7. The weight of the steel fibers for the example mixture are also shown below.

Steel Fibers (lb/ft³):

$$W_{fibers} = \rho_f(FC)$$

Equation 4-7

$$W_{fibers} = \left(490 \ ^{lb}/_{ft^3}\right)(0.02) = 9.8 \ ^{lb}/_{ft^3}$$

The amount of HRWR and VMA can be determined using Equation 4-8 and Equation 4-9. The amount of HRWR per cubic foot for the example is also shown.

HRWR (oz/ft³):

$$V_{HRWR} = v_{HRWR} \frac{(W_c + W_s + W_{sf})}{100}$$

Equation 4-8

$$W_w = \left(27.5 \ ^{oz}/_{cwt}\right)\left(43.7 \ ^{lb}/_{ft^3} + 21.8 \ ^{lb}/_{ft^3} + 7.3 \ ^{lb}/_{ft^3}\right)/100$$

$$= 20.0 \ ^{oz}/_{ft^3}$$

VMA (oz/ft³):

$$V_{VMA} = v_{VMA} \frac{(W_c + W_s + W_{sf})}{100}$$

Equation 4-9

The amount of all the different constituents in the example mixture is shown in Table 4.3. Amounts are shown per cubic foot and per 0.15 cubic foot, which was the size of the small-scale batch mixtures.

Table 4-3: Amount of materials per 1 ft³ and 0.15 ft³ for example mixture

Constituent	Amount per ft^3	Amount per 0.15ft^3
Cement [lb]	43.7	6.6
Slag [lb]	21.8	3.3
Silica Fume [lb]	7.3	1.1
Water [lb]	14.6	2.2
Fine Sand [lb]	65.5	9.8
UFR [lb]	7.3	1.1
Steel Fibers [lb]	9.8	1.5
HRWR [oz]	20.0	3.0
VMA [oz]	0.0	0.0

This procedure was performed to find the amount of material to use for each of the mixtures. A similar procedure was also used for the large-scale batches (2.2 ft^3).

4.1.3. Mixing Procedure

Due to the low w/b and the small particle size of UHPC, relatively higher mixing energy is required to complete the wetting process compared to conventional concrete. A 1.5-HP planetary mixer with 0.2 ft^3 capacity was used to make 0.15 ft^3 trial mixtures; the mixer was found to exert a sufficient amount of mixing energy.

The mixing process included two 10-minutes phases. The first 10-minute mixing phase involved mixing all the dry components (other than the fibers), and the second 10-minute mixing phase involved the addition of the liquid components (water and chemical admixtures) and the steel fibers.

The mixing procedure for the small-scale batches is shown in Figure 4.1. All constituents were premeasured in cylinder molds and graduated cylinders before the beginning of the

mixing procedure, shown in Figure 4.1 (a) and (c). The sand, cement, slag, silica fume, and UFR were all added to the mixer and mixed on low speed for 10 minutes, as shown in Figure 4.1 (b). A plastic sheet was wrapped around the mixer at this time to try and keep all the dry materials and dust in the mixer during this phase.

For the second 10-minute mixing phase, half of the HRWR was added to the required water, as shown in Figure 4.1 (d), and poured into the mixer over 2 minutes, as shown in Figure 4.1 (e). The remainder of the HRWR was then added to the mixture and left to mix until the powder material became a flowable paste, which typically took 6 to 11 minutes of additional mixing time. Once the UHPC paste was produced, the fibers were added to the mixture and allowed to mix for an additional 2 minutes, as shown in Figure 4.1 (f). The transition from a powder to a fluid takes additional time depending on the water-to-cementitious ratio and the HRWR dosage. The average total mixing time varied between 20 to 25 minutes.

Due to the very low water to binder ratio and very fine particles, UHPC is very sensitive to moisture. To avoid any variability in results, the required aggregates (fine sand and UFR) for most of the mixtures were oven-dried and stored in sealed containers to reach room temperature 24 hours before mixing. There were a few mixtures where the aggregates were not oven-dried before mixing. Not oven drying the materials led to increased variability in test results. For field cast applications, it is probably not practical to use oven-dried material. The moisture content of aggregates should be measured and monitored continuously before the mixing process.
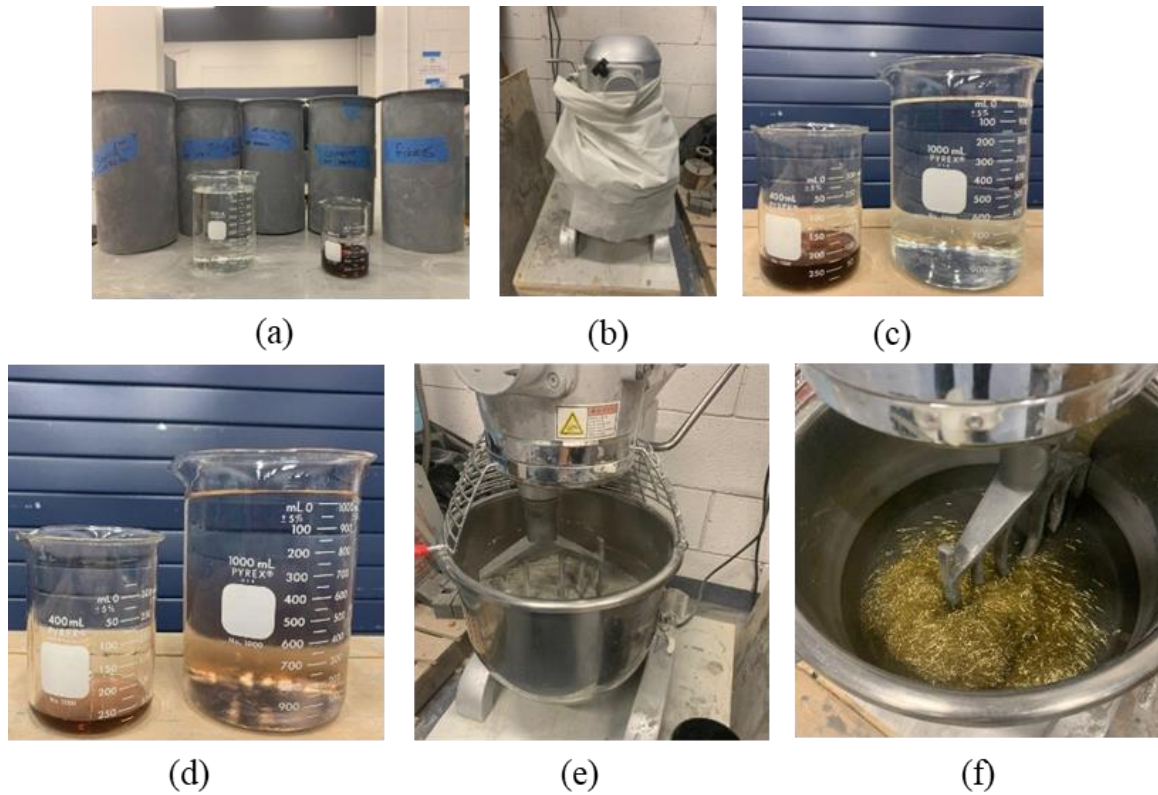
Figure 4.1: General Mixing procedure (a) weighted material, (b) dry mixing, (c) weighted water and HRWR, (d) blending half of HRWR with required water, (e) second 10 minutes of mixing with water and HRWR, and (f) adding fibers.

4.1.4. Initial Evaluation of Small-Scale Batches

The small-scale batches were evaluated based on their rheology, flowability, and compressive strength. The target compressive strength was 18 ksi at 28 days and target flowability of the fresh UHPC between 9 and 11 inches. The general working time and fiber segregation were also observed during the mixing and placing process. Each 0.15 ft^3 batch of UHPC was enough to conduct the flow table test and fill six 3 by 6-inch cylinder samples. Two-cylinder samples were tested to measure the compressive strength at 3, 7, and 28 days. The general procedure for mixture optimization is shown in Figure 4.3.
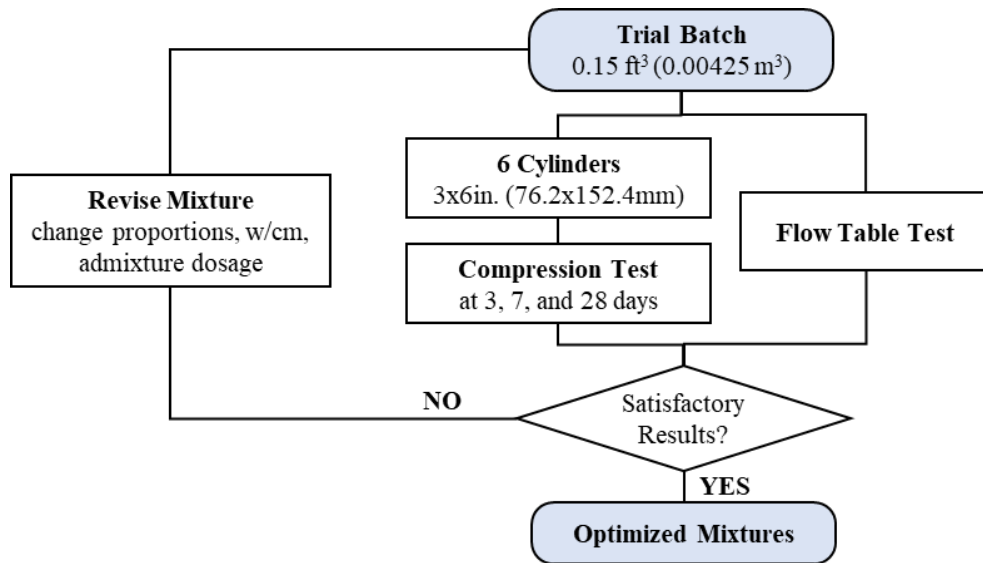
Figure 4.2: Mixture optimization process

4.1.5. Preparation and Initial Tests

Flow table tests were used to measure the flowability of the mixture and highlight any fiber segregation issues in the mixture. The UHPC was then placed into six 3 by 6-inch plastic single-use cylinder molds. After labeling and cleaning the concrete leftovers from external parts of mold, they were capped and stored in a temperature-controlled room until the test dates.

4.1.5.1. Flow Table Test Procedure

The flowability of UHPC mixtures was determined using flow table test for cement mortar in the static mode according to ASTM C230/C230M (Standard Specification for Flow Table for Use in Tests of Hydraulic Cement) [51], [104]. The spread cone, shown in Figure 4.3 (a), was filled immediately after the mixing process was finished and then slowly lifted for measuring the spreading flow. The material on the base plate was allowed to spread for 60 seconds, and then the diameter of the spread was measured in two directions. The

minimum and maximum diameters were measured, as shown in Figure 4.3 (b) and (c), and the flow for a mix was taken as the average of the two readings.
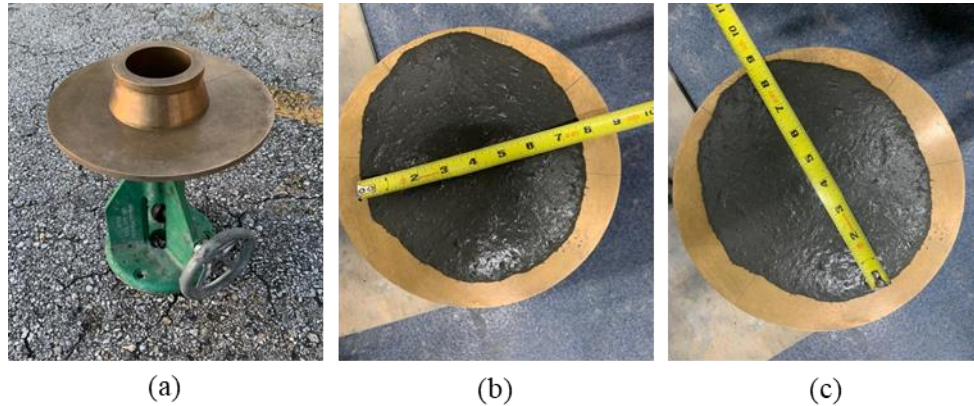
Figure 4.3: Flowability Test; (a) Flow table apparatus (b) minimum spread measurement and (c) maximum spread measurement

The flow table test was also used to determine if there were any issues with fiber distribution and fiber segregation in a mixture. Poor fiber distribution was observed in two different ways: (1) if there were not many fibers in the UHPC taken from the mixer for the flow table test, as shown in Figure 4.4 (a), and (2) if all the fibers clumped together in the middle of the spread, as shown in Figure 4.4 (b). Poor fiber distribution in the flow table test correlated well with poor fiber distribution in the overall mixture.

Figure 4.4: Photographs of two flow table tests performed on C6 with poor fiber distribution, (a) without many fibers and (b) with all fibers clumped in middle of test

4.1.5.2. Compressive Test Procedure

The compressive test was conducted in accordance with ASTM C39 (Compressive Strength of Cylindrical Concrete Specimens) and ASTM C1856 (Standard Practice for Fabricating and Testing Specimens of Ultra-High Performance Concrete) [51], [98]. All cylinder samples were capped, stored in a temperature-controlled room, and demolded 24 hours before the test. No special curing methods were used in the small-scale batch study. The surface of the cylinders after demolding is shown in Figure 4.5 (a). After demolding and before compressive tests, all samples were ground on both ends using an automatic cylinder end grinder machine, shown in Figure 4.5 (b), to satisfy the planeness required by ASTM C39 and ASTM C1856. A sample cylinder after the grinding process was completed is shown in Figure 4.5 (c). The volume and mass measurements were then taken, and all information was recorded (hand-written) in developed testing sheets. The cylinders were then placed in the compressive test machine, Figure 4.5 (d) and tested to failure using the appropriate loading rate from ASTM C39 and ASTM C1856. A cylinder after failure is shown in Figure 4.5 (e). Photographs were taken of all cylinders before and after failure.

The failure load and failure mode were documented on the testing sheets. After testing, the data for all cylinders was input into spreadsheets developed to collect the test data. The compressive strength for each cylinder was calculated in these spreadsheets using all the input data.

| (a) | (b) | (c) | (d) | (e) |
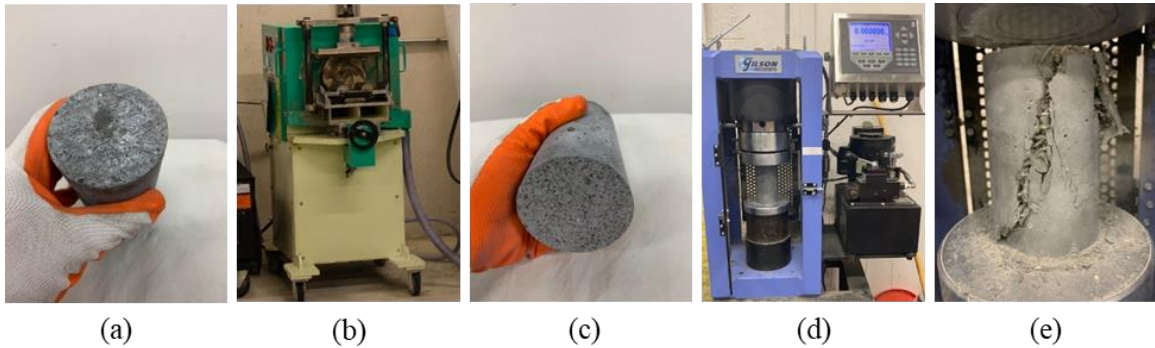
Figure 4.5: Compression testing procedure, (a) demolded sample, (b) grinding machine used to smooth each end of the cylinders, (c) sample after cylinder grinding, (d) compressive test machine with cylinder installed, and (d) diagonal break pattern of cylinder

4.1.6. Experimental Results for Small-Scale Batches

Four different series of small-scale tests were cast to study the effect of the different variables discussed above. An overview of the four different series of small-scale batches is shown in Table 4.4. All detailed large-scale experimental results are provided in0.

Table 4-4: Series OU, A, and B with aggregates in natural moisture

Series	n_mixes	Cement type	Initial goal	M.S
OU	7	C-M	Effect of C-M	N
A	10	C-T-I/II	Finding proper amount of water and HRWR dosage	N
B	20	C-T-I/II	Optimum SCM proportions	N
C	53	All cement types	Find the qualified mixtures	D

M.C: Moisture Condition: D = oven-dried; N = natural moisture

Only the results from some of the mixtures are presented in this section. The results are organized by the influence of different variables:

- Sand moisture and water content

- Cement type

- Water-to-binder ratio (w/b)

- HRWR content

- VMA content

- Effect of fiber type and content

- Effect of fine aggregate type and content

All results related to small-scale trial batches and developed spreadsheet for particle packing analysis are provided inAppendix B.

4.1.6.1. Fine Aggregate Moisture

Three different series of small-scale mixtures were cast using aggregate that was not oven dried. The aggregate for these mixtures was stored outside and moved inside 2 days before casting. There was a large variation in the results when the aggregate was not oven dried. A sample of some of similar mixtures with w/b of 0.18 and 0.20 with aggregate that was

not oven dried is shown in Table 4.5. The three mixtures with similar w/b ratios had the same mixture proportions, same mixing procedures, and similar HRWR contents.

Table 4-5: Mixture proportions and characteristics for investigation of variation in results due to moist fine aggregate

| Mix. | Cement Type | w/b | Mix Proportions | | | | | | Fiber | | Admixtures | | Density (lb/ft^3) | S.M |
			agg/cm	C	S	SF	FA	UFR	Type	Content (%)	HRWR (oz./cwt)	VMA (oz./cwt)		
B11	Titan Type I/II	0.18	1.0	0.6	0.3	0.1	1.0	0.0	-	0.0	23.81	0.00	146.10	N
B17	Titan Type I/II	0.18	1.0	0.6	0.3	0.1	1.0	0.0	-	0.0	23.81	0.00	146.40	N
B31	Titan Type I/II	0.18	1.0	0.6	0.3	0.1	1.0	0.0	-	0.0	23.81	0.00	144.90	N
B1	Titan Type I/II	0.20	1.0	0.6	0.3	0.1	1.0	0.0	-	0.0	15.75	0.00	138.60	N
B23	Titan Type I/II	0.20	1.0	0.6	0.3	0.1	1.0	0.0	-	0.0	23.81	0.00	146.00	N
B24	Titan Type I/II	0.20	1.0	0.6	0.3	0.1	1.0	0.0	-	0.0	21.97	0.00	145.80	N

S.M: Sand moisture condition

The compressive strength for these mixtures is shown in Figure 4.6. There is a large variation in the compressive strengths at different ages between the three mixtures in each w/b group. As an example, the coefficient of variation of the 28-day compressive strength between the three mixtures was 0.13 and 0.12 for w/b of 0.18 and 0.20, respectively. This is a larger coefficient of variation than was measured for similar mixtures with oven-dried aggregate.
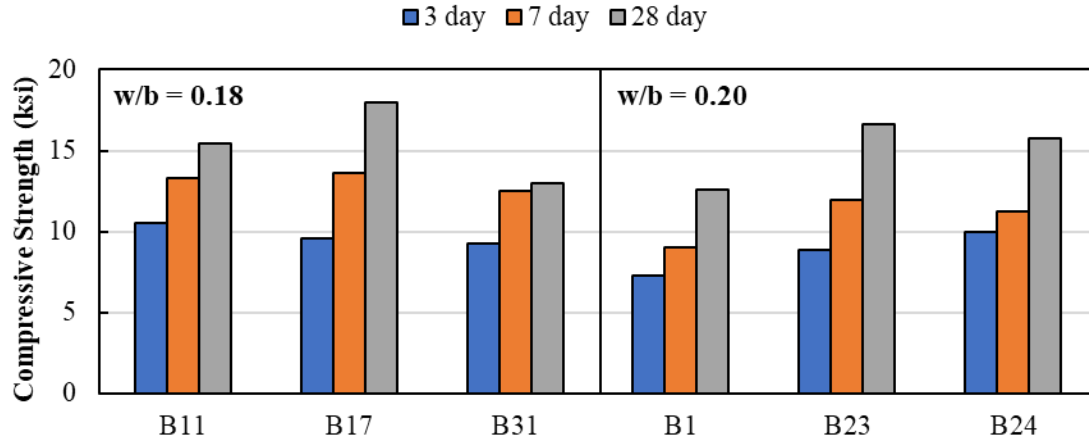
Figure 4.6: Effect of moisture content in aggregate on compressive strength

4.1.6.2. Cement Type

Five different cement types were used in this project to estimate their effect on the final properties of the UHPC. Five different mixes with the same mix proportions (OPT#1) were cast to determine the effect of cement on mixture properties. Details of each mix design are summarized in Table 4.6.

Table 4-6: Mixture proportions and characteristics for investigation of cement type

Mix.	Cement Type	w/b	Mix Proportions						Fiber		Admixtures		Density (lb/ft³)	S.M
			agg/cm	C	S	SF	FA	UFR	Type	Content (%)	HRWR (oz./cwt)	VMA (oz./cwt)		
OU2	Masonry Cement	0.20	1.0	0.6	0.3	0.1	1.0	0	A	2.0	15.77	0	135.7	N
C3	Ash Grove Type I-II	0.20	1.0	0.6	0.3	0.1	1.0	0	OL	2.0	22.25	0	149.0	D
C32	Titan Type I/II	0.20	1.0	0.6	0.3	0.1	1.0	0	OL	2.0	27.47	6.5	146.9	D
C37	Titan Type III	0.20	1.0	0.6	0.3	0.1	1.0	0	OL	2.0	27.47	0	149.0	D
C4	Lehigh White Cement	0.20	1.0	0.6	0.3	0.1	1.0	0	OL	2.0	23.35	0	146.5	D

One of the mixtures (OU2) did not use oven-dried sand and used Dramix 4D 65/35BG fibers; the other four mixtures used oven-dried sand and Dramix OL 13/.20 fibers. Flowability and compressive strengths are shown in Figure 4.7.

Specimens with masonry cement had the lowest compressive strengths of the five different types of cement. The masonry cement led to an average 28-day compressive strength of

10.2 ksi and a density less than 140 lb/ft^3; this was likely due to the masonry cement's high air content. Samples made by masonry cement all had higher porosity and lower density than other samples made by other cement. Masonry cement is not recommended for UHPC mixtures.

The Type I/II cement and Lehigh White cement had similar performance with compressive strength around 14.5 ksi at 28 days. Lehigh White cement is usually available with premium cost compared to Type I/II cement.

Specimens with Type III cement had the highest compressive strengths of the group reaching an average compressive strength of 17.9 ksi at 28 days. Type III cement had good initial flowability, but had a noticeably shorter working time than UHPC made with the other types of cement. Considering the decreased working time for Type III cement, it was not used for the large-scale batches. The working time issue would need to be addressed before Type III cement is used in UHPC.
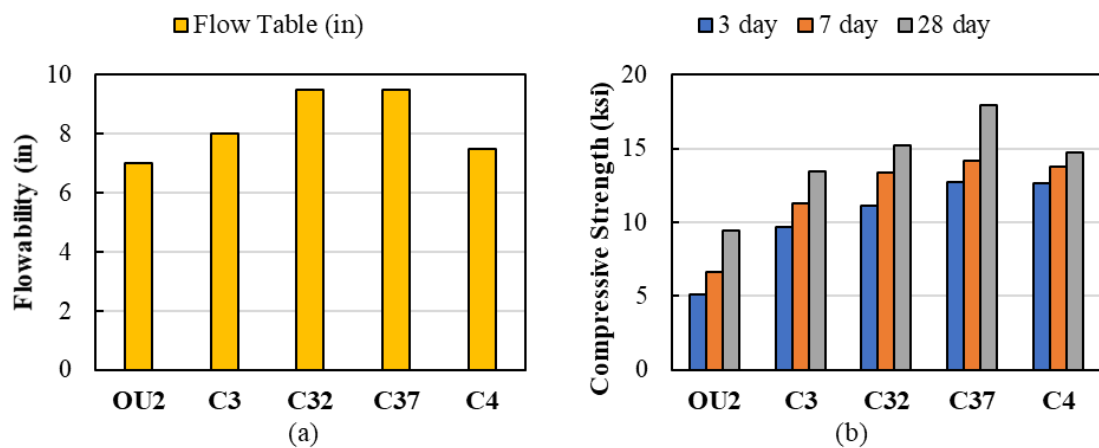
Figure 4.7: Effect of cement type on (a) flowability and (b) compressive strength

Type I/II cement was used for the majority of small-scale batches and all the large-scale batches due to its good performance, working time, and low cost.

4.1.6.3. Water-to-Binder Ratio

Water to binder ratio (w/b), discussed in §2.5, is one of the most important criteria determining the final mechanical properties of any cementitious material. Any cementitious mix needs enough water to hydrate the cementitious materials and be available for pozzolanic reactions, but excess water will lead to more pores and decreased strength. There is no exact w/b to guarantee the full hydration process, as it depends on cement fineness, the chemical composition of the clinker used, and grain size. Previous studies [112]–[114] reported numbers between 0.35 to 0.45 for full cement hydration for conventional concrete, but it differs for each mixture design and depends on the constituents used in the concrete matrix. To find the optimum w/b of the UHPC for this research, mixtures with w/b between 0.17 to 0.24 were tested, which coincides with typical w/b ratios for UHPC mixtures [3], [4], [115], [116].

Five mixtures used to compare the effect of the w/b are shown in Table 4.7. The HRWR content was increased for smaller w/b to keep a relatively consistent workability between the mixtures, although the flow still decreased with the w/b ratio even with the increased HRWR content, as shown in Figure 4.8 (a).

Table 4-7: Mixture proportions and characteristics for investigation of water to binder ratio (dried sand used in all mixtures)

Mix.	Cement Type	w/b	Mix Proportions						Fiber		Admixtures		Density (lb/ft³)
			agg/cm	C	S	SF	FA	UFR	Type	Content (%)	HRWR (oz./cwt)	VMA (oz./cwt)	
C17	Titan Type I/II	0.24	1.0	0.6	0.3	0.1	1.0	0	OL	2.0	16.39	2.47	142.8
C11	Titan Type I/II	0.22	1.0	0.6	0.3	0.1	1.0	0	OL	2.0	19.87	6.5	144.6
C32	Titan Type I/II	0.20	1.0	0.6	0.3	0.1	1.0	0	OL	2.0	27.47	6.5	146.9
C34	Titan Type I/II	0.18	1.0	0.6	0.3	0.1	1.0	0	OL	2.0	27.47	6.5	149.8
C26	Titan Type I/II	0.17	1.0	0.6	0.3	0.1	1.0	0	OL	2.0	35.52	0	150.0

The optimum w/b was found to be around 0.18 to 0.20, as shown in Figure 4.8. The compressive strength increased as the w/b decreased from 0.24 to 0.18. The compressive strength then decreased when the w/b was further reduced from 0.18 to 0.17. The w/b shown here do not include the water from the admixtures.
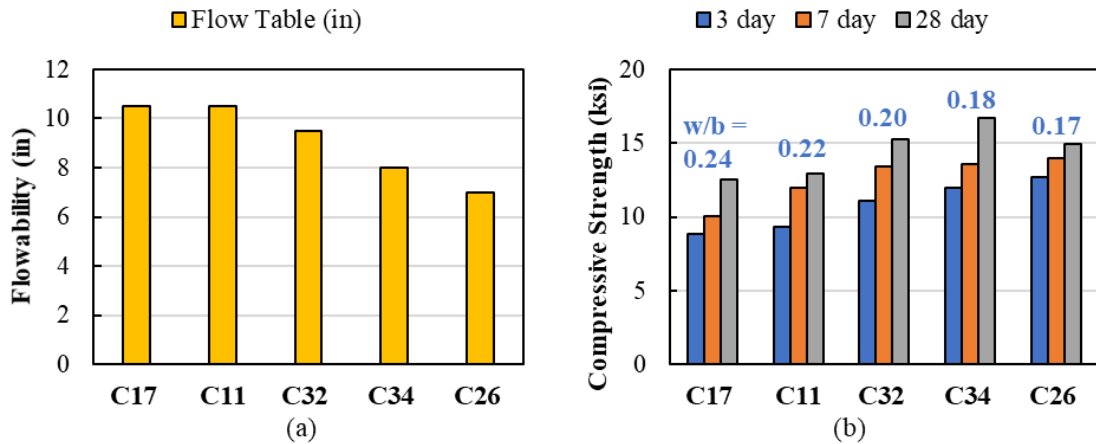
Figure 4.8: Effect of water-to-binder ratio on (a) flowability and (b) compressive strength

A w/b of 0.20 was used as the base value for the large-scale batches. One large-scale batch was cast with a w/b of 0.18.

4.1.6.4. HRWR Content

HRWR was used to provide workability and flowability of mixtures with low w/b. The base HRWR content was recommended by the University of Oklahoma (OU) as 18 oz/cwt.

This was used as the starting point and modified throughout the testing program to maintain a flow between 8 and 10 inches. Three mixtures that had similar mixture proportions with different HRWR contents are summarized in Table 4.8.

Table 4-8: Mixture proportions and characteristics for investigation of HRWR effect (dried sand used in all mixtures)

| Mix. | Cement Type | w/b | Mix Proportions | | | | | | Fiber | | Admixtures | | Density (lb/ft^3) |
			ag/cm	C	S	SF	FA	UFR	Type	Content (%)	HRWR (oz./cwt)	VMA (oz./cwt)	
C28	Titan Type I/II	0.20	1.0	0.6	0.3	0.1	1	0	OL	2.0	21.70	0	147.1
C2	Titan Type I/II	0.20	1.0	0.6	0.3	0.1	1	0	OL	2.0	22.25	0	144.5
C31	Titan Type I/II	0.20	1.0	0.6	0.3	0.1	1	0	OL	2.0	27.47	0	147.4

As expected, increasing the HRWR content increased the flow of the mixture, shown in Figure 4.9 (a). Increasing the HRWR content decreased the 28-day compressive strength for these three mixtures, as shown in Figure 4.9 (b). This was possibly due to the water content in the HRWR adding additional water to the mixture and thus increasing the w*/b, as described in §2.5. The water content of the chemical admixtures was not included in the w/b shown in Table 4.8. The water content of the chemical admixtures is typically neglected when determining the mixing water and w/b. The results from Figure 4.9 (b), showing increased HRWR decreasing the strength of the mixture, would support that the liquid part of chemical admixtures should be considered for calculation of w/b and the amount of mixing water to add to a mixture.

Due to its small flowability, the concrete for C28 needed to be actively compacted into the mold to ensure that no voids were present in the cylinder molds. In general, flowabilty below 8 inches required this active compaction, which is not practical for field applications.
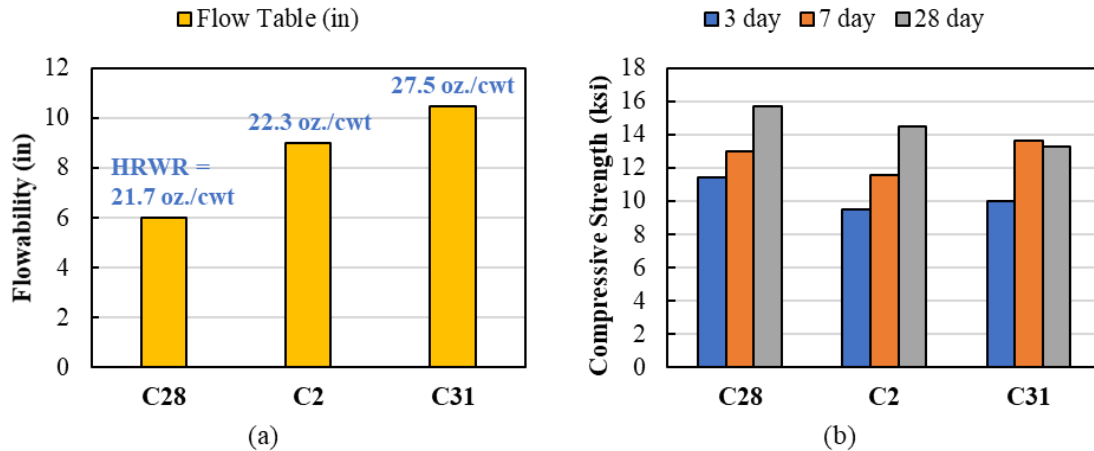
Figure 4.9: Effect of HRWR content on (a) flowability and (b) compressive strength

A HRWR content of 27.5 oz/cwt was used as the base amount for the large-scale batches to ensure sufficient workability to cast all the specimens.

4.1.6.5. VMA Content

Viscosity modifying admixture (VMA) is a water-soluble polymer that is used in concrete technology to modify the viscosity of mixing water and increase the ability of the cementitious paste to retain its constituents in suspension [95]. VMA is widely used for self-consolidating concrete (SCC) where the flowability exceeds 26 inches [95]. Its usage is not limited to SCC; VMA is also used for pumped concrete, under water concrete, lightweight concrete, sprayed concrete or shotcretes, and even for porous concrete [117].

VMA was used in this research to help prevent steel fiber segregation in the UHPC mixes, especially when heavier fibers or longer fibers were used. The effect of VMA was investigated on a fiber type that did not require VMA to stabilize the fiber in the mixture (Dramix OL 13/0.2); this allowed for a 0 oz/cwt to be compared to mixtures with VMA. The three mixture designs used to compare the effects of VMA are shown in Table 4.9.

The water content of the VMA was not considered in the w/b calculation due to its small

proportion compared to the total water.

Table 4-9: Mixture proportions and characteristics for investigation of VMA effect (dried sand used in all mixtures)

Mix.	Cement Type	w/b	Mix Proportions						Fiber		Admixtures		Density (lb/ft^3)
			ag/cm	C	S	SF	FA	UFR	Type	Content (%)	HRWR (oz./cwt)	VMA (oz./cwt)	
C28	Titan Type I/II	0.20	1.0	0.6	0.3	0.1	1.0	0	B	2.0	21.70	0	147.1
C16	Titan Type I/II	0.20	1.0	0.6	0.3	0.1	1.0	0	B	2.0	26.55	3.02	148.7
C29	Titan Type I/II	0.20	1.0	0.6	0.3	0.1	1.0	0	B	2.0	21.70	6.50	146.5

The flow and compressive strength for similar mixtures with different amounts of VMA

are shown in Figure 4.10. VMA increased the flow (comparing C28 and C29 with similar

HRWR contents); see Figure 4.10 (a). The VMA content did not change the compressive

strength of mixtures, as shown in Figure 4.10 (b).
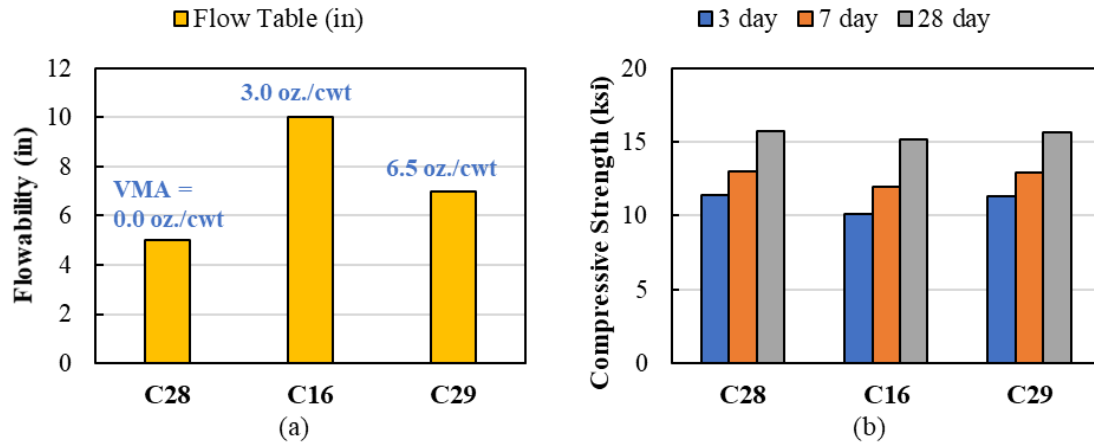
Figure 4.10:Effect of VMA content on (a) flowability and (b) compressive strength

VMA is not suggested to be used with the standard fiber types used for UHPC (i.e., 0.5-in.

length and 0.008-in. diameter), but it can be used to stabilize other kinds of fibers that may

tend to settle or clump together during the mixing procedure without affecting the strength

of the mixture. VMA was only used for the large-scale batch with Dramix 4D 65/35BG,

since these fibers are longer and heavier. Other large-scale batches did not include any VMA.

Four additional mixtures also were developed to determine the VMA influence on rheological properties and working time of the fresh UHPC. Details on these four mixtures are provided in Table 4.10.

Table 4-10: Mixture proportions and characteristics for investigation of working time (dried sand used in all mixtures)

Mix.	Cement Type	w/b	Mix Proportions						Fiber		Admixtures		Density (lb/ft^3)
			ag/cm	C	S	SF	FA	UFR	Type	Content (%)	HRWR (oz./cwt)	VMA (oz./cwt)	
C35	Titan Type I/II	0.20	1	0.60	0.3	0.1	1	0	B	2	27.47	0.00	150.5
C36	Titan Type I/II	0.20	1	0.60	0.3	0.1	1	0	B	2	27.47	6.50	150.2
C40	Titan Type I/II	0.17	1	0.6	0.3	0.1	1	0	B	2	29.39	0.00	156.5
C41	Titan Type I/II	0.17	1	0.60	0.3	0.1	1	0	B	2	29.39	9.16	151.6

The mixing procedure for these four mixtures was the same as the other mixtures. But plastic cylinders were cast in different time intervals after completing the mixing process. Two cylinders were cast at three different times after casting (6 cylinder samples for each mixture).

The flow was measured every 10 minutes for 30 to 70 minutes until the flow of the mixture dropped below 6 inches. The flow versus time for these four mixtures is shown in Figure 4.11. The mixture with a w/b of 0.20 had a higher flow over time with VMA than the same mixture without VMA, shown in Figure 4.11 (a). The VMA content did not affect the flow for the mixtures with a w/b of 0.17 and smaller initial flow, shown in Figure 4.11 (b).

All mixtures were slightly agitated by hand mixing at the end of the testing; in all cases, the hand mixing process increased the flow. This shows that UHPC can be agitated (by

hand or in a separate mixer) to increase the working time, which would be useful for field applications.
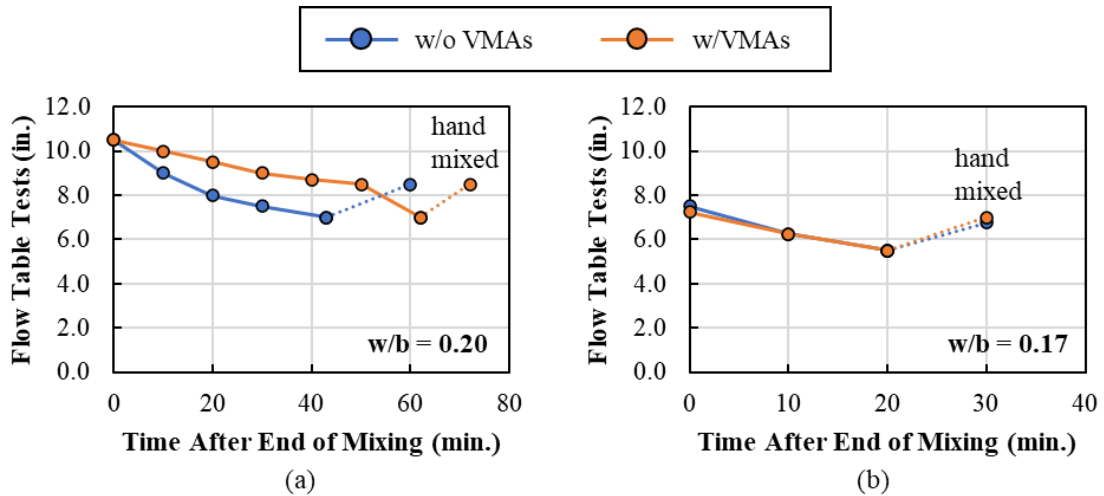
Figure 4.11: Flow versus time for mixtures with and without VMA and (a) w/b of 0.2 and (b) w/b of 0.17

There were only two samples cast for each time after mixing was complete for each w/b, so all the samples for each w/b were tested at the same age: 7 days for w/b of 0.20 and 28 days for w/b of 0.17. The compressive strength of the cylinders plotted versus the time they were cast after the end of the mixing is shown in Figure 4.12. There was a slight increase in compressive strength with time after casting for w/b of 0.20, see Figure 4.12 (a). There was no significant change in compressive strength with time after casting for w/b of 0.17. Similar compressive strengths were observed for specimens with and without VMA for both w/b ratios.
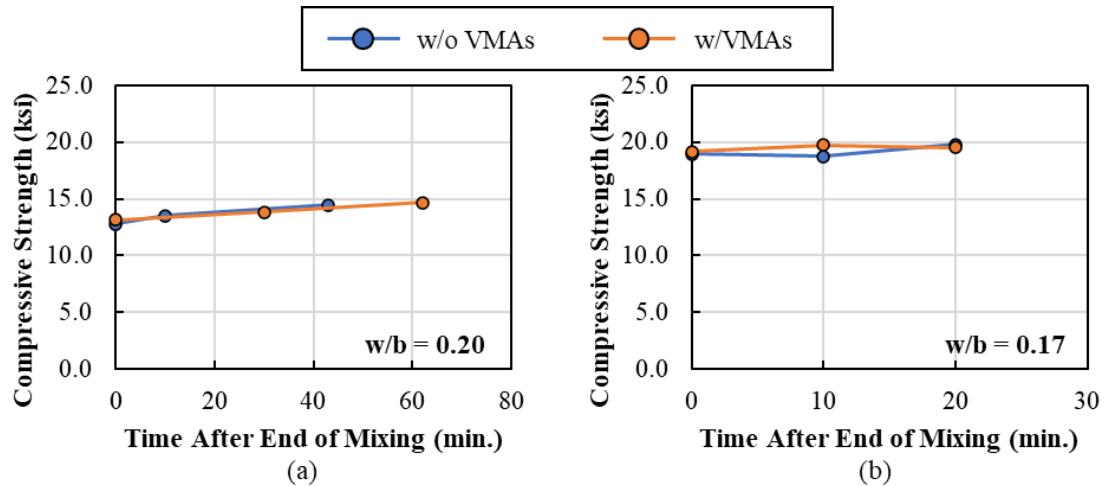
Figure 4.12: Compressive strength versus time after mixing for mixtures with and without VMA and (a) w/b of 0.2 (measured at 7 days) and (b) w/b of 0.17 (measured at 28 days)

4.1.6.6. Effect of Fiber Type

There are several studies that focused on the effect of different fiber contents ranging from 1 to 5 percent by volume [4], [72], [75], [79], [82]. The most common fiber content used by previous researchers and in field applications is 2 percent by volume. Mixtures with 0 percent fiber content and 2 percent fiber content were investigated in the small-scale batches. The results for 2 percent fibers by volume with different types of fibers are presented in this section.

Four different fiber types were investigated in the small-scale batch mixtures:

- Dramix 4D 65/35BG (A)

- Helix 5-13 Uncoated (H)

- Dramix OL 13/.20 (OL)

- Hiper Fiber Type A (HF)

See Table 2.5 for details on the fiber properties.

Details on the four mixtures used for this comparison are shown in Table 4.11. The base mix design (OPT#1) was used for the comparison. VMA was used in two mixtures containing Helix (H) fibers and Bekaert 4D 65/35BG (A) fibers to stabilize fibers. The recommended dosage by the manufacturer was 10 oz/cwt, but a smaller dosage was found to effectively prevent segregation. Bekaert 4D 65/35BG fibers were the heaviest and most challenging fiber to keep in suspension in the concrete mixture; their anchorage end shape and longer length led to them clumping together in several of the mixtures. The results provided in this section are for mixtures with good fiber distribution.

Table 4-11: Mixture proportions and characteristics for investigation of fiber type (dried sand used in all mixtures)

| Mix. | Cement Type | w/b | Mix Proportions | | | | | | Fiber | | Admixtures | | Density (lb/ft^3) |
			ag/cm	C	S	SF	FA	UFR	Type	Content (%)	HRWR (oz./cwt)	VMA (oz./cwt)	
C5	Titan Type I/II	0.20	1.0	0.60	0.3	0.1	1.0	0	H	2.0	24.72	6.41	146.2
C6	Titan Type I/II	0.20	1.0	0.60	0.3	0.1	1.0	0	A	2.0	24.72	8.24	146.4
C2	Titan Type I/II	0.20	1.0	0.60	0.3	0.1	1.0	0	OL	2.0	22.25	0	144.5
C42	Titan Type I/II	0.20	1.0	0.60	0.3	0.1	1.0	0	HF	2.0	27.47	0	148.6

The flowability and compressive strength for the four mixtures with different fiber types are shown in Figure 4.13. The fiber type did not have a significant effect on the flowability of the mixtures; flowability was kept between around 8 and 10 inches, shown in Figure 4.13 (a). The mixtures contained Hiper Fiber (HF in C42) and Dramix OL 13/.20 (B in C2) showed higher compressive strengths than the other types of fibers, shown in Figure 4.13 (b).
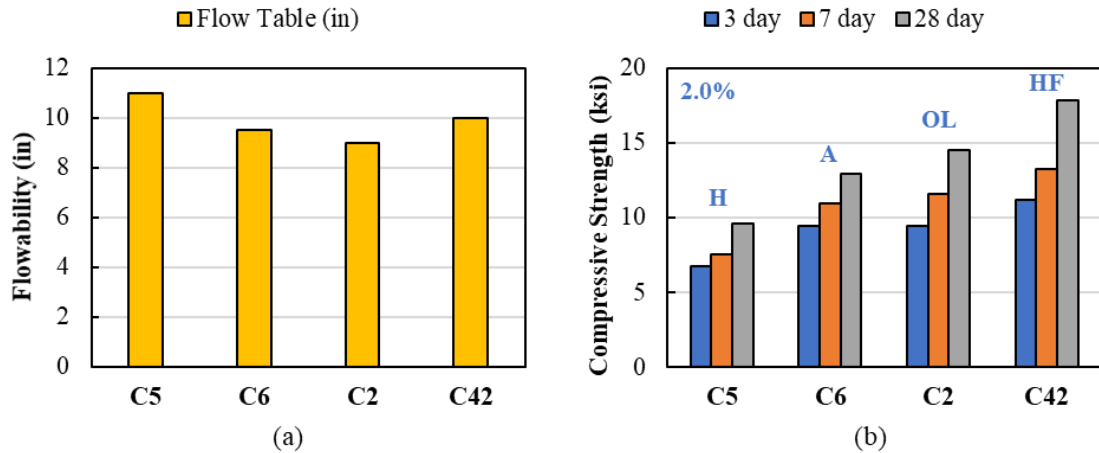
Figure 4.13: Effect of Fiber type on (a) flowability and (b) compressive strength

All mixtures in this group had a reasonable distribution of fibers, with the help of VMA

for some of the mixtures. Photographs of a representative cylinder for each mixture after

compression failure are shown in Figure 4.14.
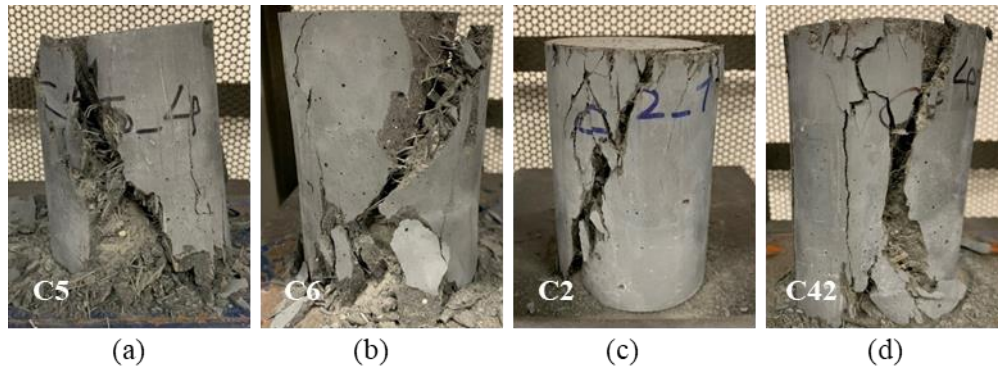
Figure 4.14: Sample cylinders after compressive failure for different fiber types: (a) Helix 5-13, (b) Dramix 4D 65/35BG, (c) OL 13/.20, and (d) Hiper Fiber Type A

The Helix 5-13 Uncoated (H) fibers had a higher zinc content and no brass coating, which

led to an expansive reaction between the fibers and UHPC paste for some of the samples,

as shown in Figure 4.15. The concrete expanded about 0.5 in. outside the top of the cylinder

before demolding, see Figure 4.15 (a). When the cylinder was removed, part of the cylinder

broke off the top, see Figure 4.15 (b). The resulting compressi expansive reaction between

93

the fibers and UHPC paste ve strength was low (5.9 ksi) relative to the samples with other fiber types. A photograph of the cylinder after failure is shown in Figure 4.15 (c). These results suggest that higher zinc content in fibers can negatively affect the mechanical properties of the UHPC mixture. This observation highlights the importance of creating trial mixes before using any new constituents in the mix design.

The manufacturer of the fiber communicated to the research team that the issue has been fixed, but the testing schedule did not allow for new samples to be cast and tested with the improved fibers.
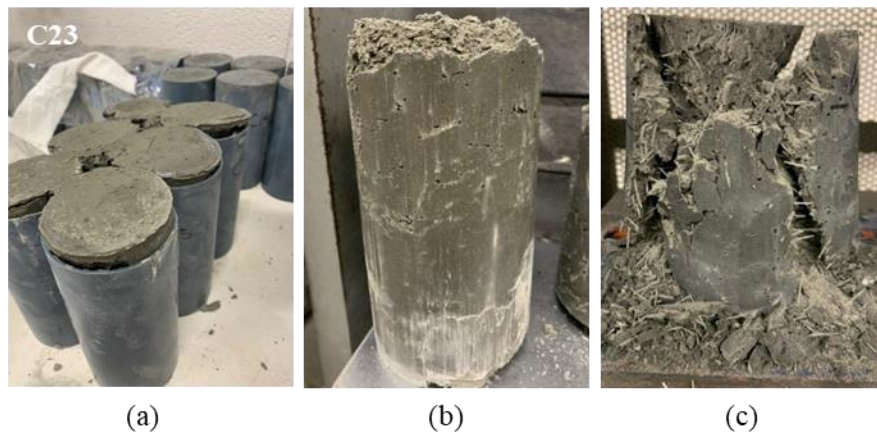
Figure 4.15: Example of expansion caused by concrete mixture reacting with zinc in fibers for C23 (a) before demolding, (b) after demolding before testing, and (c) after testing

Three of the four steel fibers (all but the Helix 5-13 Uncoated) were used in the large-scale batches. A synthetic fiber was also tested in the large-scale batches. This synthetic fiber was obtained later in the research project, so it was only tested in the large-scale batches.

4.1.6.7. Effect of Fine Aggregate Type and Content

Ultra-fines recovery (UFR) was used in some mixtures to improve the particle packing of the mixture. Its very small size allows it to fill the gap between other coarser particles in the mixture minimizing the porosity and increasing the density. UFR is made of limestone

with lower stiffness and strength than quartz particles made of rock crystal quartz. The particle packing analysis showed that replacing 10 to 35 percent of regular sand with UFR brought the base mix distribution curve (OPT#1) closer to the ideal curve (shown in Figure 3.1 and Figure 3.2).

Five mix designs with UFR replacement between 0 and 35 percent were used to determine the effect of UFR on the flowability and compressive strength. A summary of the mix designs is shown in Table 4.12. Adding UFR to the concrete mix increased the total special surface area, which required more HRWR to result in the same flowability.

Table 4-12: Mixture proportions and characteristics for investigation of using ultra-fine recovery (UFR) (dried sand used in all mixtures)

Mix.	Cement Type	w/b	Mix Proportions						Fiber		Admixtures		Density (lb/ft^3)
			ag/cm	C	S	SF	FA	UFR	Type	Content (%)	HRWR (oz./cwt)	VMA (oz./cwt)	
C28	Titan Type I/II	0.20	1.0	0.6	0.3	0.1	1.00	0.00	OL	2.0	21.70	0	147.1
C45	Titan Type I/II	0.20	1.0	0.6	0.3	0.1	0.90	0.10	OL	2.0	27.47	0	146.5
C46	Titan Type I/II	0.20	1.0	0.6	0.3	0.1	0.80	0.20	OL	2.0	27.47	0	148.4
C47	Titan Type I/II	0.20	1.0	0.6	0.3	0.1	0.70	0.30	OL	2.0	29.39	0	147.6
C48	Titan Type I/II	0.20	1.0	0.6	0.3	0.1	0.65	0.35	OL	2.0	29.39	0	147.3

The measured flow and compressive strength for these mixtures with varying UFR amounts and w/b of 0.20 are shown in Figure 4.16. Compressive strength results showed that replacing 10, 20, 30, and 35 percent of sand with UFR increased the 28-strength 7.0, 9.3, 8.9, and 13.6 percent, respectively, compared to the mixtures without any UFR. Although the flow was 8 inches, it was harder to work with the UHPC with a 35-percent UFR replacement.
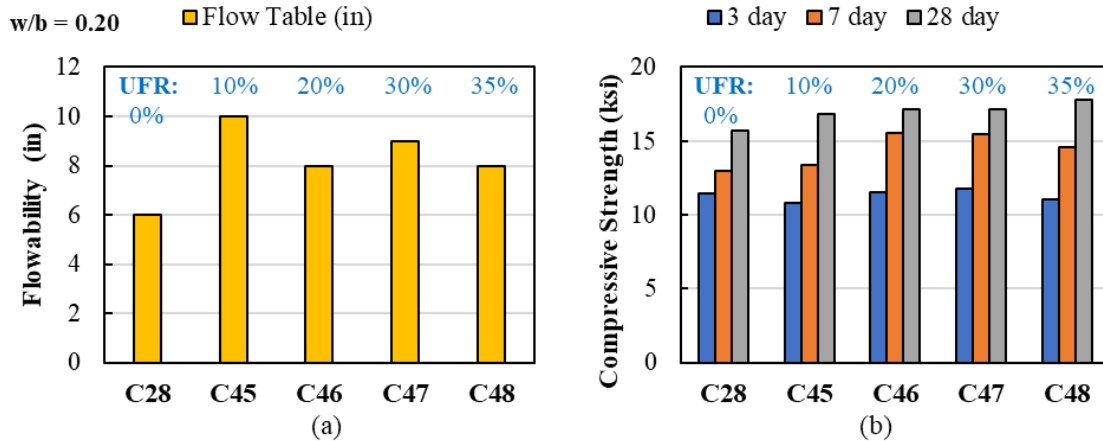
Figure 4.16:   Effect of fine aggregate content on (a) flowability and (b) compressive strength (with w/b = 0.20)

Two additional mixtures were cast with a lower w/b and and UFR contents of 20 and 30 percent. Details for these mixtures are provided in Table 4.13.

Table 4-13: Mixture proportions and characteristics for investigation of using ultra-fine recovery (UFR) with w/b of 0.18 (dried sand used in all mixtures)

| Mix. | Cement Type | w/b | Mix Proportions | | | | | | Fiber | | Admixtures | | Density (lb/ft^3) |
			ag/cm	C	S	SF	FA	UFR	Type	Content (%)	HRWR (oz./cwt)	VMA (oz./cwt)	
C33	Titan Type I/II	0.18	1	0.6	0.3	0.1	1.00	0.00	OL	2.0	27.47	0	149.4
C52	Titan Type I/II	0.18	1	0.6	0.3	0.1	0.80	0.20	OL	2.0	38.08	0	150.7
C53	Titan Type I/II	0.18	1	0.6	0.3	0.1	0.70	0.30	OL	2.0	38.08	0	150.8

The measured flow and compressive strength for these mixtures with varying UFR amounts and w/b of 0.18 are shown in Figure 4.17. Compressive strength results showed that replacing 20 and 30 percent of sand with UFR increased the 28-strength 19.1 and 17.6 percent, respectively, compared to the mixtures without any UFR.
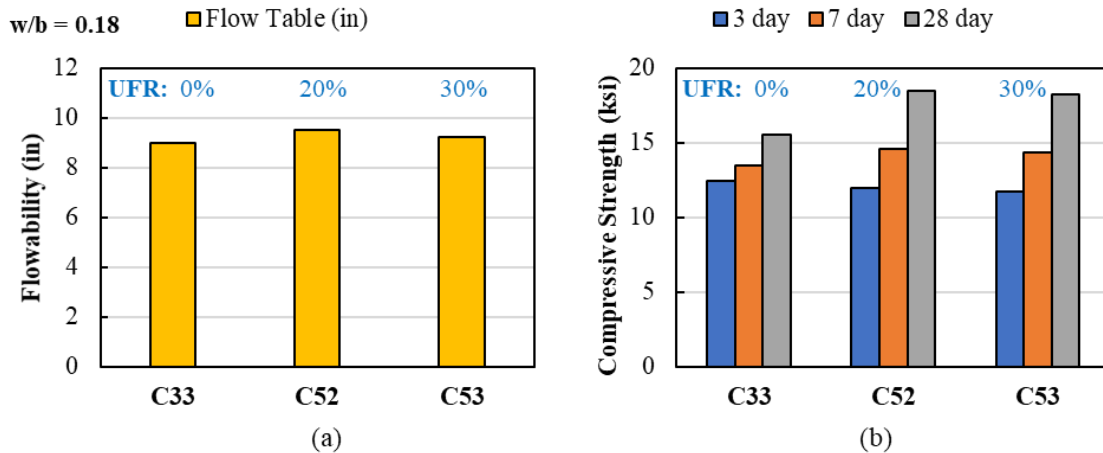
Figure 4.17: Effect of fine aggregate content on (a) flowability and (b) compressive strength (with w/b = 0.18)

A 20 and 30 percent replacement of the fine masonry sand with UFR was found to increase the compressive strength for w/b of 0.18 and 0.20. One large-scale batch with a 30-percent UFR replacement was cast. The other large-scale batches were cast without UFR to be consistent with the base mix design used by the other partner universities in this project.

4.1.7. Summary and Observations

A total of 690 3 by 6-inch cylinder from 115 0.15-ft^3 batches were cast with different mixture designs. The mixture designs were developed to investigate the effect of aggregate moisture, cement type, water-to-binder ratio, HRWR content, VMA content, fiber type, and fine aggregate type and content on the flow and compressive strength of the UHPC. The following observations were made based on these small-scale batches:

- The fine aggregate moisture content effected the repeatability of the UHPC mixtures. Fine aggregates should be oven dried to ensure consistent material properties can be achieved. This may be difficult for field applications. More research should be done to investigate mixtures with fine aggregates with natural moisture contents.

- Type I/II or Lehigh White cement resulted in similar compressive strengths and workability. Type III cement led to higher compressive strength but shortened the working time for the UHPC.

- A water-to-binder ratio between 0.18 and 0.20 produced the highest compressive strength while maintaining a good flow and working time. The water content in the chemical admixtures can affect the compressive strength and should be considered when determining how much water should be added to a mixture.

- VMA content did not influence the compressive strength. VMA can be used at dosages less than 10 oz./cwt to stabilize heavier steel fibers in the mixtures.

- The use of fibers with 0.5-inch length, 0.008-inch diameter, and tensile strength of 400 ksi led to the highest compressive strengths. This size fiber reasonably distributed in the mixture without the addition of any VMA.

- Uncoated fibers with high zinc contents can lead to an expansive reaction in the UHPC that greatly decreases its strength. This reaction can be observed in small-scale (0.15 ft^3) trial batches.

- Ultra-fines recovery (UFR) materials can replace the fine masonry sand at 20 to 30 percent replacement to increase strengths by 10 to 15 percent. More HRWR is needed for mixtures with UFR to achieve flows between 8 and 10 inches.

These observations were considered when developing the large-scale batches described in the next chapter.

4.2. Large-Scale Batches

4.2.1. Introduction

Ten large-scale batches (2.2-ft^3) were used to further evaluate the UHPC mixtures and the effect of fiber type and content on the mechanical properties. A total of 360 3-in. by 6-in. cylinders, 40 4-in. by 8-in. cylinders, 30 6-in. by 12-in. cylinders, and 50 3-in. by 3-in. by 11-in. prisms were cast in this phase to test the compressive strength, modulus of elasticity, splitting tensile strength, flexural strength, shrinkage, set time, and bulk resistivity.

4.2.2. Mixture Designs for Large-Scale Batches

The mixture design for the large-scale batches was based on the mix design from OU taking into consideration everything learned from the small-scale batches. The ten mixture designs used for the large-scale batches are summarized in Table 4-14. The water-to-binder ratio not considering the water content in the chemical admixtures (w/b) and considering the water content in the chemical admixtures (w*/b) are both shown; see §3.5 for more details on calculating w/b and w*/b. A w/b of 0.2 not considering the water content in the chemical admixtures was selected as the base value to be consistent with OU's mixture design.

Table 4-14: Mix proportions of large-scale batches

Mix.	Fiber Type	Vol. %	w*/b	w/b	Agg./b	C	Slag	SF	Sand	UFR	Cement Type	Glenium (oz/cwt)	VMA (oz/cwt)
L1	OL	2	0.21	0.20	1.00	0.60	0.30	0.10	0.7	0.3	C-T-I/II	29.4	0.00
L2	OL	2	0.21	0.20	1.00	0.60	0.30	0.10	1.0	0.0	C-A-I/II	22.0	0.00
L3	OL	2	0.21	0.20	1.00	0.60	0.30	0.10	1.0	0.0	C-T-I/II	27.5	0.00
L4	OL	2	0.19	0.18	1.00	0.60	0.30	0.10	1.0	0.0	C-T-I/II	27.5	0.00
L5	HF	2	0.21	0.20	1.00	0.60	0.30	0.10	1.0	0.0	C-T-I/II	27.5	0.00
L6	A	1.5	0.21	0.20	1.00	0.60	0.30	0.10	1.0	0.0	C-T-I/II	27.5	4.49
L7	OL	4	0.21	0.20	1.00	0.60	0.30	0.10	1.0	0.0	C-T-I/II	27.5	0.00
L8	HF	4	0.21	0.20	1.00	0.60	0.30	0.10	1.0	0.0	C-T-I/II	27.5	0.00
L9	Sy	2	0.20	0.20	1.00	0.60	0.30	0.10	1.0	0.0	C-T-I/II	27.5	0.00
L10	Sy	1	0.20	0.20	1.00	0.60	0.30	0.10	1.0	0.0	C-T-I/II	27.5	0.00

The mixtures were selected to investigate several different variables:

- L2 is the same material (shipped from Oklahoma) and same mixture design as that used by OU. The results from this mixture will be compared with results from OU in the ABC-UTC Guide document to show variability that may occur based on different people with different experience levels creating the mixture.

- L3 is the same mixture design as OU but using materials from South Florida. The results from this mixture can be compared to the mixture with Oklahoma materials to see the effect of material obtained from different parts of the country with the same mix design. Materials from South Florida were also shipped to OU for them to test at their lab.

- L1 and L4 have the same fiber type and fiber content as L3. L1 has all the same proportions as L3 except with 30 percent UFR replacement of the fine masonry sand. L4 has all the same proportions as L3 except with a w/b of 0.18. These

mixtures will give more insight to the effect of w/b and UFR replacement for mixture sizes that would be used in field applications.

- L3 and the other mixtures not mentioned so far (L5 to L10) were used to investigate the effect of three different steel fibers and one synthetic fiber at two different fiber contents on the mechanical properties of the mixtures. The OU mix design was used as the base mix design for all large-scale batches.

The actual quantity of materials for the 2.2 ft^3 mix was determined using the same procedure described in §4.1.2, but by taking the amounts per cubic foot times 2.2.

Comparisons are made in the following section based on the test.

4.2.3. Mixing Procedure

The mixing procedure and sequence of adding UHPC constituents was like the procedure followed for the small-scale batches with a slight variation in the mixing time after the water and chemical admixtures were added.

Before the mixing procedure began, the fine aggregates were all oven dried and stored in sealed containers. The proper amounts of all constituents were measured and stored in five-gallon buckets with lids prior to mixing.

Mixing of the UHPC was done using an Imer Mortarman vertical shaft paddle mixer (MIX 750 MBP). This mixer has a specified capacity of 27 ft^3 and specified batch output of 17 ft^3, but the actual amount of UHPC that can be mixed is less than the specified capacities due to the increased mix energy required by UHPC. The amount of UHPC mixed for this

project was 2.2 ft^3; this mixer has been used in other projects to successfully mix up to 2.5 ft^3.

First, all the dry materials were added through the top of the paddle mixer and allowed to mix for 10 minutes, shown in Figure 4.18 (a). The water and chemical admixtures were then added slowly to the dry mixture, shown in Figure 4.18 (b), and allowed to mix until the powder material became a flowable paste. It typically took 10 to 20 minutes for the mixture to become a flowable paste. Like the small-scale batches, the fibers were added to the mixture once the concrete paste was produced and allowed to mix for an additional 2 minutes, shown in Figure 4.18 (c).

| (a) | (b) | (c) |

Figure 4.18: Sequence of adding material, (a) adding dry constituents and mix for 10 minutes, (b) adding water and chemical admixtures, and (c) adding fibers

The UHPC was then poured into five-gallon buckets and used for the flow table test and to create all the samples required for the testing program. Photographs from the sample fabrication and flow table tests are shown in Figure 4.19. A cart with all the samples from one of large-scale batches is shown in Figure 4.19 (e).
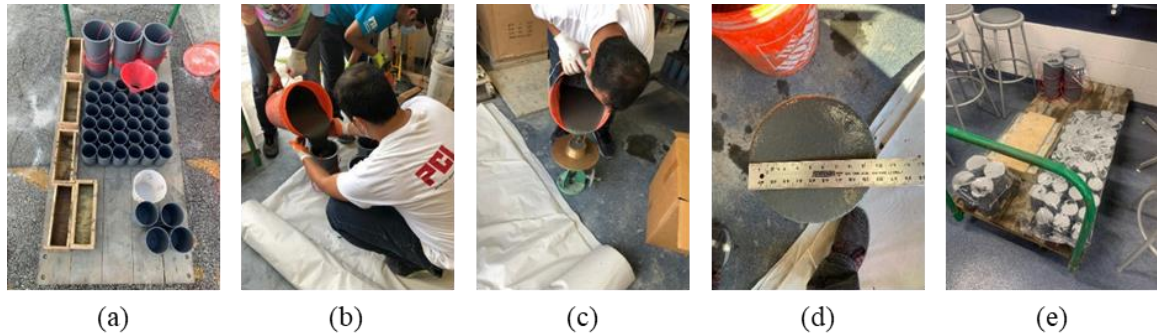
Figure 4.19: Sampling process: (a) preparing plastic and wooden molds, (b) casting samples, (c) fresh concrete flowability test, (d) spread flow, and (e) storing samples

4.2.4. Curing and Storage

The effect of curing conditions on the final compressive strength was investigated by storing half of the 3 by 6-inch cylinder samples in a lime water bath 24 hours after casting until test day. The rest of the samples were capped and kept in a temperature-controlled room until they were demolded 24 hours before testing.

4.2.5. Test Procedures

4.2.5.1. Flowability

The flowability tests for the large-scale batches were performed using the same procedure described in §4.1.5.1.

4.2.5.2. Setting Time

The setting time of UHPC mixtures was determined using mortar penetration tools according to ASTM C403/C2403M-16 (Time of Setting of Concrete Mixtures by Penetration Resistance) [103]. According to ASTM C403/C2403M-16, a cylinder container with a minimum 6-in. diameter and 6-in. height is required for the setting time test. For measuring the initial and final setting time of non-proprietary UHPC concrete, a

2-gallon bucket with 10-in. diameter and 10-in. height was used. The bucket was filled up to 80 percent height of bucket (around 8 in.) immediately after the mixing process was concluded and stored in a temperature-controlled room. Then, at specific intervals of 30 minutes or 60 minutes, the resistance of the UHPC mix to penetration was measured using standardized needles designed for the test, shown in Figure 4.20 (a). Two samples after the end of testing are shown in Figure 4.20 (b) and (c).

(a)　　　　　　　　　(b)　　　　　　　　　(c)
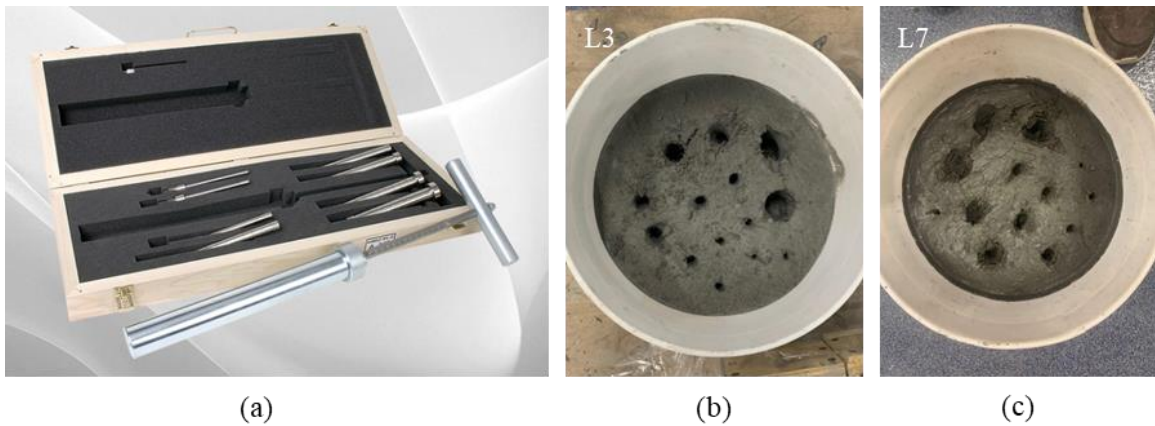
Figure 4.20: Setting time test; (a) testing apparatus [118], (b) sample left from L3, and (c) sample from L7

Sample data from the setting time test for L4 is shown in Table 4-15. The time of measurement, needle size, and resistance penetration load measured using the testing apparatus are needed to calculate the mortar resistance. The mortar resistance can be found simply by dividing the resistance penetration load by the cross-sectional area of the head of the needle.

Table 4-15: Sample data for setting time measurement (example: L4)

Time (min.)	Needle Diameter (#)	Needle Area (in²)	Resistance Penetration Load (lbf)	Mortar Resistance (psi)
0	#1	1.0	0	0
60	#1	1.0	2	2
120	#1/2	0.5	10	20
180	#1/2	0.5	20	40
240	#1/4	0.25	110	440
300	#1/10	0.1	90	900
360	#1/20	0.05	100	2000
420	#1/40	0.025	80	3200
480	#1/40	0.025	100	4000

The mortar resistance plotted versus time for L4 is shown in Figure 4.21. The standard definition for initial and final setting time is the time required for the concrete to reach specified resistance values to penetration: 500 psi and 4000 psi for initial and final set, respectively. The initial and final setting time are highlighted as 250 minutes and 480 minutes, respectively, in Figure 4.21 for the example data provided for L4. A linear interpolation was used between measurements taken at 240 minutes and 300 minutes to determine the approximate time when the mortar resistance reached 500 psi.
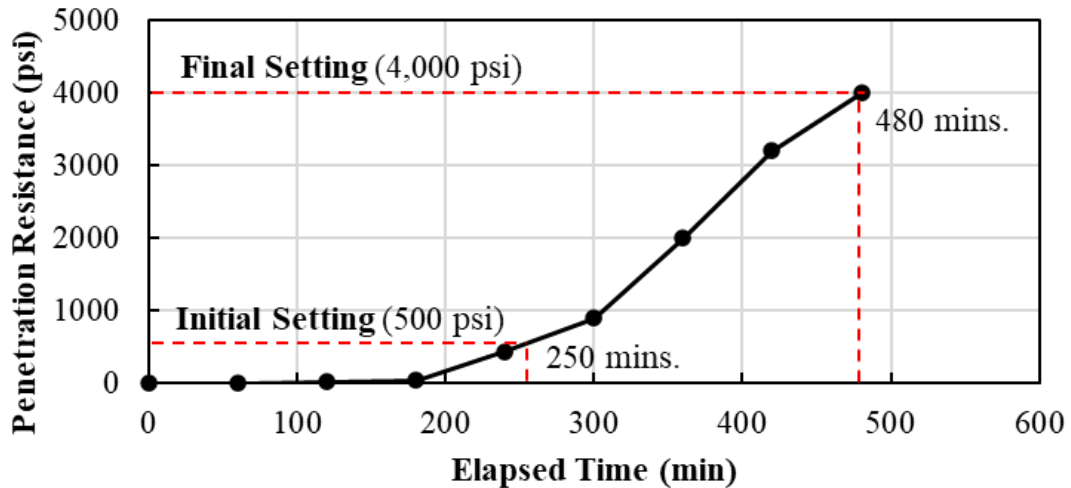
Figure 4.21: Example of initial and final setting time for L4

A similar procedure was used to determine the setting time for all large-scale batches.

4.2.5.3. Compressive Strength

The compressive strength tests for the large-scale batches were performed using the same procedure described in §4.1.5.2.

4.2.5.4. Modulus of Elasticity

The modulus of elasticity test was conducted in accordance with ASTM C469/C469M − 14 (Static Modulus of Elasticity and Poisson's Ratio of Concrete in Compressive) [100]. The modulus of elasticity of 3 in. by 6 in. cylinder samples was determined within the typical working stress range of 0 to 40 percent of the ultimate concrete strength. The compressive test machine was used to apply load at a constant rate (36.3±7 psi/s) until an applied load between 40 and 50 percent of the ultimate strength was reached. This test was done for concrete samples at 28 days for six samples (3 moist cured samples and 3 uncured samples) per batch.

All cylinders were prepared the same way as for the compressive strength cylinders, shown in Figure 4.5 and discussed in §4.5.2. Two samples were first tested in compression to determine the ultimate compressive strength of the mix. This tested strength was used to determine the 40-percent load for the modulus of elasticity testing.

The test setup for the modulus of elasticity testing is shown in Figure 4.22 (a) with a closer view of the instrumented specimen in Figure 4.22 (b). A compressometer/extensometer device with two linear strain conversion transducers (LSCT) was used to measure the longitudinal and diagonal deflections during the test, shown in Figure 4.22 (c). A basic data acquisition system, shown in Figure 4.22 (d), was used consisting of the LSCT sensors, a 250-kip capacity load cell, measurement hardware, a Campbell Scientific CR6 datalogger, and a computer with programmable software were used to collect data on load and deflection during the modulus of elasticity tests, shown in Figure 4.22 (e). Three load cycles were applied on each of the 3 in. by 6 in. cylinder samples to minimize the measurement errors during the acquisition of data.
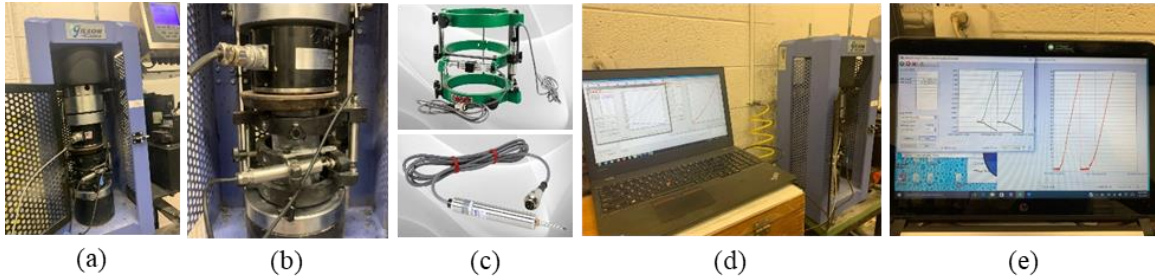
Figure 4.22: Modulus of elasticity test setup; (a) compression machine with instrumented sample, (b) closer view of instrumented sample, (c) compressometer/extensometer with LSCT [119], (d) data acquisition system, and (e) sample measured load and deflection

Data was collected at a frequency of 10 Hz, which led to large data files for each test. The data was analyzed and reduced by taking the average of specific increments of data; this helped to reduce file sizes and eliminate noise in the dataset. The reduced data was compared to the original data to ensure that the reduced data properly represented the original data set. A sample of original and reduced data is shown in Figure 4.23 for L1-21-2.
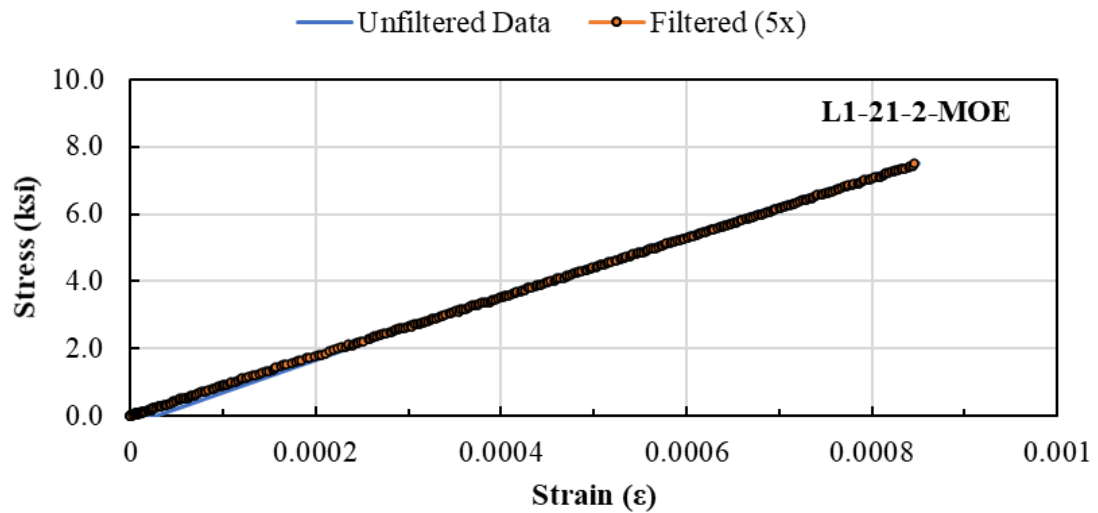
Figure 4.23: Example of noise and data reduction process for modulus of elasticity test

The data from the three tests was used to determine the modulus of elasticity using Equation 4-10 from ASTM C469/C469M [100]. The average of the three calculated modulus of elasticity values was recorded as the measured value for that sample.

$$E_c = \frac{S_2 - S_1}{\varepsilon_2 - 0.000050}$$
Equation 4-10

where:

E = chord modulus of elasticity, (ksi)

S_2 = stress corresponding to 40% of ultimate load, (ksi)

S_1 = stress corresponding to a longitudinal strain, ε_1, of 50 millionths, (ksi)

ε_2 = longitudinal strain produced by stress S_2

The values required for Equation 4-10 were determined based on the measured data for each test; an example is shown in Figure 4.24 (a) for sample L1-21-2. The calculation for the modulus of elasticity for this sample is provided below as an example.

Using Equation 4-10: $\quad E_c = \frac{S_2 - S_1}{\varepsilon_2 - 0.00005} = \frac{7.55\ ksi - 0.48\ ksi}{0.000847 - 0.00005} = 8,865\ ksi$

The modulus of elasticity was also determined based on the slope from a linear regression of the data within the range up to 40 percent of the ultimate compressive strength, as shown in Figure 4.24 (b). The stiffness for L1-21-2 was found to be 8,809 ksi using the slope of the linear regression.
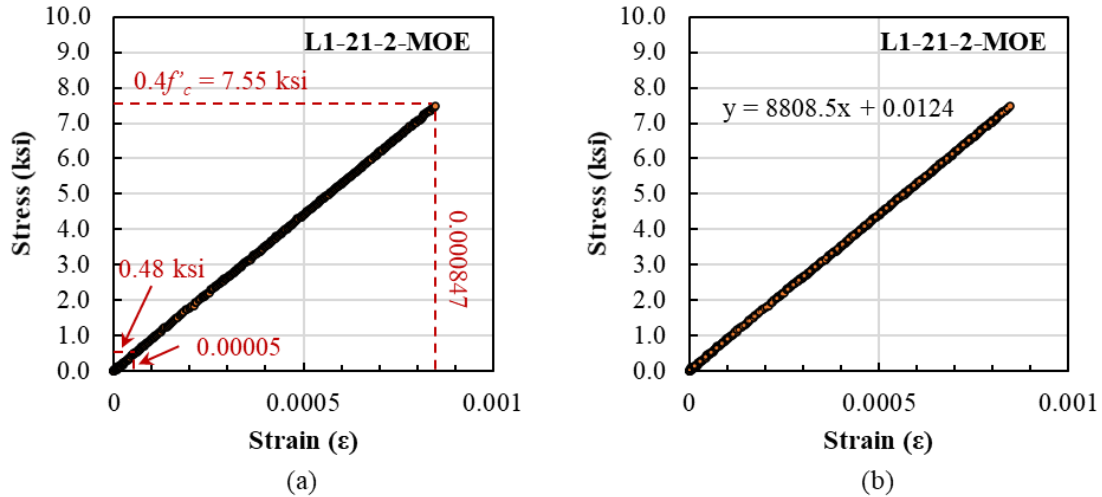
Figure 4.24: Procedures for determining modulus of elasticity with (a) ASTM C469 and (b) linear regression of measured data (L1-21-2)

The value from ASTM C469 was recorded as the modulus for the sample. The slope from the linear regression was used to verify the results from the ASTM C469 calculations.

4.2.5.5. Splitting Tensile Strength

The splitting tensile strength (f_{sp}) was determined using ASTM C496/C496M−17 (Splitting Tensile Strength of Cylindrical Concrete Specimens) [101]. The splitting tensile strength test is an indirect way to measure the tensile strength of concrete samples. The compression applied along the long side of a concrete cylinder causes transverse tension to develop along the length of the sample, as shown in Figure 4.25 (a). Splitting tensile strength is usually greater than direct tensile strength (f_t) and less than flexural strength (f_r).

All cylinders were prepared using the same end grinding procedure performed on the cylinders for compression tests, shown in Figure 4.25 and discussed in §4.1.5.2. The length of the cylinders was measured in three locations and diameter measured in two directions

110

using calipers. The weight of the cylinders was also measured prior to testing. These values were all hand recorded on a testing sheet.

The test setup used for the splitting tensile strength is shown in Figure 4.25 (b). Steel filler plates were used to decrease the space in the compression testing machine. Wood paint strips were placed on the top and bottom of a 3 by 6-inch cylinder laying on its side. The load was applied until the cylinder split in half, as shown in Figure 4.25 (c) through (e).
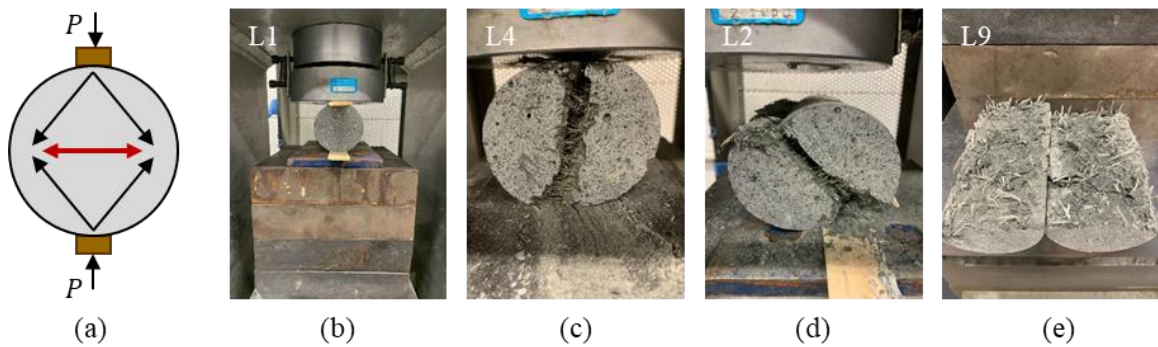
Figure 4.25: Split cylinder test, (a) stress flow in test, (b) test setup with wood bearing strips along length, (c) splitting failure from L4 with steel fibers, (d) splitting failure from L2 with steel fibers, and (e) splitting failure of L9 with synthetic fiber

The maximum applied load was recorded on the testing sheet for each of the samples. All specimen details and test results were collected in a test records spreadsheet, where the splitting tensile strength was calculated using Equation 4-11, from ASTM C496/C496M−17 [101].

$$f_{sp} = 2P/\pi l d$$

<div align="right">Equation 4-11</div>

where:

f_{sp} = splitting tensile strength (ksi)

P = maximum applied load by the testing machine (kips)

l = length (in.)

d = diameter (in,)

Examples for some of the splitting tensile strength tests for L4 are shown in Table 4-16.

Table 4-16: Splitting cylinder test for L4

Mix/Cylinder ID:	L4-SP1	L4-SP2	L4-SP3	L4-SP4	L4-SP5	L4-SP6
Curing Condition	Not Cured			Moist Cured		
Weight [lb]:	3.091	3.481	3.4295	3.1645	3.204	3.185
Length of Cylinders [in]:	5.003	5.582	5.497	5.109	5.130	5.123
	5.014	5.588	5.497	5.102	5.131	5.128
	5.008	5.583	5.501	5.107	5.132	5.126
Diameter of Cylinders [in]:	3.000	3.006	3.003	3.004	3.007	3.003
	3.003	3.009	3.006	3.007	3.006	3.005
Ultimate Load [kips]:	74.2	68.73	69.63	72.1	67.93	68.22
Splitting tensile strength [ksi]	3.14	2.60	2.68	2.99	2.80	2.82

An example of how the tensile splitting strength was calculated for L4-SP1 is shown below.

The average length and average diameter are used in the calculation.

$$f_{sp} = \frac{2P}{\pi l d} = \frac{2(74.2\ kips)}{\pi \left(\frac{5.003" + 5.014" + 5.008"}{3}\right)\left(\frac{3.003" + 3.000"}{2}\right)} = 3.14\ ksi$$

This was done for all the tensile splitting strength specimens.

4.2.5.6. Modulus of Rupture

The modulus of rupture test was conducted in accordance with ASTM C78/C78M – 18,

Flexural Strength of Concrete (Using Simple Beam with Third-Point Loading) [99].

Five 3 in. by 3 in. by 11 in. prism specimens were cast using wooden formworks for each large-scale batch, as shown in Figure 4.26 (a) and (b). Before filling the formwork with fresh concrete, all internal faces were coated with a thin layer of form oil to make the later demolding process easier. All samples were filled with fresh UHPC concrete immediately after the mixing process. The top open face of filled formworks was covered with a plastic sheet immediately after casting. All samples were stored in a temperature-controlled room until 24 hours before testing. A day before testing, they were demolded, measured, and weighted.

A four-point loading test setup according to ASTM C78 was used, as shown in Figure 4.26 (c) through (e). The loading blocks and support blocks were designed so that forces were applied to the beam perpendicularly to the side faces of the beam and applied without eccentricity. The compressive test machine was again used to apply load at a constant rate between 125 and 175 psi/min until it reached its ultimate flexural strength. Two LSCT sensors and a 250-kip loadcell were connected to the CR6 data acquisition system to measure load and displacement during the test. LSCT sensors were placed on both sides of the specimen at midspan to measure the average midspan deflection during testing.
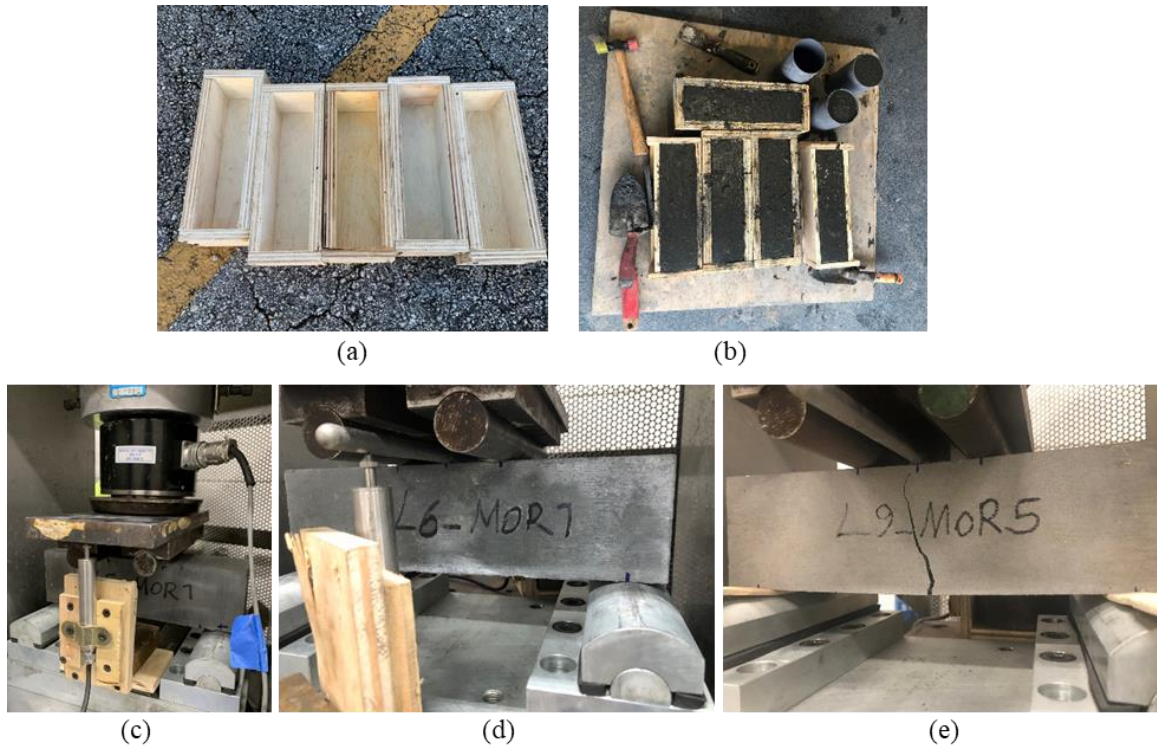
Figure 4.26: Modulus of rupture test; (a) wooden formworks, (b) filled specimens with fresh UHPC, (c) test setup, (d) LSCT sensor reads the mid-span deflection, and (e) typical flexural failure of beams

The width and depth of the specimens across one of the fractured faces were measured after conducting the test. Three measurements were taken at different locations to determine the average width and the average depth. The modulus of rupture was calculated for each sample using Equation 4-12 for failures in the middle third and Equation 4-13 for failures outside the middle third by not more than 5 percent of the span length.

Failure in middle third of span:

$$R = \frac{PL}{bd^2}$$

Equation 4-12

Failure outside middle third of span

(by not more than 0.05*L*):

$$R = \frac{3Pa}{bd^2}$$

Equation 4-13

where:

R   =   modulus of rupture, (ksi),

P   =   maximum applied load indicated by the testing machine, (kips),

L   =   span length, (in.),

b   =   average width of the specimen, (in.), at the fracture.

d   =   average depth of the specimen, (in.), at the fracture.

a   =   average distance between the line of fracture and the nearest support measured on the tension surface of the beam, (in.).

Modulus of rupture test data was collected through the data acquisition system. All modulus of ruptures were calculated based on the unfiltered stored data. The filtered data was used for creating the comparison plots, to remove noise and decrease file sizes. Filtered data, unfiltered data, and strain after crack behavior of UHPC for L6-MOR3 are shown in Figure 4.27.
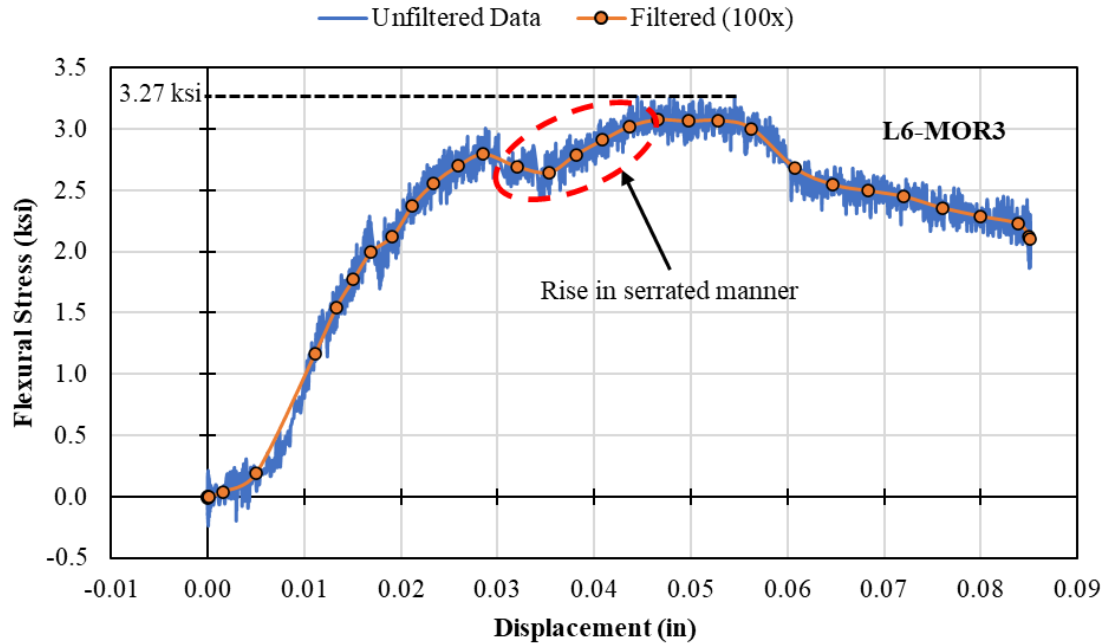
Figure 4.27: Example of modulus of rupture – L6-MOR3

The failures occurred in the middle third of the span length for all samples, so Equation 4-12 was used for calculating the modulus of rupture. An example of how the modulus of rupture was calculated for L6-MOR3 is shown below:

Using Equation 4-12:
$$R = \frac{PL}{bd^2} = \frac{(8.22\ kips)(10.989")}{(3.0030")(3.0305")^2} = 3.27\ ksi$$

This procedure was done for all the modulus of rupture specimens for all large-scale batches.

4.2.5.7. Bulk Resistivity

The durability of UHPC has been investigated in several different studies. Alkali-silica reaction tests, freeze-thaw tests, chloride ion penetrability tests, and electrical and surface resistivity tests have all been used by previous researchers [24], [26], [48]. The electrical

bulk resistivity test was used to determine the long-term durability of the UHPC in this study, based on available equipment.

ASTM C1760-12 [97] was used to determine the bulk electrical conductivity of the saturated specimens of hardened UHPC to provide a rapid indication of the resistance of the concrete to the penetration of chloride ions. Saturated cylinder samples (4 in. by 8 in.) were tested to measure the electrical current based on a constant potential difference of 60V across their ends. After 24 hours of casting, cylinder samples were demolded, ground at both ends, and measured (length and dimeter).

The resistivity of the samples was measured at different ages (3, 7, 14, 28, 56, and 90 days) using a Resipod Concrete Resistivity Meter, which has a wide range of resistance measurements (1 to 1,000 kΩ-cm), shown in Figure 4.28(a). The maximum range of the device (1,000 kΩ-cm) controlled for several of the specimens. Electrical plates with conductive foam inserts were placed at each end of the 4 in. by 8 in. concrete cylinder samples and connected to the meter through cables, shown in Figure 4.28 (b).
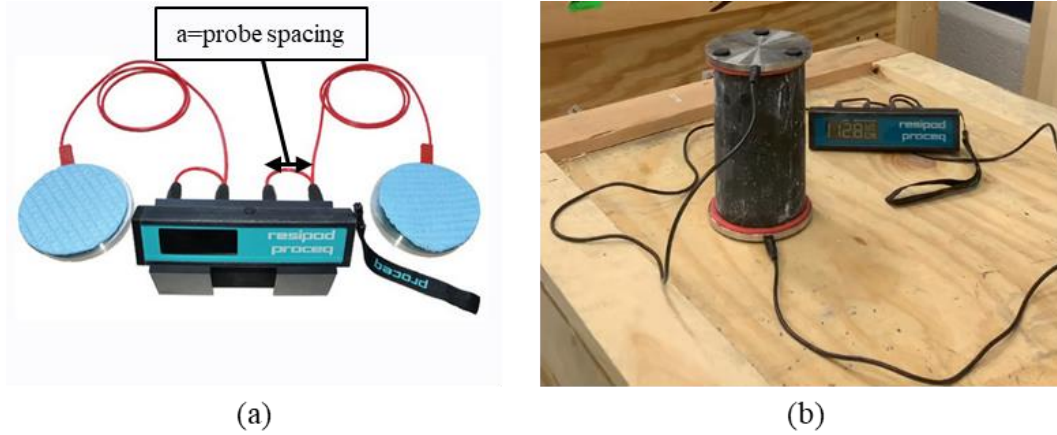
Figure 4.28: Bulk resistivity test; (a) resistivity meter device and attachments [120] and (b) test setup

The current was measured after 60 seconds of applying potential difference. The measured dimension was used to calculate the bulk resistivity using Equation 4-14 from Proceq Resipod User Manual [64], which simplifies to Equation 4-15.

$$\rho = \left(\frac{R_{Cylinder}}{2\pi a}\right)\left(\frac{A}{L}\right) \qquad \text{Equation 4-14}$$

Simplified to:
$$\rho = R_{Cylinder}\left(\frac{d^2}{8aL}\right) \qquad \text{Equation 4-15}$$

where:

$R_{cylinder}$ = measured value of resistivity by Resipod (kΩcm)

a = probe spacing (1.5 in. [3.8 cm], specified in the Resipod manual [121])

d = diameter of the sample (in.)

A = cross sectional area of tested cylinder (in.^{2})

L = length of the sample (in.)

A sample result for the bulk resistivity of cylinder samples is summarized in Table 4-17.

Table 4-17: Example of bulk resistivity test- L4

Test #:	L4					
Cylinder ID:	L4-4×8-1					
Mass of Cylinder before Capping [lb]:	7.95					
Length of Cylinders [in]:	7.2970					
	7.2900					
	7.2725					
Diameter of Cylinders [in]:	3.9890					
	3.9900					
Age [day]	3	7	14	28	56	90
K [A/L, in]:	1.72					
$R_{Cylinder}$ [kΩ-cm]:	15.5	30.1	43.1	71.2	141.8	248.9
Bulk Resistivity ρ [kΩ-cm]:	2.83	5.49	7.86	12.99	25.88	45.42

An example of how the bulk resistivity of cylinder samples of L4 at 3 days was calculated is shown below. The measurement is taken in kΩcm, using a in cm converts the data to kΩ-in.

$$\rho = R_{Cylinder}\left(\frac{d^2}{8aL}\right) = (15.5 \ k\Omega. cm)\left[\left(\frac{\left(\frac{3.9890" + 3.9900"}{2}\right)^2}{8(1.5")\left(\frac{7.2970" + 7.2900" + 7.2725"}{3}\right)}\right)\right]$$

$$= 2.83 \ k\Omega. cm$$

This procedure was done for all the bulk resistivity samples for all large-scale batches.

4.2.5.8. Shrinkage

The shrinkage test was according to ASTM C157/C157M – 17 (Length Change of Hardened Hydraulic-Cement Mortar and Concrete). GEOKON vibrating wire embedment strain gauges (VWSG) designed for direct embedment in concrete were used to measure

the strain variation of concrete due to total shrinkage. Three 6 in. by 12 in. cylinder samples

with one vertically-oriented VWSG at the center of the sample were used for the shrinkage

tests. A photograph of the VWSG, location of the VWSG in the cylinder, and photograph

of the installed VWSG before cylinder casting are shown in Figure 4.29. Steel wire was

used to hold the VWSG in the correct location during cylinder casting.

| (a) | (b) | (c) |
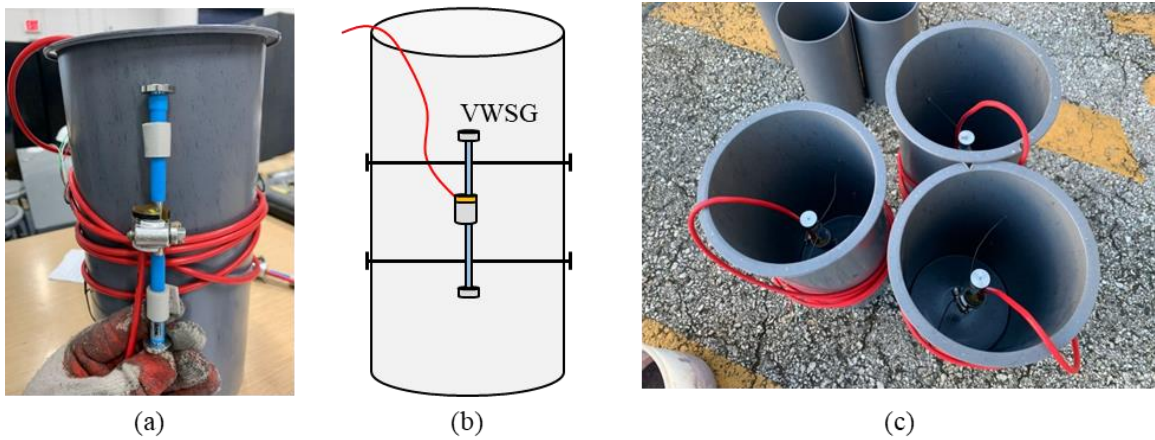
Figure 4.29: Shrinkage test; (a) Geokon Model 4200 VWGS, (b) schematic installation of the sensor, and (c) prepared samples

The UHPC samples were demolded 24 hours after casting and sensors were attached to a

data acquisition system to continuously monitor the data after casting. These samples were

stored in a climate-controlled room at temperatures between 71°F and 75°F. Photographs

of the cylinders attached to the data acquisition system are shown in Figure 4.30.
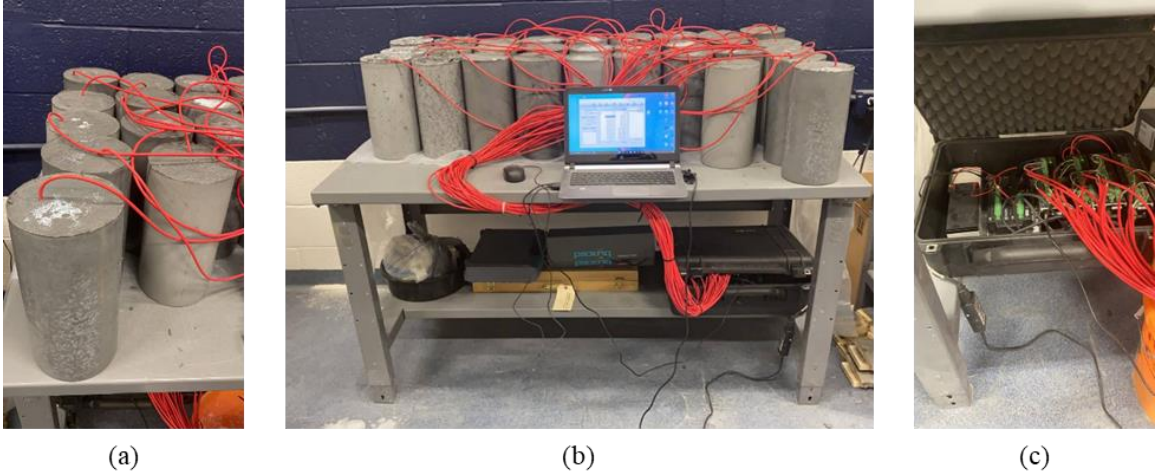
Figure 4.30: Shrinkage test; (a) shrinkage samples with embedded VWSG sensors, (b) test setup, and (c) data acquisition system

The beginning strain in the VWSG was set as zero strain; all subsequent strains are the total shrinkage that occurs in the sample. The data was reduced using the average of a specific interval of data points to reduce noise and file sizes. The reduced data was compared to the original dataset to ensure the reduced data represented the original data well. An example of data from a shrinkage test for L4 is shown in Figure 4.31.
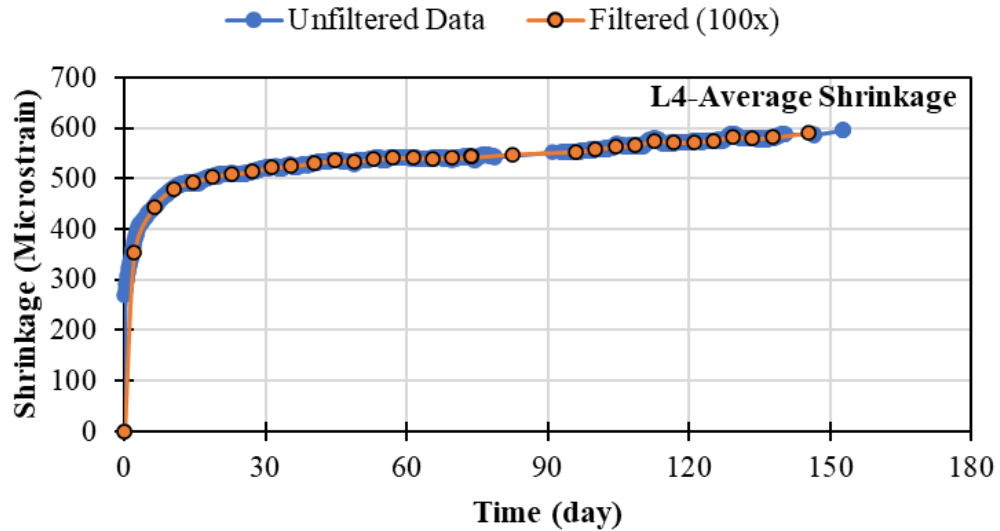
Figure 4.31: Shrinkage example (L4-2% OL fibers)

A similar procedure was followed for all large-scale batches.

4.2.6. Evaluation of Large Batches

The tests described in the previous section were performed on all ten of the large-scale batches shown in Table 5.1. Results are organized by test. Discussion of results is divided into two groups for most tests:

- *Group I – Effect of Fiber Content*: This group includes L3 and L5 to L10. All mixes in this group were made using the same mix proportions, HRWR dosage, and w/b, but with different fiber types and fiber contents.

- *Group II – Effect of w/b and UFR*: This group includes L1, L3, and L4 to study the effect of w/b and using UFR. The fiber type and fiber content were kept the same for all mixes in this group.

- *Group III – Effect of Material Source*: This group compares L2 and L3 to see the influence of the source of the material. L2 materials were shipped from Oklahoma. L3 materials were obtained from local suppliers in south Florida.

More details of all conducted tests are provided in §4.2.5.

4.2.6.1. Flowability Results

The base HRWR dosage (27.5 oz./cwt.) was modified for some of the mixtures to get between an 8- and 10-inch spread flow. The flowability for all of the mixtures is shown in Figure 4.32. L4 had less flowability than mixtures with similar HRWR contents due to its lower w/b ratio (0.18 compared to 0.2 for other mixtures). Additionally, higher fiber contents led to less flowability than other mixtures; seen by comparing the similar mixtures with 2 and 4 percent fibers.
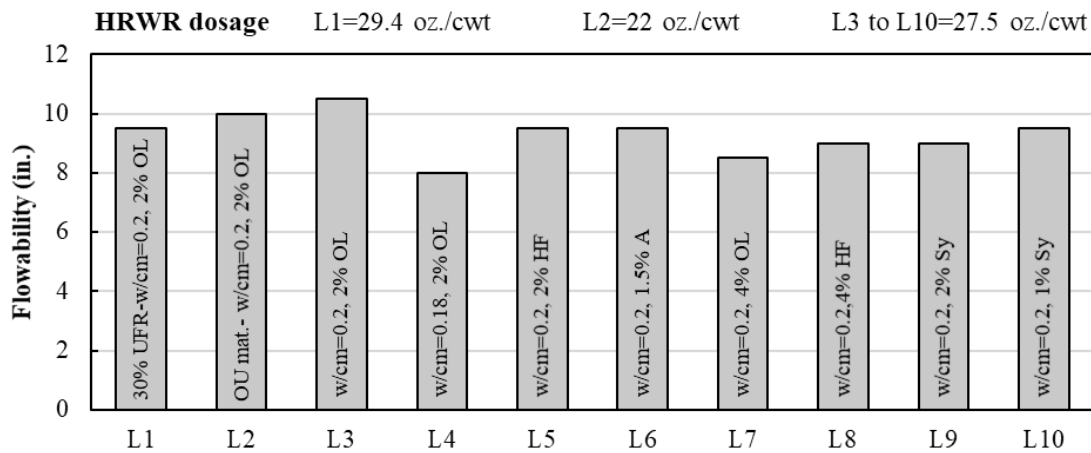
Figure 4.32: Measured flowability of large batches with HRWR dosage (oz./cwt)

4.2.6.2. Setting Time Results

The setting time of all ten large batches was measured by penetrating special needles and recording the penetration resistance, as described in § 4.2.5.2. The calculated initial and final setting times for all large-scale batches are shown in Table 4-18.

Table 4-18: Initial and final set time for all large-scale batches

Mixture	L1	L2	L3	L4	L5	L6	L7	L8	L9	L10
w/b	0.20	0.20	0.20	0.18	0.20	0.20	0.20	0.20	0.20	0.20
Sand:UFR	0.7:0.3	1:0	1:0	1:0	1:0	1:0	1:0	1:0	1:0	1:0
Fiber Type	OL	OL	OL	OL	HF	A	OL	HF	Sy	Sy
Fiber Content	2.0	2.0	2.0	2.0	2.0	1.5	4.0	4.0	2.0	1.0
Initial Set (hr)	6.3	5.8	5.5	4.1	5.2	5.1	5.0	4.3	4.6	4.6
Final Set (hr)	11.0	9.0	10.0	8.0	11.0	10.0	9.0	9.5	10.5	11.5

The penetration stress versus time for the mixtures with different fiber type and fiber contents are shown in Figure 4.33. The mixtures with higher fiber contents had shorter final set times. As an example, mixtures with 4 percent OL fibers (L7) had final set time of 9.0 hrs. compared to 10.0 hrs. for 2 percent OL fibers (L3). A similar comparison can be made for mixtures with HF fibers (L5 for 2 percent and L8 for 4 percent) and with Sy fibers (L10 for 1 percent and L9 for 2 percent). There was no clear correlation between fiber content and initial set time.
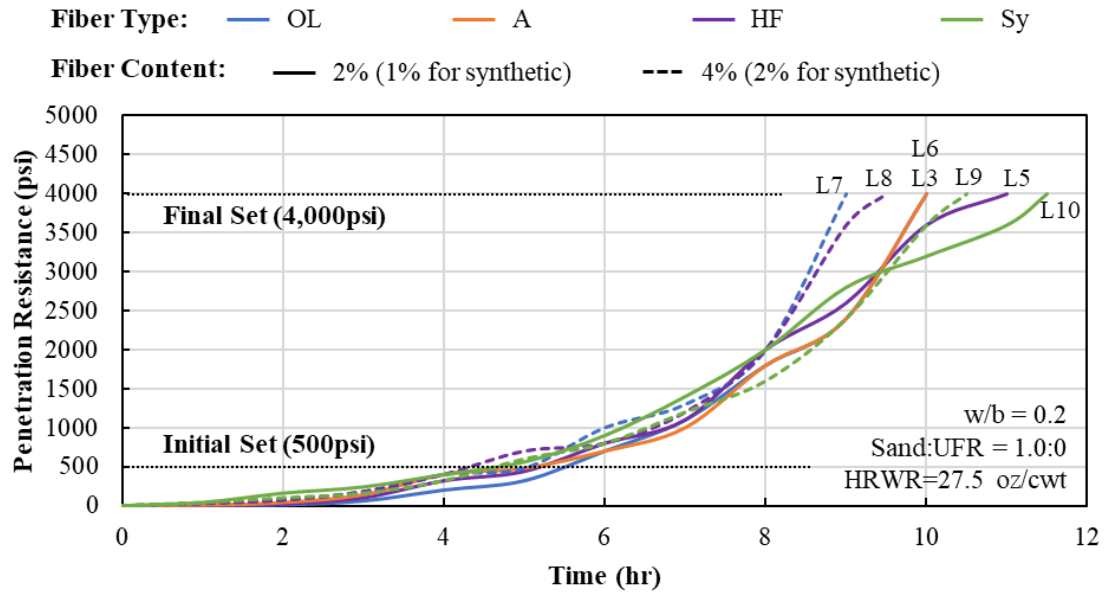
Figure 4.33: Effect of fiber type and content on setting time

The shorter final set time for mixtures with higher fiber contents may have occurred as a result of the fibers resisting the penetration needle, as shown in Figure 4.34.

(a)   (b)
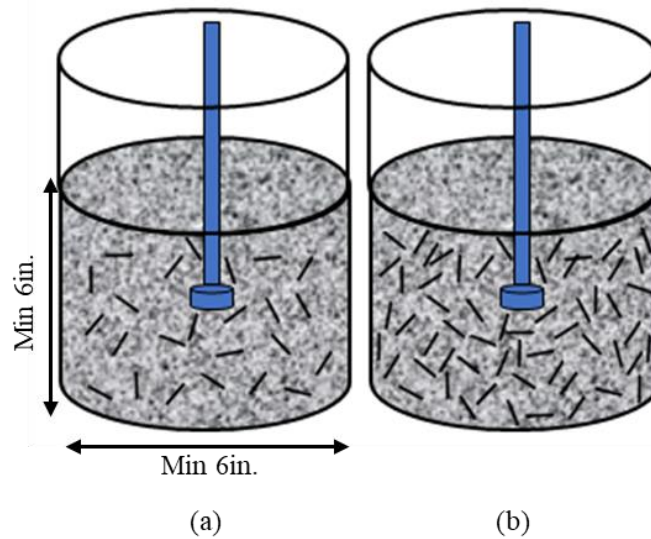
Figure 4.34: Schematic of setting time test; (a) low volume content fibers and (b) high volume content

The effect of different w/b and UFR on the penetration stress over time is shown in Figure 4.35. The smaller w/b resulted in an earlier initial set and final set time, comparing L4 with

125

w/b of 0.18 and L3 with w/b of 0.20. The use of UFR at a 30 percent replacement of the fine masonry sand led to slightly increased initial and final set times; this may be due to the larger HRWR content or that UFR leads to an improved particle packing.
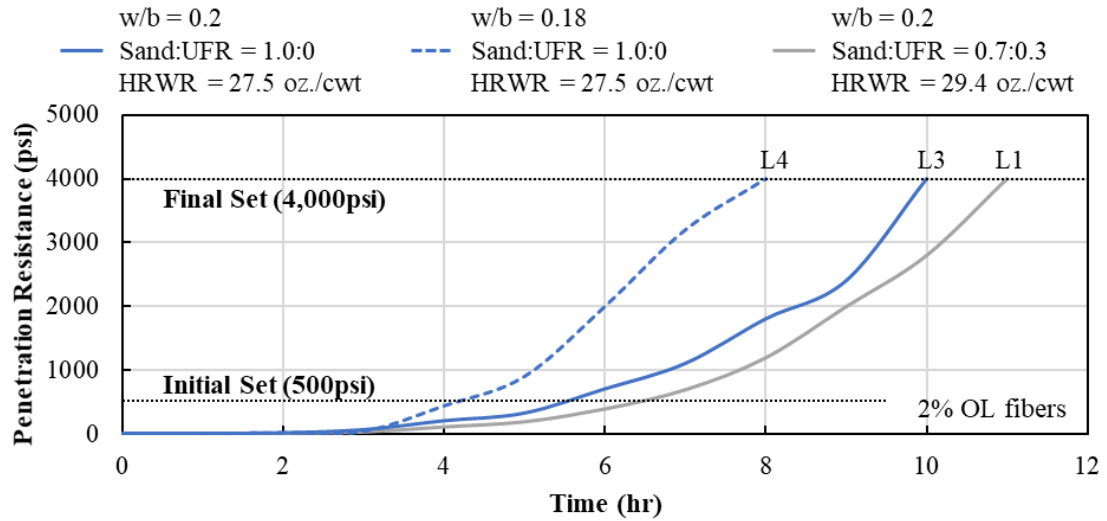
Figure 4.35: Effect of w/b and UFR on setting time

The penetration stress versus time curves for the two mixtures with similar proportions using materials from Oklahoma (OK) and south Florida (FL) are shown in Figure 4.36. The two sources of materials led to similar initial set time. The mixture with OK materials had a shorter final set time, but this may have been due to less HRWR being used.
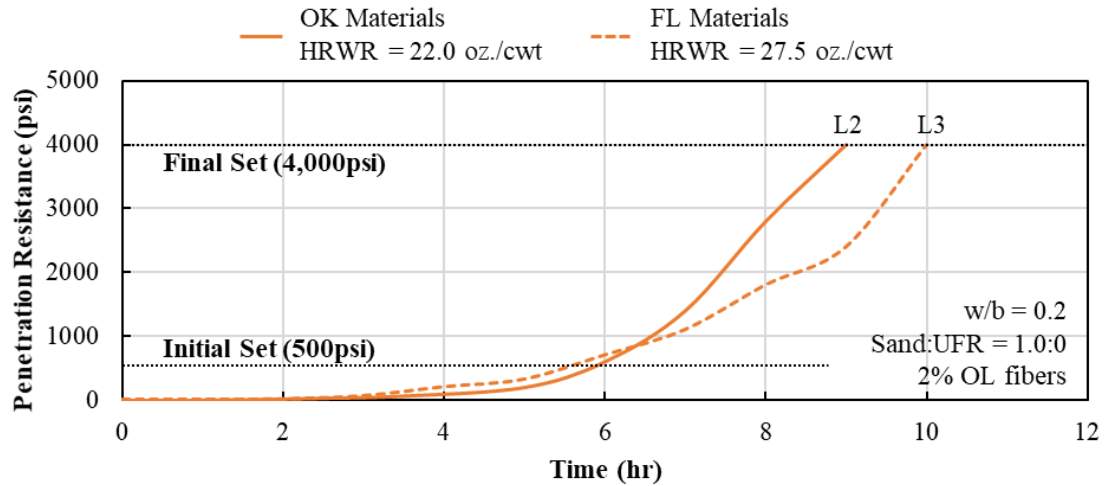
Figure 4.36: Effect of material source on setting time

4.2.6.3. Compressive Strength Results

Six 3 in. by 6 in. cylinders were tested at five different ages (3, 7, 14, 28, and 56 days). Three were moist cured and three left in the capped cylinder mold until testing at each age to determine the effectiveness of curing on compressive strength and density. The average compressive strength for all large-scale batches without moist curing are summarized in Table 4-19.

Table 4-19: Average measured compressive strength for large-scale batches

Mix.*	w/b	Sand:UFR	Fiber		Compressive Strength (ksi)				
			Type	Content	3 day	7 day	14 day	28 day	56 day
L1	0.20	0.7:0.3	OL	2.0%	11.8	14.6	15.5	16.7	18.1
L2	0.20	1:0	OL	2.0%	11.0	14.0	15.7	17.6	18.2
L3	0.20	1:0	OL	2.0%	12.2	14.4	15.5	17.1	17.6
L4	0.18	1:0	OL	2.0%	12.0	14.9	16.4	17.8	18.1
L5	0.20	1:0	HF	2.0%	12.1	14.3	15.4	17.5	18.0
L6	0.20	1:0	A	1.5%	11.7	14.9	16.2	17.3	17.6
L7	0.20	1:0	OL	4.0%	12.0	14.3	15.0	17.0	17.1
L8	0.20	1:0	HF	4.0%	12.8	14.3	15.6	17.3	17.4
L9	0.20	1:0	Sy	2.0%	9.7	10.8	11.2	11.1	13.4
L10	0.20	1:0	Sy	1.0%	10.9	12.4	13.4	15.4	16.0

*materials for L2 were shipped from Oklahoma; all other materials were obtained in South Florida

The measured compressive strength and density for the large-scale batches used to evaluate fiber type and fiber content are shown in Figure 4.37. The mixtures with steel fibers all had average 28-day compressive strengths between 17 and 18 ksi. There was no clear trend between fiber type and fiber content (for 2 and 4 percent fibers) and compressive strength for these large-scale batches. The fiber content did have a slight effect on the density of the concrete; the mixtures with 4 percent fibers had a slightly higher density than those with 2 percent fibers (3 to 4 percent increase in density).
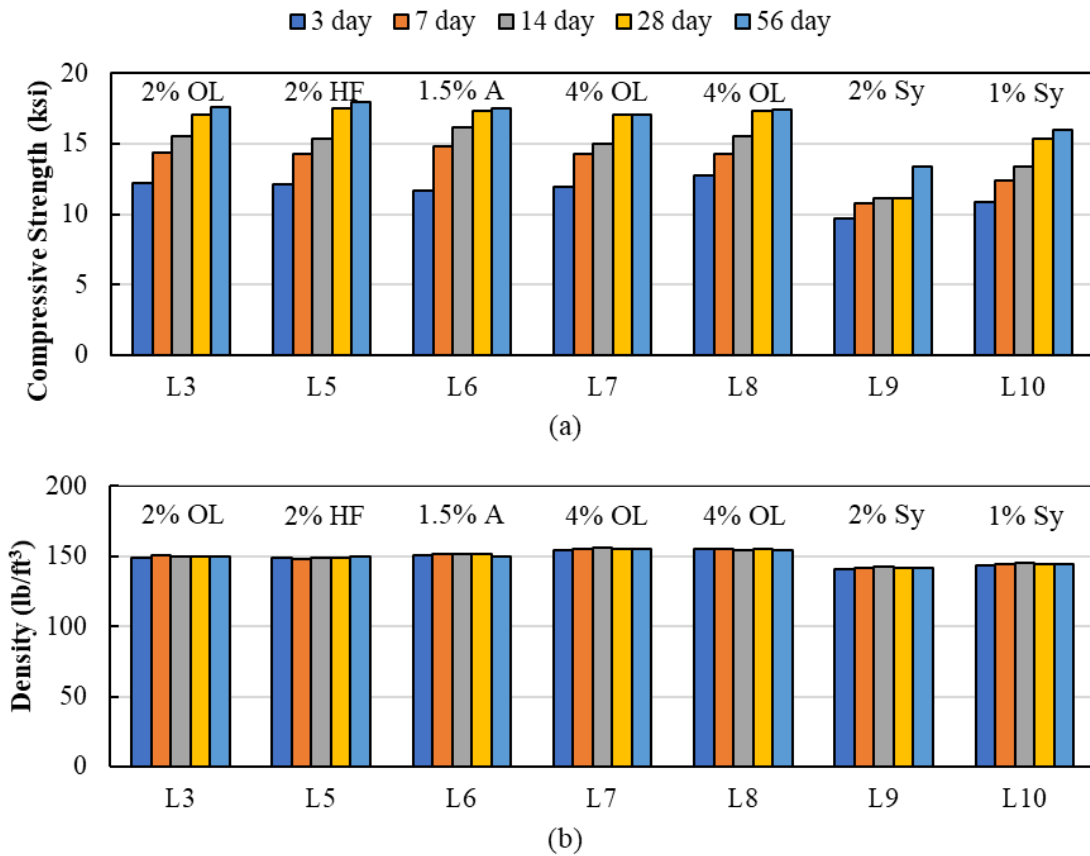
Figure 4.37: Effect of fiber type and content on (a) compressive strength and (b) density

The mixtures with synthetic fibers (L9 and L10) had lower compressive strengths and densities than those with steel fibers. The mixture with 2 percent synthetic fibers had the smallest compressive strengths of all the different fiber types and contents tested (13.4 ksi at 56 days), compared to 16.0 ksi for 1 percent synthetic fibers and between 17 and 18 ksi for steel fibers.

The lower compressive strength of the mixtures made with synthetic fibers (L9 and L10) could be due to the lower strength of the synthetic fibers compared to steel fibers. Additionally, more fiber clumps were observed in mixtures containing synthetic fibers than

129

mixtures with steel fibers. Clumping of the fibers occurred in some cases where the fibers were added rapidly to the mixer, when long or heavy fibers were used, or when synthetic fibers were used. A schematic of fiber clumping in cylinders is shown in Figure 4.38(a). Photographs after compression failure for two cylinders from mixtures with 2 percent and 1 percent synthetic fibers are shown in Figure 4.38 (b) and (c), respectively. Clumping of the fiber led to weak local spots in the cylinders, which could lead to lower compressive strengths.

(a) (b) (c)
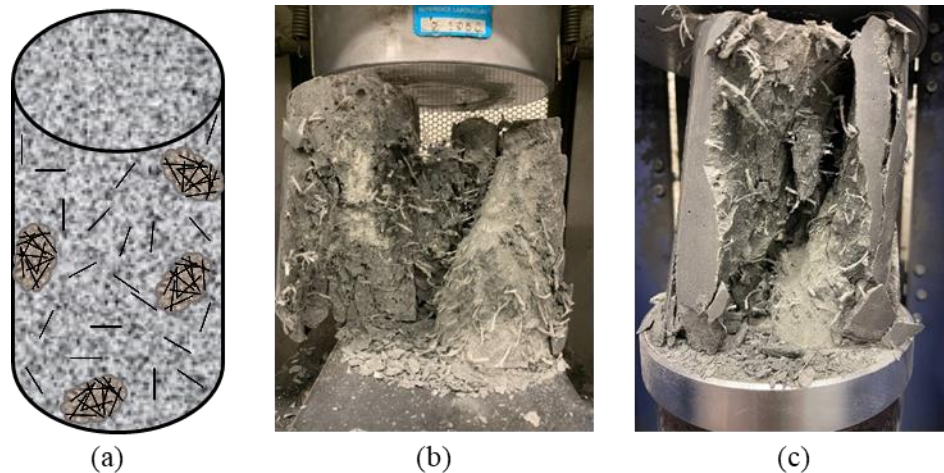
Figure 4.38: (a) Schematic of fiber clumping, (b) sample cylinder failure for L9 with 2% synthetic fibers (L9-20-28day), and (c) sample cylinder failure for L10 with 1% synthetic fibers (L10-27-56day)

The measured compressive strength and density for the large-scale batches used to evaluate the effect of w/b and UFR content are shown in Figure 4.39. Decreasing the w/b from 0.20 to 0.18 increased the compressive strength between 2 and 6 percent at different ages. The addition of UFR did not increase the strength for the large-scale batches, comparing L1 and L3 in Figure 4.39 (a). The addition of UFR was found to increase the compressive strength in the small-scale batches; it is unclear why it did not affect the strength in the

large-scale batches. The w/b and UFR content had no effect on the density of the mixtures, shown in Figure 4.39 (b).
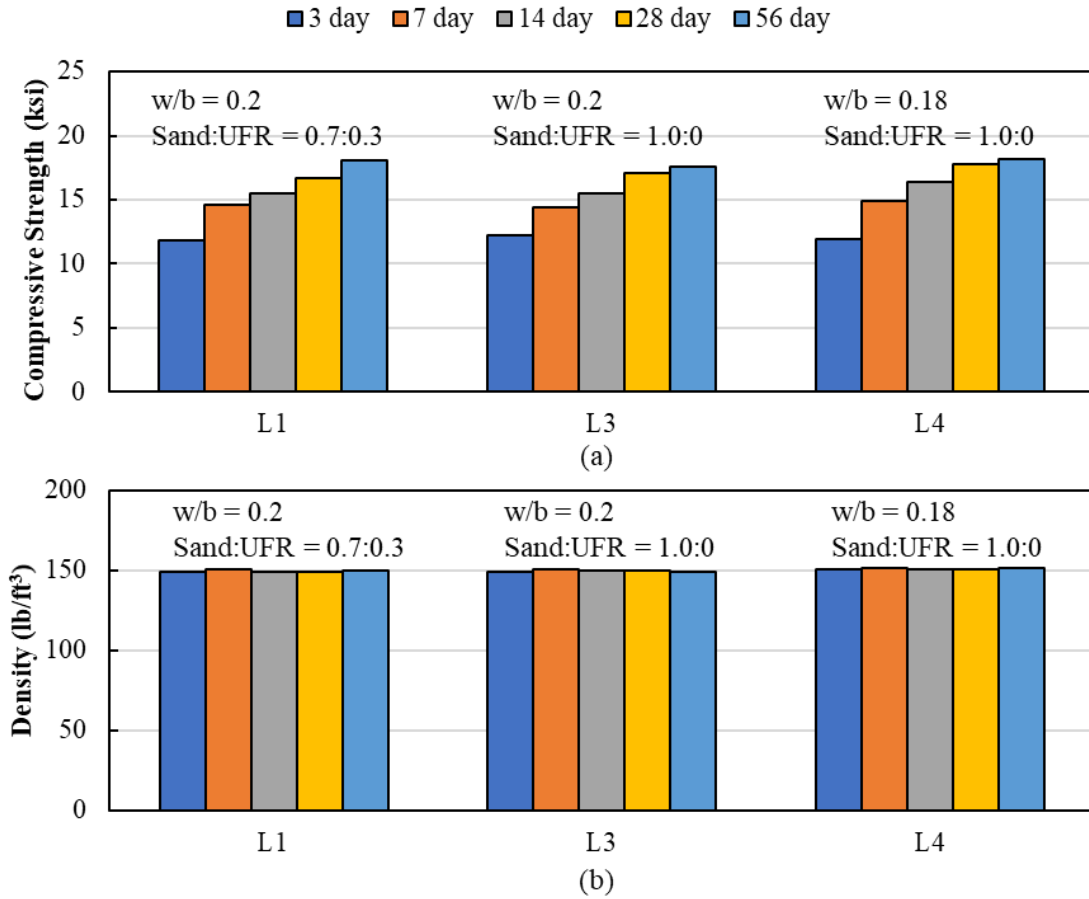
Figure 4.39: Effect w/b and UFR on (a) compressive strength and (b) density

The compressive strength and density for the two mix designs used to compare the behavior of materials from Oklahoma (OK) compared to those from south Florida (FL) are shown in Figure 4.40. The compressive strength for L2 (OK) was 2.9 and 3.4 percent higher than L3 (FL) at 28 and 56 days, respectively. The density for the mixtures with OK materials was on average 2.3 percent higher than that made with the FL materials.
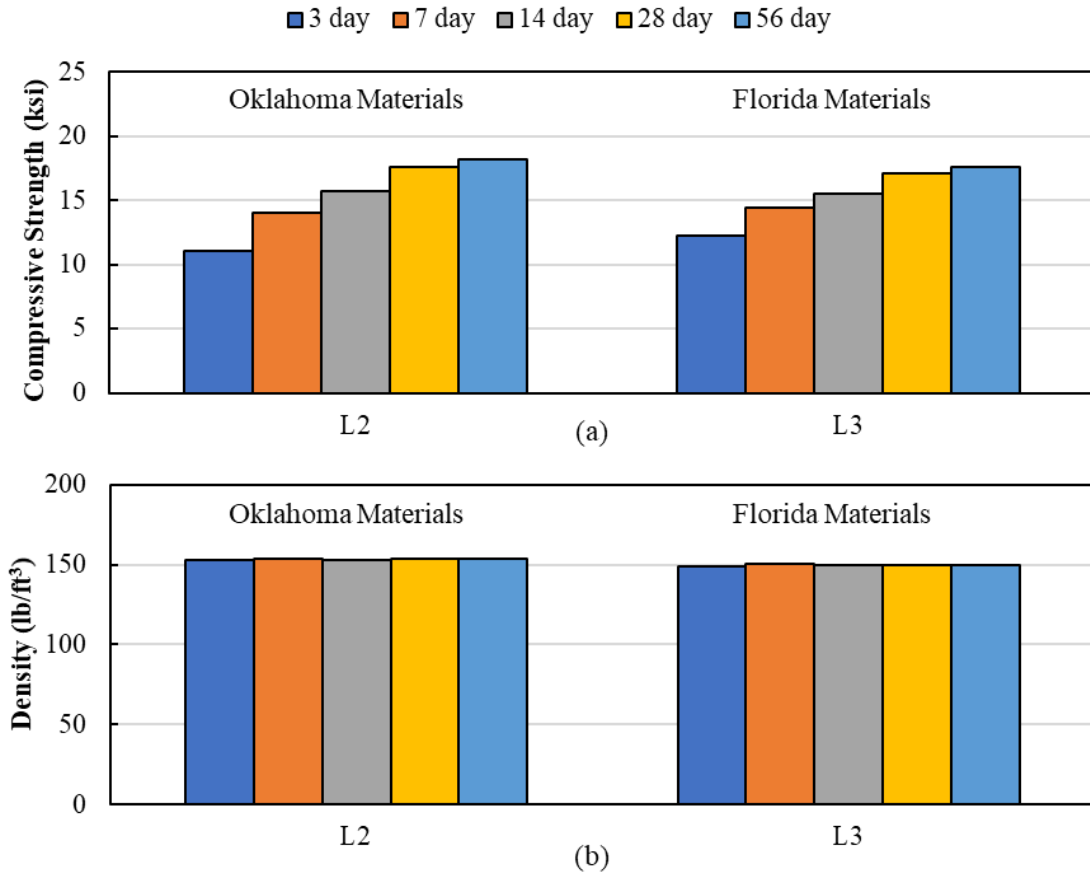
Figure 4.40: Effect of material source on (a) compressive strength and (b) density

The percent difference between the specimens that were moist-cured and those that were not moist cured for compressive strength and density is shown in Figure 4.41. The moist curing of the cylinders did not have a significant effect on the compressive strength or density of the specimens. The average of all the results was 0.8 percent higher compressive strength and 0.3 percent higher density for specimens that were moist cured compared to those that were kept in the capped cylinders until testing. Moist curing likely did not have a significant effect on compressive strength and density because of the low permeability of UHPC.
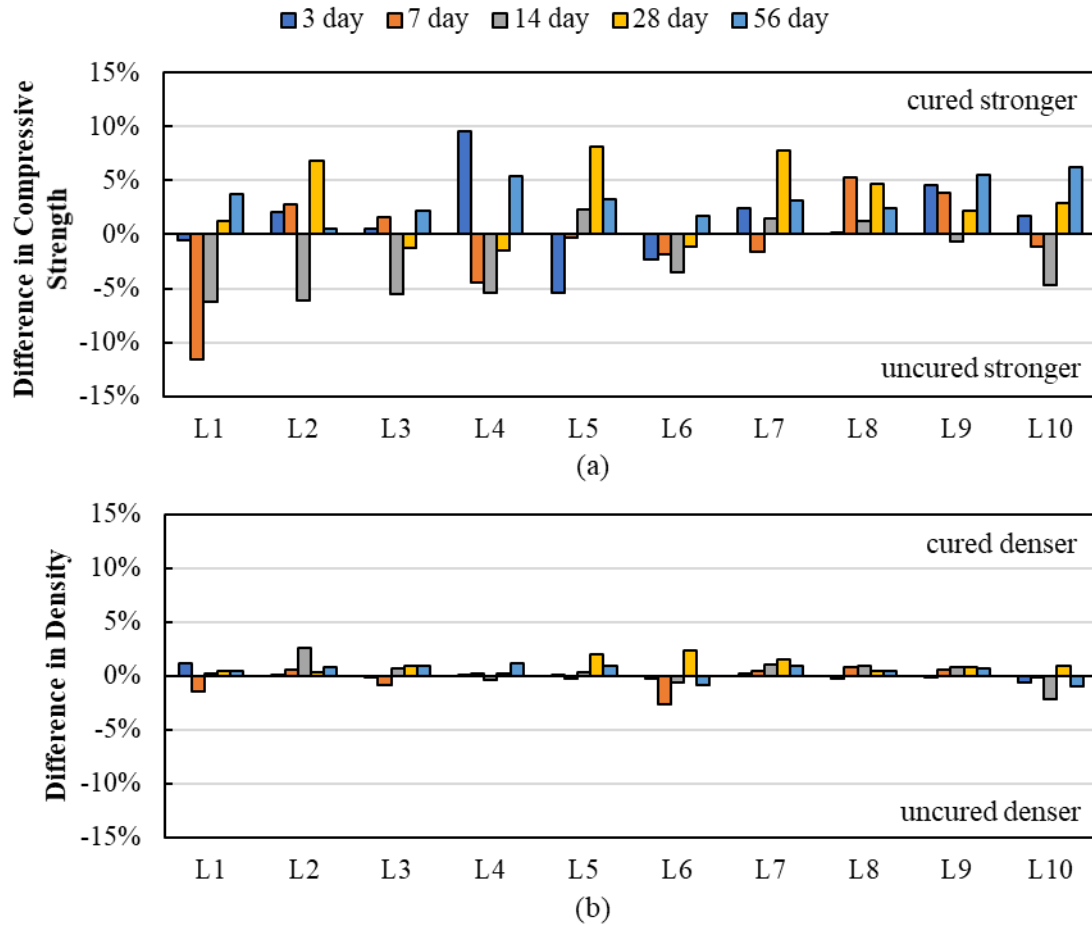
Figure 4.41: Effect of moist curing on (a) compressive strength and (b) density

4.2.6.4. Modulus of Elasticity Results

Modulus of elasticity was measured using 3 in. by 6 in. cylinders at 28 days for moist-cured and uncured samples. The modulus of elasticity was measured using ASTM C469 [100] as discussed in §4.2.5.4. A summary of the average measured modulus of elasticity for all large-scale batches is shown in Table 4-20. The measured modulus for the large-scale batches was between 7,100 and 9,500 ksi, which is in the same range for UHPC (4,250 to 8,000 ksi) found by previous researchers [48].

Moist curing did lead to a higher modulus of elasticity on average for all the specimens; the average modulus of all the moist cured samples was 7.5 percent higher than the average of all the uncured samples, as shown in Table 4-20. The effect of moist curing was more pronounced in the samples cast to investigate fiber type and fiber content (L3 and L5 to L10). L1 and L4 were positively influenced by moist curing; this is likely due to lower permeability due to better particle packing for L1 and lower w/b for L4.

Table 4-20: Results of modulus of elasticity

Mix.	w/b	Sand:UFR	Fiber		Modulus of Elasticity (ksi)		
			Type	Content	Uncured	Cured	Avg.
L1	0.20	0.7:0.3	OL	2.0%	8,867	8,734	8,767
L2	0.20	1:0	OL	2.0%	8,495	8,937	8,826
L3	0.20	1:0	OL	2.0%	7,247	7,979	7,796
L4	0.18	1:0	OL	2.0%	9,471	9,035	9,144
L5	0.20	1:0	HF	2.0%	7,863	9,202	8,867
L6	0.20	1:0	A	1.5%	8,241	9,415	9,122
L7	0.20	1:0	OL	4.0%	8,038	9,007	8,765
L8	0.20	1:0	HF	4.0%	7,884	8,940	8,676
L9	0.20	1:0	Sy	2.0%	7,158	7,699	7,293
L10	0.20	1:0	Sy	1.0%	7,865	8,241	8,147
Average =					8,113	8,719	8,540

The average measured modulus of elasticity for the large-scale batches used to evaluate fiber type and fiber content are shown in Figure 4.42. Increasing fiber content from 2 to 4 percent increased the modulus by an average of 12.2 percent for the Dramix OL 13/.20 (OL) fibers; going from 7,796 ksi for L3 to 8,765 ksi for L7). Increasing the fiber content from 2 to 4 percent decreased the average modulus for the Hiper Fiber Type A (HF) by 2.2 percent, going from 8,867 ksi for L5 to 8,676 ksi for L8. There is an inherent uncertainty

in modulus testing, which may have been the cause of the slight difference between measured moduli.

The modulus of samples with HF fibers at 2 percent was 13.7 percent higher than the modulus of samples with OL fibers at 2 percent (comparing L5 and L3). The modulus of samples with 4 percent fibers were similar between those with HF and OL fibers (comparing L7 and L8). The modulus of the samples with the Dramix 4D 65/35BG (A) was higher than the samples with HF and OL fibers.

The use of synthetic fibers led to the lowest stiffness among the samples (see L9 and L10). Decreasing the synthetic fiber content from 2 to 1 percent increased the modulus by 11.7 percent.
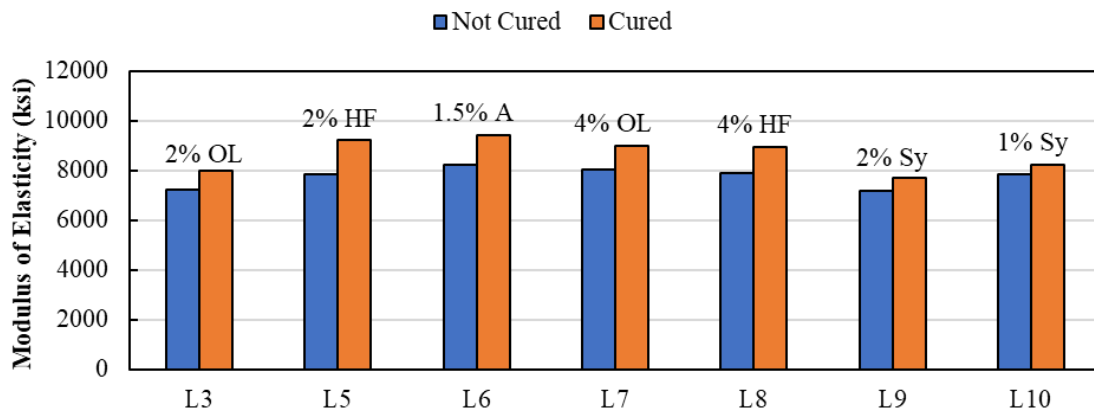
Figure 4.42: Effect of fiber type and content on modulus of elasticity

The average stress versus strain plots for the large-scale batches used to evaluate fiber type and fiber content are shown in Figure 4.43.
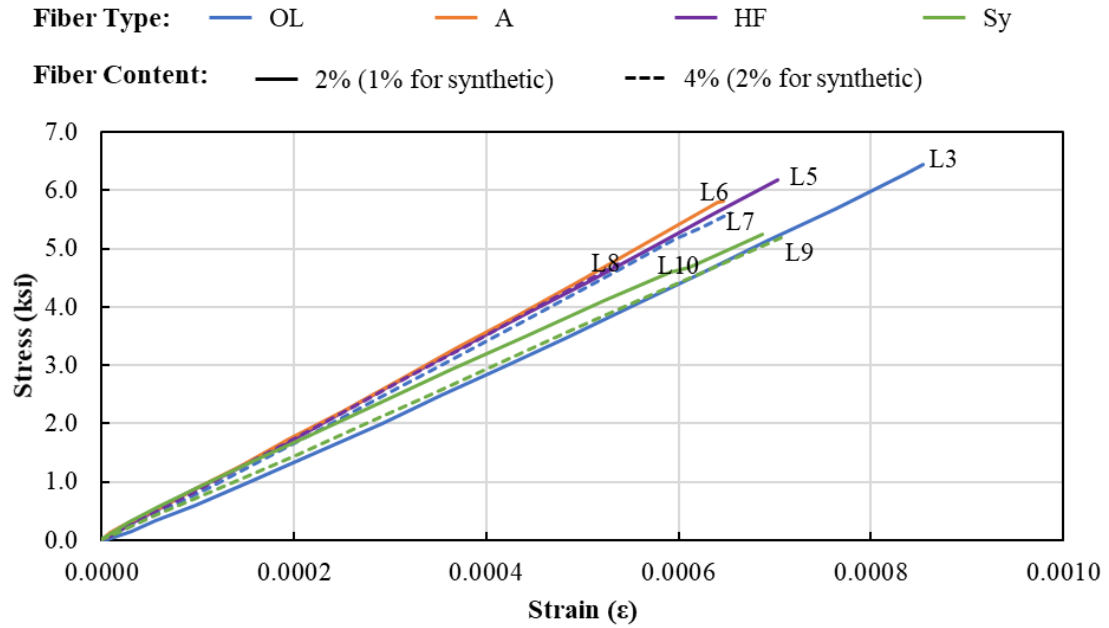
Figure 4.43: Effect of fiber type and content on the modulus of elasticity

The measured average modulus of elasticities for the large-scale batches used to evaluate the effect of w/b and UFR and the source of the constituent materials are shown in Figure 4.44. A lower w/b led to an increase in the modulus of elasticity; samples with w/b of 0.18 (L4) had an average 17.3 percent larger modulus than the similar samples with w/b of 0.20 (L3). The use of UFR also increased the average modulus of elasticity; samples with 30 percent UFR replacement (L1) had an average 12.5 percent higher modulus than the similar samples with all fine masonry sand (L3).

The samples with material from Oklahoma (OK, L2) had an average 13.2 percent higher modulus than the similar sample with materials from south Florida (FL, L3).
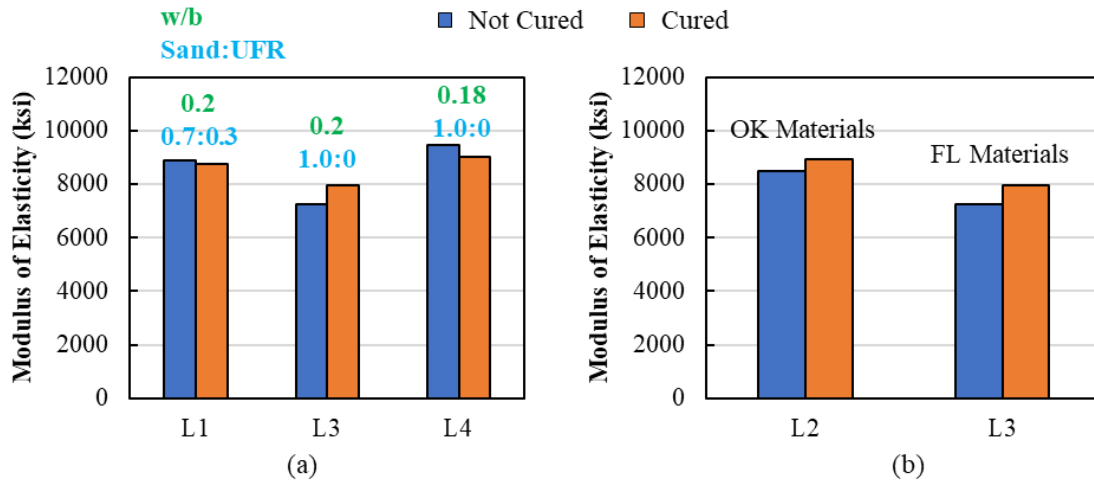
Figure 4.44: Effect of (a) w/b and UFR and (b) material source on modulus of elasticity

4.2.6.5. Splitting Tensile Strength Results

Splitting tensile strength tests were conducted on both moist cured (3 samples) and uncured samples (3 samples) at 28 days after casting the UHPC. Results of the average splitting tensile strength tests for all large-scale batches are summarized in Table 4-21. Similar to the compressive strength, moist curing did not have an effect on the splitting tensile strength, see similar averages in Table 4-21.

Table 4-21: Splitting tensile strength at 28 days

Mix.	w/b	Sand:UFR	Fiber		Split Tensile Strength (ksi)		
			Type	Content	Uncured	Cured	Avg.
L1	0.20	0.7:0.3	OL	2.0%	2.68	2.54	2.61
L2	0.20	1:0	OL	2.0%	2.49	2.76	2.62
L3	0.20	1:0	OL	2.0%	2.61	2.73	2.67
L4	0.18	1:0	OL	2.0%	2.81	2.87	2.84
L5	0.20	1:0	HF	2.0%	3.06	2.80	2.93
L6	0.20	1:0	A	1.5%	2.45	2.33	2.39
L7	0.20	1:0	OL	4.0%	2.80	2.90	2.85
L8	0.20	1:0	HF	4.0%	2.85	2.75	2.80
L9	0.20	1:0	Sy	2.0%	1.45	1.30	1.38
L10	0.20	1:0	Sy	1.0%	1.46	1.53	1.49

The average measured splitting tensile strength for the large-scale batches used to evaluate fiber type and fiber content are shown in Figure 4.45. There was a slight increase in the average tensile strength with an increased fiber content for the Dramix OL 13/.20 (OL) fibers (L3 and L7), increasing from 2.67 ksi to 2.85 ksi (6.7 percent increase). There was actually a slight decrease in the splitting tensile strength with increased fiber content for the Hiper Fiber Type A (HF) fibers (L5 and L8), decreasing from 2.93 ksi to 2.80 ksi (4.4 percent decrease). The splitting tensile strength with HF fibers at 2 percent was 11.2 percent higher than the splitting tensile of samples with OL fibers at 2 percent (comparing L5 and L3). The Dramix 4D 65/35BG (A) had the lowest splitting tensile strength for the steel fibers, 2.39 ksi average for L6. The synthetic fibers had a 47 percent lower splitting tensile strength than the steel fibers on average (2.71 ksi average for steel fibers compared to 1.44 ksi average for synthetic fibers).
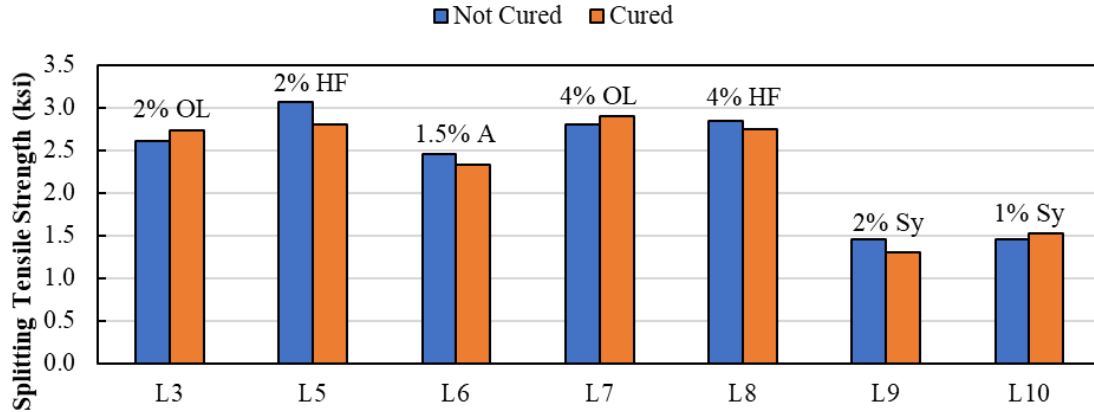
Figure 4.45: Effect of fiber type and content on splitting tensile strength

The splitting tensile strengths for the large-scale batches cast to investigate w/b and UFR

content are shown in Figure 4.46. Using a w/b ratio of 0.18 led to an increase in the splitting

tensile strength of 6.4 percent (average of 2.67 ksi for L3 and 2.84 ksi for L4). Using UFR

led to a slight (2.3 percent) decrease in the splitting tensile strength (average of 2.61 ksi for

L1 and 2.67 ksi for L3).
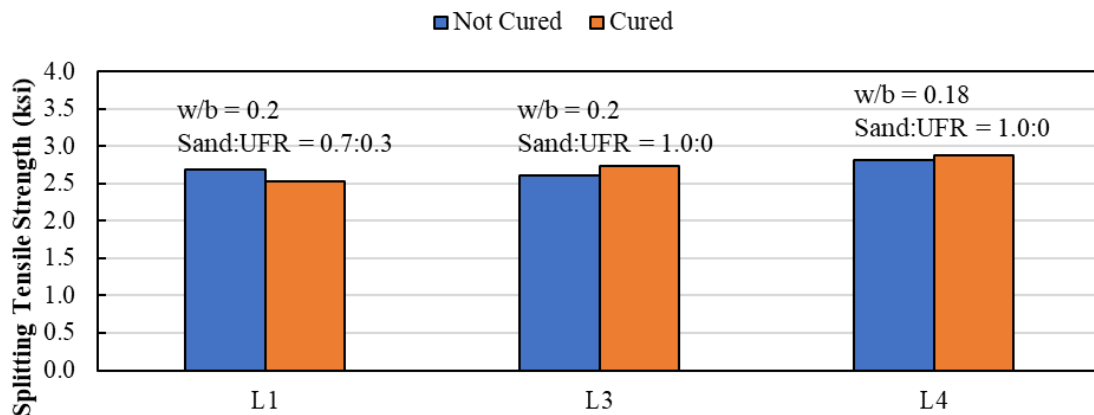
Figure 4.46: Effect of w/b and UFR on splitting tensile strength

The splitting tensile strength for the similar large-scale batches with Oklahoma (OK, L2)

and south Florida (FL, L3) materials are shown in Figure 4.47. The mixtures with the FL

materials had a slightly higher (1.7 percent) splitting tensile strength compared to the mixtures with OK materials.
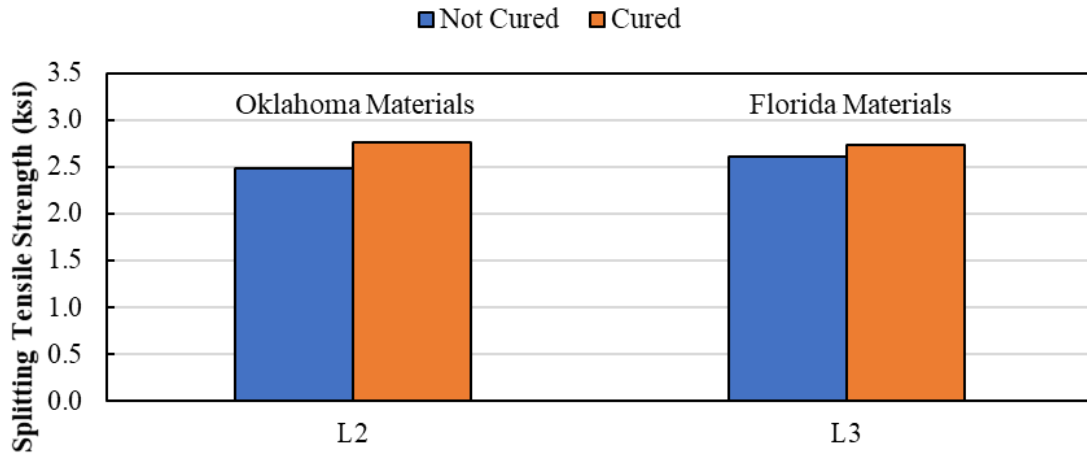
Figure 4.47: Effect of material source on splitting tensile strength

4.2.6.6. Modulus of Rupture Results

Modulus of rupture (MOR) tests were conducted on 3 in. by 3 in. by 11 in. prism beams to measure the flexural strength of UHPC samples. This test can be considered as an indirect way of evaluating the tensile behavior of UHPC. The MOR test was performed based on ASTM C78 [99] as described in §4.2.5.6. Equipment capable of testing the direct tensile strength of the UHPC was not available to the research team at the time of this project. A summary of the average MOR results is shown in Table 4-22. The average splitting tensile strength from §4.2.5.6 are also included in Table 4-22 for comparison. On average, the MOR test resulted in a 7.6 percent higher estimated tensile strength than the splitting tensile strength test. MOR and splitting tensile strengths were within 10 percent of each other for L1, L3, L4, L7, and L9.

Table 4-22: Average measured modulus of rupture for large-scale batches

Mix.	w/b	Sand:UFR	Fiber		MOR (ksi)	Avg. Split Tensile Strength (ksi)	Percent Difference
			Type	Content			
L1	0.20	0.7:0.3	OL	2.0%	2.83	2.61	7.8%
L2	0.20	1:0	OL	2.0%	-*	2.62	-
L3	0.20	1:0	OL	2.0%	2.49	2.67	-7.3%
L4	0.18	1:0	OL	2.0%	2.89	2.84	1.8%
L5	0.20	1:0	HF	2.0%	3.65	2.93	19.8%
L6	0.20	1:0	A	1.5%	3.24	2.39	26.0%
L7	0.20	1:0	OL	4.0%	3.13	2.85	8.9%
L8	0.20	1:0	HF	4.0%	4.05	2.80	30.9%
L9	0.20	1:0	Sy	2.0%	1.34	1.38	-3.3%
L10	0.20	1:0	Sy	1.0%	1.29	1.49	-15.8%
Average =					2.77	2.46	7.6%

*Modulus of rupture for the L2 mix design was initially found based on a 3-point-load test setup; additional samples could not be cast due to limited amount of material from OU. Modulus or rupture strengths were found using a 4-point-load test setup for all other mixes.

The average measured MOR for the large-scale batches used to evaluate fiber type and fiber content are shown in Figure 4.48. An increased fiber content increased the average MOR for both Dramix OL 13/.20 (OL) and Hiper Fiber Type A (HF) fibers; increasing from 2 to 4 percent fiber content increased the MOR by 25.8 percent for the OL fibers and 10.9 percent for the HF fibers. The HF led to a higher MOR than the OL fibers for similar fiber contents: 46.8 percent higher MOR for 2 percent and 29.4 percent higher for 4 percent fiber contents. The difference in MOR between OL and HF was unexpected since these fibers have the same dimensions and specified properties.

The Dramix 4D 65/35BG (A) had a MOR higher than the OL fibers, but less than the HF fibers. The MOR for the synthetic fibers was about half of the MOR for batches with 2 percent OL fibers.
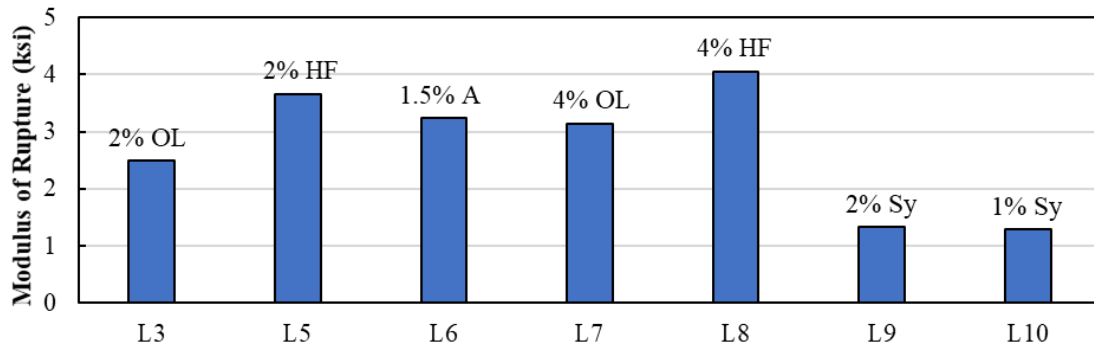
Figure 4.48: Effect of fiber type and fiber content on modulus of rupture

The average flexural stress versus displacement curves for the large-scale batches used to evaluate fiber type and fiber content are shown in Figure 4.49. These curves show the average peak flexural stress and the ductility of the beams in flexure before failure. This behavior is much different than typical concrete MOR beams, which fail immediately after cracking.
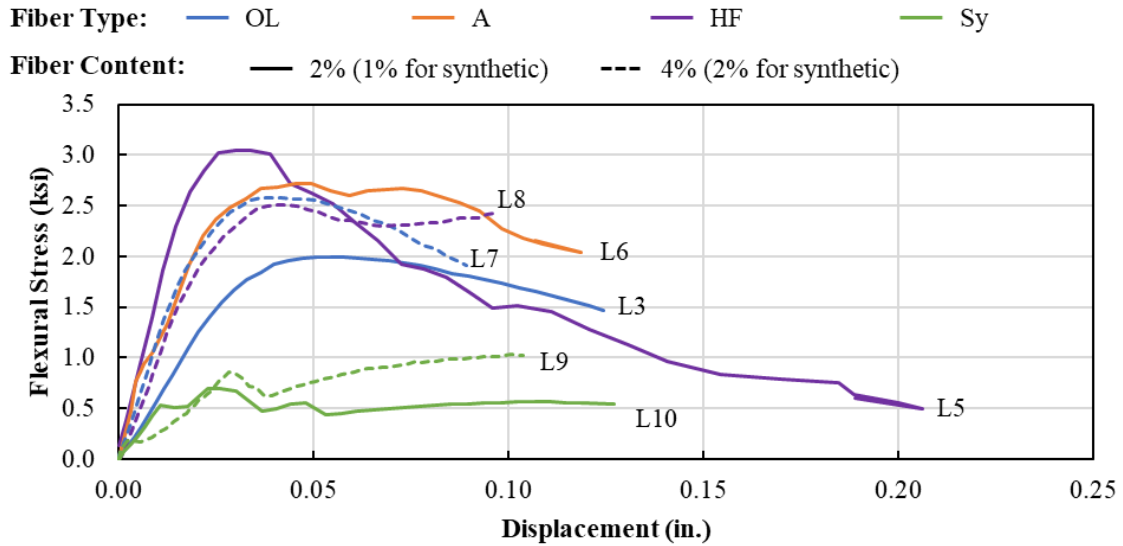
Figure 4.49: Flexural stress versus midspan displacement curves for samples investigating the effect of fiber type and content on the modulus of rupture

The measured MOR used to evaluate the effect of w/b and UFR content are shown in Figure 4.50. The average MOR was 16.3 percent higher when the w/b was decreased from 0.20 to 0.18. The MOR was 13.6 percent higher for the specimens with a 30 percent UFR replacement.
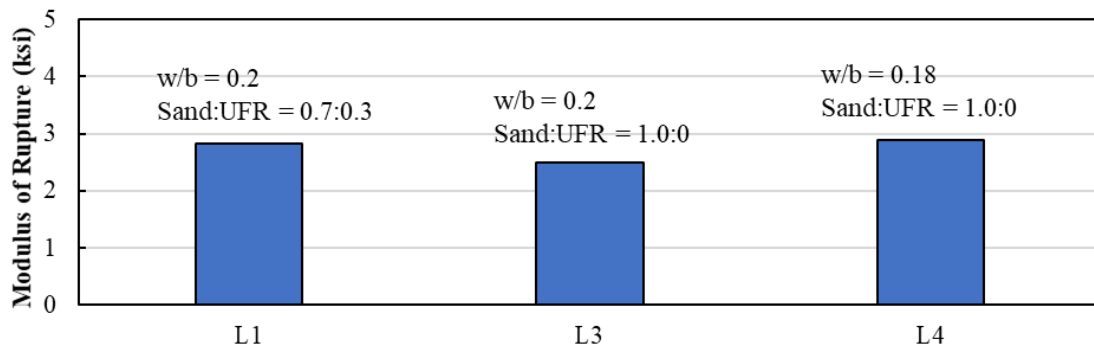
Figure 4.50: Effect of w/b and UFR on modulus of rupture

The average flexural stress versus displacement curves for the large-scale batches used to evaluate w/b and UFR are shown in Figure 4.51.
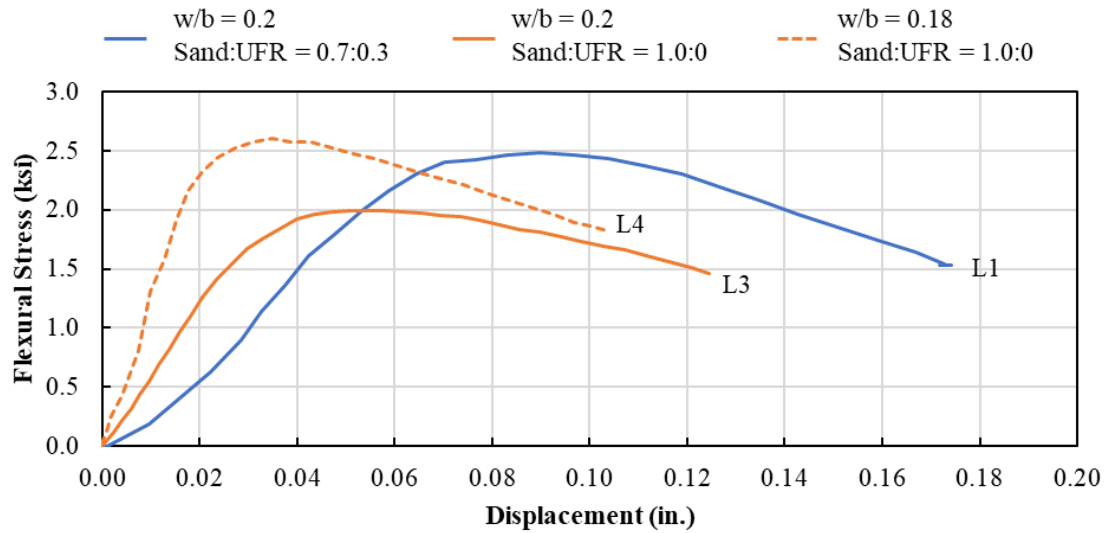
Figure 4.51: Flexural stress versus midspan displacement curves for samples investigating the effect of w/b and using UFR on the modulus of rupture

4.2.6.7. Bulk Resistivity Test Results

Many current uses for UHPC require good chloride penetration resistance especially where it is used in structural elements subject to marine or deicer exposures or in contact with chloride-containing soils or groundwater, e.g., joints, overlays, splash zone repairs. The bulk resistivity test was performed according to ASTM C1760-12 [97] as described in §4.2.5.7. The average bulk resistivity readings for all large-scale batches are summarized in

Table 4-23. The steel fibers seemed to influence the results. The researchers could not find any bulk resistivity comparison points for UHPC, so two additional mixtures were tested

using Ductal® (one with 0 percent fibers, D1, and one with 2 percent fibers, D2). The measurement shown for D1 was based on the maximum range for the Resipod device.

Table 4-23: Bulk resistivity test results

Mix.	w/b	Sand:UFR	Fiber		Bulk Resistivity (kΩ.cm)					
			Type	Content	3 day	7 day	14 day	28 day	56 day	90 day
L1	0.20	0.7:0.3	OL	2.0%	1.4	2.3	4.9	6.6	12.9	21.9
L2	0.20	1:0	OL	2.0%	1.1	3.6	5.0	5.4	11.7	23.1
L3	0.20	1:0	OL	2.0%	4.5	7.0	9.6	15.5	23.8	38.9
L4	0.18	1:0	OL	2.0%	3.1	6.5	9.9	15.5	31.7	56.5
L5	0.20	1:0	HF	2.0%	5.2	8.2	8.3	11.7	23.8	44.9
L6	0.20	1:0	A	1.5%	3.9	5.4	7.5	10.9	16.3	31.9
L7	0.20	1:0	OL	4.0%	2.2	4.2	8.6	11.6	16.2	31.2
L8	0.20	1:0	HF	4.0%	1.4	3.0	7.1	9.4	13.1	25.0
L9	0.20	1:0	Sy	2.0%	9.7	13.7	30.4	59.2	114.8	182.1
L10	0.20	1:0	Sy	1.0%	8.7	11.5	27.2	64.3	137.6	183.4
D1	C-UHPC		OL	0.0%	204.5	204.5	204.5	204.5	204.5	204.5
D2	C-UHPC		OL	2.0%	9.7	15.1	26.2	47.1	78.3	125.3

The typical classification of permeability measurements for bulk resistivity and surface resistivity are shown in Table 4-24 based on Nugent [122]. The measured bulk resistivity for all large-scale batches would be in the very low classification for concrete permeability.

Table 4-24: Classification of permeability measurements by test method [122]

Classification	RCP (C)	Bulk Resistivity (kΩ-cm)	Surface Resistivity (kΩ-cm)
High	> 4000	< 5	< 12
Moderate	2000 to 4000	5 to 10	12 to 21
Low	1000 to 2000	10 to 20	21 to 37
Very Low	100 to 1000	20 to 200	37 to 254
Negligible	< 100	> 200	> 254

The average measured bulk resistivity over time for the large-scale batches used to evaluate fiber type and fiber content are shown in Figure 4.52. The specimens with steel fibers had significantly smaller bulk resistivity measurements than those without steel fibers or with synthetic fibers. The measured bulk resistivity of the mixtures with synthetic fibers (L9 and L10) was about 3.5 times larger that of the similar mixtures with steel fibers (L3 and L5 to L8).
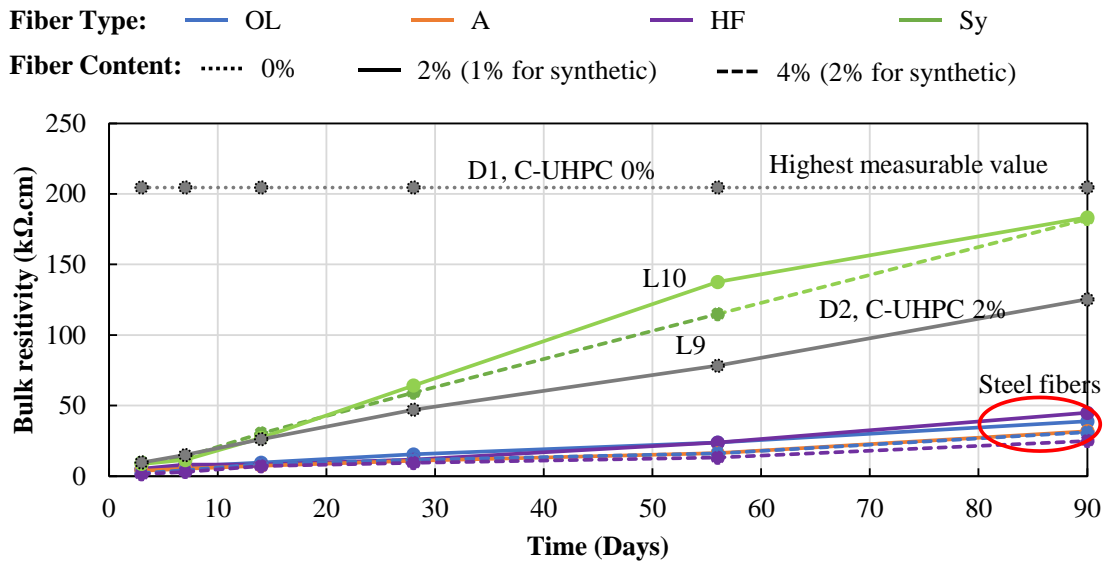
Figure 4.52: Effect of fiber type and content on bulk resistivity

The average measured bulk resistivity over time for the large-scale batches used to evaluate steel fiber type and content are shown in Figure 4.53. A higher fiber content led to a lower bulk resistivity measurement: going from 2 to 4 percent fibers decreased the bulk resistivity by 44 percent for HF fibers and 20 percent for OL fibers.
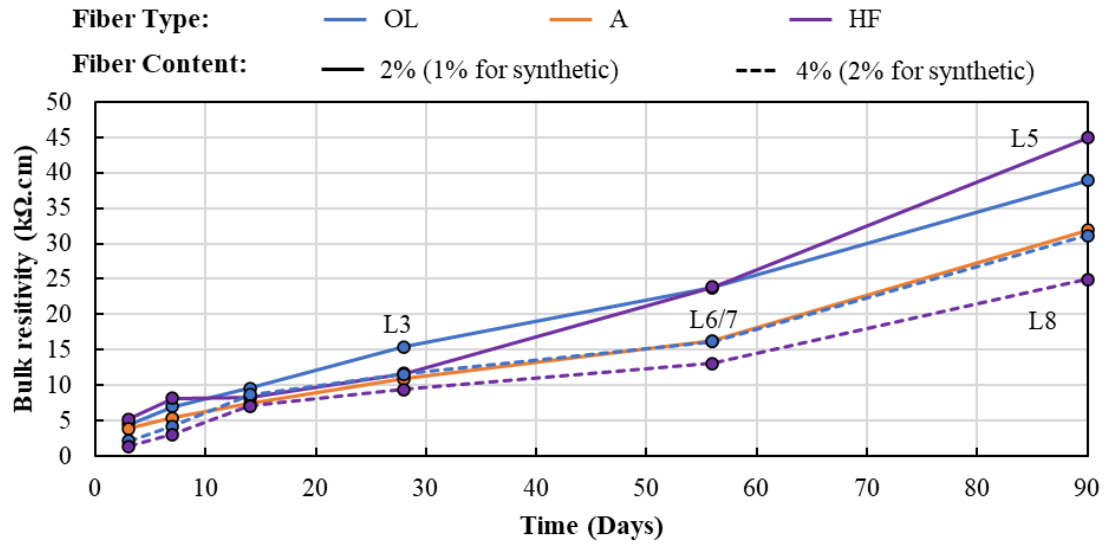
Figure 4.53: Effect of steel fiber type and content on bulk resistivity

The measured bulk resistivity values used to evaluate the effect of w/b and UFR content are shown in Figure 4.54. The bulk resistivity was 45 percent higher at 90 days for w/b of 0.18 compared to 0.20, which is consistent with the specimens with w/b of 0.18 having a lower permeability. The bulk resistivity was lower for the specimens with UFR than those without. It is unclear why the use of UFR led to lower bulk resistivity, but this could have had to do with fiber alignment in the UFR specimens.
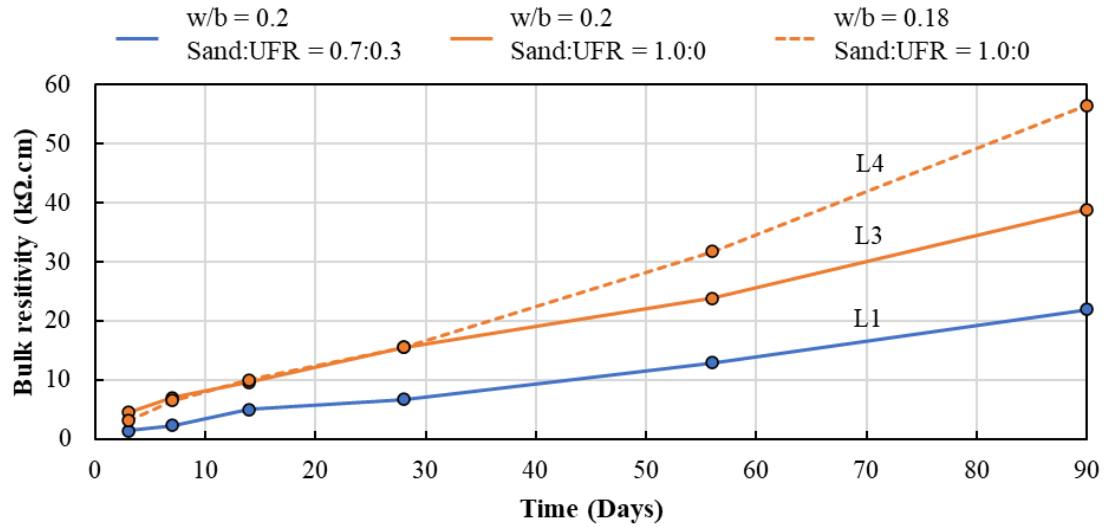
Figure 4.54: Effect of w/b and UFR on bulk resistivity

The bulk resistivity for the similar large-scale batches with Oklahoma (OK, L2) and south Florida (FL, L3) materials are shown in Figure 4.55. The specimens with FL materials had a 68 percent higher bulk resistivity than those with the OK materials.
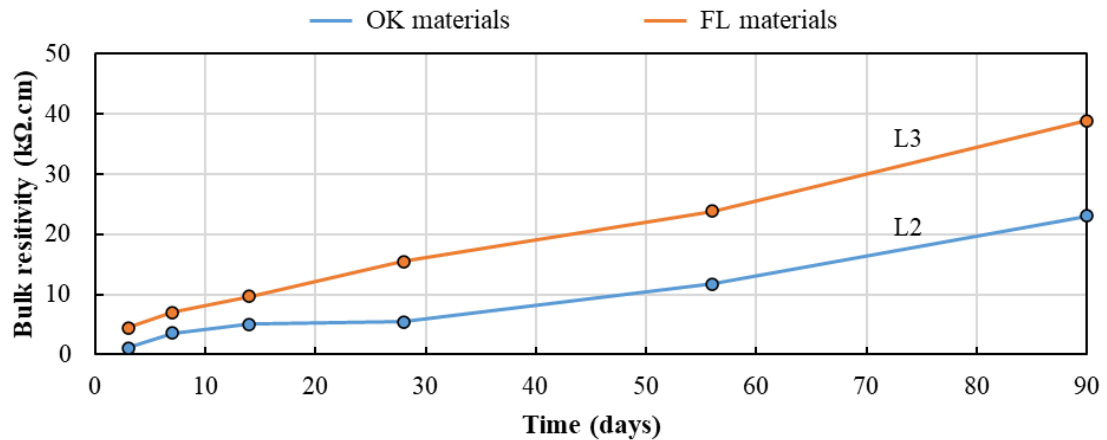
Figure 4.55: Effect of material source on bulk resistivity

In general, the presence of steel fibers in UHPC seems to influence the reading of bulk resistivity. The fibers help to create a path for current flow with less resistance than the concrete matrix itself, as illustrated in Figure 4.56. Specimens with synthetic fibers with

148

similar fiber content would give a better approximation of the bulk resistivity of the concrete matrix with fibers.
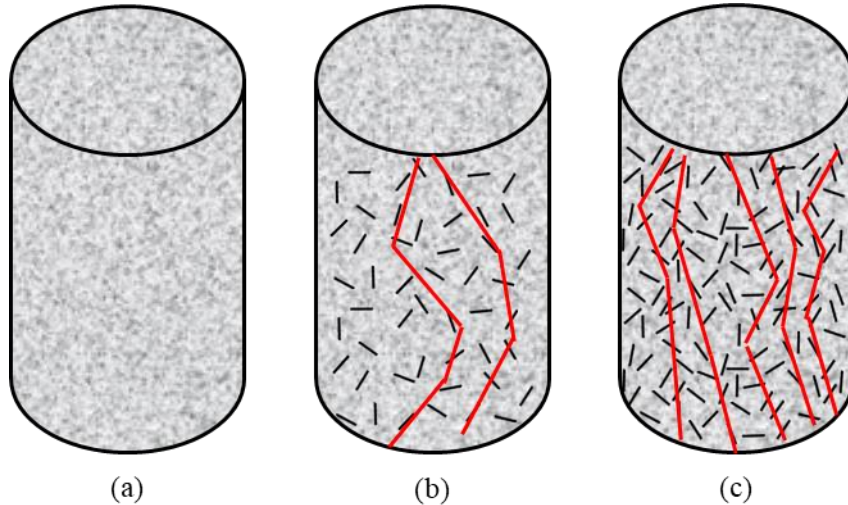
Figure 4.56: Schematic of formation of the conductive path in cylinder samples; (a) 0% fiber content, (b) medium fiber content, and (c) high fiber content

No additional weight or clamping was applied to the bulk resistivity end plates for the general testing. An additional study was performed on the bulk resistivity samples when the samples were between 178 and 200 days old to investigate the effect of different clamping forces on the change in bulk resistivity reading with change in clamping force. Different numbers of half-pound weights were stacked on top of the top electrical plate to investigate if there was any effect on the readings. A summary of the raw data readings for the four samples from L1 are shown in Table 4-25. The additional weight provided on the testing apparatus decreased the resistivity by an average of 0.5 percent for all the test specimens (ranging between 0 and 2.2 percent).

Table 4-25: Example of raw bulk resistivity readings under different weights from L1 samples

L1 Sample	K (A/L)	Bulk Resistivity Readings (kΩ-cm)							
		0.0 lb	0.5 lb	1.0 lb	1.5 lb	2.0 lb	2.5 lb	3.0 lb	3.5 lb
1	1.78	491	487	484	483	482	481	481	480
2	1.73	588	586	585	584	583	583	583	583
3	1.70	363	360	359	359	358	358	357	356
4	1.71	529	528	528	527	527	526	526	526

The results were also compared to four-point Wenner array probe resistivity readings when the samples were between 178 and 200 days also using the Resipod device. The resistivity measured by the Resipod was modified based on two different correction factors from Morris et al. [123] and the Resipod Operating Instructions [121]. Morris et al. [123] proposed Figure 4.57 for determining the correction factor. The following values can be determined based on the cylinder dimensions and probe spacing for the Resipod device.

$$\frac{L}{a} = \frac{8"}{1.5"} = 11.1 \qquad\qquad \frac{d}{a} = \frac{4"}{1.5"} = 2.67$$

Using these values in Figure 5.40 gives a correction factor of $k = 2.0$.
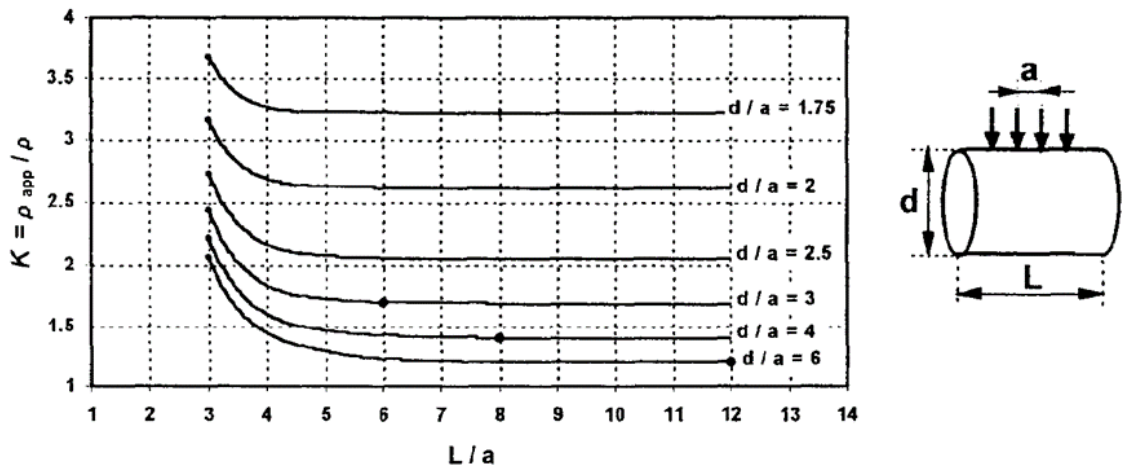
Figure 4.57: Cell constant correction to determine concrete resistivity [123]

The Resipod Operating Instructions [121] recommends the geometric correction factor shown in Equation 4-16.

$$k = \frac{2\pi}{1.09 - \dfrac{0.527}{d/a} + \dfrac{7.34}{\left(d/a\right)^2}} \qquad \text{Equation 4-16}$$

$$k = \frac{2\pi}{1.09 - \dfrac{0.527}{4"/1.5"} + \dfrac{7.34}{\left(4"/1.5"\right)^2}} = 3.26$$

A comparison between the average bulk resistivity and average four-point Wenner array probe using the two different correction factors are shown in Figure 4.58. Results should be consistent between the bulk resistivity and Wenner array probe measurements. There is a reasonable consistency between bulk resistivity and Wenner array probe measurements using the Morris et al. [123] correction factor for mixes L1 through L8 (average difference of 17 percent). There was a larger difference using the correction from the Resipod Operating Instructions [121] (average difference of 44 percent).
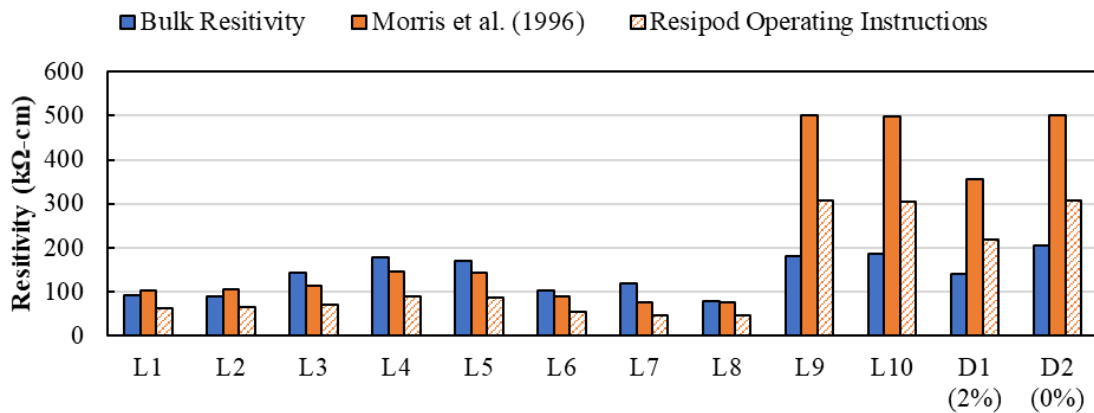
Figure 4.58: Comparison between bulk resistivity and 4-point Wenner array probe measurements using the average of all test results in each mix design

There was noticeably more variation between readings for the Wenner array probe measurements compared to those from the bulk resistivity. The mean, standard deviation, and coefficient of variation for the resistivity measurements taken on samples from the large-scale batches are shown in Table 4-26. For L1 through L8, the average coefficient of variation for the bulk resistivity measurements was 0.153 compared to 0.222 for the measurements using the Wenner array probe. The increased variability for the Wenner array probe may have been due to the steel fiber distribution in the samples having a larger impact on the measurement than in the bulk resistivity test.

Table 4-26: Mean, standard deviation, and coefficient of variation for resistivity measurements taken on large-scale batch samples

Mix		L1	L2	L3	L4	L5	L6	L7	L8	L9	L10
Bulk Resistivity	Mean	90.8	89.6	142.5	177.5	170.6	102.6	118.9	78.0	179.5	185.9
	St. Dev.	18.0	8.8	32.6	7.6	7.2	16.9	39.4	9.1	1.6	5.9
	CoV	0.198	0.098	0.228	0.043	0.042	0.165	0.331	0.117	0.009	0.032
Wenner Array Probe	Mean	103.2	106.0	114.7	146.0	141.9	90.1	76.3	76.5	500.0	499.2
	St. Dev.	24.8	24.3	17.1	22.5	13.9	36.2	19.5	18.9	0.0	2.7
	CoV	0.240	0.229	0.149	0.154	0.098	0.402	0.255	0.247	0.000	0.005

Bulk resistivity appears to be more consistent than four-point resistivity measurements using the Wenner array probe.

4.2.6.8. Shrinkage Results

Shrinkage was measured on 6 in. by 12 in. cylinders using vibrating wire strain gauges (VWSG) using the procedure described in §4.2.5.8. Three specimens were prepared per large batch, and all were connected to the data acquisition center. Unfortunately, due to

some issues (e.g., power shut down, software programing issues, and human errors) some early readings were lost. The research team is planning on repeating the shrinkage tests for the mixture designs with incomplete data.

A summary of the available shrinkage data for the large-scale batches is provided in Table 4-27 with shrinkage strains highlighted at 7, 30, and 90 days after casting.

Table 4-27: Summary of shrinkage strains for large-scale batches (will be updated later for other mixtures)

Mix.	w/b	Sand:UFR	Fiber		Shrinkage Strain (με)		
			Type	Content	7-day	30-day	90-day.
L1	0.20	0.7:0.3	OL	2.0%	556	668	711
L2	0.20	1:0	OL	2.0%	-	-	-
L3	0.20	1:0	OL	2.0%	595	696	740
L4	0.18	1:0	OL	2.0%	451	521	552
L5	0.20	1:0	HF	2.0%	450	530	560
L6	0.20	1:0	A	1.5%	413	496	526
L7	0.20	1:0	OL	4.0%	593	668	718
L8	0.20	1:0	HF	4.0%	470	555	594
L9	0.20	1:0	Sy	2.0%	403	475	552
L10	0.20	1:0	Sy	1.0%	513	600	670
Average =					470	549	596

The shrinkage development over time during the first few months after casting for four of the large-scale batches is shown in Figure 4.59. A higher volume (2 percent versus 1 percent) of synthetic fibers led to an average 21.4 percent decrease in the total measured shrinkage strain at 90 days after casting.
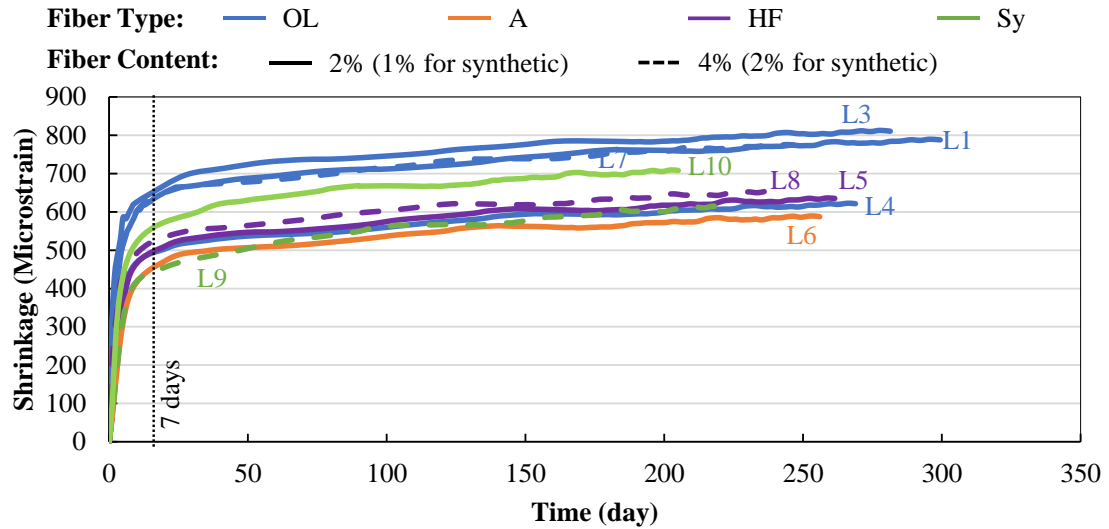
Figure 4.59: Effect of fiber type and content on shrinkage

4.2.6.9. Summary and Observations

Ten (10) large-scale batches were cast to investigate the effect of (a) different fiber types and fiber contents, (b) w/b and UFR content, and (c) source of constituent materials on the performance of the developed UHPC mixtures. The following tests were performed to determine the mechanical properties of the UHPC mixtures:

- Flowability

- Setting time

- Compressive strength

- Modulus of elasticity

- Splitting tensile strength

- Modulus of rupture

- Bulk resistivity

- Shrinkage

Some of main observations from the large-scale batches are listed below (organized by test).

1. **Flowability**: Flow should be kept between 8 and 10 inches to help prevent fiber settlement and ensure sufficient workability and working time. This was achieved using a HRWR dosage between 22 and 29.4 oz./cwt. A typical dosage of 27.5 oz./cwt could be used for all mixtures with w/b of 0.20 and with only fine masonry sand (i.e., no UFR).

2. **Set Time**: Initial set times varied between 4.3 and 6.3 hours; final set times varied between 8.0 and 11.5 hours. Mixtures with higher fiber contents had shorter final set times. Lower w/b and UFR substitution had shorter initial and final set times.

3. **Compressive Strength**: Mixtures with steel fibers, w/b of 0.2, and no UFR had average compressive strengths between 17.0 and 17.6 ksi at 28 days. There was no clear trend between steel fiber type and fiber content and compressive strength. The mixtures with synthetic fibers had a 36 percent lower strength than steel fibers for 2 percent synthetic fibers and 12.4 percent lower strength for 1 percent synthetic fibers (at 28 days). Decreasing the w/b from 0.20 to 0.18 slightly increased the compressive strength (between 2 and 6 percent depending on concrete age). The compressive strength for the concrete with materials from Oklahoma had a slightly higher compressive strength (around 3 percent higher). Moist curing did not consistently affect the compressive strength.

4. **Density**: The average measured density of the UHPC varied between 148 and 155 pcf for the mixtures with steel fibers. The average measured density was less for the mixtures with synthetic fibers, between 141 and 145 pcf. Mixtures with 4

percent steel fibers had about a 3 percent higher density than the similar mixtures with 2 percent steel fibers. The higher amount of synthetic fibers (2 percent) decreased the density of the mix by about 2 percent compared to the 1 percent synthetic fiber mixture.

5. **Modulus of Elasticity**: The average modulus of elasticity varied between 7,796 and 9,144 ksi for the mixtures with steel fibers and 7,293 and 8,147 ksi for mixtures with synthetic fibers. Increasing the steel fiber content from 2 to 4 percent increased the modulus by an average of 12.2 percent for OL fibers and decreased modulus by 2.2 percent for HF fibers. The use of 2 percent HF fibers produced samples with a 13.7 percent higher modulus than similar samples with OL fibers. Samples with 4 percent of OL and HF fibers had comparable moduluses. The use of synthetic fibers led to the lowest moduluses among the large-scale batches. A lower w/b and use of UFR increased the modulus. Samples made with the Oklahoma materials had an average 13.2 percent higher modulus than those made with materials from south Florida. Moist curing of samples led to an average 7.5 higher modulus than those not moist cured.

6. **Splitting Tensile Strength**: The average splitting tensile strength varied between 2.39 and 2.93 ksi for the mixtures with steel fibers and 1.38 and 1.49 ksi for mixtures with synthetic fibers. There was a slight increase in splitting tensile strength when increasing from 2 to 4 percent OL fibers and a slight decrease for HF fibers. Decreasing the w/b to 0.18 increased the average splitting tensile strength by 6.4 percent compared to w/b of 0.20. Using UFR decreased the splitting tensile

156

strength slightly (2.3 percent). Moist curing did not consistently affect the splitting tensile strength of the samples.

7. **Modulus of Rupture**: The average modulus of rupture varied between 2.49 ksi and 4.05 for the mixtures with steel fibers and 1.29 and 1.34 for synthetic fibers. An increased steel fiber content (2 to 4 percent) increased the average MOR for samples with OL and HF fibers. The use of HF fibers led to the highest MOR. The Dramix 4D 65/35BG (A) had a higher MOR than the OL fibers but less than HF fibers. The MOR increased with a w/b of 0.18 (compared to w/b of 0.20) and with the use of UFR.

8. **Bulk Resistivity**: All mixtures had average bulk resistivities in the very low classification of permeability measurements. The presence of steel fibers dramatically decreased the bulk resistivity. Higher steel fiber contents led to lower bulk resistivity.

9. **Shrinkage**: The average shrinkage strains were 470, 549, and 596 microstrain for 7, 30, and 90 days after casting. Shrinkage was only measured in some of the large-scale batches at the time of this report. Additional samples were being constructed to measure shrinkage in the other mixtures.

The best mix design based on the large-scale batches is summarized in Table 4-28.

Table 4-28: Proposed non-proprietary UHPC mix designs

Mix.	Cement Type	W/B	Mix Proportions						Fiber		Admixtures	
			ag/cm	C	S	SF	FA	UFR	Type	Content (%)	HRWR (oz./cwt)	VMA (oz./cwt)
L3	Titan Type I/II	0.20	1.0	0.6	0.3	0.1	1.00	0.00	HF or OL	2.0	27.5	0
L1	Titan Type I/II	0.20	1.0	0.6	0.3	0.1	0.70	0.30	HF or OL	2.0	29.5	0

4.2.7. Recommendations for use of N-UHPC in the field:

According to all observations during the second independent research work on developing non-proprietary UHPC, following cased should be followed to get proper results:

- As UHPC is very sensitive to moisture content, it is recommended to control the moisture content of aggregates before using and deduct the amount of moisture in aggregated from required free water for mix design.

- Controlling the heat of hydration plays an important role in final mechanical properties. It is recommended to use ice or cold water to keep the temperature of fresh concrete in the permitted range of temperature by ACI.

- It is so important to do particle packing analysis design and do trial small scale batches before using the material in the field.

- Adding fibers to the mixture should be done slowly to prevent any fiber clumping during the mixing process.

4.2.8. Cost Analysis

4.2.8.1. Introduction

The main reason of all research efforts to develop non-proprietary UHPC was reducing the premium cost of commercial UHPC. Developing this material from locally-produced raw available material significantly decreased the material cost itself.

4.2.8.2. Material Cost

The approximate cost of these mixtures was determined based on approximate costs obtained from the suppliers of the different materials. These approximate costs do not include any freight costs to ship the materials or costs associated with mixing and placing the mixtures. Table 4-29 summarizes the supplier quotes for each material. The mentioned costs are approximate prices provided by suppliers and would be subject to specific quantities being ordered, job location, and time after publication of this dissertation.

Table 4-30 summarizes the amount of each constituent in large scale mix designs for one cubic yard. All values were derived from the experimental section of this study.

Table 4-29: The cost of each used material in N-UHPC

Component	Cost
Type I/II Cement [cost per lb]	$ 0.050
Slag [cost per lb]	$ 0.050
Silica Fume [cost per lb]	$ 0.500
Water [cost per lb]	$ 0.00048
Masonry Sand [cost per lb]	$ 0.008
UFR [cost per lb]	$ 0.025
HRWR [cost per oz.]	$ 0.15
VMA [cost per oz.]	$ 0.14

Steel Fibers [cost per lb]	$ 2.00
Synthetic Fibers [cost per lb]	$ 6.00

Table 4-30: Required amount of each material for one cubic yard of different mix designs

Material per 1 yd³	L1	L2	L3	L4	L5	L6	L7	L8	L9	L10
Type I Cement [lb/yd³] =	1179.6	1179.6	1179.6	1179.6	1179.6	1185.6	1155.5	1155.5	1179.6	1191.6
Slag [lb/yd³] =	589.8	589.8	589.8	589.8	589.8	592.8	577.8	577.8	589.8	595.8
Silica Fume [lb/yd³] =	196.6	196.6	196.6	196.6	196.6	197.6	192.6	192.6	196.6	198.6
Water [lb/yd³] =	393.2	393.2	393.2	353.9	393.2	395.2	385.2	385.2	393.2	397.2
Fine Masonry Sand [lb/yd³] =	1376.2	1966.0	1966.0	1966.0	1966.0	1976.0	1925.9	1925.9	1966.0	1986.0
UFR [lb/yd³] =	589.8	0.0	0.0	0.0	0.0	0.0	0.0	0.0	0.0	0.0
Fibers [lb/yd³] =	264.6	264.6	264.6	264.6	264.6	258.5	529.3	529.3	30.7	15.3
HRWR [oz/yd³] =	578.0	432.5	540.6	540.6	540.6	543.4	529.6	529.6	540.6	546.2
VMA [oz/yd³] =	0.0	0.0	0.0	0.0	0.0	88.7	0.0	0.0	0.0	0.0

Considering the required amount of material and their unite price, Table 4-31 summarizes

the final price break down of each mix designs used in this study.

Table 4-31: Cost break down and total cost of each N-UHPC mix design

Cost per 1 yd³	L1	L2	L3	L4	L5	L6	L7	L8	L9	L10
Type I Cement [$/yd³] =	59.0	59.0	59.0	59.0	59.0	59.3	57.8	57.8	59.0	59.6
Slag [$/yd³] =	29.5	29.5	29.5	29.5	29.5	29.6	28.9	28.9	29.5	29.8
Silica Fume [$/yd³] =	98.3	98.3	98.3	98.3	98.3	98.8	96.3	96.3	98.3	99.3
Water [$/yd³] =	0.2	0.2	0.2	0.2	0.2	0.2	0.2	0.2	0.2	0.2
Fine Masonry Sand [$/yd³] =	10.3	14.7	14.7	14.7	14.7	14.8	14.4	14.4	14.7	14.9
UFR [$/yd³] =	14.7	0.0	0.0	0.0	0.0	0.0	0.0	0.0	0.0	0.0

Fibers [$/yd^3] =	529.3	529.3	529.3	529.3	529.3	517.0	1058.5	1058.5	61.4	30.7
HRWR [$/yd^3] =	86.7	64.9	81.1	81.1	81.1	81.5	79.4	79.4	81.1	81.9
VMA [$/yd^3] =	0.0	0.0	0.0	0.0	0.0	12.4	0.0	0.0	0.0	0.0
Total Cost [$/yd^3] =	828.0	795.8	812.1	812.0	812.1	813.7	1335.6	1335.6	466.8	377.7

Using reported costs by suppliers, the cost for the proposed mixes (L1 and L3) is around $800 per cubic yard (with around $530 per cubic yard of this amount being for the steel fibers). The cost of manufacturing the steel fibers is high due to the lack of domestic manufacturers and low demands. This value is about 40% lower than the cost of commercial UHPC. The minimum cost per cubic yard of commercial UHPC is reported $2000 which may increase according to fiber type and content [124]. Several different values were reported for the price of commercial UHPC from $3,270/yd^3 to $5,886/yd^3 [125] based on the fiber type and content but this value decreased by increasing the number of steel fiber suppliers in the North America but still no practical value below $2000/yd^3 is reported. On the other hand, the overestimated cost of conventional concrete (f'$_c$=6500 psi) is around $200/yd^3 which is 10 times less expensive than commercial UHPC.

There are few studies that compared and estimated the cost analysis due to using UHPC concrete. A comprehensive study in Nevada revealed that using C-UHPC with average price of $2500/yd^3 increase for a concrete bridge (continuous span-normal concrete) with UHPC piers increase the overall cost of construction between 11 to 18% [126]. This value differs based on the application and the required volume of UHPC. Same study revealed that if non-Proprietary UHPC with average price of $550/yd^3 was used, the increase in the total price was between 1.5 to 3%. It is completely clear that using non-proprietary UHPC

concrete addresses both long term performance and costs concerns related to bridge structures and infrastructures.

4.2.8.3. Other cost considerations

Beside the initial cost of the material itself, there are other costs that must be considered for cost comparison. N-UHPC and C-UHPC are needed to be mix on site before casting, this procedure needs more time, special equipment and even quality control specialist.

Although UHPC mixing increases the required on-site time, but its initial high strength reduces the overall construction time.

UHPC mixing requires more amount of energy input during the missing procedure due to its fine particles and low water content, hence, conventional mixing methods may not work for UHPC. A high shear mixer that can evenly release the water to dry components without heating the mixture during the mixing is required which will increase the initial cost of using UHPC [15]. Temperature control during the mixing process and probably using ice in hot climate condition is another factor that may increase the initial cost and add challenges for using UHPC.

Although the initial cost of using UHPC is significantly higher than conventional concrete due to all mentioned requirements and limitations, very high durability of UHPC will decrease the long-term costs due to less required maintenance activity over UHPC material.

Considering all high initial cost of using UHPC, long-term saving due to less required maintenance is the UHPC's merit. There were no data related to environmental impact of using UHPC or CC in this study, therefore no life-cycle cost analysis was conducted. There are few published works that shed light on the life cycle costs due to using UHPC.

A life cycle analysis refers to an analysis that determines the structure's environmental impact during its lifetime. A comprehensive life-cycle study on three bridges located in Germany, USA and Canada revealed that using UHPC can contribute between 45 to 85% of the environmental impact according to GWP environmental metric comparison [127]. Clearly more investigations are required to determine the exact environmental impact of UHPC and specially for non-proprietary UHPC when different supplementary cementitious material can be replaced by cement. This fact is highly affected by the application of UHPC and the required amount of it for entire construction.

Chapter 5: **Numerical Analysis of Joint Performance**

5.1. Introduction

The main goal of the research summarized in this chapter was to evaluate the performance of female-to-female connections with straight bars between FDPC deck panels with different joint widths and joint materials. Three primary joint materials were used: conventional concrete (CC), commercial UHPC (C-UHPC) and non-proprietary UHPC (N-UHPC) mixture developed in this research. Additional joint materials were also investigated with varying compression strength, tensile strength, and post-cracking tensile behavior. This analysis could be used as a starting point for future experimental work on N-UHPC bridge applications.

As discussed in Chapter 2:, the most frequent observed issue in FDPC system in or around connections. In other words, joints were recognized as weak regions of FDPC system. For this reason, the maximum load capacity of system and maximum deflection before failure were captured to compare the performance of different joint filler materials in this study. Using high-performance materials in connections has been a typical solution for improving the performance of bridge decks, but there has always been a question as to if C-UHPC could be replaced by other less expensive materials. The analyses performed and summarized in this chapter show that the use of N-UHPC (with significantly lower cost) in joints leads to similar performance as C-UHPC in joint applications. Also, the minimum required joint material properties for showing same performance of joints filled with C-UHPC were estimated.

5.2. Field-Cast Ultra-High Performance Concrete Joints

The earliest use of C-UHPC in joints between slab elements data back to 1995 in Europe [15]. More recently, using UHPC in connection between precast elements was noticed in North America and nine bridges in Canada and two bridges in the U.S. were constructed by UHPC connections by the end of 2011 [15]. At the same duration, several research studies were conducted to investigate the effect and performance of UHPC filled joints between bridge elements. The most recent and comprehensive study in this field was sponsored by Highway Transportation Officials (AASHTO) and resulted in a report, titled "Full-Depth Precast Concrete Deck Panel System" which is known also as NCHRP 12-65 report. This program defined the concept of full-depth precast concrete deck panels and developed an economical, non-post tensioned transverse connection details using C-UHPC that decrease the joint width significantly [1]. Figure 5.1 shows the typical deck panel configurations and different joint types which were recommended to fill by UHPC.

(a)   (b)
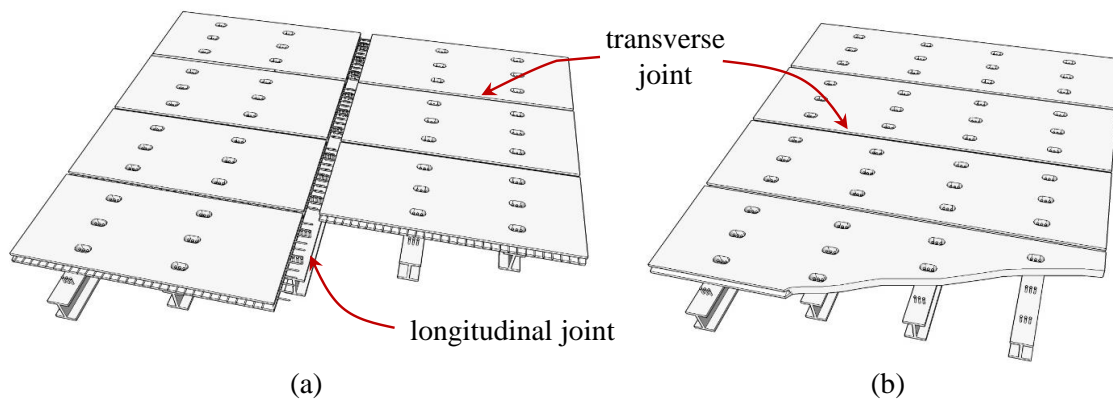
Figure 5.1: Conventional deck panel configurations for (a) bridge widths greater than 40 to 50 feet and (b) bridge widths less than 40 to 50 feet [10]

After NCHRP 12-65, more detailed studies were conducted to evaluate the structural performance of C-UHPC filled joints. In 2010, first comprehensive joint performance test

utilizing C-UHPC was conducted, and the performance of longitudinal and transverse joints filled with C-UHPC was evaluated under cyclic and static structural loading [15].

Four specimens were tested for transverse joints and two specimens were used for evaluating the longitudinal joints. Typical load protocols that were used for transverse joints and longitudinal joints are shown in Figure 5.2.
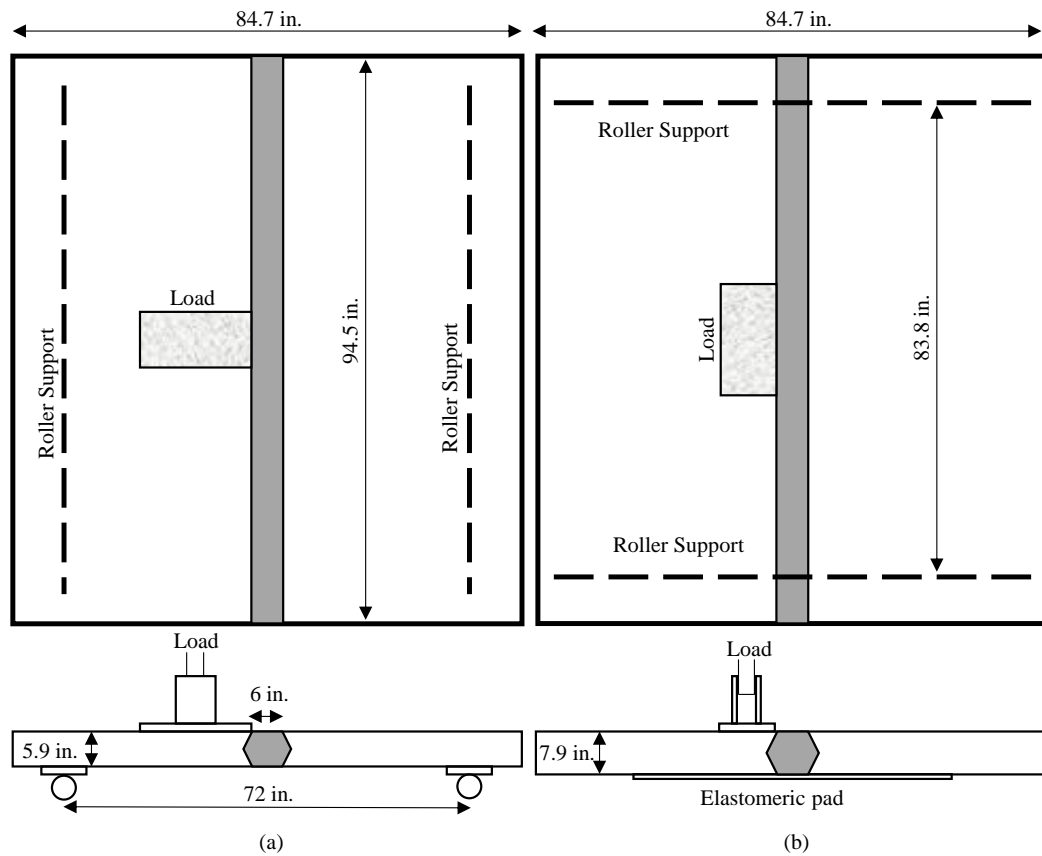
Figure 5.2: Test setup; (a) Transverse joint, (b) Longitudinal joint

The transverse joint setup (Figure 5.2 (a)) simulated the connection between precast deck panels while longitudinal joint setup (Figure 5.2 (b)) simulated the connections between the top flanges of deck-bulb-tee girders. The results revealed that field cast UHPC joints (C-UHPC) with shorter joint widths can perform similar or even better than a conventional

cast in place bridge deck with normal concrete joint. The load deflection curve for the test

setup shown in Figure 5.2 (a) is shown in Figure 5.3.
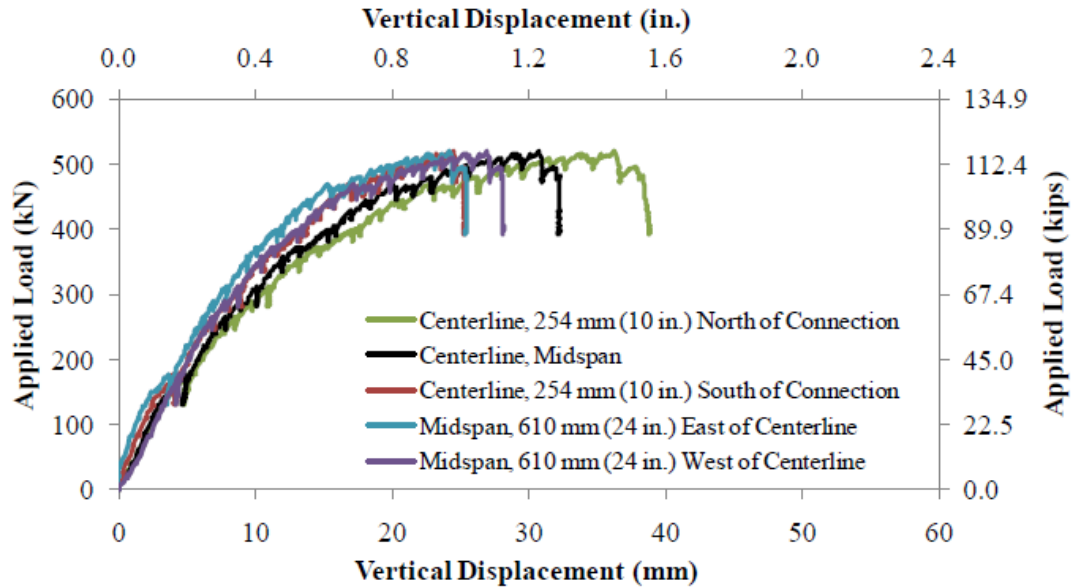
Figure 5.3: Load-deflection response of 6-inch thickness panel using C-UHPC under static loading [15]

Almost same test setup and load configuration for deck with 6-inch thickness was used in

a recent study by the University of Nevada, Reno. A developed N-UHPC mix design using

local material in Nevada and C-UHPC were used to fill the joint between deck panels and

performance of each material was investigated experimentally by static loading [128]. The

load deflection curve resulted from this study is shown in Figure 5.4.
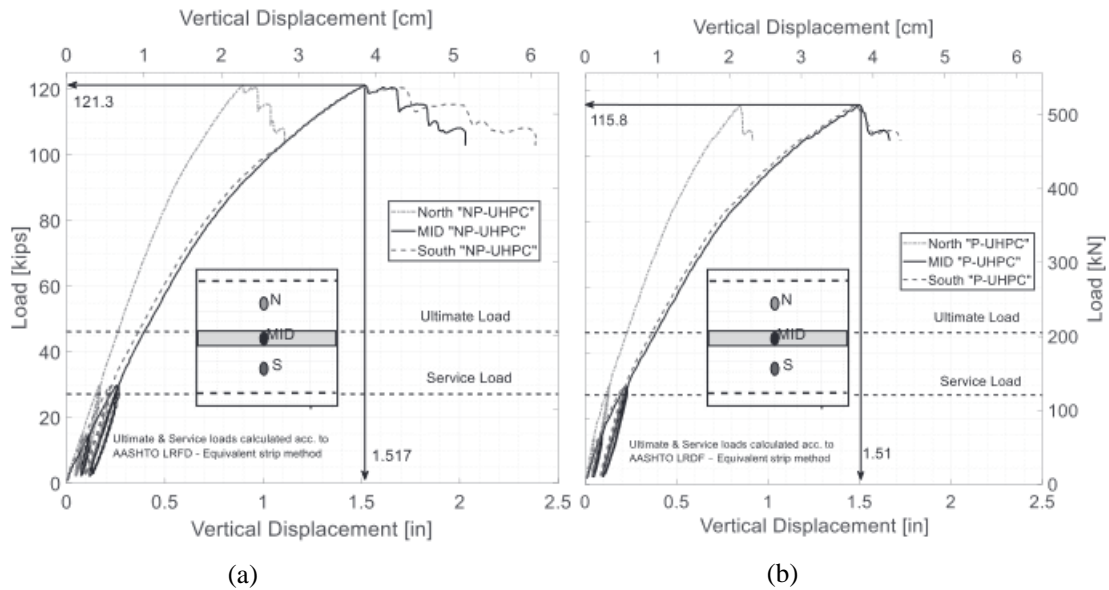
Figure 5.4: Load versus vertical displacements at quarter- and mid-span locations of the N-UHPC specimen (a) and C-UHPC specimen (b)[128]

The load deflection curves resulted from previous studies, revealed that the maximum peak load before failure is in the range of 112 to 120 kips with maximum mid span deflection in the range of 1.2 to 1.5 inches for the 6-inch deck panels.

As these both major studies were focused on the experimental aspect of performance comparison, this study was focused on numerical modeling of this problem.

For this reason, a 3D finite element based modelling was used initially to verify the experimental results by Graybeal and Abokifa et al [15], [128] and then the calibrated material in model was used for typical 8-inch deck of full depth precast concrete deck panels (FDPC) to compare the performance of CC filled joint with C-UHPC and N-UHPC filled joint with different joint widths.

5.3. Numerical Modelling (ATENA)

For comparing the performance of different materials in a joint setup, ATENA, a user-friendly software for nonlinear analysis of reinforced concrete structures was used. ATENA is developed by "Červenka Consulting" one of pioneer companies in nonlinear structural analysis of concrete and reinforced concrete structures.

ATENA is specially designed for concrete and is a great tool for understanding the real behavior of concrete members. ATENA simulated the real behavior of cementitious material and can demonstrate the crack propagation clearly.

5.3.1. Geometry and Model Creation

Most of the required documents, basic and advanced tutorial for modelling with ATENA are available in "Cervenka Consulting" website [129]. In this study, some modelling points, learned lessons and observed challenges during modeling with ATENA was mentioned. For full detailed information and step by step modelling ATENA documentation section available in website is recommended.

Like any other finite element tools, there are two typical ways for drawing the geometry in software space. Direct way which is usually can be done through drawing tools of program or indirect way which is based on importing the geometry from other drawing software like AutoCAD®, SolidWorks®, etc. Direct way is basically recommended for simple and small geometries, but for complicated models with many details it is much better to utilized indirect way of drawing the geometry. In this study, it was found that generating the 3D geometry of deck elements in AutoCAD, were more accurate and friendly user than

generating them directly in program drawing module. Hence, a 3D geometry of all assumed models was created in AutoCAD and then was imported in ATENA for modelling. As ATENA supports "IGES" format, it is required to export from AutoCAD to this format and then import the saved "IGES" file into the ATENA. For minimizing drawing efforts, it is better to define surfaces and volumes in AutoCAD, to make them recognizable for ATENA. ATENA recognize predefined surfaces and volumes and it is easier if the whole geometry includes complete surfaces and volumes instead of lines/polylines. Extra task will be required to define surfaces and volumes in ATENA, if the "IGES" file just contains the basic elements (lines/polylines). The quickest way was found to create the whole geometry in AutoCAD and then define the surfaces using the command "region". For 3D symmetric models, initially completed 2D section of model can be transformed to 3D volumes using "Extrude" command. It is very important to define all closed area between lines/polylines as "region" before extruding them to make volumes. For unsymmetric 3D models, it is required to define all volumes in AutoCAD before importing to ATENA.

Some minor changes on geometry are always required. Defining a center point on a plate for applying load or defining a line on a surface to apply the boundary condition are such examples. Based on the modelling experience on this project, it is suggested to apply these minor changes using command "edit/divide" in ATENA platform after importing the whole required geometry.

5.3.2. Material Modelling

After defining and importing the required geometry to ATENA, it is time to define the used material and assigned them to different components of geometry. ATENA has several

predefined models for modeling the cementitious material. The detailed information about different predefined material models can be found on ATENA tutorials and theory manual. ATENA has a wide variety of predefined models for steel and concrete. It also has some Fracture-Plastic constitutive models that were designed for modelling the fiber reinforced concrete.

These models are the combination of "Rankine-Fracturing Model for Concrete Cracking" model and "Plasticity Model for Concrete Crushing". Several material models are proposed by ATENA with difference of some predefined valued and assumptions in different sections of material modeling. The "CC3DNonLinCementitious2User" model is suggested and used previously by Červenka Consulting's team for fiber reinforced concrete. This material models allows user to define the tensile and softening behavior, shear retention factor and the effect of the lateral compression on tensile strength of the material. An example of tensile and compressive behavior of fiber reinforced material is shown in Figure 5.5.
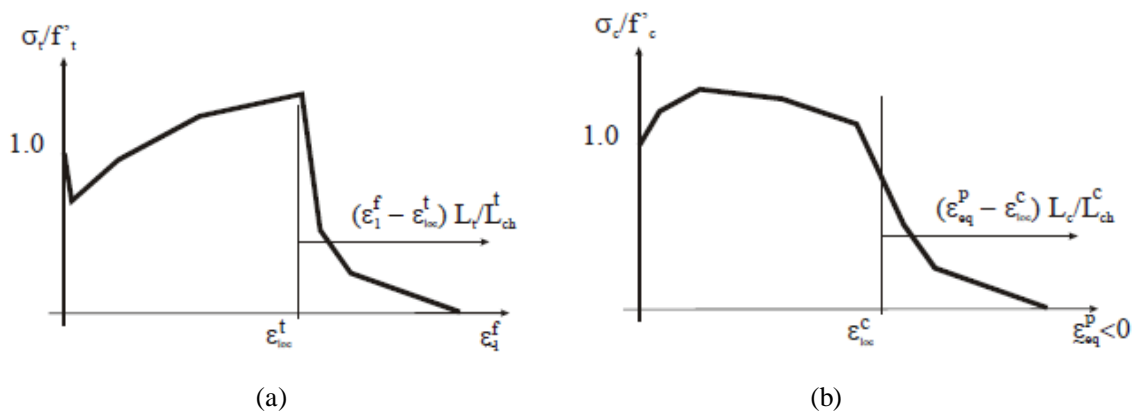

Figure 5.5: Example of user defined tensile and compressive behavior of fiber reinforced concrete; (a) tensile behavior and (b) softening behavior or compression behavior

For modelling the N-UHPC and C-UHPC in this study, material model "CC3DNonLinCementitious2User" was used and for conventional concrete (CC), predefined material models according to Eurocode 2 was chosen.

All basic material properties were assigned based on the experimental tests conducted during Graybeal work [15] and experimental test that were conducted during this study for non-UHPC concrete.. The 28-day compressive strength of C-UHPC and conventional concrete (CC) used by Graybeal was reported 31.5 and 6.5 ksi respectively, and the modulus of elasticity for C-UHPC was reported 8900 ksi. In this study, all reported values by Graybeal were considered as constant and all other unknown values like the modulus of elasticity of conventional concrete were driven from reverse engineering and trial and error process.

5.3.3. Assumptions for Material Models

In all models, several different materials were used including steel plates as supports and loading plate, reinforcement bars, conventional concrete, non-proprietary UHPC concrete and commercial UHPC. Following are the initial considered material properties. The material properties related to conventional concrete and commercial UHPC were modified later based on the validation process.

As the compressive strength of conventional concrete was considered equal to 6.5 ksi, the concrete class 70/85 with same compressive strength was chosen in ATENA.

For N-UHPC and C-UHPC, material model "CC3DNonLinCementitious2User" was used as was recommended by ATENA for defining fiber reinforcement concrete. This model

allows users to define desired tensile and compressive behavior of concrete according to the material response in the test. Initially only basic parameters were assigned to ATENA and all other parameters for tension and compressive function were assigned the default values from the program; tension and compressive function were modified later during the validation process. Table 5-1 summarize the initial considered material properties for numerical modelling with ATENA. Highlighted cells were initial assumptions and modified during the validation process.

Table 5-1: Basic cementitious material properties for modelling in ATENA

Material	Young's Modulus (E)	Poisson Ratio (υ)	Tension Strength (Fₜ)	Compression Strength (Fᴄ)
	ksi	-	ksi	ksi
CC	4595	0.2	0.32	6.5
C-UHPC	8900	0.2	1.38	31.5

All highlighted values in Table 5-1 were estimated according to proposed equations for normal concrete in ACI 318 [130] and UHPC equations according to Graybeal work [3]:

Modulus of elasticity of Normal Concrete

$$\mathrm{E}_c = 57000\sqrt{f_c'} = \frac{57000 \times \sqrt{6500}}{1000} = 4595 \; ksi \qquad \text{Equation 5-1}$$

Tensile Strength of Normal Concrete

$$f_t = 4\sqrt{f_c'} = 4 \times \sqrt{f_c'} = \frac{4 \times \sqrt{6500}}{1000} = 0.32 \; ksi \qquad \text{Equation 5-2}$$

Tensile Strength of UHPC

$$f_t = 7.8\sqrt{f_c'} = 7.8 \times \sqrt{f_c'} = \frac{7.8 \times \sqrt{31500}}{1000} = 1.38 \; ksi \qquad \text{Equation 5-3}$$

Table 5-2: Basic material properties of steel plates and reinforcement for modelling in ATENA

Material	Young's Modulus (E)	Poisson Ratio (υ)	Characteristic Yield Strength
	ksi	-	ksi
Steel Plates and Reinforcement*	29000	0.3	72

*#5 reinforcement bars with 0.625 diameter

The important point about the defining the reinforcement bars with 1D linear elements, is their bonding behavior with surrounding material which is mostly concrete. By default, ATENA assumes a perfect bonding between reinforcement bars and surrounding material. In most of the cases, this perfect bonding represents the real response of material, and no future action is required. However, the bond model becomes important when only short development lengths are provided as is the case with the joint between FDPC deck panels. Hence, a bond-slip strength function according to ATENA predefined models was used in this study to model bonding behavior between reinforcement bars and surrounding concrete. ATENA contains three bond-slip models: CEB-FIB model code 1990, slip law by Bigaj [131]and the user defined law. In this study, the slip law by Bigaj was used to define the bonding behavior in ATENA. This bond model depends on the bond quality, bar diameter and concrete strength. Bond quality can be assigned "Bad", "Good" or "Excellent". The excellent condition performs almost as well as the default perfect bonding condition. There were no pull-out test results in this study, so determining the exact bond-slip model was impossible. An unconservative "Good" bonding quality in Bigaj model was used to define the bonding behavior. Figure 5.6 shows the general bond law developed by Bigaj 1999 and Table 5-3 summarizes the parameters for defining the bond function according to bar diameter (D) and cubical compressive strength of concrete (f_{cu}).
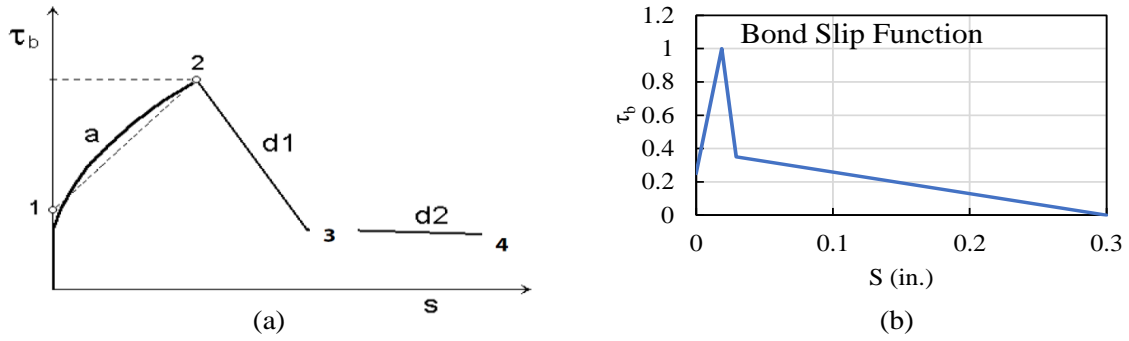
Figure 5.6: Bond- slip function; (a) Bond law by Bigaj 1999 [131], (b) Assumed function

Table 5-3: Parameters for defining the bond strength-slip relationship based on Bigaj 1999

Concrete Type	Bond Quality		Point 1	Point 2	Point 3	Point 4
$f'_c < 60$ (Mpa)	Excellent	S/D	0	0.02	0.044	0.48
		$\tau_b / \sqrt{0.8 f'_{cu}}$	0.5	3	0.7	0
	Good	S/D	0	0.03	0.047	0.48
		$\tau_b / \sqrt{0.8 f'_{cu}}$	0.5	2	0.7	0
	Bad	S/D	0	0.04	0.047	0.48
		$\tau_b / \sqrt{0.8 f'_{cu}}$	0.5	1	0.7	0
$f'_c > 60$ (Mpa)	Excellent	S/D	0	0.012	0.03	0.34
		$\tau_b / \sqrt{0.88 f'_{cu}}$	0.5	2.5	0.9	0
	Good	S/D	0	0.020	0.03	0.34
		$\tau_b / \sqrt{0.88 f'_{cu}}$	0.5	1.9	0.9	0
	Bad	S/D	0	0.025	0.03	0.34
		$\tau_b / \sqrt{0.88 f'_{cu}}$	0.5	1.1	0.9	0

5.4. Model Calibration

The validation process for the numerical models was done according to previous research conducted by Graybeal [15]. The same test setup and slab thickness (6-inches), as shown in Figure 5.2 (a), were used for the calibration model in ATENA. Many trials and error analysis were performed to get same load- deflection curve shown in Figure 5.3 resulted from experimental results. A lot of efforts were conducted to refine the mesh and keep the mesh element type "Hexahedra" for all volumes. Some geometrical issues resolved to remove the mesh error. Mesh element size and mesh size are two very important variable that can affect the results. Figure 5.7 shows outputs from trial-and-error process to for several different mesh element types and size. The average mesh size of 1.5 considered for both analysis and only mesh element type changed from Tetrahedra to Hexahedra. Results clearly shows the importance of mesh type and size on results. Then the response of deck under different mesh size from 0.5 to 3 inches were recorded. According to the speed of analysis and required space for each complete analysis and also the total number of models, the mesh size of 1.5 was chosen for all performed models.
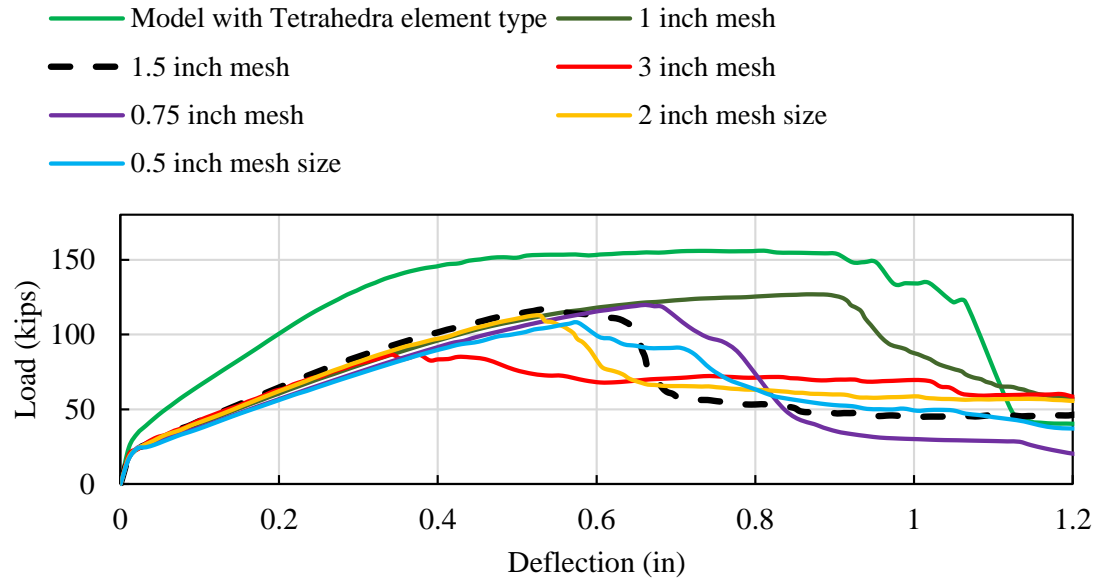
Figure 5.7: An example of load deflection response for two different mesh element types

After many trials analysis, the closest numerical result to experimental result was determined, as shown in Figure 5.8.
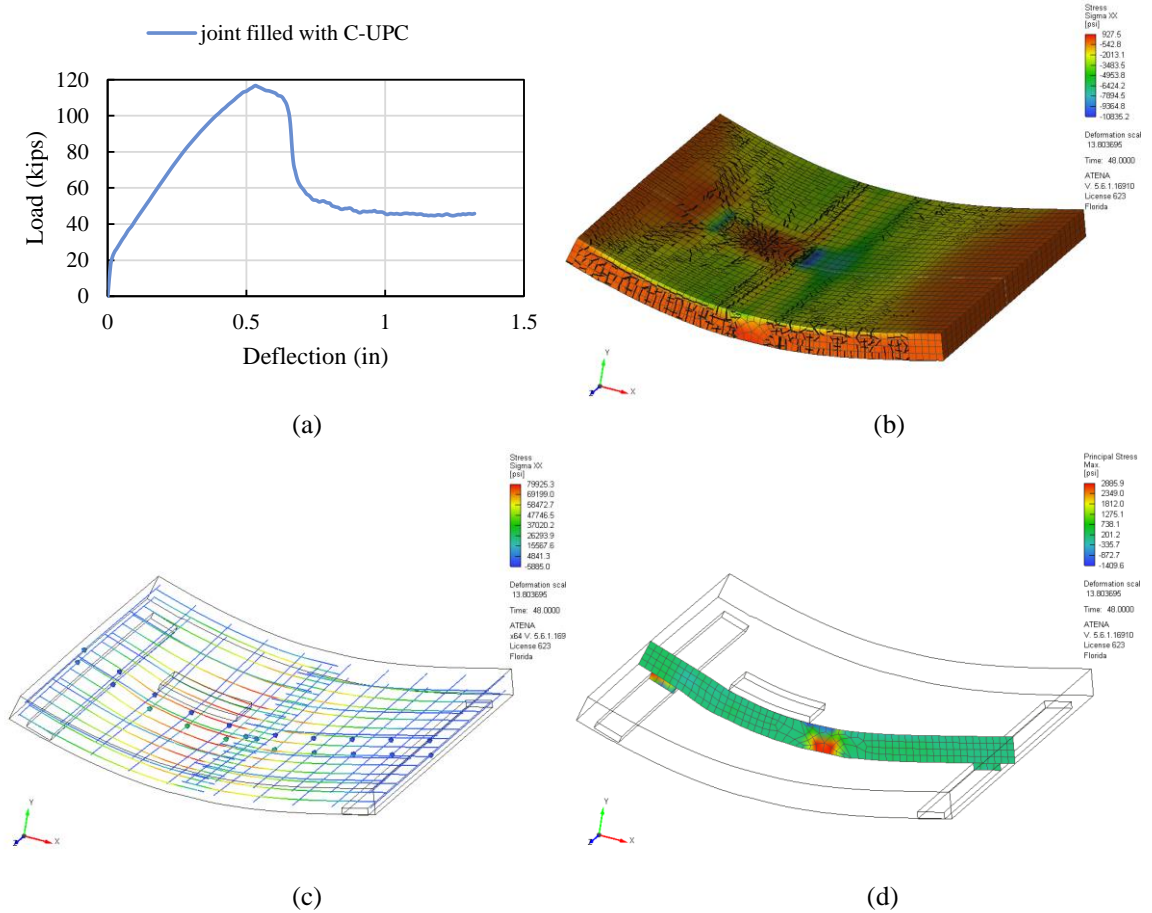
The failure load of model was 116.7 kips accompanied by 0.55-inch deflection in midspan while the experimental results of same test setup conducted by Graybeal showed 116.8-kip failure load and 1.18-inch deflection at ultimate load. This point was defined as failure of specimen while decrease in ultimate load capacity concurrent with increase in deflection. This model calibrated with other specimen tested by Graybeal and was able to get same experimental failure load.

Beside of the load and deflection, same crack pattern also was observed during the numerical modelling shown in Figure 5.8 (b).

 The total capacity was found accurately close but resulted deflection from modelling was less than actual deflection in test. This incompatibility could be due to several factors in modelling including boundary conditions, mesh size and bonding behavior between bars and surrounded concrete and was not necessarily related to the concrete material properties. Hence, in trial-and-error process, it was tried to keep material properties with 5% difference from laboratory test results include modulus of elasticity and compressive strength. On the other hand, the goal of this study was to compare the performance of three different concrete material numerically and finding the exact amount of failure deflection was not the priority in this study. Hence, the calibrated model which resulted in same failure load compared to experimental study, was used for additional models with different joint width and material.

5.5. Qualified Material and Joint Configuration

To shed light on the performance of joints and determine the effect of material properties on joint width, three different materials were used. Conventional concrete (CC), non-proprietary UHPC (N-UHPC) mix and commercial UHPC (C-UHPC) with 28-day compressive strength of 6.5, 17 and 31 ksi accordingly were modelled to determine the effect of each one on overall performance of joints. The non-proprietary UHPC material used for modeling was based on the experimental results of Mix L1 as a qualified mix designs from experimental work of this study.

Based on all laboratory test results and material validation efforts, the final material properties considered for the numerical modeling are provided in the following sections:

5.5.1. Final Assumed Material Properties for Modelling

For defining the UHPC material, "CC3DNonLinCementitious2User" model was used. Finalized material properties for modeling after validation process are summarized in Table 5-4. The final material properties for steel plates and reinforcement bars were kept constant according to Table 5-2.

Table 5-4: Final assumed material properties for modelling

Material	Young's Modulus (E)	Poisson Ratio (υ)	Tension Strength (F$_t$)	Compression Strength (F$_c$)
	ksi	-	ksi	ksi
CC	4950	0.2	0.3	-6.5
C-UHPC	8900	0.2	1.4	-31.5
N-UHPC	7800	0.2	1	-17

After crack behavior functions for C-UHPC and N-UHPC were considered same and are shown in Figure 5.9.

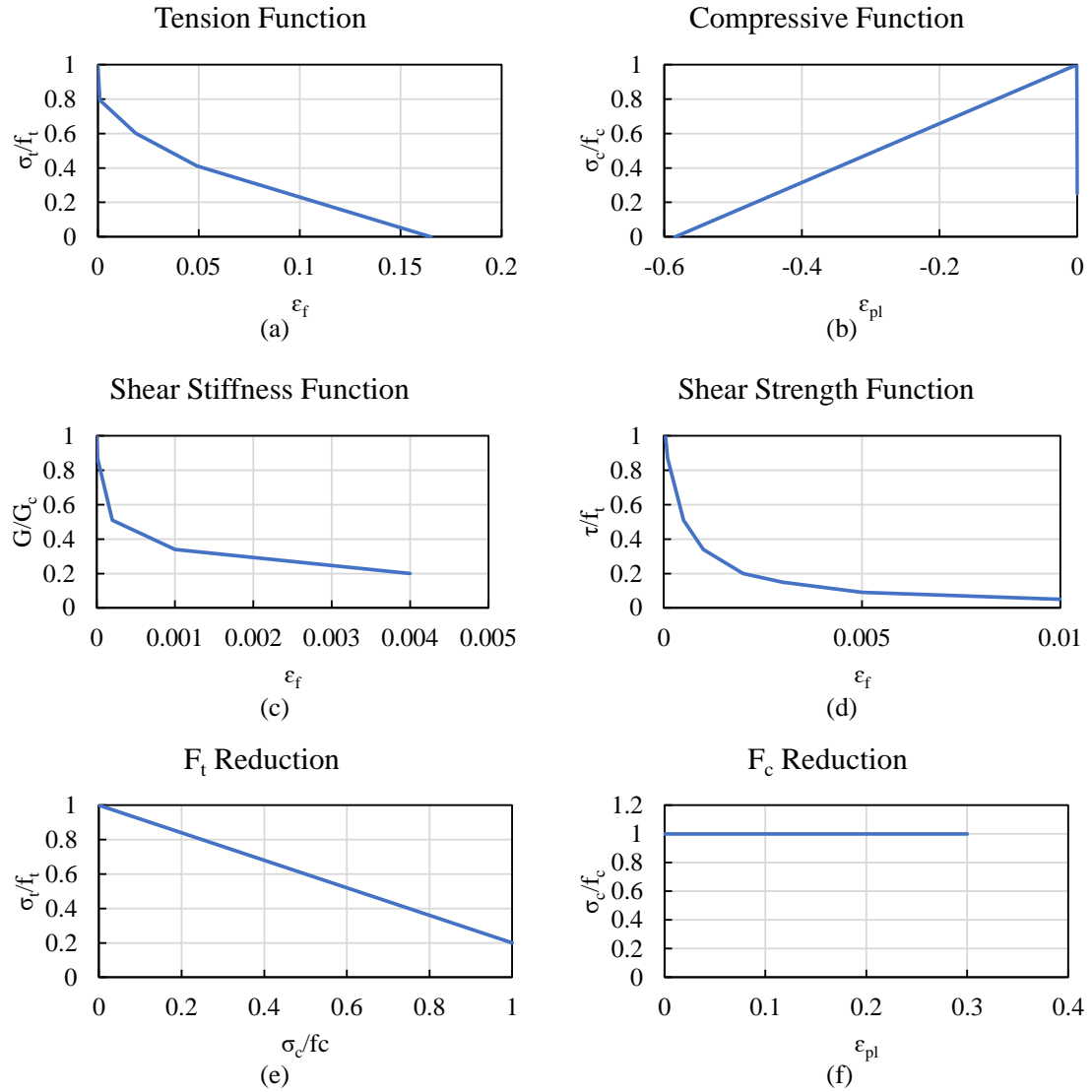*Figure 5.9: After crack behavior functions of UHPC; (a) Tension function, (b) Compressive function, (c) shear stiffness function, (d) shear strength function, (e) tension reduction function and (f) compressive reduction function*

These properties were considered for comparison purpose and were driven according to available information on previous studies, experimental works of this study and model validation process.

5.5.2. Joint Configuration

Several different joint widths (based on popular field used width) were considered to show joint width versus performance for these three materials. Reinforcement configuration, deck thickness (8-inch) and load setup were considered constant like the work conducted by Graybeal [15].

UHPC joints with straight bars shown in Figure 5.10 (a) are one of the most used details in the field, survey results for DOTs revealed that this detail has been used in 25.3% of bridges constructed with FDPC system. Conventional concrete with straight bars joint shown in Figure 5.10 (b) is also the other popular used joint details (13.7 % of previous bridges) and was considered here to for comparison purpose. For the ease of use and minimize the variables, the joint geometry shown in Figure 5.10 (a) was used for numerical modelling in this study even for conventional concrete.

(a)   (b)
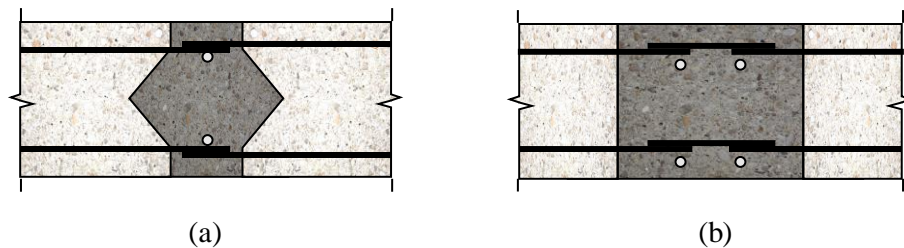
Figure 5.10: Joints with straight bar details; (a) typical joint geometry for UHPC filled joints and (b) typical joint geometry for joints filled with conventional concrete

5.5.3. Reinforcement Development Length for Straight Bars

To determine different joint width, development length of rebars all used material is required. The provisions of AASHTO LRFD 5.10.8.2.1.a was used for calculating the development length of bars, when the compressive strength of concrete is less than 15 ksi

[132]. The following table summarizes the development length calculation of #5 rebars based on different compressive strength of concrete.

Table 5-5: Required development length of reinforcement based on compressive strength of normal concrete

#	d_b (in.)	f_y (ksi)	f'_c (ksi)	l_{db} (in.)=2.4×d_b×f_y×(f'_c)^0.5	l_d=l_{db} ×(λ_{rl}×λ_{cf}×λ_{rc}×λ_{er}/λ)= l_{db} ×0.4
5	0.625	60	4	45.0	18.0
			5	40.2	16.1
			6	36.7	14.7
			7	34.0	13.6
			8	31.8	12.7
			9	30.0	12.0
			10	28.5	11.4
			6.5	35.3	14.1

As the compressive strength CC was considered 6500psi, the last row of Table 5-5, summarized the calculated development length of rebars in 6500 psi normal concrete.

All modification factors (λ) shall be taken equal to 1.0 unless they are specified to increase or decrease in AASHTO provisions in Articles 5.10.8.2.1.b and 5.10.8.2.1.c. In this case the only factor which is not equal to 1.0 is λ_{rc}.

$$0.4 \le \lambda_{rc} \le 1.0$$

Where $\lambda_{rc} = \dfrac{d_b}{c_b + k_{tr}}$

and $k_{tr} = 40 \, A_{tr}/(sn)$

Where:

c_b = the smaller of the distance from center of bar being developed to the nearest concrete surface of the bars being developed (in.)

k_{tr} = transverse reinforcement index

A_{tr} = total cross-sectional area of all transverse reinforcement which is within the spacing S and which crosses the potential plane of splitting through the reinforcement being developed (in.^{2})

In this case, conservatively A_{tr} was taken zero and consequently the λ_{rc} will be equal to d_b/c_b which was less than 0.4 for all configuration assumed in this study and therefore the minimum amount of 0.4 considered for calculations. The compression strength of normal concrete for casting the deck panels was considered 6.5 ksi. According to this amount and considering the AASHTO provisions, the minimum development length for reinforcements was equal to 14.1 inches. On the other hand, the required lap splice length for bar in tensions is equal to development length for Class A splice and must be more than 12 inches.

In this case conservatively, the development length was considered 18 inches with 16 inches lap splice length. More details are shown in Figure 5.11.
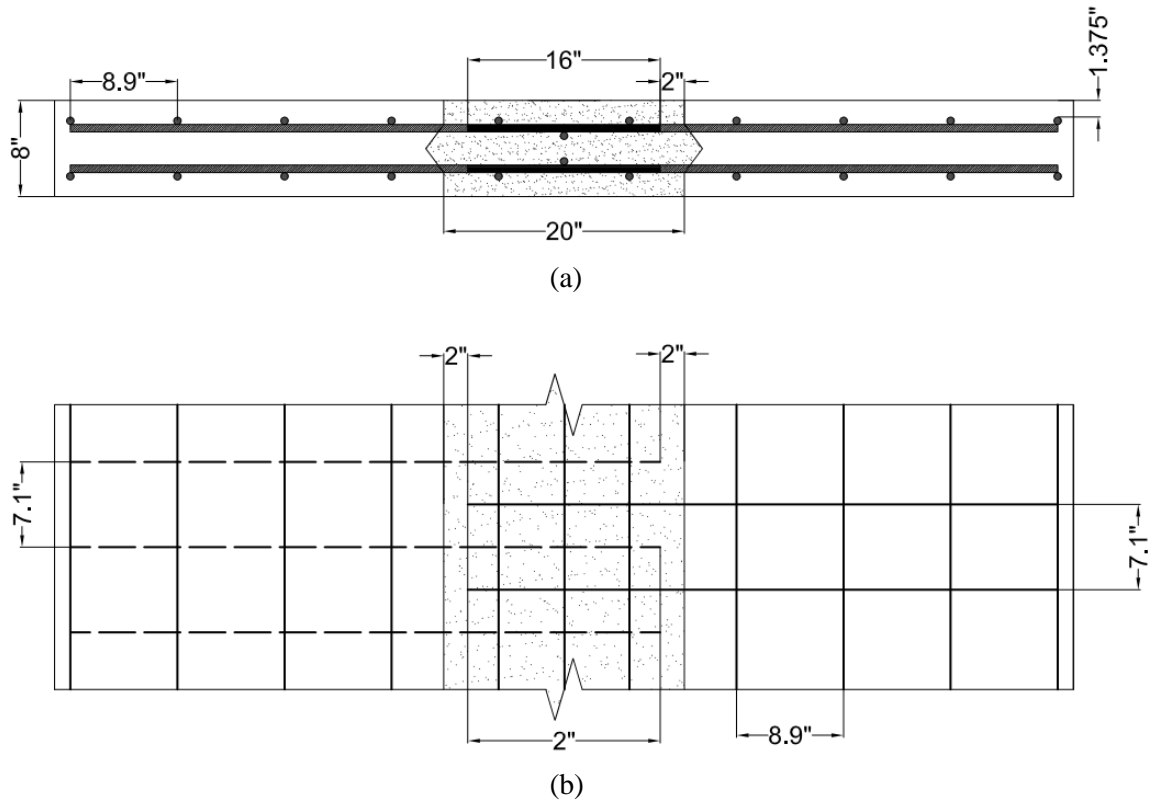
(a)

(b)

Figure 5.11: Development length of reinforcement for normal concrete (f'$_c$=6.5 ksi); (a) cross section view and (b) plan view

5.5.4. Numerical Specimen Details

The joint detail shown in Figure 5.11 was the widest joint detail modelled during this research. Shorter joint widths also were modelled to determine the joint width versus performance of different materials. Table 5-6 summarizes the details related to all modelled joints with straight bars. It was tried to consider 2-inch gap from each end for all sections except the 6-inch joint which was developed specially for UHPC and tested by Graybeal [133].

Table 5-6: Different studied sections with straight bars and different material

Model Name	Geometry	Gap from both sides (in.)	Splice length (in.)	Joint width
S6	Female to female (decagon shape)	1.1	3.8	6
S9		2	12	16
S12		2	8	12
S16		2	12	16
S20		2	16	20
S0	Jointless Deck (ideal condition)			

In all models the depth, length and width of whole model were considered constant and equal to 8, 94.5 and 84.7" respectively. Beside the dimension, reinforcement configuration was kept constant to minimize the number of variables. These dimensions were driven from the previous works done [15], [58]. One model also dedicated to an ideal system without joint (Model S0). This section modeled with normal concrete and same reinforcement configuration with this difference that all bars were extended along the width of model. Figure 5.18 shows the jointless deck which was considered for comparison purpose to see how models with joint behave compared to ideal deck without joint. Figure 5.12 shows the schematic load setup for numerical modelling in this study.
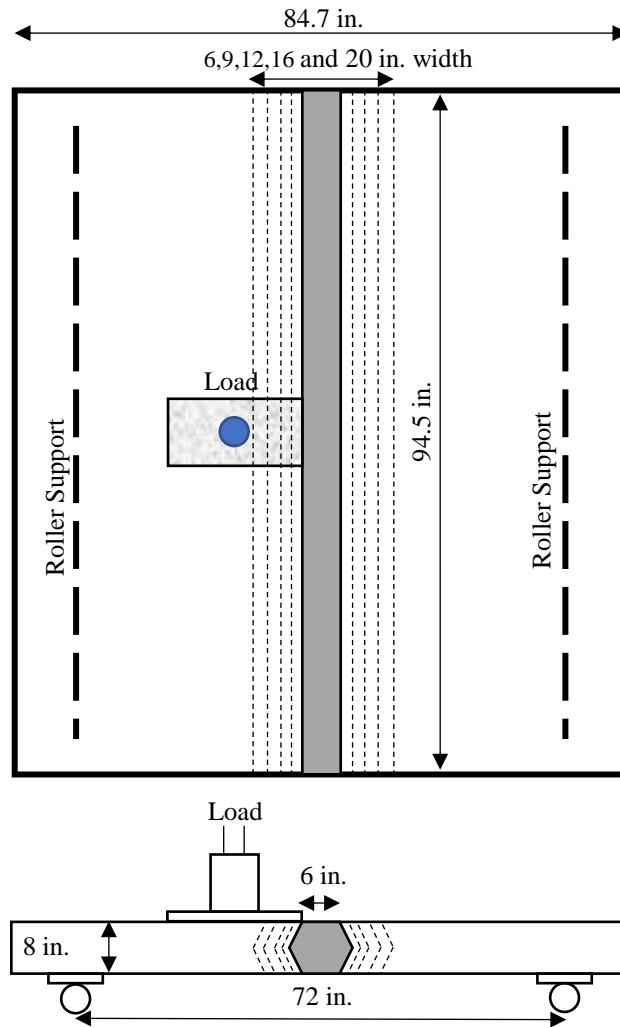
Figure 5.12: Considered load setup for all models with different joint widths

Figure 5.13 to Figure 5.17 demonstrate the geometry of all different models with straight
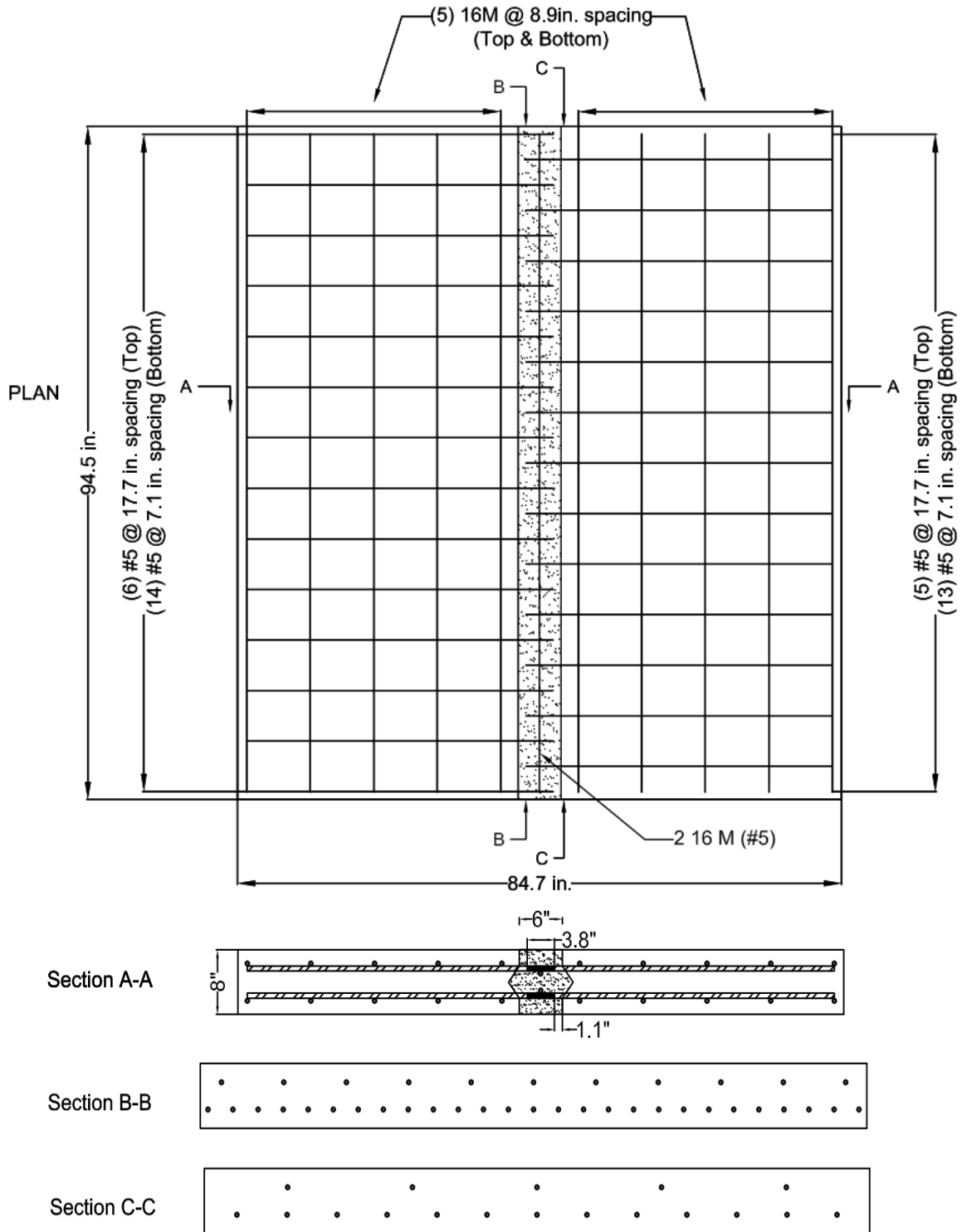
bars.

Figure 5.13: 6-inch joint with straight bar details (Model S6)
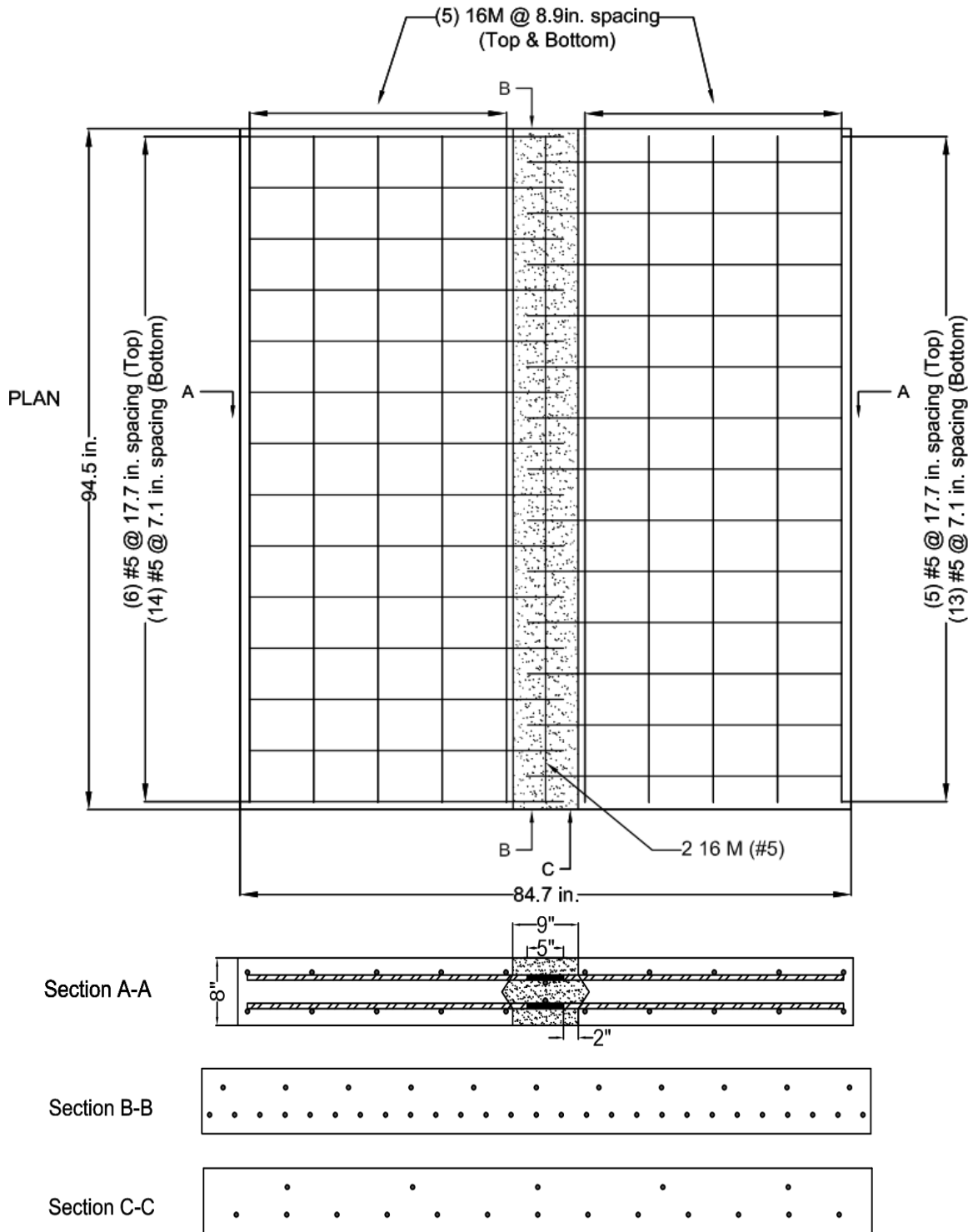
Figure 5.14: 9-inch joint with straight bar details (Model S9)
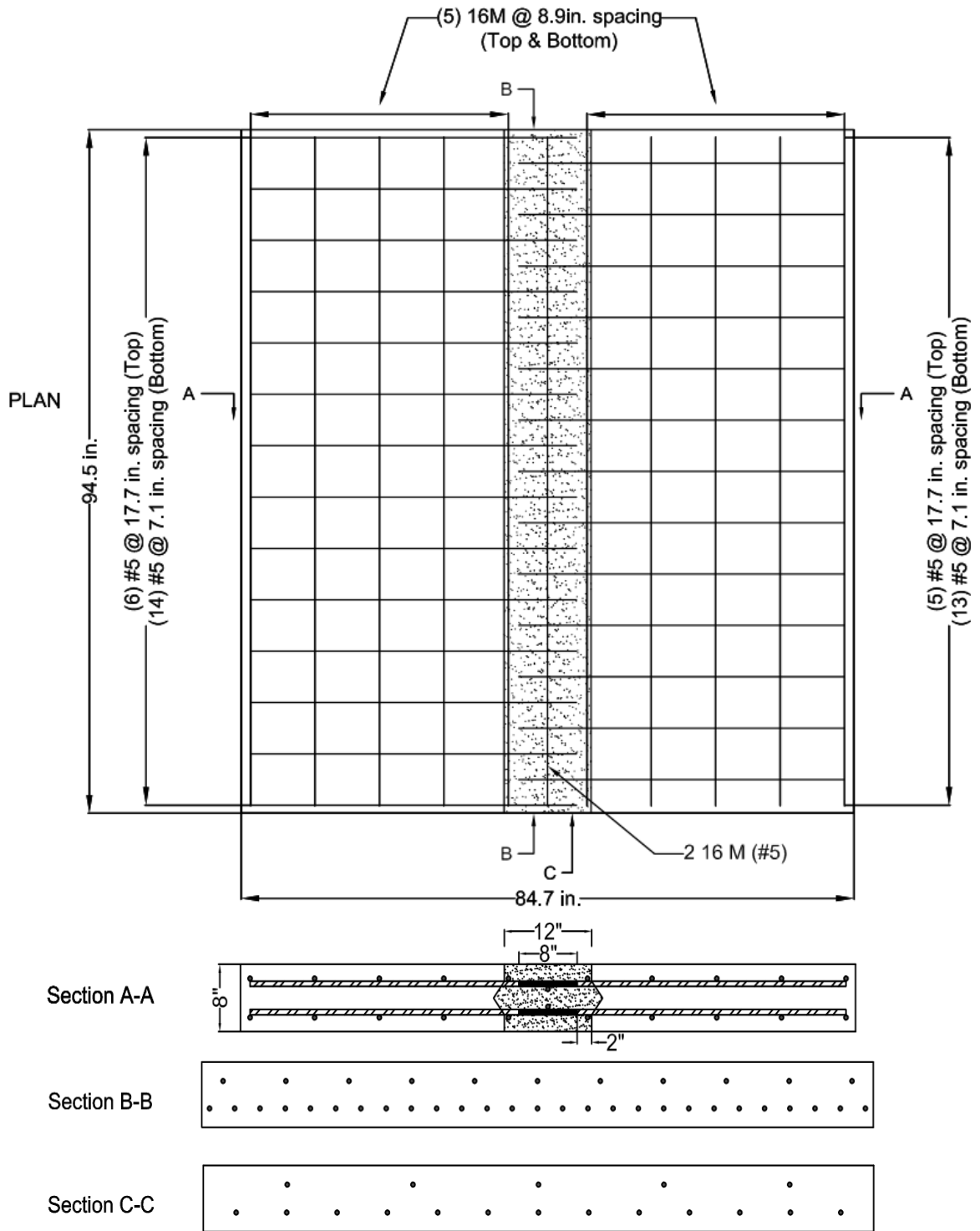
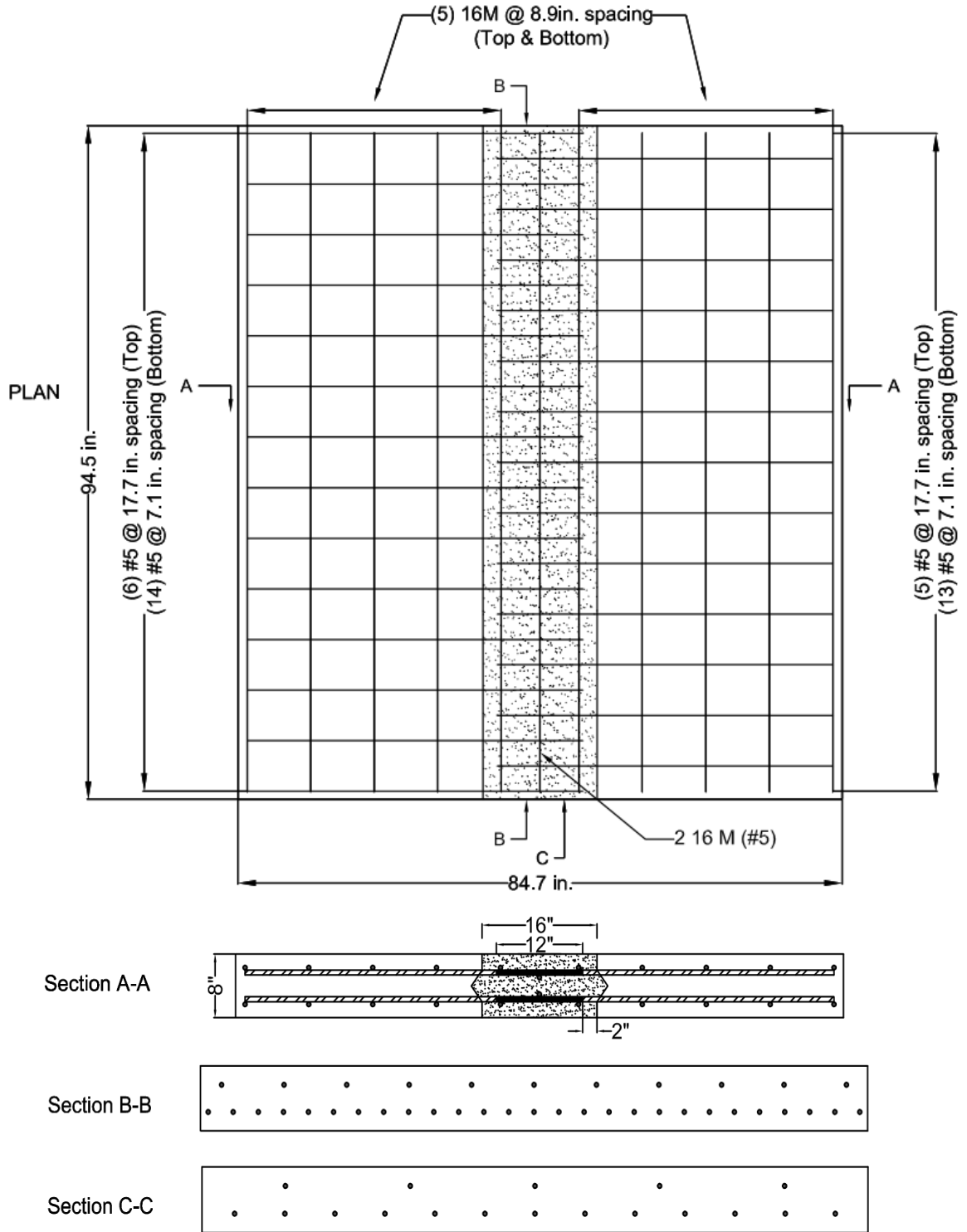*Figure 5.15: 12-inch joint with straight bar details (Model S12)*

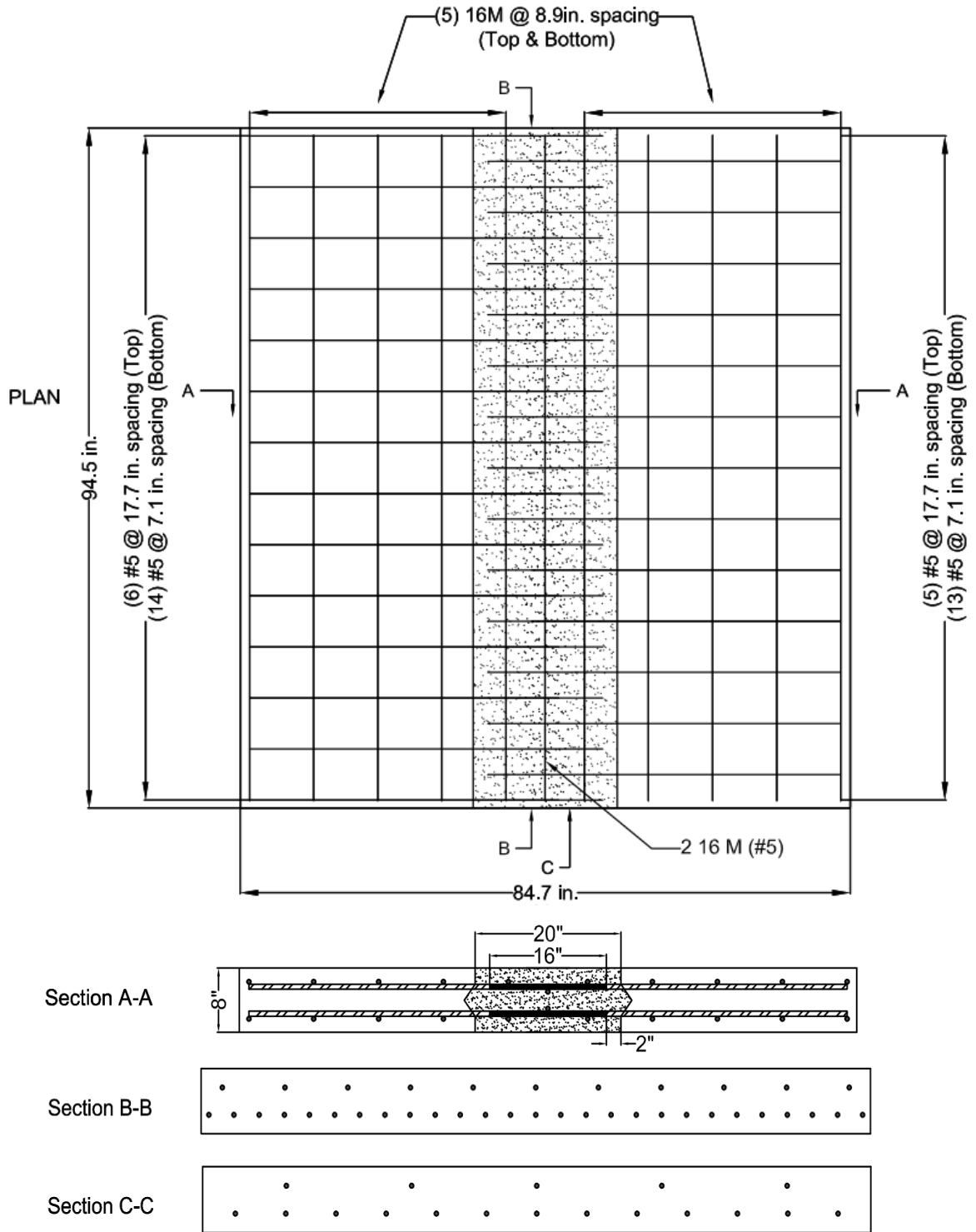*Figure 5.16: 16-inch joint with straight bar details (Model S16)*

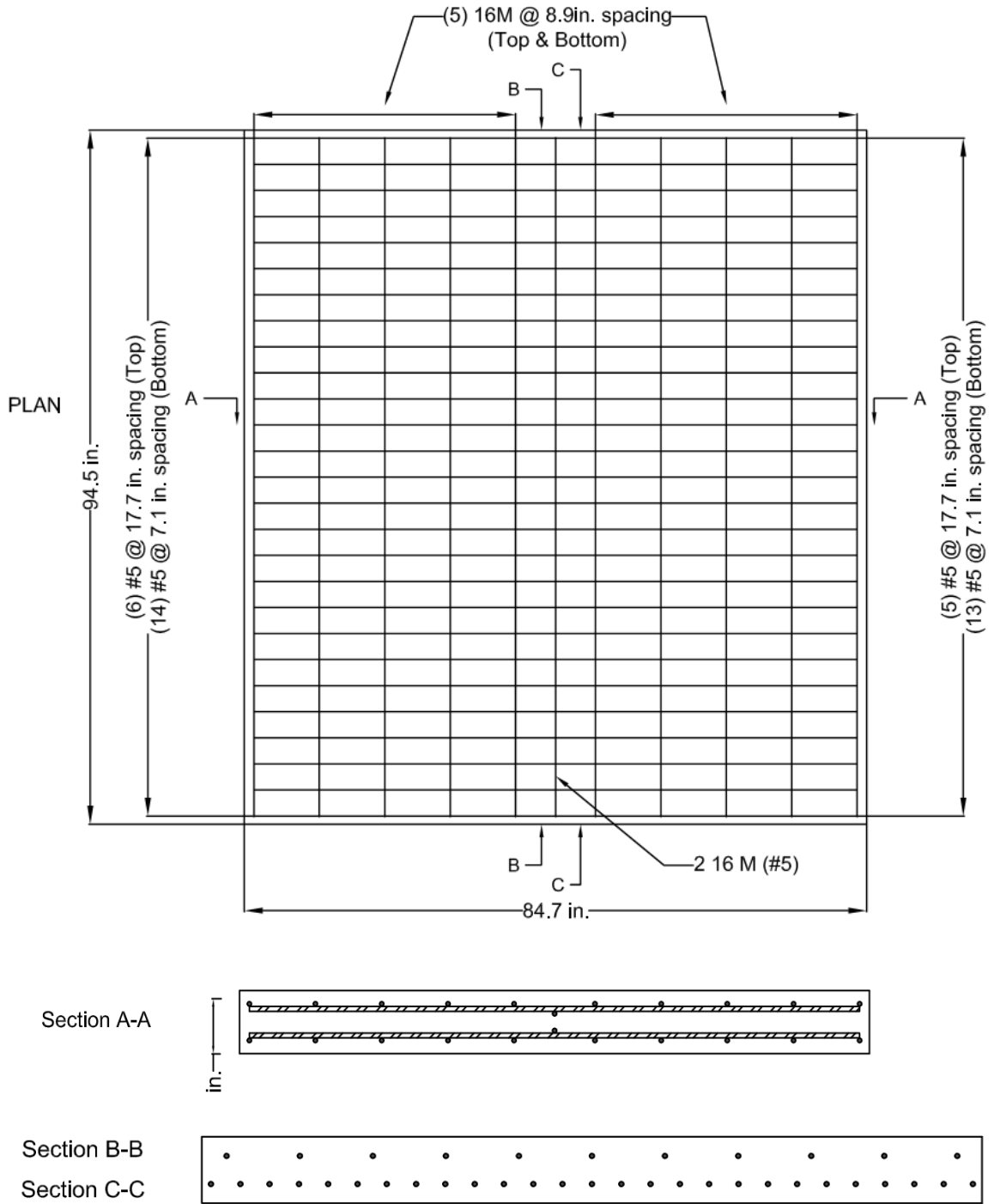*Figure 5.17: 20-inch joint with straight bar details (Model S20)*

Figure 5.18: Jointless deck (Model S0)

5.6. Results and Discussion

5.6.1. Experimental Matrix for Numerical Analyses

Several trial-and-error processes were performed before validating the model with experimental results. Table 5-7 summarizes the material properties of used for numerical analysis after validation process. The basic mechanical properties of all three primary material include compressive strength and modulus of elasticity were assumed similar to previous experimental works and tensile strength of material was estimated according to recommended equations between compressive strength and tensile strength. estimated based on the recommended equations.

Table 5-7: Mechanical properties of primary material for numerical study

Material	Young's Modulus (E)	Poisson Ratio (υ)	Tension Strength (F_t)	Compression Strength (F_c)	F_c Reduction Factor
	ksi	-	ksi	ksi	-
CC	4950	0.2	0.3	-6.5	0.2
C-UHPC	8900	0.2	1.4	-31.5	1
N-UHPC	7800	0.2	1	-17	1

All mentioned values in Table 5-7, were kept constant and play and error process was focused on after crack behavior of UHPC material in validation process. The compressive strength reduction factor of material was also determined during the validation process. This reduction factor determines the reduction of compressive strength capacity after cracking. For UHPC material, due to fibers this factor was set to one that shows no reduction in compressive strength after cracking. The other important part of validation was related to determining the tension function of C-UHPC.

Based on the calibrated mechanical properties, 16 different models initially were analyzed through ATENA, to compare the performance of three primarily material in joint between FDPC panels. Table 5-8 summarizes different models' specification in this study.

Table 5-8: Summary of different numerically analyzed models

#	Numerical Specimen	Model Name	Joint Material	Splice Length (in.).
1	S6-6-inch joint width	S6-C-UHPC	Commercial UHPC	3.8
2		S6-CC	Conventional Concrete	
3		S6-N-UHPC	Non-proprietary UHPC	
4	S9-9-inch joint width	S9-C-UHPC	Commercial UHPC	5
5		S9-CC	Conventional Concrete	
6		S9-N-UHPC	Non-proprietary UHPC	
7	S12-12-inch joint width	S12-C-UHPC	Commercial UHPC	8
8		S12-CC	Conventional Concrete	
9		S12-N-UHPC	Non-proprietary UHPC	
10	S16-16-inch joint width	S16-C-UHPC	Commercial UHPC	12
11		S16-CC	Conventional Concrete	
12		S16-N-UHPC	Non-proprietary UHPC	
13	S20-20-inch joint width	S20-C-UHPC	Commercial UHPC	16
14		S20-CC	Conventional Concrete	
15		S20-N-UHPC	Non-proprietary UHPC	
16	S0-Jointless Deck	S0-CC	Conventional Concrete	-

In all analyzed models, same reinforcement configuration was used with different development length. For S0-CC model, all bars were extended along the length of deck to associate the ideal jointless system for comparison purpose. Detailed output of ATENA for all analyzed models are provided in Appendix B.

Primary comparing the load deflection curves, maximum mid span deflection before failure and failure load of different models, revealed that using the UHPC in both shape of commercial and non-proprietary version, increases the total capacity of deck system. In other words, the maximum deflection before failure and failure load of system increases by using the high-performance material.

5.6.2. Effect of Three Primary Material Types

Result showed that for this specific application (joints), both C-UHPC and N-UHPC perform similar. It seems that the C-UHPC was over designed and N-UHPC with lower mechanical properties lead to same results. The load deflection curve of five different numerical specimen is shown in Figure 5.20. In all five different specimen, N-UHPC and C-UHPC performed similar and increased the failure load. In S6, S9 and S12, use of high-performance material in joint also increased the maximum mid-span deflection before failure. In S16 and S20 with wider joint width, use of high-performance material led to lower deflection. This effect is shown in Figure 5.19 and Figure 5.20. Figure 5.19 (a) shows the effect of different material on numerical specimens and Figure 5.19 (b) shows the of deflection based on the different material used in specimen joints.
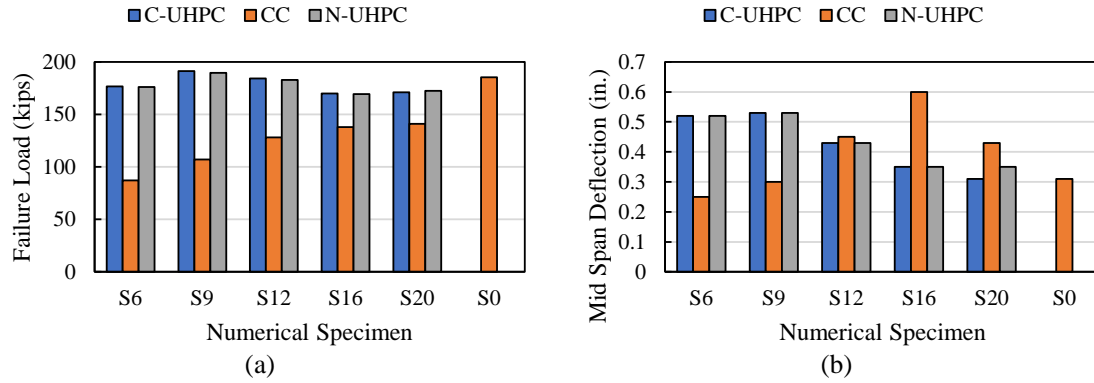
Figure 5.19: Effect of material on different numerical specimens; (a) failure load and (b) mid span deflection before failure

Figure 5.20 also shows the load deflection curves of different specimens. It should be emphasized that choosing different joint width initially was considered to show how wider joints with weaker material perfume compared to shorter joints with stronger material. But as it is shown in Figure 5.20, even 20-inch joint width filled with normal concrete could not perform as well as 6-inch joint filled with C-UHPC.
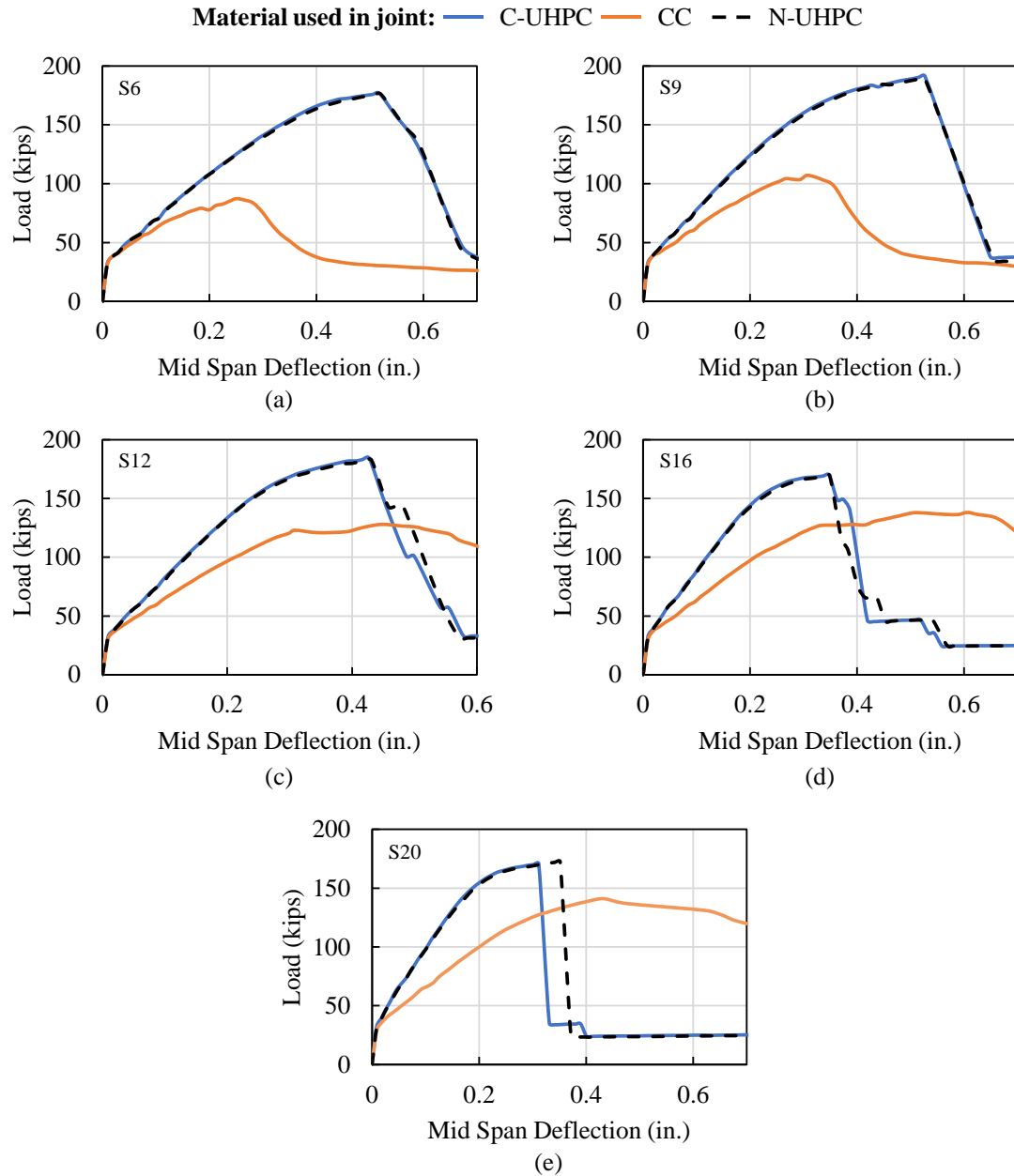
Figure 5.20: Load-deflection response of numerical specimens; (a) 6 in. joint width-S1, (b) 9 in. joint width-S2, (c) 12 in. joint width-S3, (d) 16 in. joint width-S4 and (e) 20 in. joint width-S5

As the load setup and monitoring point of deflection for all models were assumed same, the place of maximum deflection in deck system shifted toward the critical section between normal concrete and high-performance concrete (joint limit). Hence the reported mid span

deflection reported for specimen with wider joints (16 and 20 inches) was lower compared to specimen with shorter joint width (6,9 and 12 inches)

As shown in Figure 5.20 (d) and (e), the lower mid span deflection of specimen S16 and S20, when high performance material was used to fill the joint compared to specimen with shorter joint can be probably due to shorter distance between the load and material interface between high performance concrete and normal concrete. As the load setup was assumed for all specimen, in specimen with wider joints, the critical bonding surface between normal concrete and high performance would be closer to load center line and lead to lower capacity (lower failure load and lower deflection) before failure. This condition is illustrated schematically in Figure 5.21.
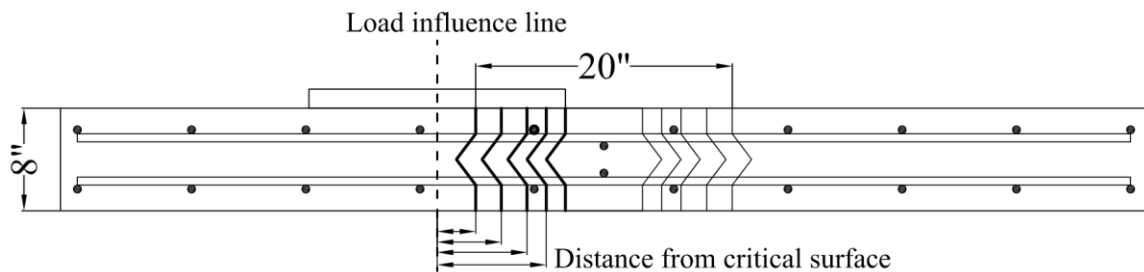
Figure 5.21: closer distance between load and critical bonding surface in wider specimens

5.6.3. Effect of Development Length and Joint Width

Figure 5.22 shows the effect of joint width which is directly related to development length of reinforcement with different used material in specimen joints. Results showed that increasing the joint width and development length did not change the failure load of system significantly when high performance material was used in joints. This can be explained and verify the findings of Graybeal [133] about required development length of high-performance material. In other words, the minimum calculated joint width according to

required development length of rebars in high-performance concrete (6-inch width) was adequate and increasing this amount by did not change the maximum failure load of system. Regard to mid span deflection and according to discussion in §5.6.2, mid span deflection decreased by increasing the joint width.
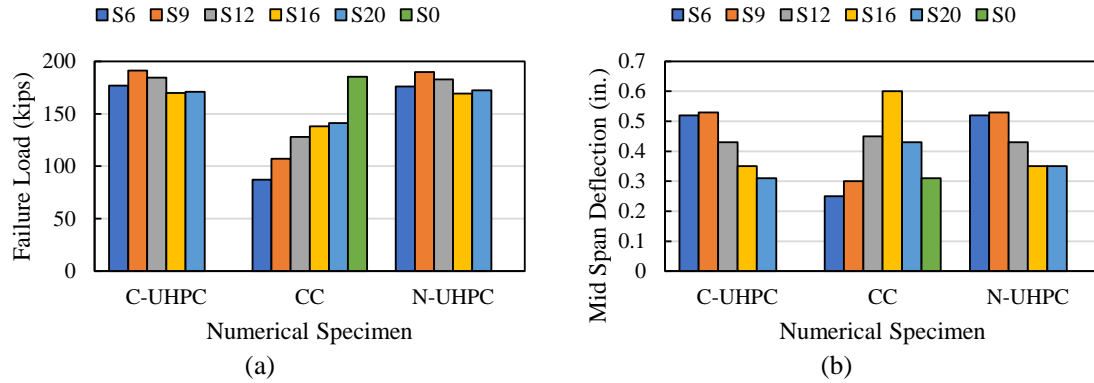

Figure 5.22:Effect of joint width on (a) failure load and (b) mid span deflection before failure

Focusing on conventional concrete, results revealed that increasing the development length of rebars in conventional concrete and consequently increasing the joint width, led to higher failure load. Considering the calculation of required development length (14 inches) and splice length for reinforcement in conventional concrete in §5.5.3, the failure load of specimen increased by enhancing the development length and joint width. The growth of failure load was significant until reaching to required development length in S16. After satisfying the minimum required development length for straight bars in conventional concrete no significant change observed comparing between S16 and S20. In this amount, jointless deck specimen (S0), showed the highest failure load compared to other specimens due its extended bars over the whole length of specimen. Comparing the ideal jointless deck system (S0) with rest of the specimens revealed that a S6-C-UHPC and S6-N-UHPC

with around 176 kips failure load and 0.5 deflection were performed similar to S0-CC with 185 kips failure load and 0.31 inches mid span deflection.

5.6.4. Effect of Material Properties

Very similar performance of all models that used N-UHPC and C-UHPC to fill the joint, shed light on this question that how much the minimum is required mechanical properties to get same results as joints filled with C-UHPC. For this purpose, a reverse analysis started to reduce to mechanical properties and compare their performance with base models filled with C-UHPC.

In this regard, first the weakest experimental results of this study were used as a start point and then other variants of mechanical properties were also modeled to fill the joint in specimens. S6-C-UHPC and S6-N-UHPC model were considered as based and the only material in joint were modified. In all figures of this section the results of S6-CC, S6-NHPC and S6-C-UHPC are shown for comparison with other modified models.

Several different material properties were modeled to evaluate the sensitivity of results to the mechanical properties of material in joints. Three group of weakened material were used for evaluating the response of whole model. Also, the weakest results of experimental section L9 was used for sensitivity analysis and represents the behavior of existing mix design, but all other weakened material (marked by "W" sign) were produced theoretically and may not reflect the actual mechanical properties of any UHPC.

Table 5-9 summarizes the models in them, tension strength and tension function were considered constant and compressive strength and modulus of elasticity were reduced to

see how model response changed. As it shown in Figure 5.23, changing the value of tensile strength itself, doesn't create as significant difference from S6-C-UHPC and S6-N-UHPC.

Table 5-9: Assumed material properties with same tension strength and tension function

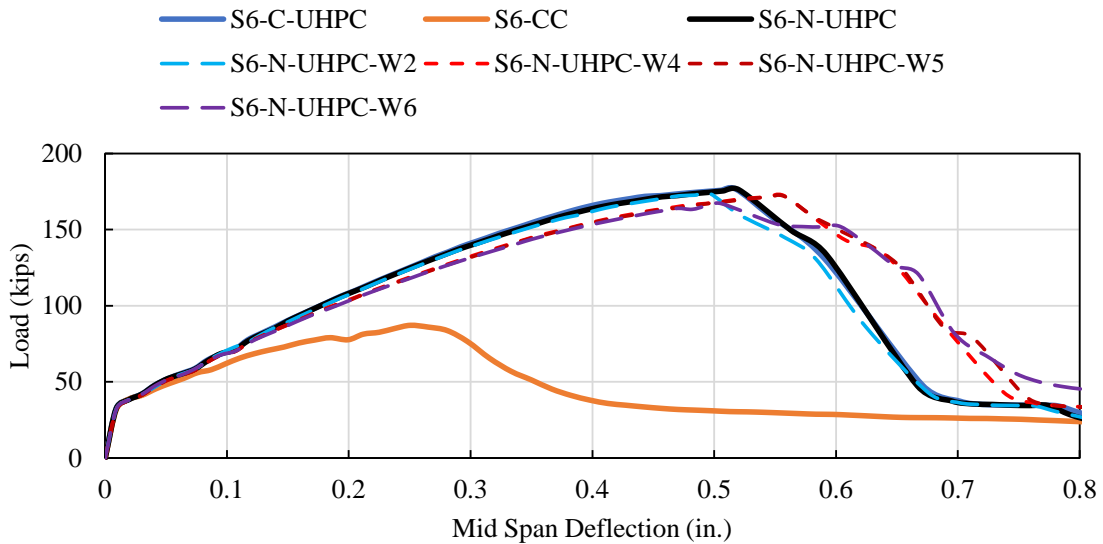| Material	Young's Modulus (E)	Poisson Ratio (υ)	Tension Strength (F$_t$)	Compression Strength (F$_c$)
	ksi	-	ksi	ksi
S6-N-UHPC-W2	7290	0.2	1	-11
S6-N-UHPC-W4	6000	0.2	1	-10
S6-N-UHPC-W5	6000	0.2	1	-6.7
S6-N-UHPC-W6	7290	0.2	1	-12
S6-CC	4950	0.2	0.3	-6.5
S6-C-UHPC	8900	0.2	1.4	-31.5
S6-N-UHPC	7800	0.2	1	-17

Figure 5.23: Load deflection response for models with lower compressive strength and modulus of elasticity

The second group of material were analyzed by keeping the compressive strength and modulus of elasticity constant and reducing the tensile strength. Compressive strength and modulus of elasticity of L9 were considered as a base and the amount of tensile strength

was changed to see how it affect the final response. Table 5-10 summarizes the mechanical properties of material that were evaluated in this group.

Table 5-10: Assumed material properties with same compressive strength, modulus of elasticity and tension function

Material	Young's Modulus (E)	Poisson Ratio (υ)	Tension Strength (F_t)	Compression Strength (F_c)
	ksi	-	ksi	ksi
S6-N-UHPC-L9	7290	0.2	0.83	-11
S6-N-UHPC-W1	7290	0.2	2.5	-11
S6-N-UHPC-W2	7290	0.2	1	-11
S6-N-UHPC-W8	7290	0.2	1.2	-11
S6-CC	4950	0.2	0.3	-6.5
S6-C-UHPC	8900	0.2	1.4	-31.5
S6-N-UHPC	7800	0.2	1	-17

All the material were modeled by considering the same tension function as C-UHPC and N-UHPC.

Figure 5.24 shows the importance of tensile strength value on the overall behavior of deck.

As it is shown in Figure 5.24, the value of tensile strength doesn't change the overall response of deck significantly.
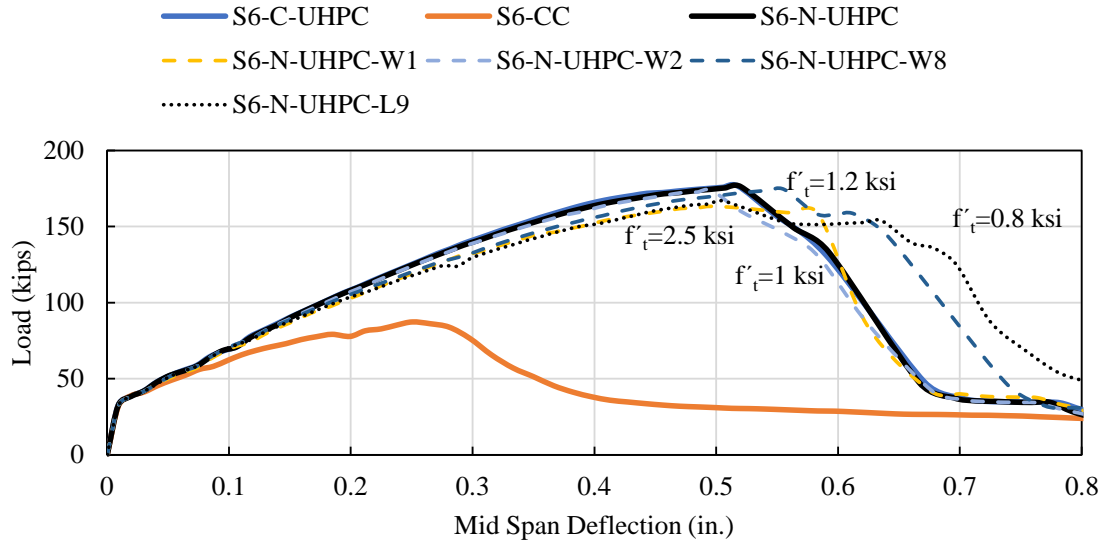
Figure 5.24: Load deflection response for models with lower tensile strength

In the third group, the effect of tension function or existing the fiber in UHPC were investigated. As discussed earlier, the main source of after cracking behavior and high tensile strength of UHPC is fiber. In this group, two different models were analyzed twice, and results were compared. Mechanical properties of CC and N-UHPC-L9 were considered as start point. Each one of them was modeled once with after cracking behavior and once like normal concrete. More details are summarized in Table 5-11.

Table 5-11: Assumed material properties for evaluating the effect of fibers

Material	Young's Modulus (E)	Poisson Ratio (υ)	Tension Strength (F_t)	Compression Strength (F_c)	Fiber
	ksi	-	ksi	ksi	
S6-CC	6000	0.2	0.3	-6.7	No
S6-CC*					Yes
S6-N-UHPC-L9	7290	0.2	0.83	-11.25	Yes
S6-N-UHPC-L9*					No

For S6-CC and S6-N-UHPC-L9*, no tension and compression function were assumed, and it means that these two models behave like normal concrete without any fiber in their mix designs. On the other hand, S6-CC* and S6-N-UHPC-L9 were modeled using user defined tension and compression function similar to found functions for C-UHPC in validation section. It means that these two models are reinforced with fibers and were able to demonstrate after cracking behavior like C-UHPC. Figure 5.25 shows the overall response of deck using these four different materials in 6-inch width joint. Comparing the load-deflection curves revealed that the tension function and after crack behavior are the critical factors that changed the system response significantly.

Comparing S6-CC* with 0.3 ksi tensile strength and tension function values similar to C-UHPC performed much better than S6-N-UHPC-L9* with 0.83 ksi and normal concrete behavior. It is worth to remind again that, S6-CC* and S6-N-UHPC-L9* were not related to any actual mix design and were created theoretically to evaluate the effect of different material properties.
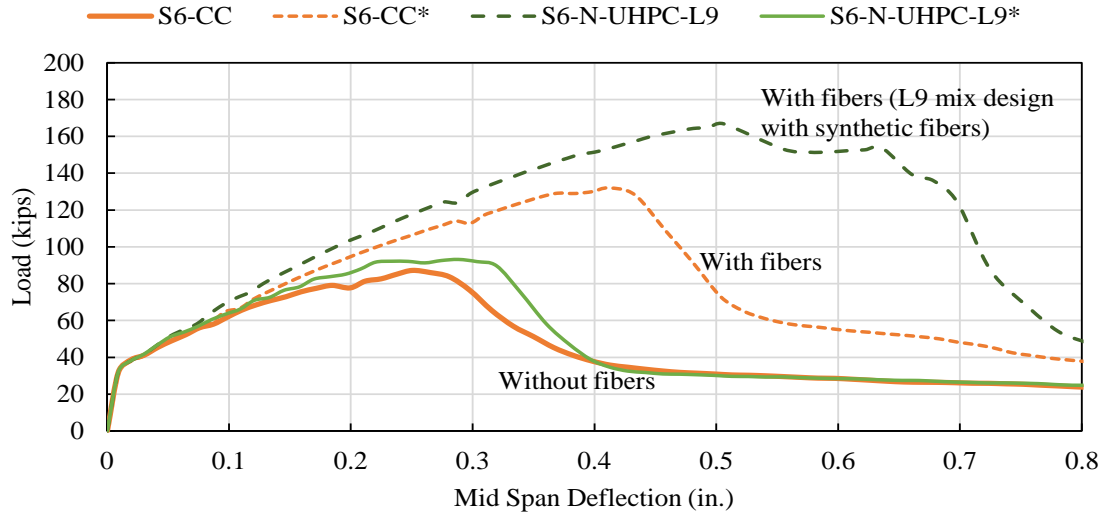
Figure 5.25: Load deflection response for models using no fiber in the material

Considering all analysis and comparing their results together revealed that, tensile strength and tension function plays the main role on overall response of deck panel system. Modulus of elasticity and compressive strength did not change the results significantly but the amount of tension strength and the tension function for after cracking behavior were critical factors.

Chapter 6: **Conclusions and Recommendations**

6.1. Summary and Conclusions

The main goal of this study was to improve the long-term performance of FDPC deck panel system by using non-proprietary UHPC concrete. Results revealed that using non-proprietary UHPC concrete instead of conventional concrete in connection between panels, improved the long-term performance of FDPC system significantly and lead to significant higher failure load and deflection. It also revealed that using non-proprietary UHPC concrete instead of the C-UHPC in joint between deck panels, lead to a significant saving. More detailed findings are summarized in the following sections:

6.1.1. FDPC Deck Panels

Full-depth, precast concrete (FDPC) deck panels have been used for new construction and rehabilitation since 1965 [1]. There have been surveys [2] conducted to attempt to determine the performance of bridges with FDPC deck panels, but not recently.

The work conducted under this project was aimed at determining the bridges that have been constructed in the US utilizing FDPC deck panels and evaluating their long-term performance. A state DOT survey was used to determine DOT practice and opinion and compile the FDPC deck panel projects completed in each state. The FDPC Deck Panel Database was created based on the survey results and information obtained from the ABC Project Database. This database contained detailed information on 280 bridges throughout the U.S. specifically for those constructed with FDPC deck panels. The performance of the bridges in the FDPC Deck Panel Database was analyzed based on NBI inspection data and

the influential variables according to linear regression and deep learning model. The following conclusions were made based on this analysis:

- **Joint Type**: The three joints with better performance in terms of higher estimated service life coming from estimation models, were the UHPC with straight bar (C1.f) (for transverse or longitudinal joints), longitudinal post-tensioned (C1.a) (for transverse joints), and conventional concrete with hooped bar details (C1.h) (for longitudinal joints).

- **Climate Zone**: As expected, bridges with FDPC deck panels have the shortest average estimated service life in cold climate zones. More freeze-thaw cycles compare to very cold zones has made the most damages to bridges constructed in cold zones.

- **Wearing Surface**: FDPC deck panel bridges with monolithic concrete, integral concrete, epoxy overlay, and bituminous wearing surfaces have shown similar performance. Bridges with other wearing surfaces (including microsilica concrete, polyester polymer, and silica fume concrete) have longer estimated service lives. Anyway, using a proper protection layer prevent aggressive ions like chloride to reach the concrete surface and enhance the durability of protected elements

- **Traffic**: As expected, bridges with FDPC deck panels and high traffic volumes have a shorter average estimated service life than similar bridges with lower traffic volumes. A more detailed study is required to investigate the effect of passing traffic based on the bridge function.

- **Construction Type**: There was no difference in performance between bridges using FDPC deck panels for new construction compared with those using them for rehabilitation projects.

There are limitations to the approach and analysis described in this study due to a limited sample size and the subjectivity of the NBI inspection data. These findings were made based on statistical analyses of the NBI inspection data and more general observations on performance from state DOTs. The FDPC Deck Panel Database can be used as a starting point for future investigations with more in-depth inspection techniques (e.g., non-destructive testing) and revisited every 5 to 10 years as the bridges continue to age and new bridges are constructed. There is no question that precast and prefabricated elements are the future of bridge construction. The results of this study may suggest though there is room for improvement in joint performance.

6.1.2. Non-Proprietary UHPC Concrete

Ultra-high performance concrete (UHPC) is generally known as a cementitious composite material with compressive strength (greater than 18 ksi) and high tensile strength (greater than 1 ksi) [44], [46]. UHPC is continually becoming more popular among academia, engineers, and owners due to its unique properties. Commercially available UHPC products offer consistent quality and material properties, but their use has been limited due to their high cost, which can be 25 to 30 times more expensive than conventional concrete.

The research effort conducted under this project aimed to study the effect of different variables, including fiber type, fiber content, cement type, cement content, HRWR dosage,

VMA dosage, w/b, and UFR content, on the final mechanical properties of UHPC mixtures. Knowledge gained from this investigation was then used to develop a non-proprietary UHPC mix design made with locally-produced raw materials achieving the necessary mechanical properties and durability for use in bridge components, repair, and connections. A total of 115 small-scale batches (0.15 ft^3) and 10 large-scale batches (2.2 ft^3) were cast to investigate the different variables and develop the final mixture design.

Some of the major conclusions from this research are summarized below:

1. Particle packing theory can be used with simple spreadsheets as a first step in the UHPC mixture development phase.

2. The fine aggregate moisture content affected the repeatability of the UHPC mixtures. Fine aggregates should be oven dried to ensure consistent material properties can be achieved.

3. Type I/II or Lehigh White cement resulted in similar compressive strengths and workability. Type III cement led to higher compressive strength but shortened the working time for the UHPC.

4. A water-to-binder ratio between 0.18 and 0.20 produced the highest compressive strength while maintaining a good flow and working time. The water content in the chemical admixtures can affect the compressive strength and should be considered when determining how much water should be added to a mixture.

5. Flow should be kept between 8 and 10 inches to help prevent fiber settlement and ensure sufficient workability and working time. This was achieved using a HRWR

dosage between 22 and 29.4 oz./cwt. A typical dosage of 27.5 oz./cwt could be used for all mixtures with w/b of 0.20 and with only fine masonry sand (i.e., no UFR).

6. VMA content did not influence the compressive strength. VMA can be used at dosages less than 10 oz./cwt to stabilize heavier steel fibers in the mixtures.

7. The use of fibers with 0.5-inch length, 0.008-inch diameter, and tensile strength of 400 ksi led to the best overall performance of the UHPC. This size fiber reasonably distributed in the mixture without the addition of any VMA.

8. Uncoated fibers with high zinc contents can lead to an expansive reaction in the UHPC that greatly decreases its strength. This reaction can be observed in small-scale (0.15 ft^3) trial batches.

9. The use of synthetic fibers led to lower compressive strength, density, modulus of elasticity, and tensile strength compared to similar mixtures with steel fibers. The use of synthetic fibers did lead to higher bulk resistivity than similar mixtures with steel fibers.

10. Higher steel fiber contents (2 versus 4 percent) generally led to higher tensile strength but similar compressive strength and modulus of elasticity. Higher steel fiber contents also decreased the bulk resistivity.

11. The use of ultra-fines recovery (UFR) materials at a 30 percent replacement generally led to improved performance. In the small-scale batches, its use was found to increase compressive strengths by 10 to 15 percent. The large-scale batches resulted in similar compressive strength and modulus of elasticity, and higher tensile strength. More HRWR is needed for mixtures with UFR to achieve flows between 8 and 10 inches.

12. All mixtures had average bulk resistivities in the very low classification of permeability measurements. The presence of steel fibers dramatically decreased the bulk resistivity. Higher steel fiber contents led to lower bulk resistivity.

13. The average shrinkage strains were 470, 549, and 596 microstrain for 7, 30, and 90 days after casting.

14. Variation in results did not show any specific correlation between time and how moist curing affects the mechanical properties. More investigation is required to find the exact effect of moist curing.

15. The cost comparison analysis revealed that the N-UHPC mixtures with 2% fibers cost between $466 to $830 which is between 23 to 41% of minimum reported value for C-UHPC ($2000). This significant drop in price can save a significant portion of construction budget and will develop the use of non-proprietary UHPC concrete more than before.

Two mix designs were developed based on the availability of UFR and summarized in Table 6-1. These mixtures gave compressive strengths close to the 18-ksi minimum and had modulus of rupture strengths above the 1.5-ksi first crack and 2.0-ksi peak minimum values typically used for UHPC [46].

Table 6-1: Proposed non-proprietary UHPC mix designs

Mix.	Cement Type	W/B	Mix Proportions						Fiber		Admixtures	
			ag/cm	*C*	*S*	*SF*	*FA*	*UFR*	*Type*	*Content (%)*	*HRWR (oz./cwt)*	*VMA (oz./cwt)*
1	Titan Type I/II	0.20	1.0	0.6	0.3	0.1	1.00	0.00	HF or OL	2.0	27.5	0
2	Titan Type I/II	0.20	1.0	0.6	0.3	0.1	0.70	0.30	HF or OL	2.0	29.5	0

These mix designs can be used with the procedure outlined in §4.1.2 to determine the specific amounts of material to use based on the desired quantity of UHPC.

6.1.3. Numerical Analysis of Joint Performance

Numerical analyses were performed with ATENA to evaluate the performance of typical joints between FDPC deck panels with straight bars and different joint material properties and joint widths. Six (6) different joint widths and many different material types were analyzed. Three of the primary materials investigated included conventional concrete, commercial UHPC and non-proprietary UHPC. Additional variations of the material properties were made to see the specific effect of compressive strength, tensile strength, and post-cracking behavior (i.e., fiber content) on the joint performance. The validation process was completed using previous experimental research. Results revealed that N-UHPC with lower mechanical properties than C-UHPC, lead to similar performance.

It was concluded that for joints, the tensile strength and tension function (i.e., post-cracking behavior based on fiber type and content) of concrete influence the joint behavior more than compressive strength and modulus of elasticity. In other words, for connection precast members like deck panels under flexural load, the tensile characteristics of filler material and its bond with precast elements has higher priority than compressive strength and modulus of elasticity. Results from the numerical analysis showed that a joint material with a minimum tensile strength of 0.8 ksi and similar post-cracking tensile behavior to UHPC and at least 12 ksi compressive strength at 28 days led to similar results as commercial UHPC. These minimum values should be validated with additional research.

It should be emphasized that the tensile strength of the concrete itself will not lead to satisfactory joint performance; the tensile strength needs to be accompanied by a proper after crack behavior (tension function).

Based on the results from the numerical analyses, even the non-proprietary UHPC mixtures with synthetic fibers (L9 and L10), which had the smallest compression and modulus of rupture strengths could likely be used for joint application. Although, using synthetic fibers did not result in high compressive strength and modulus of elasticity, these fibers appear to create a proper tensile strength and after cracking behavior that could fit for joint applications.

6.2. Contribution to the Field

Precast concrete elements can be connected to form a complete structure and speed up the construction speed while addressing the durability and long-term maintenance of whole system. One of the popular precast elements are FDPC deck panels that have been widespread in the past decades. Commercial UHPC was known as a filler material for connecting the precast members like FDPC deck panels. The high mechanical properties of UHPC have made it a good potential for improving the long-term performance of FDPC deck panels and minimize the previously observed issue in joints filled with conventional concrete include cracking, leaking and other related issues. Although, the mechanical properties of commercial UHPC have satisfied all the requirements for filling the joints, but its relatively high cost has limited its widespread use.

Non-proprietary UHPC is the economical version of this material and was developed using the locally-produced raw materials. Although the mechanical properties of non-proprietary UHPC were lower than commercial UHPC, it showed that they can lead to similar performance when they are used in the joints between deck panels.

According to this finding, bridge owners, contractors, engineers, and designers can use same procedure used in this study to develop their own non-proprietary UHPC concrete with locally available material in the location of the project and use it as joint filler in the future bridge construction.

6.3. Recommendation for Future Research

There are limitations to the approach and analysis in this project and some numerical assumptions were considered that need to be validate with full scale experimental specimen. The finding of this study can be used a start point for further investigations on the application of non-proprietary UHPC concrete. All in all, the following items should be considered for future work:

- Additional experimental tests should be done to prove the proper performance of non-proprietary UHPC in joint application.

- More load setup and more analysis like fatigue test under cyclic load has to be done to validate the performance of non-proprietary UHPC.

- Additional experimental testing should be done with different bonded and unbonded reinforcement models to confirm the findings from the numerical efforts of this research.

- More studies are required to be done on synthetic fibers, mix designs with synthetic fibers were estimated 80% lower than the minimum cost of commercial UHPC and modifying the length and other properties of these fiber types can led to significant saving.

- Using fibers increased the compressive strength of samples slightly compared to samples without fiber. More studies are required to investigate this fact based on the fiber type and content before applying any modification on design strength.

- More studies are required to investigate the effect of higher stiffness in joints. Using UHPC in joints increase the stiffness of joints significantly. This higher stiffness will attract more forces and may cause higher deterioration rate and make some long-term concerns which need to be investigated in future works.

- Although using UHPC reduces future maintenance costs, but the maintenance and repair of regions constructed with UHPC is another challenge that need to be studied in more details.

References

[1]   S. S. Badie and M. K. Tadros, "NCHRP Report 584: Full-Depth, Precast-Concrete Bridge Deck Panel Systems," National Cooperative Highway Research Program (NCHRP) Report 584, 2008.

[2]   B. Graybeal, "UHPC in the US Highway Infrastructure," *Des. Build. UHPFRC Marseille Fr.*, 2009.

[3]   H. Russel and B. Graybeal, "Ultra-High-Performance Concrete: A State-of-the-Art Report for the Bridge Community. Federal Highway Administration; McLean, VA," 2013.

[4]   M. Berry, R. Snidarich, and C. Wood, "Development of Non-Proprietary Ultra-High Performance Concrete," Montana Dept. of Transportation Research Programs, 2017.

[5]   E. Shahrokhinasab and D. Garber, "Long-term performance of full-depth precast concrete (FDPC) deck panels," *Eng. Struct.*, vol. 244, p. 112738, 2021.

[6]   E. Shahrokhinasab and D. Garber, "Development of 'ABC-UTC Non-Proprietary UHPC' Mix," 2021.

[7]   D. Garber, "ABC Project Database," 2016. http://utcdb.fiu.edu/ (accessed May 24, 2016).

[8]   H. Russell, M. Ralls, and B. Tang, "Part 3: Concrete Bridges: Prefabricated Bridge Elements and Systems in Japan and Europe," *Transp. Res. Rec. J. Transp. Res. Board*, no. 1928, pp. 101–109, 2005.

[9]   M. P. Culmo, "Connection details for prefabricated bridge elements and systems," 2009.

[10] D. Garber and E. Shahrokhinasab, "Performance Comparison of In-Service, Full-Depth Precast Concrete Deck Panels to Cast-in-Place Decks," Accelerated Bridge Construction University Transportation Center (ABC-UTC), 2019.

[11] L. S. Pheng and C. J. Chuan, "Just-in-time management of precast concrete components," *J. Constr. Eng. Manag.*, vol. 127, no. 6, pp. 494–501, 2001.

[12] G. Polat, "Factors affecting the use of precast concrete systems in the United States," *J. Constr. Eng. Manag.*, vol. 134, no. 3, pp. 169–178, 2008.

[13] B. Graybeal, "Design and construction of field-cast UHPC connections.," United States. Federal Highway Administration, 2014.

[14] B. A. Graybeal, "Fatigue response in bridge deck connection composed of field-cast ultra-high-performance concrete," *Transp. Res. Rec.*, vol. 2251, no. 1, pp. 93–100, 2011.

[15] B. A. Graybeal, "Behavior of field-cast ultra-high-performance concrete bridge deck connections under cyclic and static structural loading," United States. Federal Highway Administration, 2010.

[16] H. M. Afefy, K. Sennah, S. Tu, M. Ismail, and R. Kianoush, "Development and study of deck joints in prefabricated concrete bulb-tee bridge girders: Experimental evaluation," *Bridge Struct.*, vol. 11, no. 1, 2, pp. 55–71, 2015.

[17] M. Sayed-Ahmed and K. Sennah, "Fatigue Resistance of GFRP-Reinforced Precast Full-Depth Deck Panel with Transverse Joints," *Cairo Egypt*, 2015.

[18] S. S. K. Dolati and A. Mehrabi, "Review of Mechanical Bar Couplers for Splicing Precast Concrete Members".

[19] M. Sayed-Ahmed and K. Sennah, "Structural behavior of UHPFRC-filled, transverse C-joint in full-depth, GFRP-reinforced, precast bridge deck panels resting over steel girders," presented at the Proceedings of the 4th International Conference on Engineering Materials and Mechanics, Regina, SK, Canada, 2015.

[20] M. Sayed-Ahmed, K. Sennah, and D. Lai, "Development of transverse joints for full-depth precast normal strength concrete deck panels incorporating ribbed-surface GFRP bars and UHPFRC," 2014, pp. 1–10.

[21] H. M. Afefy, N. M. Kassem, and S. E.-D. F. Taher, "Retrofitting of defected closure strips for full-depth precast concrete deck slabs using EB-CFRP sheets," *Pract. Period. Struct. Des. Constr.*, vol. 24, no. 4, p. 04019025, 2019.

[22] M. Sherif, "Flexure strength prediction of closure strip between prefabricated deck slabs supported over bridge girders incorporating GFRP bars and UHPFRC," *Tor. Ryerson Univ*, 2017.

[23] C. Ribeiro do Valle, H. Abdalla, S. Islam, and M. A. Issa, "Performance of transverse joint grout materials in full-depth precast concrete bridge deck systems," *PCI J.*, vol. 48, no. 4, 2003.

[24] B. A. Graybeal, "Development of Non-Proprietary Ultra-High-Performance Concrete for Use in the Highway Bridge Sector: TechBrief," United States. Federal Highway Administration, 2013.

[25] I. De la Varga, R. P. Spragg, J. F. Muñoz, C. A. Nickel, and B. A. Graybeal, "Application of internal curing in cementitious grouts for prefabricated bridge concrete elements connections," *Adv. Civ. Eng. Mater.*, vol. 7, no. 4, pp. 628–643, 2018.

[26] Z. B. Haber and B. A. Graybeal, "Experimental Evaluation of Prefabricated Deck Panel Connections," 2015.

[27] Utah Department of Transportation (UDOT), "Performance of Accelerated Bridge Construction Projects in Utah: As of May 2009 (Lessons Learned Report)," 2009.

[28] Utah Department of Transportation (UDOT), "Performance of Accelerated Bridge Construction Projects in Utah: As of June 2010 (Lessons Learned Report)," 2010.

[29] Utah Department of Transportation (UDOT), "Performance of Accelerated Bridge Construction Projects in Utah: As of September 2011 (Lessons Learned Report)," 2011.

[30] Utah Department of Transportation (UDOT), "Performance of Accelerated Bridge Construction Projects in Utah: As of October 2013 (Lessons Learned Report)," 2013.

[31] Utah Department of Transportation (UDOT), "Performance of Accelerated Bridge Construction Projects in Utah: As of August 2016 (Lessons Learned Report)," 2016.

[32] D. Garber, "Compilation of Accelerated Bridge Construction (ABC) Bridges," Florida International University (FIU), Miami, 2016.

[33] Office of Energy and Renewable Energy, "Climate Zones.," *Department of Energy*, Mar. 2019.

[34] Federal Highway Administration, "LTBP InfoBridge." https://infobridge.fhwa.dot.gov/

[35] Federal Highway Administration (FHWA), "National Bridge Inventory (NBI)," 2016. https://www.fhwa.dot.gov/bridge/nbi.cfm (accessed May 05, 2016).

[36] E. Shahrokhinasab and D. Garber, "ABC-UTC Guide for: Full-Depth Precast Concrete (FDPC) Deck Panels," 2019.

[37] "LTBP: Long-Term Bridge Performance Program-- | Federal Highway Administration." https://www.fhwa.dot.gov/research/tfhrc/programs/infrastructure/structures/ltbp/products.cfm#sec4 (accessed Mar. 13, 2018).

[38] W. Weseman, "Recording and coding guide for the structure inventory and appraisal of the nation's bridges," *U. S. Dep. Transp. Ed Fed. Highw. Adm. USA*, 1995.

[39] D. Garber and E. Shahrokhinasab, "Performance Comparison of In-Service, Full-Depth Precast Concrete Deck Panels to Cast-in-Place Decks," Accelerated Bridge Construction University Transportation Center (ABC-UTC), ABC-UTC-2013-C3-FIU05-Final, Mar. 2019.

[40] J. Nehme and P. Lu, "New Bridge Deck Condition Forecasting Models," TRB 2020 Annual Meeting, Jan. 2020.

[41] Y. J. Kim and D. K. Yoon, "Identifying critical sources of bridge deterioration in cold regions through the constructed bridges in North Dakota," *J. Bridge Eng.*, vol. 15, no. 5, pp. 542–552, 2009.

[42] Heng Liu, Jean A. Nehme and Ping L, "Bridge Deck Condition Rating Forecast— Machine Learning Models." US Department of Transportation, Federal Highway Administration, Apr. 22, 2020. [Online]. Available: https://highways.dot.gov/research/long-term-infrastructure-performance/ltbp/data-analysis/bridge-deck-condition-rating-machine

[43] D. M. Frangopol, M. Kallen, and J. M. van Noortwijk, "Probabilistic models for life-cycle performance of deteriorating structures: review and future directions," *Prog. Struct. Eng. Mater.*, vol. 6, no. 4, pp. 197–212, 2004.

[44] B. Graybeal, "Ultra-High-Performance Concrete--| Federal Highway Administration," *Accedido Marzo*, vol. 23, 2015.

[45] R. Karim, M. Najimi, and B. Shafei, "Assessment of transport properties, volume stability, and frost resistance of non-proprietary ultra-high performance concrete," *Constr. Build. Mater.*, vol. 227, p. 117031, 2019, doi: https://doi.org/10.1016/j.conbuildmat.2019.117031.

[46] M. K. Tadros et al., "Implementation of Ultra-High-Performance Concrete in Long-Span Precast Pretensioned Elements for Concrete Buildings and Bridges," *Precast. Concr. Inst. PCI*, Jan. 2020, doi: https://doi.org/10.15554/pci.rr.mat-012.

[47] K. Wille, A. E. Naaman, and G. J. Parra-Montesinos, "Ultra-High Performance Concrete with Compressive Strength Exceeding 150 MPa (22 ksi): A Simpler Way.," *ACI Mater. J.*, vol. 108, no. 1, 2011.

[48] B. Graybeal, "Design and construction of field-cast UHPC connections.," United States. Federal Highway Administration, 2019.

[49] ACI Committee 239, "Ultra-High Performance Concrete: An Emerging Technology Report (ACI 239R-18)," *Farmington Hills MI Am. Concr. Inst.*, 2018.

[50] Association Francaise de Normalisation (AFNOR), "Concrete - Ultra-high performance fibre-reinforced concrete - Specifications, performance, production and conformity.," *AFNOR Fr.*, pp. 18–470, France 2016.

[51] American Society for Testing and Materials (ASTM), "C1856/C1856M - 17 - Standard Practice for Fabricating and Testing Specimens of Ultra-High Performance Concrete," 2017, doi: https://doi.org/10.1520/c1856_c1856m-17.

[52] Canadian Standards Association, "CSA A23.1 Concrete materials and methods of concrete construction, Annex U - Ultra-high Performance Concrete (UHPC).," *Mississauga Ont. Can. Stand. Assoc.*, 2019.

[53] Swiss Society of Engineers and Architects (SIA). (2016)., "SIA 2052 Béton fibré ultra-performant (BFUP) - Matériaux, dimensionnement et exécution (Ultra-High Performance Fibre Reinforced Cement-based Composites [UHPFRC]- Construction material, dimensioning and application).," *Zurich SIA*, 2016.

[54] Z. Haber, I. D. la Varga, B. A. Graybeal, B. Nakashoji, and R. El-Helou, "Properties and Behavior of UHPC-Class Materials," Federal Highway Administration (FHWA), FHWA-HRT-18-036, Mar. 2018.

[55] J. Resplendino, "State of the art of design and construction of UHPFRC structures in France," 2012, pp. 27–41.

[56] C. Sosa Cardenas, I. M. Mantawy, and A. Azizinamini, "Repair of Timber Piles Using Ultra-High-Performance Concrete," 2021.

[57] A. Azizinamini, S. Rehmat, and A. Sadeghnejad, "Enhancing resiliency and delivery of bridge elements using ultra-high performance concrete as formwork," *Transp. Res. Rec.*, vol. 2673, no. 5, pp. 443–453, 2019.

[58] B. A. Graybeal, "Fatigue response in bridge deck connection composed of field-cast ultra-high-performance concrete," *Transp. Res. Rec.*, vol. 2251, no. 1, pp. 93–100, 2011.

[59] A. Khodayari, I. M. Mantawy, and A. Azizinamini, "Introducing a New Connection Detail for Connecting Prefabricated Barrier to Concrete Deck Using UHPC," 2021.

[60] J. Juhart, N. Randl, W. Schneider, and A. Pichler, "Study on the Application of UHPC for Precast Tunnel Segments," in *International Symposium on Ultra High Performance Concrete*, 2012, pp. 981–988.

[61] H. Aoude, S. De Carufel, and C. Melançon, "Blast Behavior of One-Way Panel Components Constructed with UHPC," 2016, vol. 1, no. 1. doi: https://doi.org/10.21838/uhpc.2016.60.

[62] S. Sritharan and G. M. Schmitz, "Design of tall wind turbine towers utilizing UHPC," presented at the 2nd International Symposium on Ultra-High Performance Fibre-Reinforced Concrete (UHPFRC). Marseille, France, 2013.

[63] S. Aaleti, B. Petersen, and S. Sritharan, "Design guide for precast UHPC waffle deck panel system, including connections," 2013.

[64] J. Heimann, "The implementation of full depth UHPC waffle bridge deck panels," United States. Federal Highway Administration, 2013.

[65] "hhbc-consulting - UHPC Onshore windmill tower and foundation." / (accessed Feb. 25, 2021).

[66] P. Acker and M. Behloul, "Ductal® technology: A large spectrum of properties, a wide range of applications," 2004, pp. 11–23. [Online]. Available: https://www.ductal.com/en

[67] P. Fontana *et al.*, "Composite UHPC façade elements with functional surfaces," *HiPerMat 2016*, pp. 9–11, 2016.

[68] "Ductal® | Innovative UHPC Solution," *Ductal®*, Jul. 27, 2015. https://www.ductal.com/en (accessed Feb. 25, 2021).

[69] B. A. Graybeal, "Material property characterization of ultra-high-performance concrete," United States. Federal Highway Administration. Office of Infrastructure …, 2006.

[70] P. Li, Q. Yu, and H. Brouwers, "Effect of coarse basalt aggregates on the properties of Ultra-high Performance Concrete (UHPC)," *Constr. Build. Mater.*, vol. 170, pp. 649–659, 2018.

[71] A. Arora, Y. Yao, B. Mobasher, and N. Neithalath, "Fundamental insights into the compressive and flexural response of binder-and aggregate-optimized ultra-high performance concrete (UHPC)," *Cem. Concr. Compos.*, vol. 98, pp. 1–13, 2019.

[72] S. El-Tawil, M. Alkaysi, A. E. Naaman, W. Hansen, and Z. Liu, "Development, Characterization and Applications of a Non Proprietary Ultra High Performance Concrete for Highway Bridges," Michigan Dept. of Transportation, 2016.

[73] M. S. Meddah, S. Zitouni, and S. Belâabes, "Effect of content and particle size distribution of coarse aggregate on the compressive strength of concrete," *Constr. Build. Mater.*, vol. 24, no. 4, pp. 505–512, 2010, doi: https://doi.org/10.1016/j.conbuildmat.2009.10.009.

[74] M. Alkaysi and S. El-Tawil, "Effects of variations in the mix constituents of ultra high performance concrete (UHPC) on cost and performance," *Mater. Struct.*, vol. 49, no. 10, pp. 4185–4200, 2016, doi: https://doi.org/10.1617/s11527-015-0780-6.

[75] B. A. Graybeal, "Development of Non-Proprietary Ultra-High-Performance Concrete for Use in the Highway Bridge Sector: TechBrief," United States. Federal Highway Administration, 2013.

[76] R. Yu, P. Spiesz, and H. Brouwers, "Effect of nano-silica on the hydration and microstructure development of Ultra-High Performance Concrete (UHPC) with a low binder amount," *Constr. Build. Mater.*, vol. 65, pp. 140–150, 2014.

[77] A. Tafraoui, G. Escadeillas, S. Lebaili, and T. Vidal, "Metakaolin in the formulation of UHPC," *Constr. Build. Mater.*, vol. 23, no. 2, pp. 669–674, 2009.

[78] A. M. Matos, S. Nunes, C. Costa, and J. L. Barroso-Aguiar, "Characterization of non-proprietary UHPC for use in rehabilitation/strengthening applications," in *Rheology and Processing of Construction Materials*, Springer, 2019, pp. 552–559. doi: https://doi.org/10.1007/978-3-030-22566-7_64.

[79] M. Berry, "Feasibility of Non-Proprietary Ultra-High Performance Concrete (UHPC) for Use in Highway Bridges in Montana: Phase II Field Application," 2018, [Online]. Available: https://scholarworks.montana.edu/xmlui/handle/1/15911

[80] S. El-Tawil, Y.-S. Tai, J. A. Belcher II, and D. Rogers, "Open-Recipe Ultra-High-Performance Concrete," *Formwork*, p. 33, 2020.

[81] A. J. Giesler, S. B. Applegate, and B. D. Weldon, "Implementing nonproprietary, ultra-high-performance concrete in a precasting plant," *PCI J.*, vol. 61, no. 6, pp. 68–80, 2016, doi: https://doi.org/10.15554/pcij61.6-03.

[82] T. Looney, A. McDaniel, J. Volz, and R. Floyd, "Development and characterization of ultra-high performance concrete with slag cement for use as bridge joint material," *Development*, vol. 1, no. 02, 2019.

[83] A. Neville and an O. M. C. Safari, *Properties of Concrete, Fifth Edition*. 2012. Accessed: Feb. 22, 2021. [Online]. Available: https://www.safaribooksonline.com/complete/auth0oauth2/&state=/library/view//9780273786337/?ar

[84] American Society for Testing and Materials (ASTM), "C109/C109M - Standard Test Method for Compressive Strength of Hydraulic Cement Mortars (Using 2-in. or [50-mm] Cube Specimens)," 2016.

[85] A. Tafraoui, G. Escadeillas, and T. Vidal, "Durability of the ultra high performances concrete containing metakaolin," *Constr. Build. Mater.*, vol. 112, pp. 980–987, 2016.

[86] R. Yu, P. Spiesz, and H. Brouwers, "Development of an eco-friendly Ultra-High Performance Concrete (UHPC) with efficient cement and mineral admixtures uses," *Cem. Concr. Compos.*, vol. 55, pp. 383–394, 2015.

[87] E. Shahrokhinasab, F. D. Chitty, M. Vahedi, and S. Zolfagharysaravi, "Improvement of Concrete Characterization Using Nanosilica," *Comput. Eng. Phys. Model.*, vol. 4, no. 2, pp. 39–52, 2021.

[88] A. Nasution, I. Imran, and M. Abdullah, "Improvement of concrete durability by nanomaterials," *Procedia Eng.*, vol. 125, pp. 608–612, 2015.

[89] A. Ehsani, M. Nili, and K. Shaabani, "Effect of nanosilica on the compressive strength development and water absorption properties of cement paste and concrete containing Fly Ash," *KSCE J. Civ. Eng.*, vol. 21, no. 5, pp. 1854–1865, 2017.

[90] A. Çevik, R. Alzeebaree, G. Humur, A. Niş, and M. E. Gülşan, "Effect of nano-silica on the chemical durability and mechanical performance of fly ash based geopolymer concrete," *Ceram. Int.*, vol. 44, no. 11, pp. 12253–12264, 2018.

[91] A. M. Fadzil, M. M. Norhasri, M. Hamidah, M. Zaidi, and J. M. Faizal, "Alteration of nano metakaolin for ultra high performance concrete," in *InCIEC 2013*, Springer, 2014, pp. 887–894.

[92] M. M. Norhasri, M. Hamidah, A. M. Fadzil, and O. Megawati, "Inclusion of nano metakaolin as additive in ultra high performance concrete (UHPC)," *Constr. Build. Mater.*, vol. 127, pp. 167–175, 2016.

[93] A. E. Naaman, "Fiber reinforced concrete: Five decades of progress," 2018, pp. 22–25.

[94] A. E. Naaman, *Fiber reinforced cement and concrete composites*. Techno Press 3000, 2018.

[95] M. Lachemi, K. Hossain, V. Lambros, P.-C. Nkinamubanzi, and N. Bouzoubaa, "Performance of new viscosity modifying admixtures in enhancing the rheological properties of cement paste," *Cem. Concr. Res.*, vol. 34, no. 2, pp. 185–193, 2004, doi: http://dx.doi.org/10.1016/S0008-8846(03)00233-3.

[96] J. S. Lawler, M. K. Tadros, M. Lampton, and E. N. Wagner, "Development of Non-Proprietary UHPC for Florida Precast Applications," 2019, vol. 2, no. 1. doi: https://doi.org/10.21838/uhpc.9689.

[97] American Society for Testing and Materials (ASTM), "ASTM C1760-12-Standard Test Method for Bulk Electrical Conductivity of Hardened Concrete," 2012.

[98] American Society for Testing and Materials (ASTM), "C39/C39M-21 - Standard Test Method forCompressive Strength of Cylindrical Concrete Specimens," 2021.

[99] American Society for Testing and Materials (ASTM), "C78/C78M-18 - Standard Test Method for Flexure Strength of Concrete (Using Simple Beam with Third-Point Loading)," 2018.

[100] American Society for Testing and Materials (ASTM), "C469/C469M-14 - Standard Test Method for Static Modulus of Elasticity and Poisson's Ratio of Concrete in Compression," 2014.

[101]   American Society for Testing and Materials (ASTM), "C496/C496M-17 - Standard Test Method for Splitting Tensile Strength of Cylindrical Concrete Specimens," 2017.

[102]   American Society for Testing and Materials (ASTM), "C1437-20 - Standard Test Method for Flow of Hydraulic Cement Mortar," 2020.

[103]   American Society for Testing and Materials (ASTM), "C403/C403M - 16 - Standard Test Method for Time of Setting of Concrete Mixtures by Penetration Resistance," 2016.

[104]   American Society for Testing and Materials (ASTM), "C230/C230M - 21 - Standard Specification for Flow Table for Use in Tests of Hydraulic Cement," 2021.

[105]   A. Andreasen, "Über die Beziehung zwischen Kornabstufung und Zwischenraum in Produkten aus losen Körnern (mit einigen Experimenten)," *Kolloid-Z.*, vol. 50, no. 3, pp. 217–228, 1930, doi: https://doi.org/10.1007/bf01422986.

[106]   D. Dinger and J. Funk, "Predictive process control of crowded particulate suspensions," 1994, doi: https://doi.org/10.1007/978-1-4615-3118-0.

[107]   Z. Rong, W. Sun, H. Xiao, and W. Wang, "Effect of silica fume and fly ash on hydration and microstructure evolution of cement based composites at low water–binder ratios," *Constr. Build. Mater.*, vol. 51, pp. 446–450, 2014.

[108]   S. A. Fennis and J. C. Walraven, "Using particle packing technology for sustainable concrete mixture design," *Heron 57 2012 2*, 2012.

[109]   H. Brouwers and H. Radix, "Self-compacting concrete: the role of the particle size distribution," 2005, pp. 109–118. doi: https://doi.org/10.1617/2912143624.010.

[110]   S. Pradhan, S. Kumar, and S. V. Barai, "Recycled aggregate concrete: Particle Packing Method (PPM) of mix design approach," *Constr. Build. Mater.*, vol. 152, pp. 269–284, 2017.

[111]   A. Rahul, M. Santhanam, H. Meena, and Z. Ghani, "3D printable concrete: Mixture design and test methods," *Cem. Concr. Compos.*, vol. 97, pp. 13–23, 2019.

[112]   D. P. Bentz, "Influence of water-to-cement ratio on hydration kinetics: simple models based on spatial considerations," *Cem. Concr. Res.*, vol. 36, no. 2, pp. 238–244, 2006, doi: https://doi.org/10.1016/j.cemconres.2005.04.014.

[113] X. Pang, "The effect of water-to-cement ratio on the hydration kinetics of Portland cement at different temperatures," 2015, vol. 13, p. 16. doi: http://dx.doi.org/10.13140/RG.2.1.4526.2800.

[114] D. M. Kirby and J. J. Biernacki, "The effect of water-to-cement ratio on the hydration kinetics of tricalcium silicate cements: Testing the two-step hydration hypothesis," *Cem. Concr. Res.*, vol. 42, no. 8, pp. 1147–1156, 2012, doi: http://dx.doi.org/10.1016/j.cemconres.2012.05.009.

[115] A. J. Giesler, S. B. Applegate, and B. D. Weldon, "Implementing nonproprietary, ultra-high-performance concrete in a precasting plant," *PCI J.*, vol. 61, no. 6, pp. 68–80, 2016, doi: https://doi.org/10.15554/pcij61.6-03.

[116] T. Looney, A. McDaniel, J. Volz, and R. Floyd, "Development and characterization of ultra-high performance concrete with slag cement for use as bridge joint material," *Development*, vol. 1, no. 02, 2019.

[117] "Viscosity Modifying Admixtures (VMAs) in Concrete," *The Constructor*, Dec. 02, 2018. https://theconstructor.org/concrete/viscosity-modifying-admixture-vma-concrete/5903/ (accessed Apr. 09, 2021).

[118] "Mortar Penetration Resistance Apparatus." https://www.humboldtmfg.com/mortar-penetration-resistance-apparatus.html (accessed Apr. 23, 2021).

[119] "Compressometer, Extensometer with LSCT." https://www.humboldtmfg.com/compressometerextensometer-with-lsct.html (accessed Apr. 23, 2021).

[120] "Bulk Resistivity Accessory," *GlobalGilson.com*. https://www.globalgilson.com/bulk-resistivity-accessory (accessed Mar. 15, 2021).

[121] Proceq SA, "Resipod Family Operating Instructions," p. 28, 2017.

[122] J. T. Nugent, "Chloride Penetration Resistance of Concrete: An Examination and Comparison of Short-Term Testing Methods," Thesis, Jan. 2020.

[123] W. Morris, E. I. Moreno, and A. A. Sagues, "Practical Evaluation of Resistivity of Concrete in Test Cylinders using a Wenner Array Probe," *Cem. Concr. Res.*, vol. 26, no. 12, pp. 1779–1787, 1996.

[124] M. K. Tadros, "building BLOCKS".

[125]   Y. J. Kim, "Development of Cost-Effective Ultra-High Performance Concrete (UHPC) for Colorado's Sustainable Infrastructure," 2018.

[126]   C. D. Joe, *Cost and ecological feasibility of using ultra-high performance concrete in highway bridge piers*. University of Nevada, Reno, 2016.

[127]   T. Stengel and P. SCHIEßL, "Life cycle assessment of UHPC bridge constructions: Sherbrooke footbridge, Kassel Gärtnerplatz footbridge and Wapello road bridge," *Arch. Civ Eng Env.*, vol. 1, pp. 109–118, 2009.

[128]   M. Abokifa and M. A. Moustafa, "Full-scale testing of non-proprietary ultra-high performance concrete for deck bulb tee longitudinal field joints," *Eng. Struct.*, vol. 243, p. 112696, 2021.

[129]   "ATENA Documentation", [Online]. Available: https://www.cervenka.cz/products/atena/documentation/

[130]   American Concrete Institute, *Building Code Requirements for Structural Concrete (ACI 318-14): Commentary on Building Code Requirements for Structural Concrete (ACI 318R-14): an ACI Report*. American Concrete Institute. ACI, 2014.

[131]   A. J. Bigaj, "Structural dependence of rotations capacity of plastic hinges in RC beams and slobs," 1999.

[132]   L. AASHTO, "Bridge Design Specifications (8th edition September 2017)," *Am. Assoc. State Highw. Transp. Off. Wash. DC*, vol. 4, 2017.

[133]   B. A. Graybeal, "Behavior of Ultra-High Performance Concrete Connections between Precast Bridge Deck Elements," presented at the 2010 Concrete Bridge Conference: Achieving Safe, Smart & Sustainable Bridges, 2010.

Appendix A: Results from Small-Scale Trial Tests

Detailed results from small-scale experimental section are summarized in this section.

A.1. OU Series Mix Designs Using Masonry Cement

Seven different mix designs according to initial proposed proportions by Oklahoma University were cast. Sand used in these mixtures were in natural moisture condition and made significant variability in the flowability and compressive test results in in different ages.

Table A- 1 summarizes OU series mix proportions accompanied by flow table results and compressive strength.

Table A- 1: OU mixtures

Mix.	Fiber Type	Vol. %	W*/B	W/B	Agg./b	C	Slag	SF	Sand	UFR	Cement Type	Glenium (oz/cwt)	VMA (oz/cwt)	Flow Table (in)	f'c (ksi)			Density (lb/ft³)		
															3	7	28	3	7	28
OU1	-	0	0.21	0.20	1	0.60	0.30	0.10	1	0	C-M	15.77	0.00	-	4.1	3.8	7.1	121.6	122.7	119.4
OU2	A	2	0.21	0.20	1	0.60	0.30	0.10	1	0	C-M	15.77	0.00	7.00	5.1	6.6	9.5	-	136.5	134.8
OU3	-	0	0.21	0.20	1	0.60	0.30	0.10	1	0	C-M	31.54	0.00	-	4.2	5.8	7.5	120.8	121.2	121.0
OU4	-	0	0.21	0.20	1	0.60	0.30	0.10	1	0	C-M	23.66	0.00	-	4.0	5.1	6.7	114.8	116.2	116.4
OU5	-	0	0.17	0.16	1	0.60	0.30	0.10	1	0	C-M	23.66	0.00	-	5.5	5.7	8.2	126.5	119.5	122.7
OU6	-	0	0.19	0.18	1	0.60	0.30	0.10	1	0	C-M	25.23	0.00	-	3.3	4.3	4.5	110.3	109.3	109.9
OU7	A	2	0.18	0.17	1	0.60	0.30	0.10	1	0	C-M	23.66	0.00	-	3.4	4.2	5.2	110.1	109.6	109.9

Table A- 2 summarizes the information related to A series of mixtures. All mixtures in this group were made by cement type I/II and aggregate with natural moisture content.

Table A- 2: Series A; mixtures with cement type I/II and natural moisture content in aggregates

Mix.	Fiber Type	Vol. %	W*/B	W/B	Agg./b	C	Slag	SF	Sand	UFR	Cement Type	Glenium (oz/cwt)	VMA (oz/cwt)	Flow Table (in)	f'c (ksi)			Density (lb/ft³)		
															3	7	28	3	7	28
A1	-	0	0.21	0.20	1	0.60	0.30	0.10	1	0	C-T-I/II	31.54	0.00	-	9.9	10.6	-	140.2	140.5	-
A2	-	0	0.19	0.18	1	0.60	0.30	0.10	1	0	C-T-I/II	24.19	0.00	-	10.9	13.0	-	145.2	145.5	-
A3	-	0	0.18	0.17	1	0.60	0.30	0.10	1	0	C-T-I/II	20.31	0.00	-	10.3	11.0	-	139.1	139.3	-
A4	A	1	0.19	0.18	1	0.60	0.30	0.10	1	0	C-T-I/II	18.99	0.00	-	8.8	10.9	-	138.2	141.2	-
A5	A	2	0.19	0.18	1	0.60	0.30	0.10	1	0	C-T-I/II	19.52	0.00	-	9.8	11.0	-	146.3	145.4	-
A6	-	0	0.19	0.18	1	0.60	0.30	0.10	1	0	C-T-I/II	15.75	0.00	-	8.1	10.1	-	130.2	137.7	-
A7	-	0	0.19	0.18	1	0.60	0.30	0.10	1	0	C-T-I/II	16.76	0.00	-	9.0	11.2	-	137.4	137.8	-
A8	-	0	0.19	0.18	1	0.60	0.30	0.10	1	0	C-T-I/II	16.48	0.00	-	8.5	-	9.7	142.7	142.5	-
A9	-	0	0.19	0.18	1	0.60	0.30	0.10	1	0	C-T-I/II	15.56	0.00	-	-	8.4	10.9	-	137.6	138.7
A10	A	1	0.19	0.18	1	0.60	0.30	0.10	1	0	C-T-I/II	15.56	0.00	-	-	10.3	11.0	-	141.1	139.8
A11	A	2	0.19	0.18	1	0.60	0.30	0.10	1	0	C-T-I/II	15.56	0.00	-	-	8.4	12.3	-	143.8	146.5
A12	OL	1	0.19	0.18	1	0.60	0.30	0.10	1	0	C-T-I/II	15.56	0.00	-	8.7	10.8	11.9	142.2	143.6	142.2
A13	OL	2	0.19	0.18	1	0.60	0.30	0.10	1	0	C-T-I/II	15.56	0.00	-	9.8	10.1	11.7	145.0	144.5	142.6
A14	H	1	0.19	0.18	1	0.60	0.30	0.10	1	0	C-T-I/II	15.56	0.00	-	5.6	7.6	10.1	139.1	138.7	138.4
A15	H	2	0.19	0.18	1	0.60	0.30	0.10	1	0	C-T-I/II	15.56	0.00	-	4.7	6.5	8.7	141.6	140.4	142.1
A16	OL	1	0.19	0.18	1	0.60	0.30	0.10	1	0	C-T-I/II	15.56	0.00	-	-	9.9	11.7	-	139.4	139.3
A17	OL	2	0.19	0.18	1	0.60	0.30	0.10	1	0	C-T-I/II	15.56	0.00	-	-	10.5	12.7	-	144.4	142.9
A18	-	0	0.19	0.18	1	0.60	0.25	0.15	1	0	C-T-I/II	15.56	0.00	-	6.5	8.2	10.5	134.8	133.2	132.4
A19	H	1	0.19	0.18	1	0.60	0.25	0.15	1	0	C-T-I/II	15.56	0.00	-	6.3	9.5	11.1	137.8	136.0	136.1
A20	H	2	0.18	0.17	1	0.60	0.25	0.15	1	0	C-T-I/II	15.56	0.00	-	5.9	8.7	10.6	138.1	136.9	136.1

Table A- 3 summarizes the information related to the B series of mixtures. All mixtures in this group were made by cement type I/II and aggregate with natural moisture content and were initially made to optimize the mix proportions.

Table A- 3: Series B; optimization process with natural moisture aggregates

Mix.	Fiber Type	Vol. %	W*/B	W/B	Agg./b	C	Slag	SF	Sand	UFR	Cement Type	Glenium (oz/cwt)	VMA (oz/cwt)	Flow Table (in)	f'c (ksi) 3	f'c (ksi) 7	f'c (ksi) 28	Density (lb/ft³) 3	Density (lb/ft³) 7	Density (lb/ft³) 28
B1	-	0	0.21	0.20	1	0.60	0.30	0.10	1	0	C-T-I/II	15.75	0.00	-	7.2	9.0	12.6	134.9	135.8	138.6
B2	-	0	0.21	0.20	1	0.60	0.25	0.15	1	0	C-T-I/II	15.75	0.00	-	6.9	7.8	10.3	133.8	131.2	130.8
B3	-	0	0.21	0.20	1	0.65	0.25	0.10	1	0	C-T-I/II	15.75	0.00	-	9.0	9.6	13.6	140.8	140.1	140.5
B4	-	0	0.21	0.20	1	0.65	0.20	0.15	1	0	C-T-I/II	15.75	0.00	-	7.6	8.4	11.4	137.3	137.3	135.9
B5	-	0	0.21	0.20	1	0.70	0.20	0.10	1	0	C-T-I/II	15.75	0.00	-	7.9	8.6	12.8	137.5	139.4	139.2
B6	-	0	0.21	0.20	1	0.70	0.15	0.15	1	0	C-T-I/II	15.75	0.00	-	7.5	8.0	11.6	136.4	135.1	136.2
B7	-	0	0.21	0.20	1	0.65	0.23	0.13	1	0	C-T-I/II	15.75	0.00	-	7.4	7.9	11.3	134.7	134.0	135.8
B8	-	0	0.21	0.20	1	0.70	0.18	0.13	1	0	C-T-I/II	15.75	0.00	-	7.1	8.3	11.7	135.2	136.4	135.6
B9	-	0	0.21	0.20	1	0.65	0.25	0.10	1	0	C-T-I/II	18.31	0.00	-	7.5	4.8	13.4	140.3	139.3	144.6
B10	H	2	0.21	0.20	1	0.65	0.25	0.10	1	0	C-T-I/II	18.31	0.00	-	8.8	8.8	15.0	144.2	143.3	144.2
B11	-	0	0.19	0.18	1	0.60	0.30	0.10	1	0	C-T-I/II	23.81	0.00	-	10.5	13.3	15.5	146.8	146.2	146.1
B12	-	0	0.19	0.18	1	0.65	0.23	0.13	1	0	C-T-I/II	18.31	0.00	-	8.6	9.8	11.7	135.2	136.0	137.5
B13	-	0	0.21	0.20	1	0.65	0.23	0.13	1	0	C-T-I/II	18.31	0.00	-	7.9	10.0	14.0	140.4	141.0	142.5
B14	-	0	0.21	0.20	1	0.70	0.18	0.13	1	0	C-T-I/II	18.31	0.00	-	7.7	9.3	12.7	138.7	137.8	140.4
B15	H	1	0.21	0.20	1	0.65	0.25	0.10	1	0	C-T-I/II	15.75	0.00	-	6.9	10.3	12.6	141.6	141.7	141.9
B16	H	2	0.21	0.20	1	0.65	0.25	0.10	1	0	C-T-I/II	15.75	0.00	-	6.3	10.8	13.6	139.3	140.4	140.8
B17	-	0	0.19	0.18	1	0.60	0.30	0.10	1	0	C-T-I/II	23.81	0.00	-	9.6	13.6	18.0	144.4	145.4	146.4
B18	-	0	0.19	0.18	1	0.65	0.25	0.10	1	0	C-T-I/II	23.81	0.00	-	9.2	11.5	16.8	145.2	145.1	146.0
B19	-	0	0.19	0.18	1	0.70	0.20	0.10	1	0	C-T-I/II	23.81	0.00	-	10.9	13.1	15.1	146.7	146.4	146.8
B20	H	2	0.19	0.18	1	0.60	0.30	0.10	1	0	C-T-I/II	23.81	0.00	-	9.8	13.0	15.2	145.2	144.7	144.8
B21	OL	1.5	0.18	0.18	1	0.60	0.30	0.10	1	0	C-T-I/II	11.17	0.00	-	6.6	8.4	10.9	134.6	136.1	137.1
B22	OL	2	0.19	0.18	1	0.60	0.30	0.10	1	0	C-T-I/II	23.81	0.00	-	7.4	10.0	15.2	144.1	146.0	149.0
B23	-	0	0.21	0.20	1	0.60	0.30	0.10	1	0	C-T-I/II	23.81	0.00	-	8.9	12.0	16.6	143.3	145.0	146.0
B24	-	0	0.21	0.20	1	0.60	0.30	0.10	1	0	C-T-I/II	21.97	0.00	-	10.0	11.2	15.8	145.0	134.6	145.8
B25	OL	2	0.21	0.20	1	0.60	0.30	0.10	1	0	C-T-I/II	21.97	0.00	11.00	9.0	12.5	16.7	149.3	150.2	149.6

Mix.	Fiber Type	Vol. %	W*/B	W/B	Agg./b	C	Slag	SF	Sand	UFR	Cement Type	Glenium (oz/cwt)	VMA (oz/cwt)	Flow Table (in)	f'_c (ksi)			Density (lb/ft^3)		
															3	7	28	3	7	28
B26	OL	2	0.21	0.20	1	0.60	0.30	0.10	1	0	C-T-I/II	20.14	0.00	11.00	8.1	12.9	16.0	146.2	146.1	145.2
B27	OL	2	0.21	0.20	1	0.60	0.30	0.10	1	0	C-T-I/II	18.31	0.00	11.00	9.7	11.1	15.5	144.6	148.0	142.4
B28	OL	2	0.21	0.20	1	0.60	0.30	0.10	1	0	C-T-I/II	16.48	0.00	11.00	4.5	5.4	11.0	136.6	138.6	139.1
B29	OL	2	0.14	0.14	1	0.60	0.30	0.10	1	0	C-T-I/II	11.47	0.00	-	7.0	10.4	10.7	137.5	138.1	138.0
B30	OL	2	0.16	0.16	1	0.60	0.30	0.10	1	0	C-T-I/II	12.60	0.00	-	6.6	9.2	9.0	135.8	135.5	136.4
B31	-	0	0.19	0.18	1	0.60	0.30	0.10	1	0	C-T-I/II	23.81	0.00	-	9.3	12.5	13.0	145.2	145.2	144.9
B32	-	0	0.20	0.18	1	0.60	0.30	0.10	1	0	C-T-I/II	41.93	0.00	-	10.8	13.9	15.8	148.4	148.9	149.2
B33	-	0	0.19	0.18	1	0.60	0.30	0.10	1	0	C-T-I/II	24.17	0.00	-	-	13.6	14.6	-	153.3	148.2

Table A- 4 summarizes the information related to the C series of mixtures. All mixtures in this group were made with oven-dried aggregates.

Table A- 4: Series C; optimization process with oven-dried aggregates

Mix.	Fiber Type	Vol. %	W*/B	W/B	Agg./b	C	Slag	SF	Sand	UFR	Cement Type	Glenium (oz/cwt)	VMA (oz/cwt)	Flow Table (in)	f'$_c$ (ksi)			Density (lb/ft^3)		
															3	7	28	3	7	28
C1	OL	2	0.21	0.20	1	0.60	0.30	0.10	1	0	C-A-I/II	20.60	0.00	10.00	9.4	11.6	12.8	148.4	148.6	148.3
C2	OL	2	0.21	0.20	1	0.60	0.30	0.10	1	0	C-T-I/II	22.25	0.00	9.00	9.5	11.6	14.5	144.9	144.5	144.2
C3	OL	2	0.21	0.20	1	0.60	0.30	0.10	1	0	C-A-I/II	22.25	0.00	8.00	9.7	11.3	13.4	148.9	148.2	150.0
C4	OL	2	0.21	0.20	1	0.60	0.30	0.10	1	0	C-W-I	23.35	0.00	7.50	12.7	13.8	14.8	146.3	146.9	146.2
C5	H	2	0.21	0.20	1	0.60	0.30	0.10	1	0	C-T-I/II	24.72	6.41	11.00	6.7	7.6	9.6	146.1	147.0	145.6
C6	A	2	0.22	0.20	1	0.60	0.30	0.10	1	0	C-T-I/II	24.72	8.24	9.50	9.5	10.9	13.0	146.3	147.3	145.5
C7	OL	2	0.22	0.20	1	0.60	0.30	0.10	1	0	C-A-I/II	24.72	8.24	10.00	9.6	12.2	14.6	150.3	149.3	149.6
C8	OL	2	0.22	0.20	1	0.60	0.30	0.10	1	0	C-T-I/II	24.72	8.24	9.50	9.6	11.1	13.4	146.1	146.0	146.3
C9	OL	2	0.21	0.20	1	0.60	0.30	0.10	1	0	C-A-I/II	18.00	0.00	5.00	9.5	12.3	13.9	147.3	148.4	148.5
C10	OL	2	0.24	0.22	1	0.60	0.30	0.10	1	0	C-A-I/II	24.72	8.24	11.50	9.3	12.1	12.1	151.1	151.6	151.0
C11	OL	2	0.23	0.22	1	0.60	0.30	0.10	1	0	C-T-I/II	19.87	6.50	10.50	9.4	11.9	12.9	145.4	144.4	143.9
C12	H	2	0.23	0.22	1	0.60	0.30	0.10	1	0	C-W-I	22.89	6.50	5.00	8.8	9.3	10.8	143.9	143.9	144.7
C13	H	2	0.23	0.22	1	0.60	0.30	0.10	1	0	C-T-I/II	18.49	6.50	9.00	5.5	6.8	7.2	142.5	141.5	142.0
C14	H	2	0.21	0.20	1	0.60	0.30	0.10	1	0	C-T-I/II	22.89	6.50	9.00	5.1	5.9	7.0	143.0	143.3	144.4
C15	OL	2	0.23	0.22	1	0.60	0.30	0.10	1	0	C-T-I/II	18.31	5.86	7.00	9.9	11.4	14.6	142.4	142.1	144.8
C16	OL	2	0.21	0.20	1	0.60	0.30	0.10	1	0	C-T-I/II	26.55	3.02	10.00	10.2	11.9	15.2	-	148.3	149.0
C17	OL	2	0.25	0.24	1	0.60	0.30	0.10	1	0	C-T-I/II	16.39	2.47	10.50	8.8	10.0	12.5	143.0	142.6	142.8
C18	OL	2	0.23	0.22	1	0.65	0.25	0.10	1	0	C-T-I/II	24.72	1.56	11.00	9.3	12.2	13.9	147.1	147.6	147.5
C19	OL	2	0.23	0.22	1	0.70	0.20	0.10	1	0	C-T-I/II	22.43	2.11	11.00	10.5	10.9	13.7	146.5	146.3	146.4
C20	H	2	-	-	-	-	-	-	-	-	Ductal	-	-	-	-	-	5.6	-	-	149.6
C21	OL	2	0.23	0.22	1	0.65	0.23	0.13	1	0	C-T-I/II	22.16	5.22	9.50	9.3	12.1	13.9	142.0	145.9	145.6
C22	OL	2	0.19	0.17	1	0.60	0.30	0.10	1	0	C-T-I/II	41.97	3.27	8.00	11.0	12.9	-	149.9	148.2	-
C23	H	2	-	-	-	-	-	-	-	-	Ductal	-	-	7.00	-	5.6	5.9	-	135.5	140.9
C24	OL	2	0.20	0.18	1	0.60	0.30	0.10	1	0	C-W-I	34.06	0.00	7.00	11.9	14.5	15.1	147.7	148.4	147.8
C25	OL	2	0.23	0.22	1	0.60	0.30	0.10	1	0	C-W-I	24.72	0.00	9.00	11.2	12.7	13.7	144.4	144.5	144.0
C26	OL	2	0.18	0.17	1	0.60	0.30	0.10	1	0	C-T-I/II	35.52	0.00	7.00	12.7	14.0	15.0	150.2	149.6	150.2
C27	OL	2	0.23	0.22	1	0.60	0.30	0.10	1	0	C-T-I/II	22.89	4.30	11.50	10.0	11.7	12.9	145.2	145.1	145.5

Mix.	Fiber Type	Vol. %	W*/B	W/B	Agg./b	C	Slag	SF	Sand	UFR	Cement Type	Glenium (oz/cwt)	VMA (oz/cwt)	Flow Table (in)	f'c (ksi)			Density (lb/ft³)		
															3	7	28	3	7	28
C28	OL	2	0.21	0.20	1	0.60	0.30	0.10	1	0	C-T-I/II	21.70	0.00	6.00	11.4	13.0	15.7	146.8	146.9	147.7
C29	OL	2	0.21	0.20	1	0.60	0.30	0.10	1	0	C-T-I/II	21.70	6.50	7.00	11.3	12.9	15.7	145.7	146.3	147.4
C30	OL	2	0.21	0.20	1	0.60	0.30	0.10	1	0	C-A-I/II	19.81	0.00	6.00	9.8	13.2	14.8	148.9	149.7	149.3
C31	OL	2	0.21	0.20	1	0.60	0.30	0.10	1	0	C-T-I/II	27.47	0.00	10.50	10.0	13.7	13.3	146.7	147.4	148.1
C32	OL	2	0.22	0.20	1	0.60	0.30	0.10	1	0	C-T-I/II	27.47	6.50	9.50	11.1	13.4	15.2	146.1	147.7	147.0
C33	OL	2	0.19	0.18	1	0.60	0.30	0.10	1	0	C-T-I/II	27.47	0.00	9.00	12.4	13.5	15.5	150.5	148.6	149.1
C34	OL	2	0.20	0.18	1	0.60	0.30	0.10	1	0	C-T-I/II	27.47	6.50	8.00	12.0	13.6	16.7	151.1	149.4	148.9
C35	OL	2	0.21	0.20	1	0.60	0.30	0.10	1	0	C-T-I/II	27.47	0.00	10.50	-	13.6	-	-	150.5	-
C36	OL	2	0.22	0.20	1	0.60	0.30	0.10	1	0	C-T-I/II	27.47	6.50	10.50	-	13.9	-	-	150.2	-
C37	OL	2	0.21	0.20	1	0.60	0.30	0.10	1	0	C-T-III	27.47	0.00	9.50	12.8	14.2	17.9	148.4	149.6	149.0
C38	OL	2	0.22	0.20	1	0.60	0.30	0.10	1	0	C-T-III	27.47	6.50	9.50	12.3	14.0	17.3	148.3	147.6	149.3
C39	OL	2	0.19	0.18	1	0.60	0.30	0.10	1	0	C-T-III	27.47	0.00	7.50	13.6	14.9	17.1	149.8	150.1	149.7
C40	OL	2	0.18	0.17	1	0.60	0.30	0.10	1	0	C-T-I/II	29.39	0.00	7.50	-	-	19.2	-	-	156.5
C41	OL	2	0.19	0.17	1	0.60	0.30	0.10	1	0	C-T-I/II	29.39	9.16	7.25	-	-	19.5	-	-	151.6
C42	HF	2	0.21	0.20	1	0.60	0.30	0.10	1	0	C-T-I/II	27.47	0.00	10.00	11.2	13.3	17.9	151.4	146.7	147.8
C43	HF	2	0.22	0.20	1	0.60	0.30	0.10	1	0	C-T-I/II	27.47	6.50	10.00	10.5	13.8	16.7	148.5	148.1	148.5
C44	HF	2	0.19	0.18	1	0.60	0.30	0.10	1	0	C-T-I/II	27.47	0.00	8.50	12.3	14.9	18.8	149.7	149.0	152.0
C45	OL	2	0.21	0.20	1	0.60	0.30	0.10	0.9	0.1	C-T-I/II	27.47	0.00	10.00	10.8	13.4	16.8	145.9	146.6	147.0
C46	OL	2	0.21	0.20	1	0.60	0.30	0.10	0.8	0.2	C-T-I/II	27.47	0.00	8.00	11.5	15.5	17.2	147.9	148.8	148.6
C47	OL	2	0.21	0.20	1	0.60	0.30	0.10	0.7	0.3	C-T-I/II	29.39	0.00	9.00	11.8	15.5	17.1	147.6	147.4	147.9
C48	OL	2	0.21	0.20	1	0.60	0.30	0.10	0.65	0.35	C-T-I/II	29.39	0.00	8.00	11.1	14.6	17.8	146.9	146.3	148.6
C49	-	0	0.20	0.16	1	0.60	0.30	0.10	0.65	0.35	C-T-I/II	85.15	0.00	6.00	-	11.5	14.3	-	140.0	-
C50	-	0	0.20	0.16	1	0.60	0.30	0.10	0.65	0.35	C-T-I/II	85.15	0.00	6.50	-	12.0	13.5	-	140.4	-
C51	-	0	0.19	0.15	1	0.60	0.30	0.10	0.65	0.35	C-T-I/II	92.84	0.00	7.50	-	10.9	15.0	-	138.8	-
C52	OL	2	0.20	0.18	1	0.60	0.30	0.10	0.8	0.2	C-T-I/II	38.08	0.00	9.50	12.0	14.6	18.5	150.7	150.4	151.1
C53	OL	2	0.20	0.18	1	0.60	0.30	0.10	0.7	0.3	C-T-I/II	38.08	0.00	9.25	11.7	14.3	18.3	150.1	150.1	152.3

A.2. Spreadsheet Development for Non-Proprietary UHPC Mixture Design

The link of the developed spreadsheet will be posted later on the website.

	mm(μm/1000)	μm	Cement Average	Slag Average	Silica Fume Average	Sand Average	UFR Average
4	0.001	1	4.93	5.60	1.17	3.72	0.15
5	0.002	2	9.68	11.49	2.27	3.72	0.28
6	0.003	3	14.35	17.49	3.38	3.73	0.41
7	0.004	4	18.78	23.31	4.48	3.73	0.53
8	0.005	5	22.83	28.78	5.58	3.74	0.66
9	0.006	6	26.52	33.88	6.82	3.74	0.79
10	0.007	7	29.95	38.66	8.06	3.74	0.92
11	0.008	8	33.17	43.14	9.30	3.75	1.04
12	0.010	10	39.23	51.30	11.77	3.76	1.30
13	0.012	12	44.94	58.46	13.44	3.77	1.55
14	0.014	14	50.36	64.68	14.35	3.78	1.81
15	0.016	16	55.49	70.04	15.27	3.78	2.06
16	0.018	18	60.32	74.65	16.18	3.79	2.32
17	0.020	20	64.82	78.58	17.10	3.80	2.57
18	0.022	22	68.97	81.95	17.59	3.81	2.83
19	0.024	24	71.76	84.02	18.09	3.82	3.08
20	0.025	25	74.54	86.09	18.26	3.83	3.21
21	0.028	28	79.34	89.35	18.80	3.84	3.59
22	0.030	30	82.13	91.12	19.15	3.85	3.85
23	0.032	32	84.62	92.64	19.51	3.86	4.10
24	0.034	34	86.83	93.92	19.73	3.87	4.36
25	0.036	36	88.77	95.01	20.07	3.87	4.61
26	0.037	37	89.63	95.48	20.21	3.88	4.74
27	0.038	38	90.48	95.94	20.33	3.88	4.87
28	0.040	40	91.98	96.73	20.57	3.89	6.02
29	0.043	43	93.87	97.68	20.93	3.91	7.75
30	0.044	44	94.40	97.93	21.05	3.91	8.33
31	0.045	45	94.93	98.19	21.15	3.92	8.91
32	0.050	50	96.99	99.13	21.64	3.94	11.79
33	0.053	53	97.90	99.49	21.94	3.95	13.52
34	0.055	55	98.40	99.67	22.10	3.96	14.67
35	0.056	56	98.62	99.74	22.18	3.96	15.25
36	0.060	60	99.31	99.94	22.50	3.98	17.55
37	0.063	63	99.57	99.97	22.74	4.00	19.28
38	0.066	66	99.84	99.99	22.93	4.01	21.01
39	0.071	71	99.99	100.00	23.24	4.03	23.89
40	0.074	74	100.00	100.00	23.43	4.05	25.62
41	0.075	75	100.00	100.00	23.48	4.05	26.20
42	0.080	80	100.00	100.00	23.71	4.27	30.14
43	0.085	85	100.00	100.00	23.94	4.49	34.08
44	0.088	88	100.00	100.00	24.08	4.63	36.44
45	0.090	90	100.00	100.00	24.13	4.71	38.02
46	0.095	95	100.00	100.00	24.26	5.51	41.96
47	0.112	112	100.00	100.00	24.71	8.22	55.36
48	0.125	125	100.00	100.00	25.06	10.29	65.60
49	0.150	150	100.00	100.00	25.72	14.27	85.30
50	0.210	210	100.00	100.00	27.88	41.53	99.90
51	0.500	500	100.00	100.00	100.00	100.00	100.00

Proportions — Try different proportions of each contituents to get closet curve from ideal curve

$$D(P) = \frac{D^q - D_{min}^q}{D_{max}^q - D_{min}^q}$$

Mixes	Cement	Slag	Silica Fume	Sand	UFR
OPT#1	0.60	0.30	0.10	1.00	0.00
OPT#2	0.65	0.25	0.10	1.00	0.00
OPT#3	0.70	0.20	0.10	1.00	0.00
OPT#4	0.67	0.23	0.10	1.00	0.00
OPT#5	0.67	0.30	0.13	0.90	0.00
OPT#6	0.60	0.30	0.10	0.90	0.10
OPT#7	0.60	0.30	0.10	0.80	0.20
OPT#8	0.60	0.30	0.10	0.70	0.30
OPT#9	0.60	0.30	0.10	0.60	0.40

Cells required to be filled by user

Other Inputs

D_{min} [mm] = 0.001
D_{max} [mm] = 0.5
q = 0.25

Figure B-1: The developed spreadsheet by FIU for the mix optimization

Appendix B: Results From Large-Scale Tests

Detailed results from the large-scale experimental section are summarized in this section.

A.3. Large -Scale Series

Two qualified mixtures resulting from the small-scale trial alongside the mix proportions suggested by OU were cast using a large, 2.2 ft3 mixer to study other mechanical and durability properties and the effect of fiber type and content non-proprietary UHPC mix. Table B- 1 summarizes the mix proportions of 10 large mixtures with their compressive strength and density.

Table B- 1 summarizes the large-scale UHPC batches -mix proportions, compressive strength, and their density.

Table B- 1: Large-scale UHPC batches -mix proportions, compressive strength, and density

Mix.	Fiber Type	Vol. %	W*/B	W/B	Agg./b	C	Slag	SF	Sand	UFR	Cement Type	Glenium (oz/cwt)	VMA (oz/cwt)	Flow Table (in)	f'c (ksi)					Density (lb/ft³)				
															3	7	14	28	56	3	7	14	28	56
L1	OL	2	0.21	0.20	1	0.60	0.30	0.10	0.7	0.3	C-T-I/II	29.4	0.00	9.50	11.8	14.6	15.5	16.7	18.1	149.5	151.0	149.4	149.4	149.6
L2	OL	2	0.21	0.20	1	0.60	0.30	0.10	1	0	C-A-I/II	22.0	0.00	10.00	11.0	14.0	15.7	17.6	18.2	153.1	153.4	152.9	153.5	153.2
L3	OL	2	0.21	0.20	1	0.60	0.30	0.10	1	0	C-T-I/II	27.5	0.00	10.50	12.2	14.4	15.5	17.1	17.6	148.8	150.8	149.8	149.6	149.5
L4	OL	2	0.19	0.18	1	0.60	0.30	0.10	1	0	C-T-I/II	27.5	0.00	8.00	12.0	14.9	16.4	17.8	18.1	150.4	151.6	151.0	151.1	151.5
L5	HF	2	0.21	0.20	1	0.60	0.30	0.10	1	0	C-T-I/II	27.5	0.00	9.50	12.1	14.3	15.4	17.5	18.0	148.4	147.6	149.0	148.5	149.9
L6	A	1.5	0.21	0.20	1	0.60	0.30	0.10	1	0	C-T-I/II	27.5	4.49	9.50	11.7	14.9	16.2	17.3	17.6	150.6	151.3	151.7	151.4	150.2
L7	OL	4	0.21	0.20	1	0.60	0.30	0.10	1	0	C-T-I/II	27.5	0.00	8.50	12.0	14.3	15.0	17.0	17.1	154.2	155.6	155.8	155.2	155.0
L8	HF	4	0.21	0.20	1	0.60	0.30	0.10	1	0	C-T-I/II	27.5	0.00	9.00	12.8	14.3	15.6	17.3	17.4	154.9	154.9	154.4	155.1	154.4
L9	S	2	0.20	0.20	1	0.60	0.30	0.10	1	0	C-T-I/II	27.5	0.00	9.00	9.7	10.8	11.2	11.1	13.4	141.1	141.6	142.2	142.0	141.4
L10	S	1	0.20	0.20	1	0.60	0.30	0.10	1	0	C-T-I/II	27.5	0.00	9.50	10.9	12.4	13.4	15.4	16.0	143.5	144.3	144.9	144.1	144.5

Table B- 2summarizes the splitting tensile strength, modulus of elasticity, and modulus of rupture for large-scale mixtures.

Table B- 2: Large-scale UHPC batches - splitting tensile strength, modulus of elasticity, and modulus of rupture

Mix.	Split T (ksi)-28days			MOE (ksi)-28days			MOR(ksi)-28days
	N.Cured	Cured	Avg.	N.Cured	Cured	Avg.	Avg.
L1	2.68	2.54	2.61	8866.77	8733.62	8766.91	2.827
L2	2.49	2.76	2.62	8494.85	8936.67	8826.22	-
L3	2.61	2.73	2.67	7246.64	7978.68	7795.67	2.489
L4	2.81	2.87	2.84	9471.15	9034.57	9143.72	2.894
L5	3.06	2.80	2.93	7862.58	9201.79	8866.99	3.652
L6	2.45	2.33	2.39	8241.42	9415.38	9121.89	3.235
L7	2.80	2.90	2.85	8038.32	9006.73	8764.63	3.130
L8	2.85	2.75	2.80	7883.74	8940.07	8675.99	4.051
L9	1.45	1.30	1.38	7157.54	7698.71	7292.83	1.336
L10	1.46	1.53	1.49	7865.41	8240.88	8147.01	1.290

Figure B-1and Figure B-2 show the average compressive strength and density of large-scale mixtures, respectively.
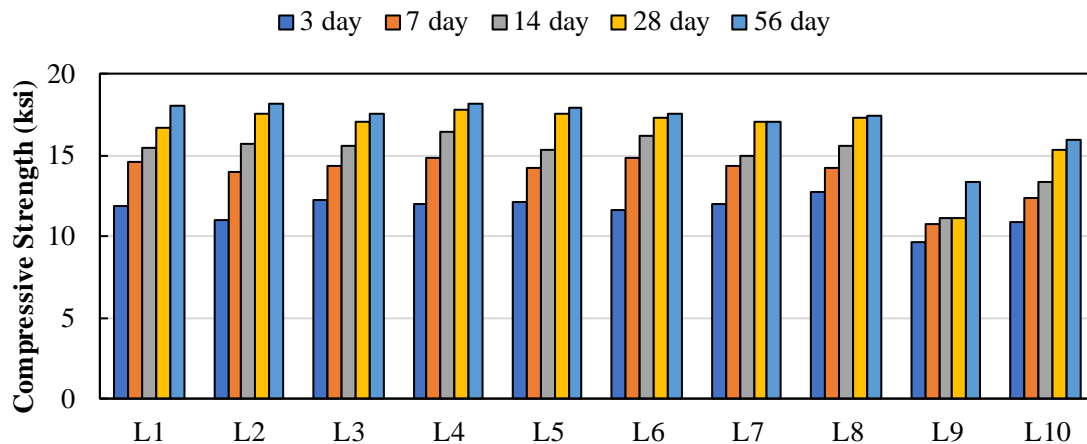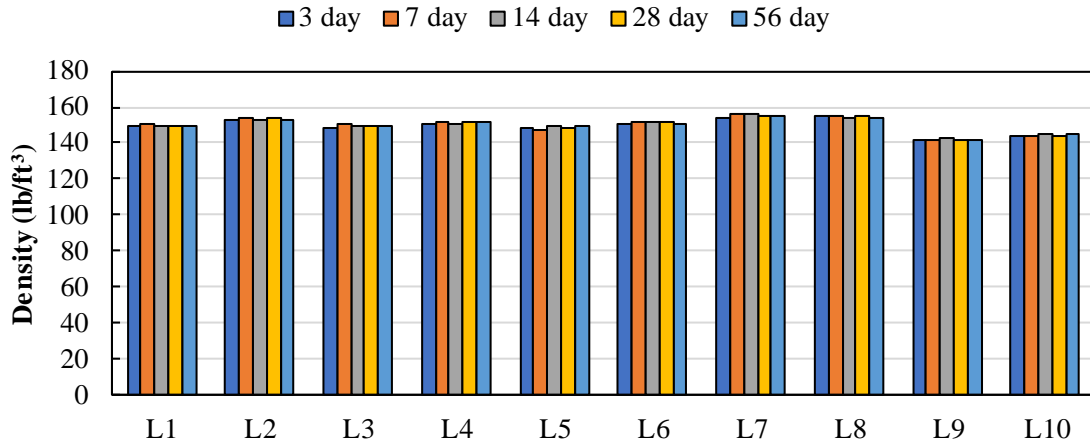
Figure B-2:Average Density

Figure B-3 and Figure B-4show the average compressive strength of large–scale mixtures for cured samples and uncured samples, respectively.
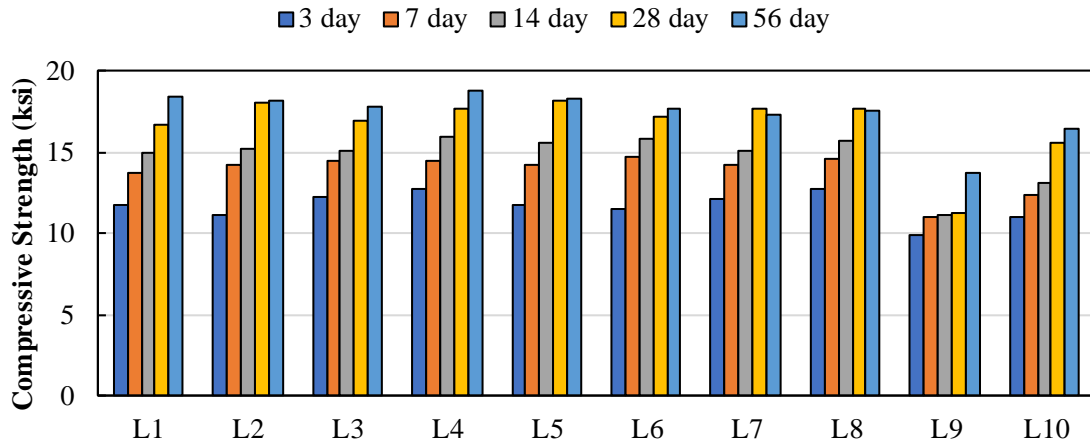
Figure B-3: Average compressive strength of cured samples
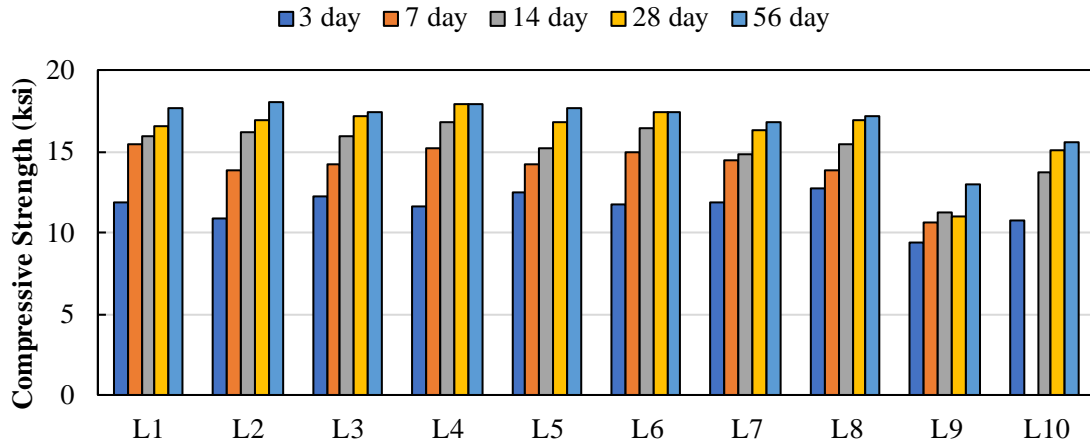
Figure B-4: Average compressive strength of uncured samples

Figure B-5 and Figure B-6 show the average density of large–scale mixtures for cured samples and uncured samples, respectively.
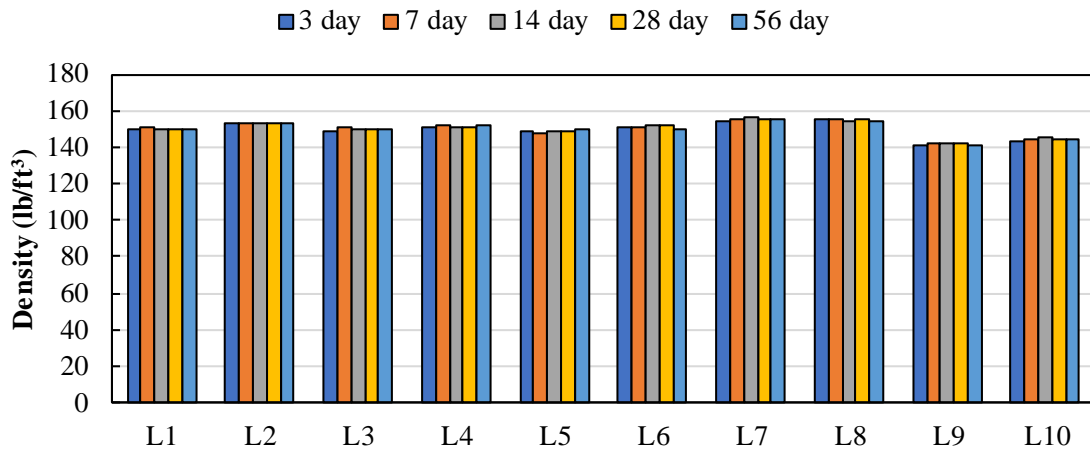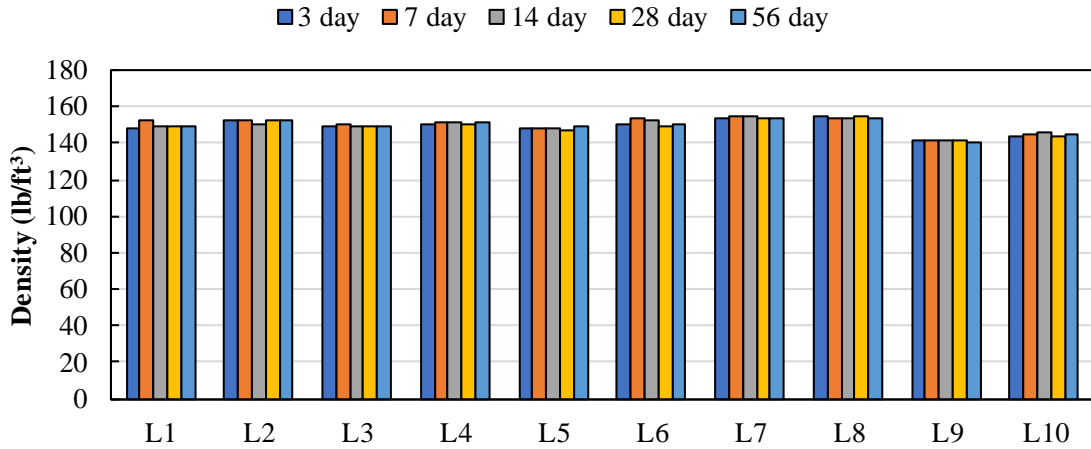
Figure B-6: Average density of uncured samples

Figure B-7 shows the results of the tensile splitting test for large-scale mixtures and the effect of moist curing on the final results.
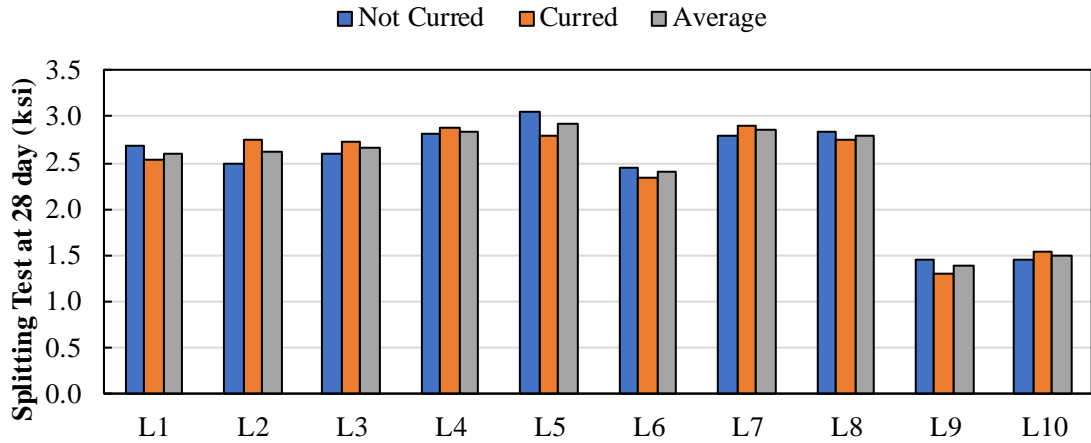
Figure B-7: Result of 28 days tensile splitting test

Figure B-8 shows the results of setting time test for large-scale mixtures.
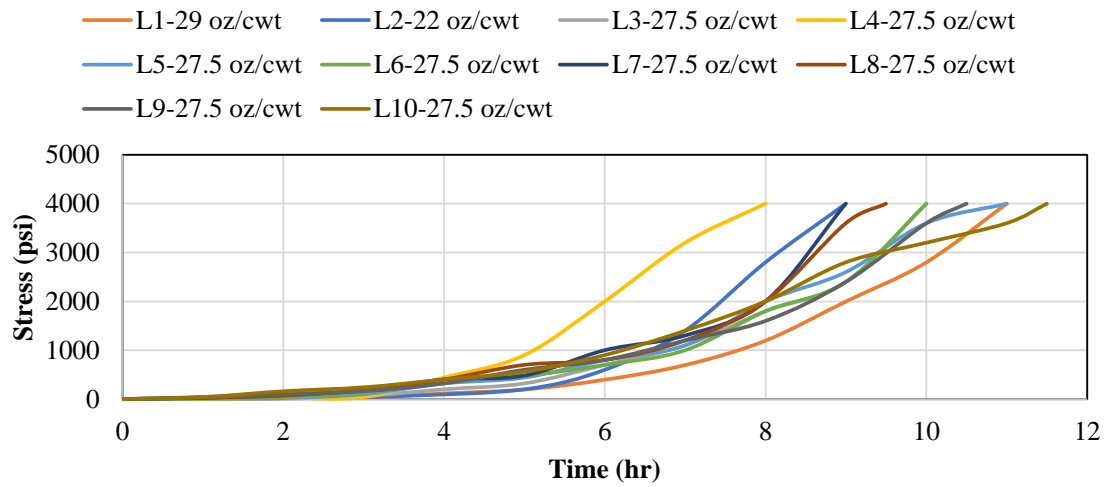
Figure B-8:Setting time results

6
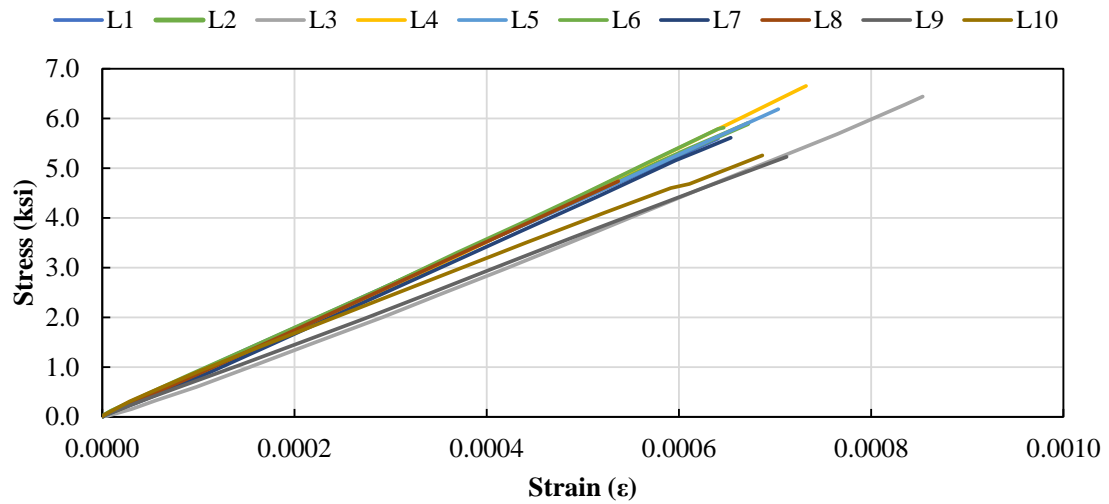
Figure B-9 shows the comparison of modulus of elasticity for large-scale mixtures;
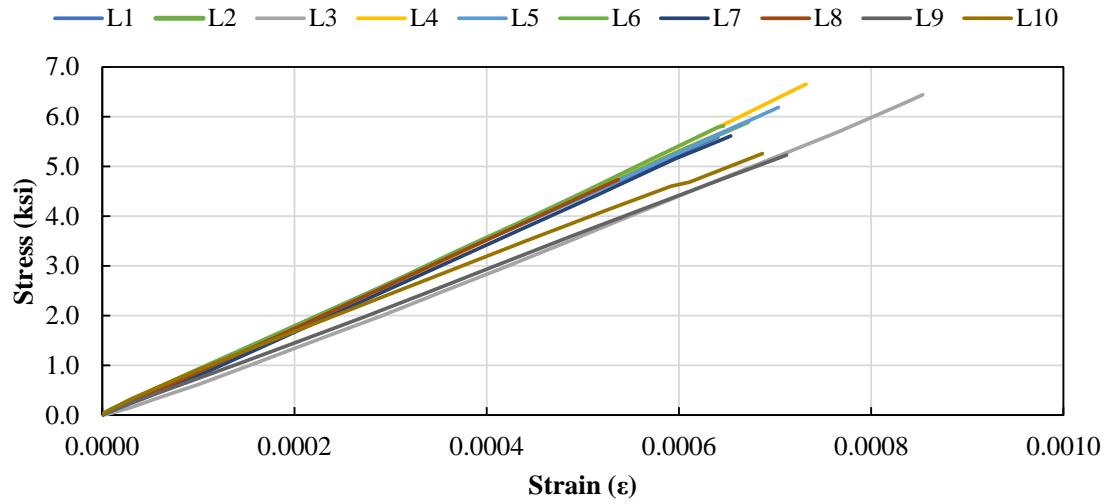
Figure B-9: Comparison of modulus of elasticity L1 to L10

Figure B-10 and Figure B-11show the detailed results (modulus of elasticity) for each large-scale mixture and related samples.
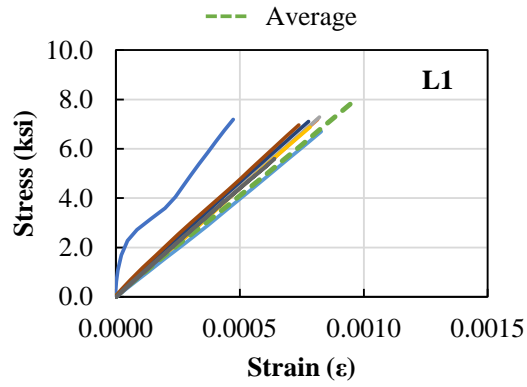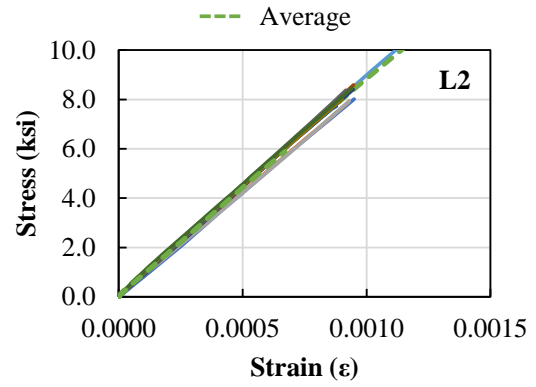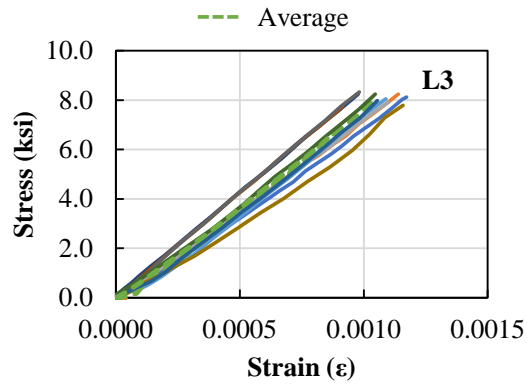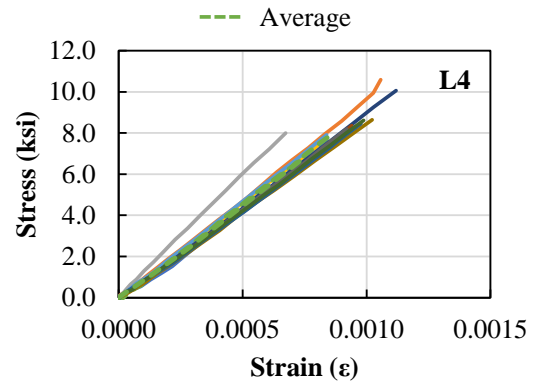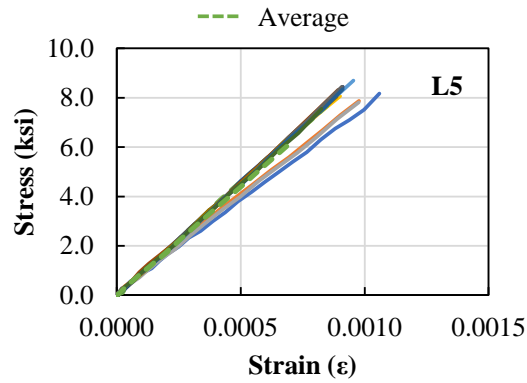
Figure B-10: Modulus of elasticity L1 to L5

(a)

(b)

(c)

(d)

(e)
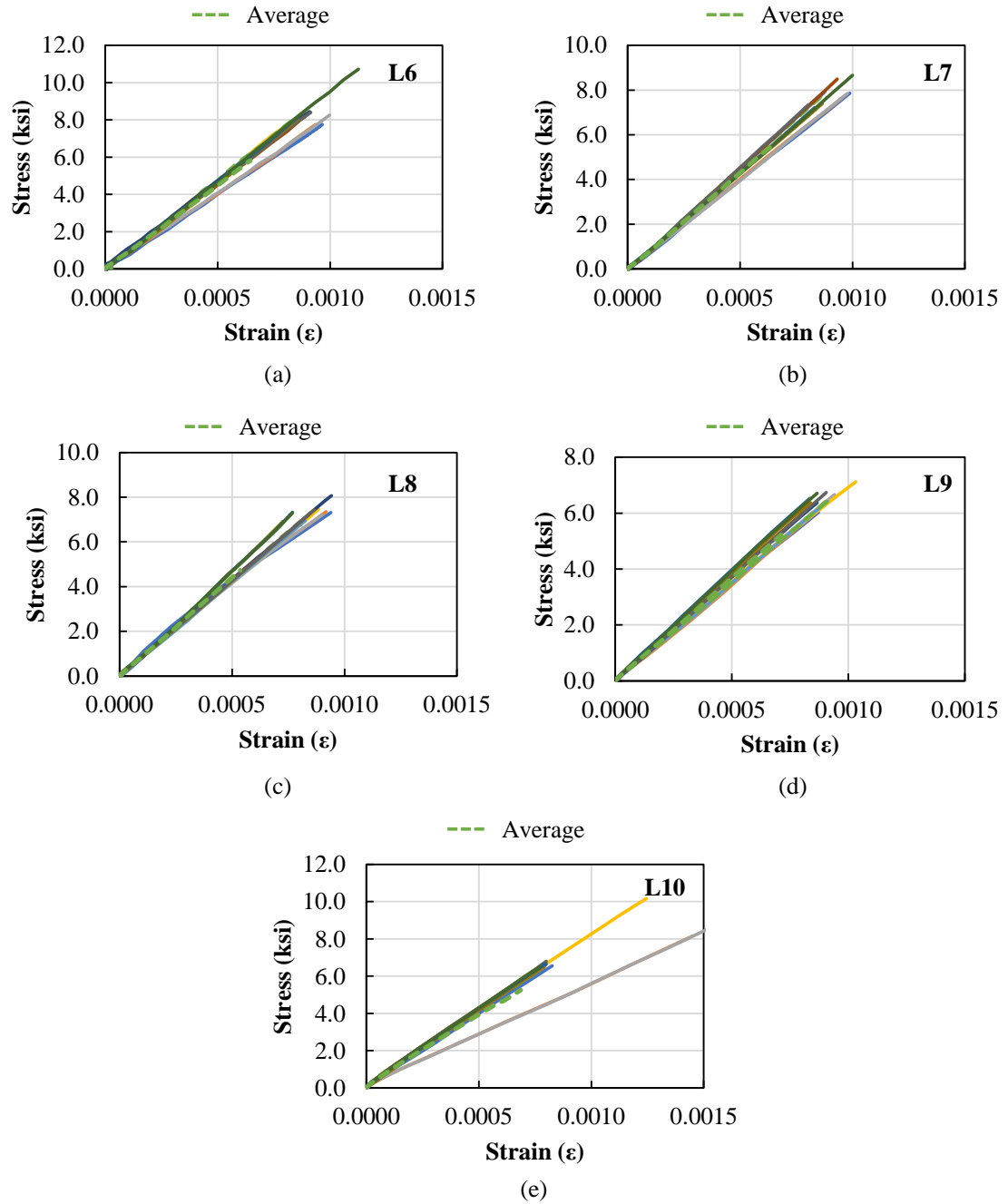
Figure B-11: Modulus of elasticity L6 to L10

Figure B-12 Shows the average response during the modulus of rupture.
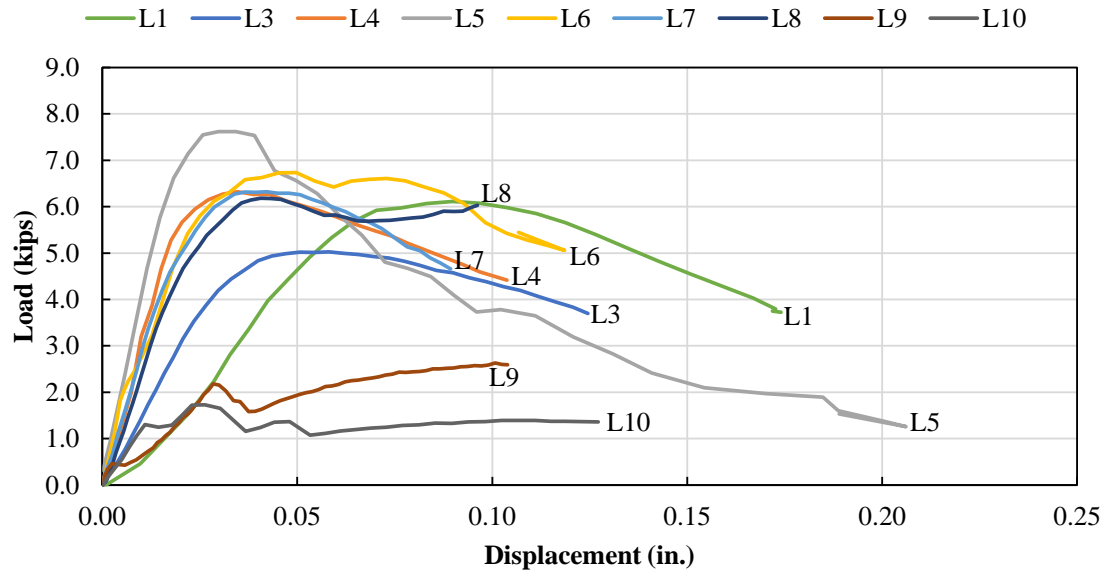
Figure B-12: Average load-displacement curves for large-scale mixtures-MOR test

Figure B-13 and Figure B-14show the modulus of rupture for each large-scale mixture and related samples.
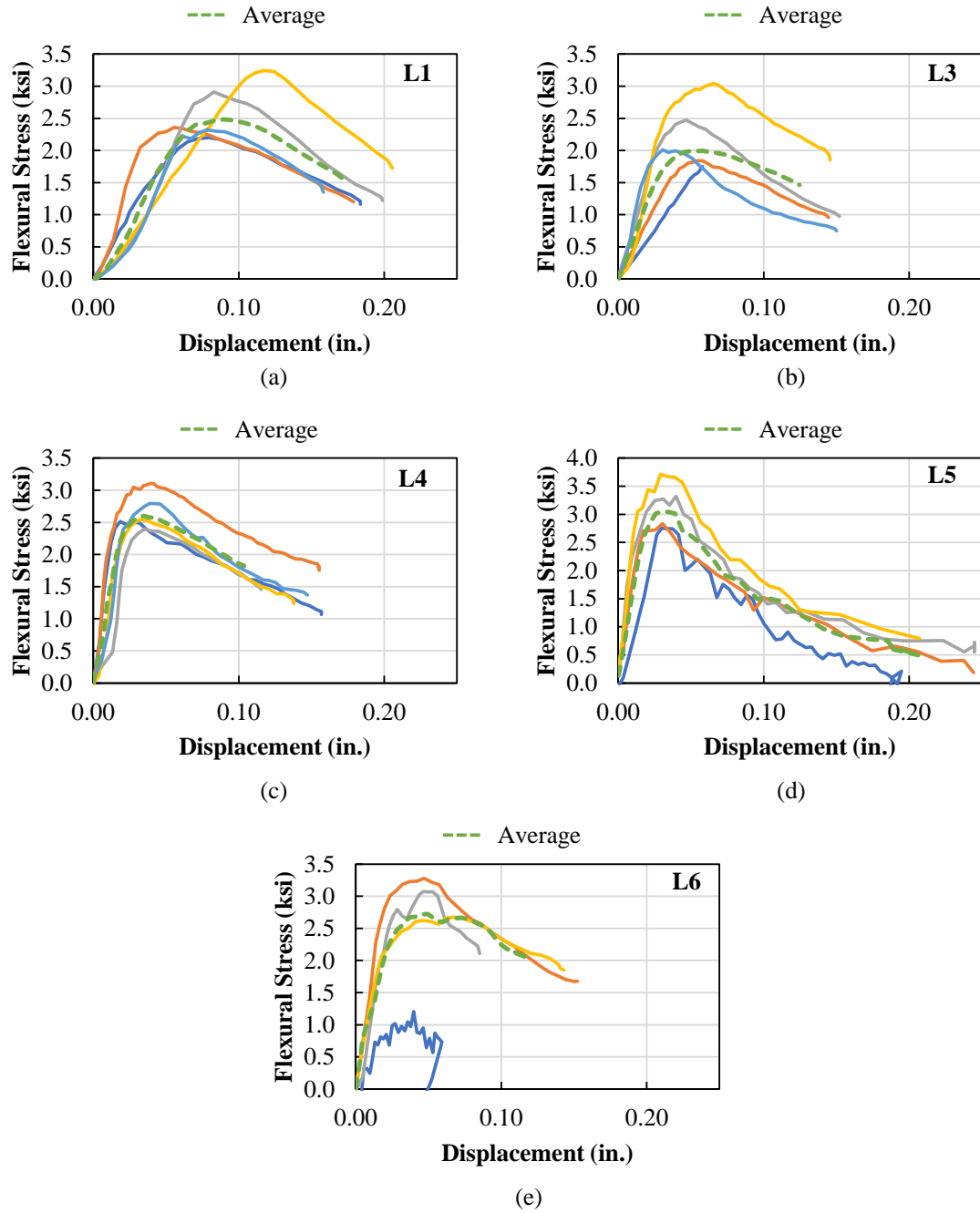
Figure B-13: Modulus of rupture, L1 and L3 to L6
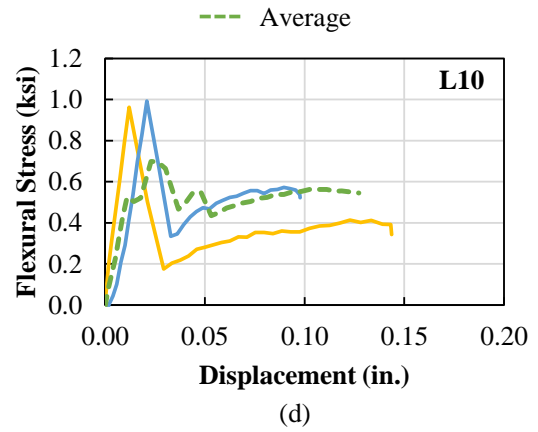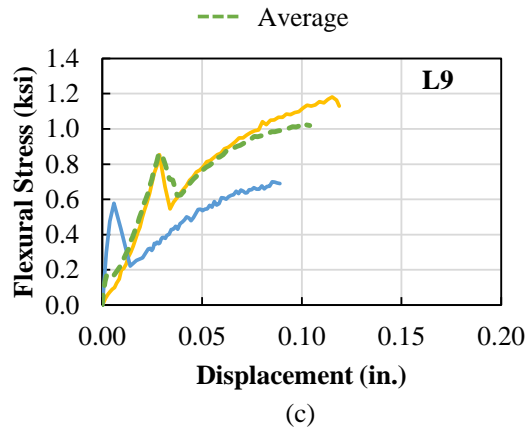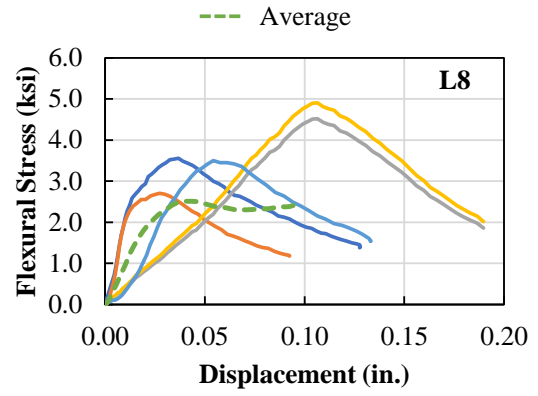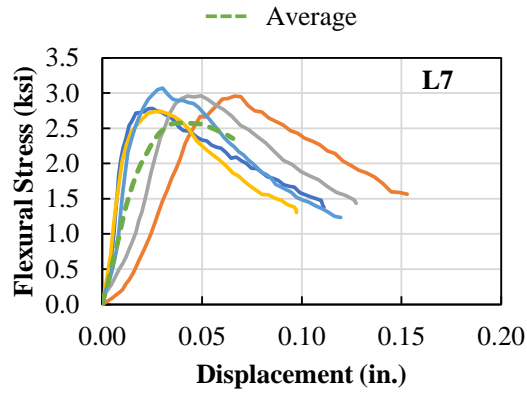
Figure B-14: Modulus of rupture, L7 to L10

Figure B-15 shows the shrinkage test results for each large-scale mixture and related samples.
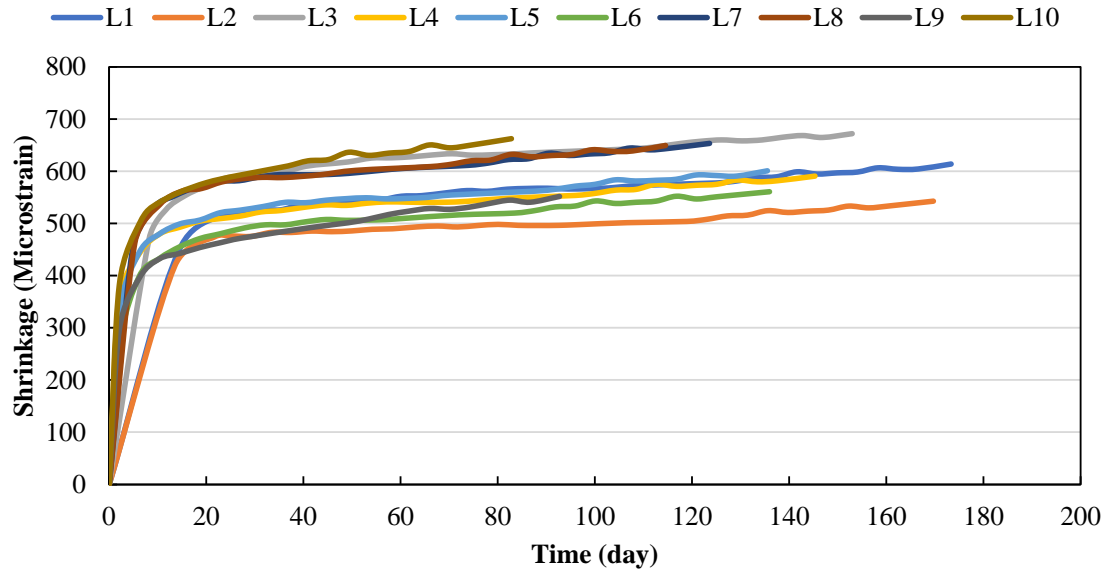
Figure B-15: Shrinkage test results

Appendix B: **NUMERICL ANALYSIS RESULTS**

This section summarizes the modelling outputs (ATENA) for different studies models.

(a)

(b)

(c)

(d)
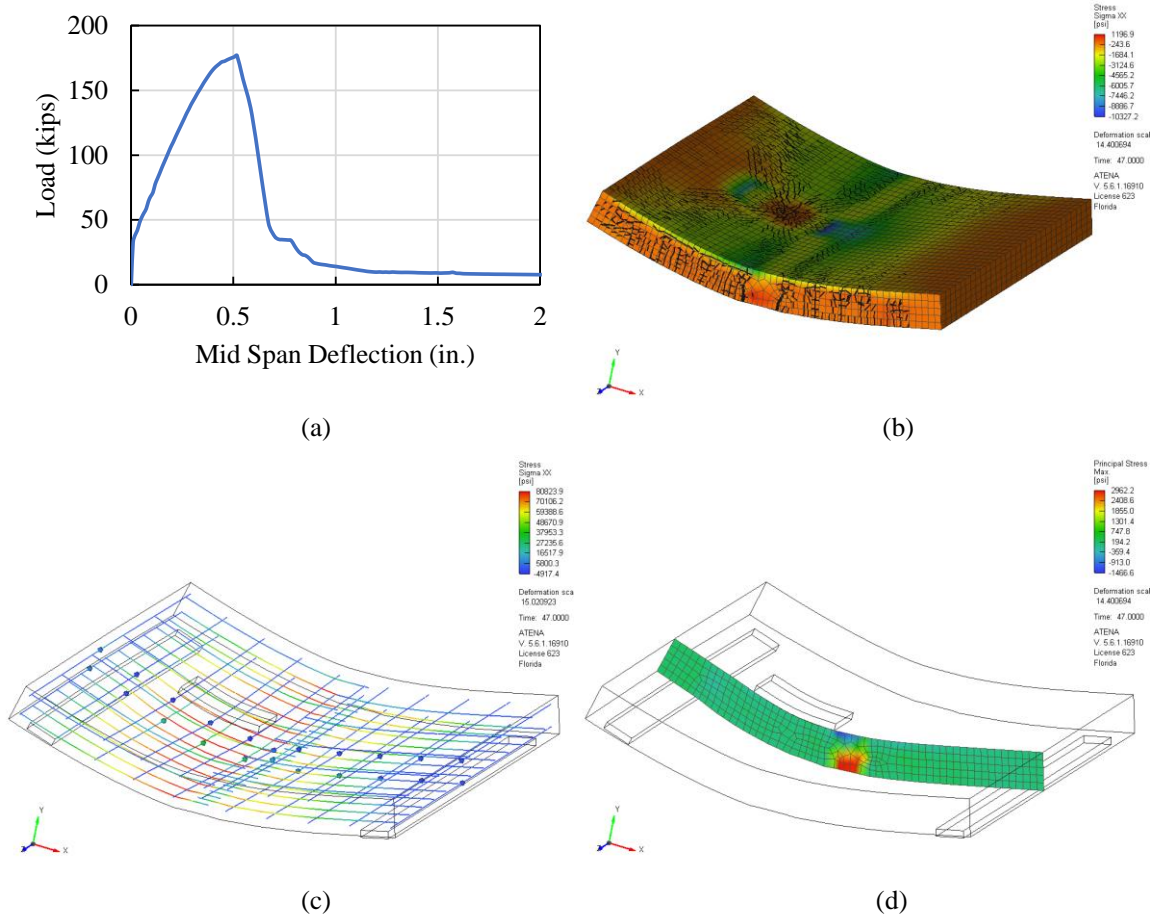
Figure B-1: Results for Model S1-C-UHPC; (a) load-deflection curve, (b) crack pattern of deck, (c) reinforcements stress and (d) Max. principal stress at joint
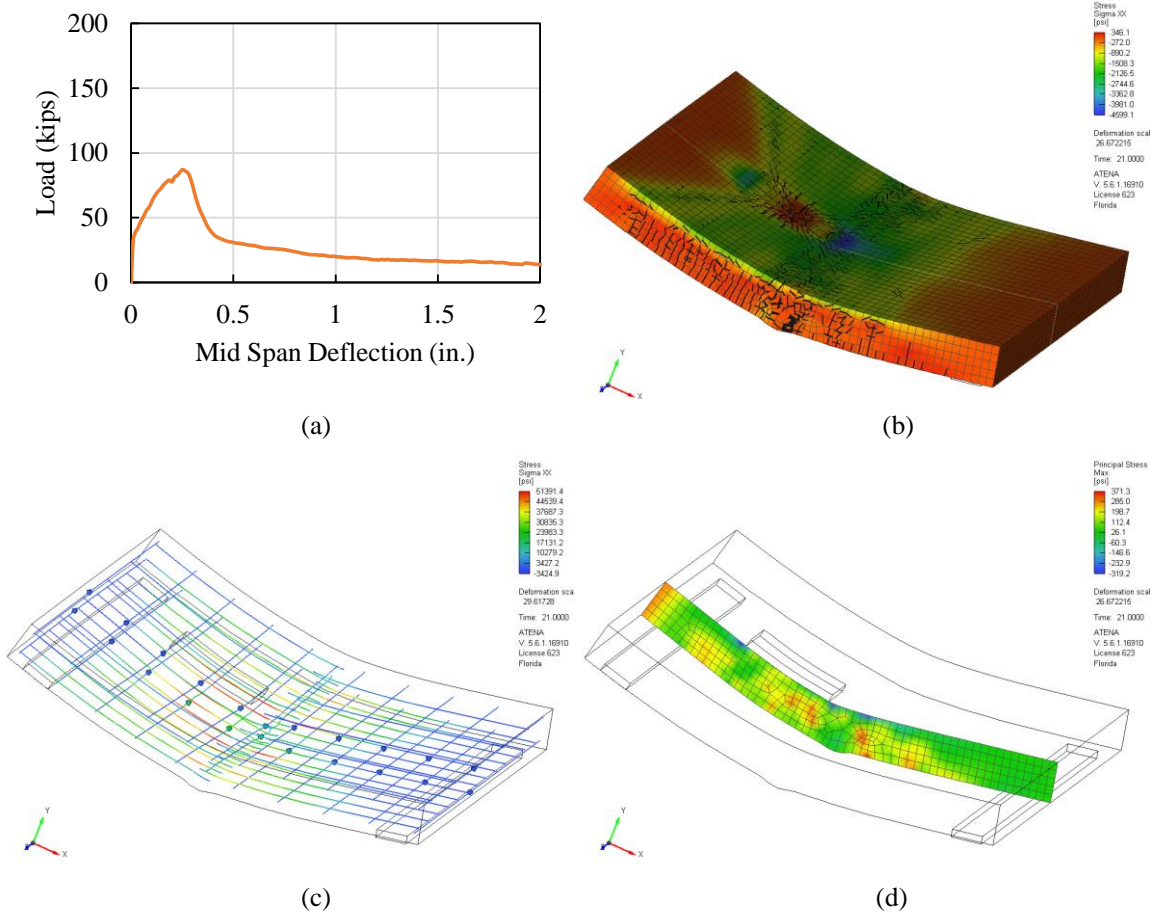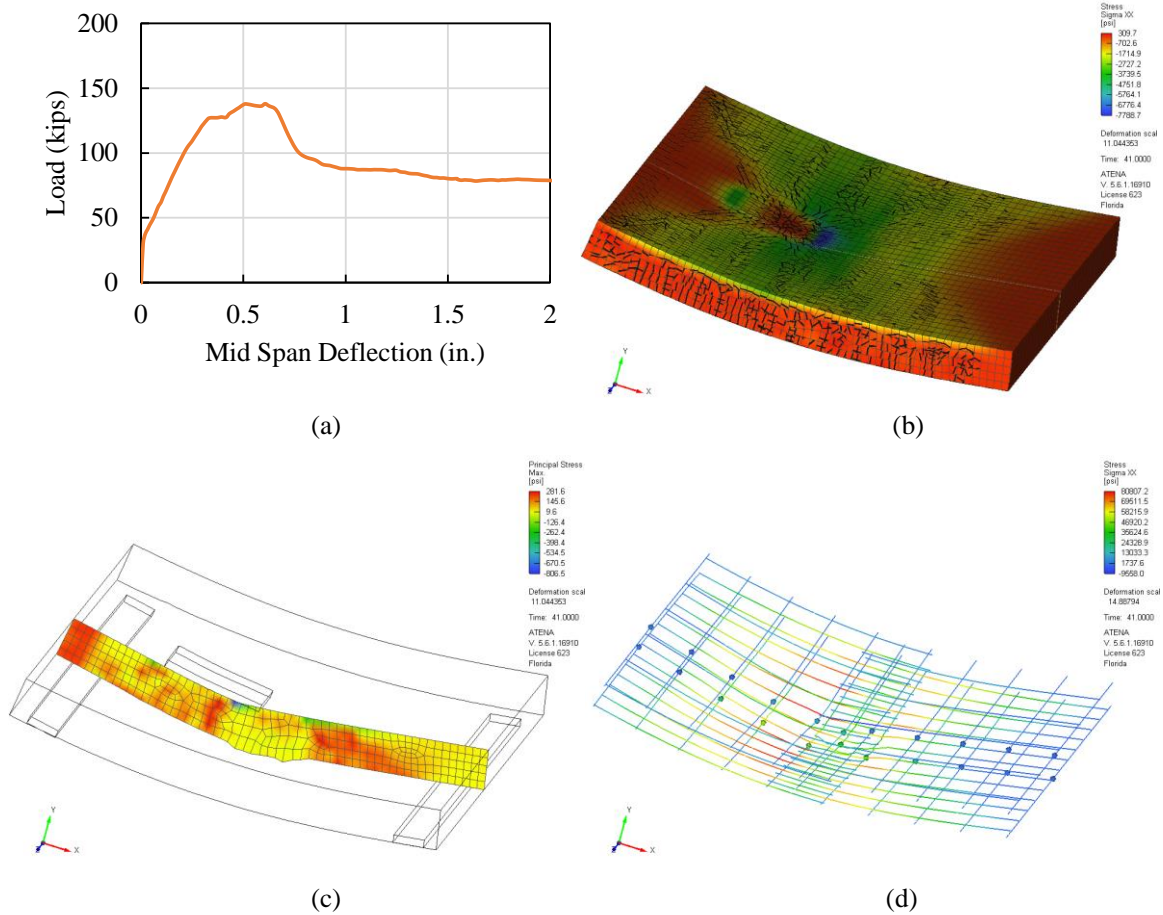
Figure B-2: Results for Model S1-CC; (a) load-deflection curve, (b) crack pattern of deck, (c) reinforcements stress and (d) Max. principal stress at joint
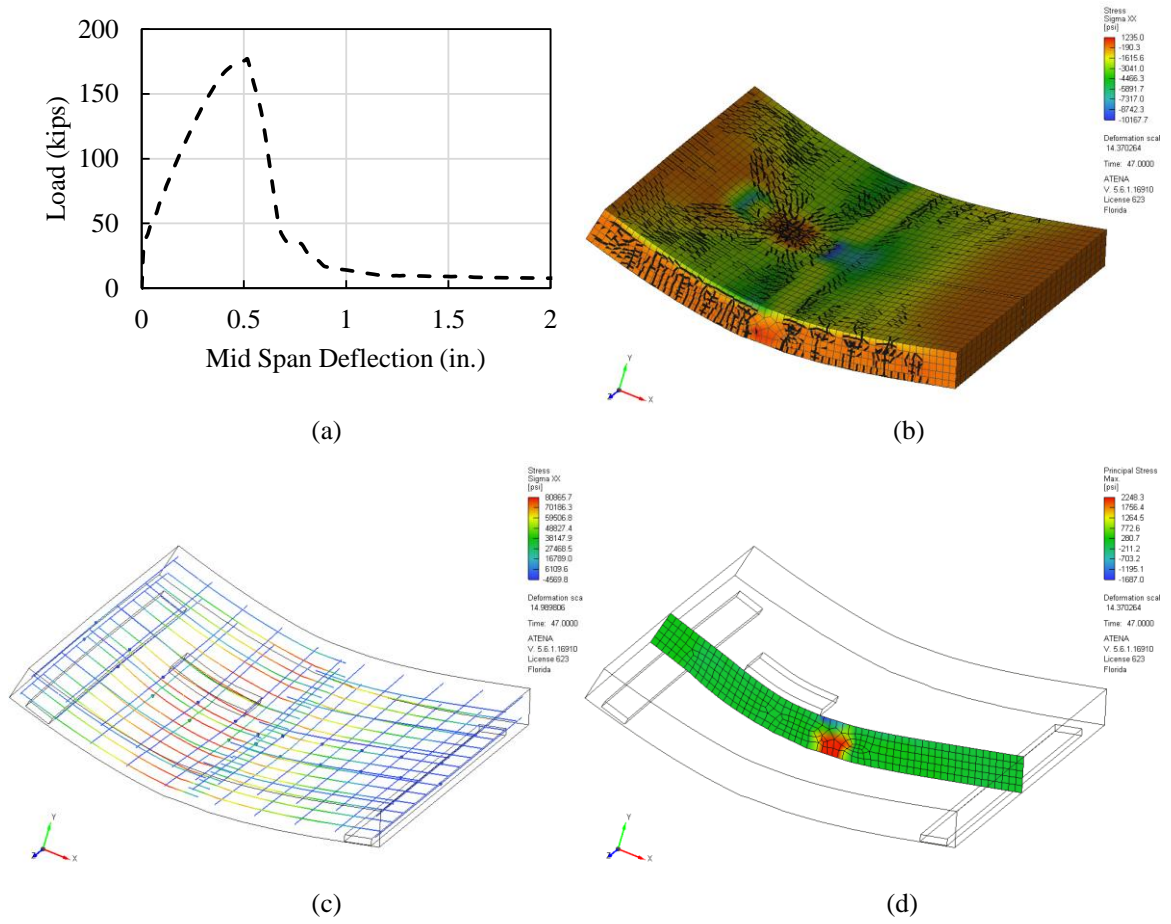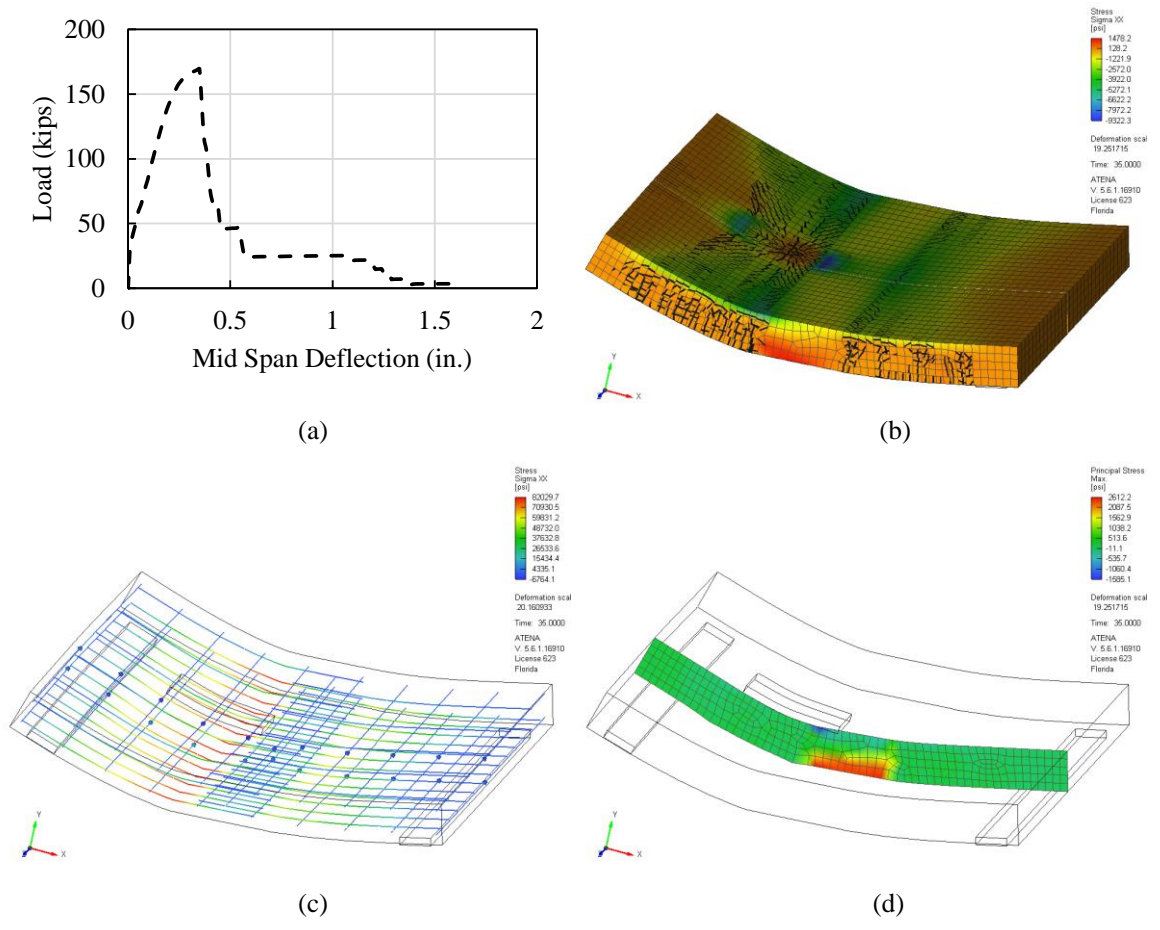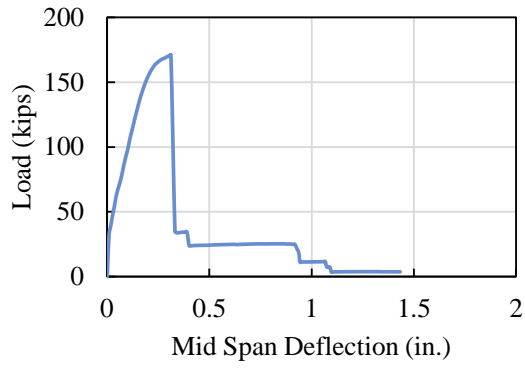
Figure B-3: Results for Model S1-N-UHPC; (a) load-deflection curve, (b) crack pattern of deck, (c) reinforcements stress and (d) Max. principal stress at joint
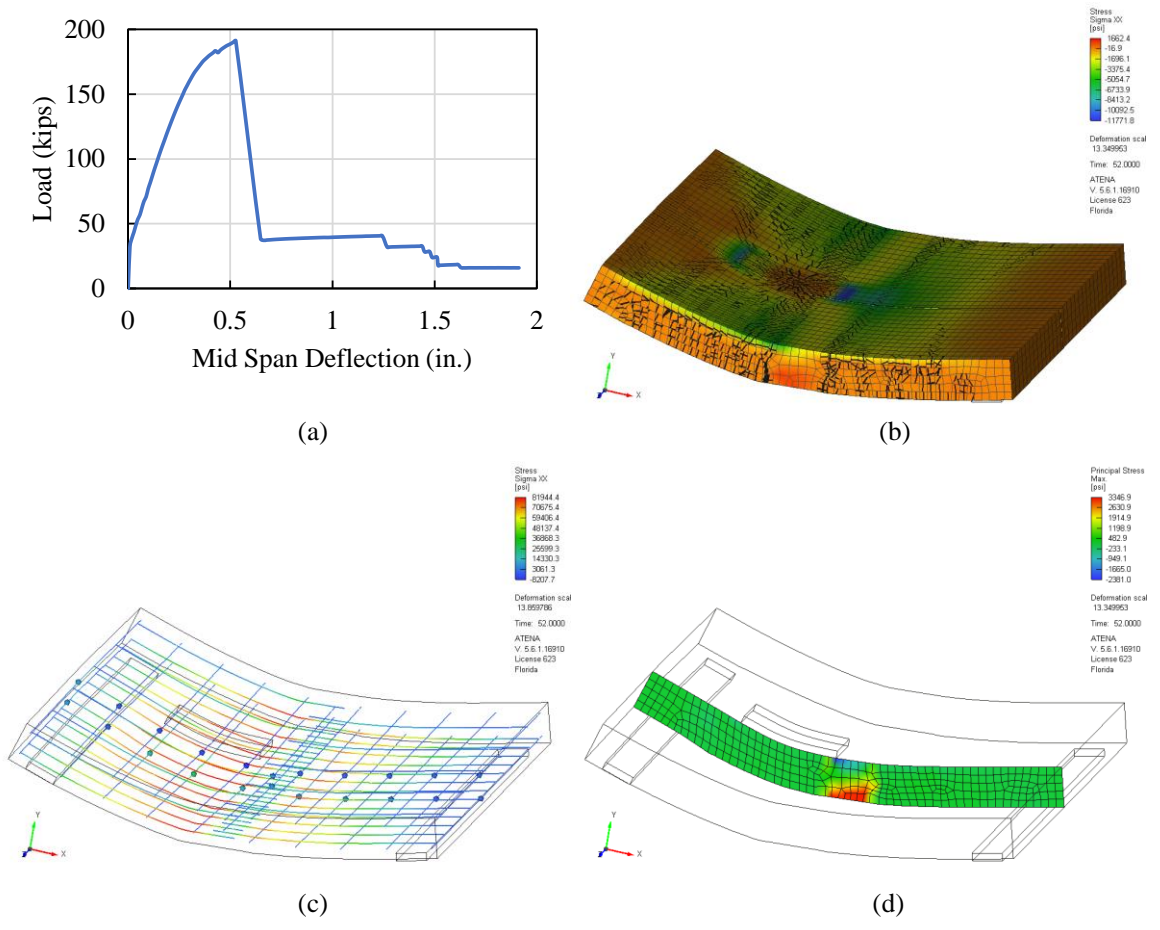
Figure B-4: Results for Model S2-C-UHPC; (a) load-deflection curve, (b) crack pattern of deck, (c) reinforcements stress and (d) Max. principal stress at joint
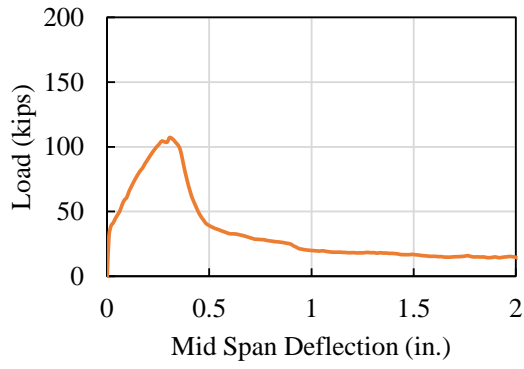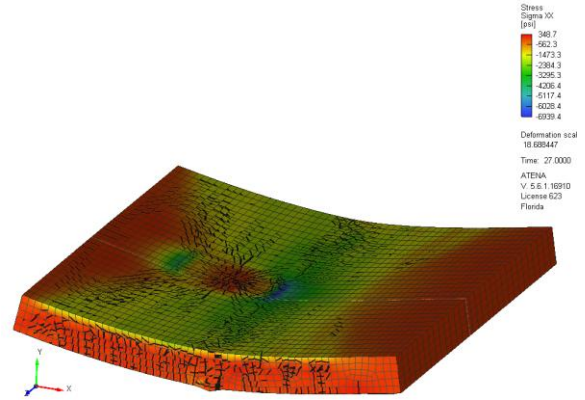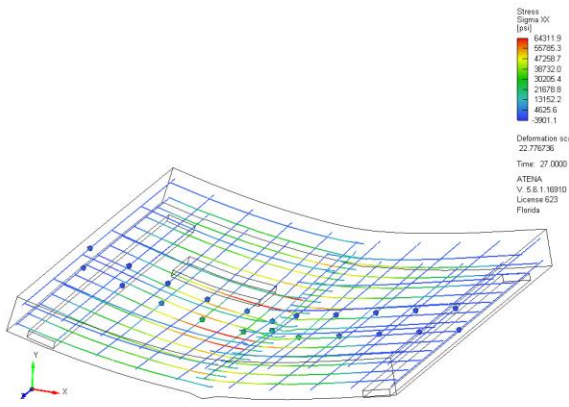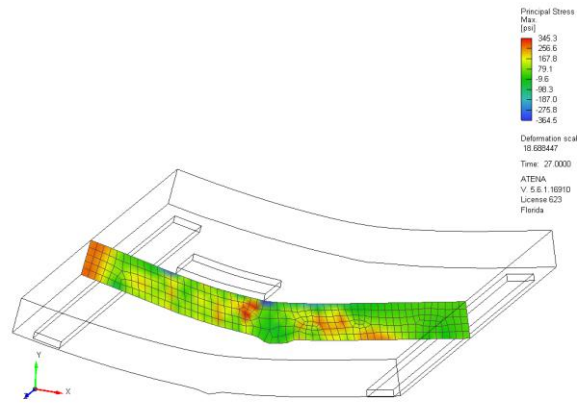
Figure B-5: Results for Model S2-CC; (a) load-deflection curve, (b) crack pattern of deck, (c) reinforcements stress and (d) Max. principal stress at joint
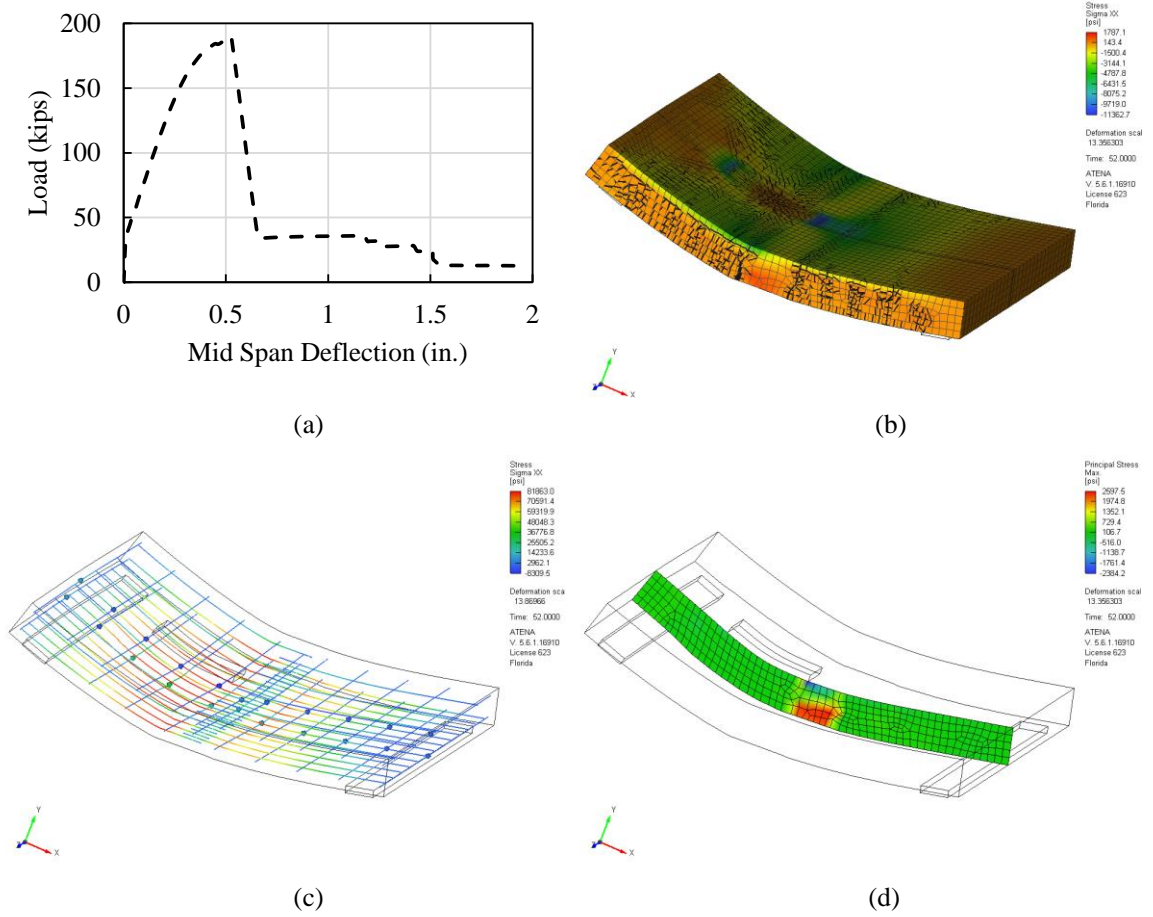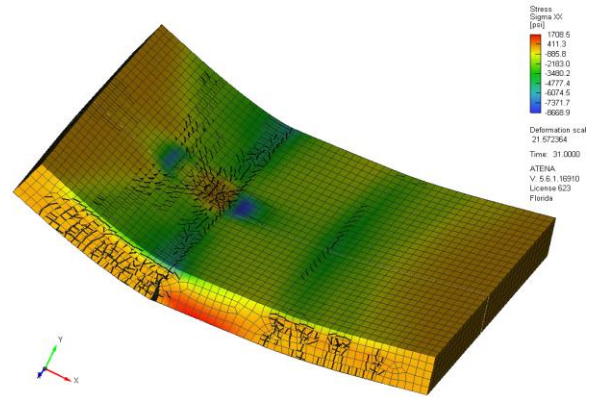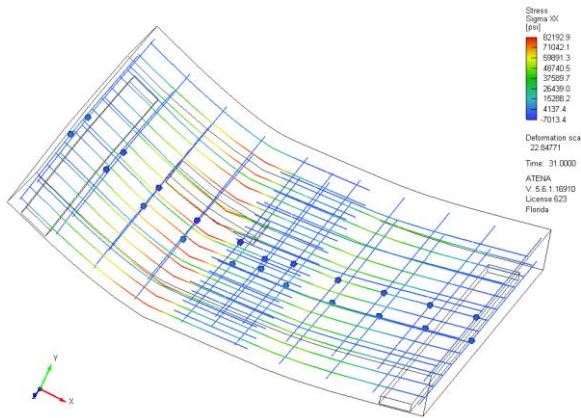
Figure B-6: Results for Model S2-N-UHPC; (a) load-deflection curve, (b) crack pattern of deck, (c) reinforcements stress and (d) Max. principal stress at joint
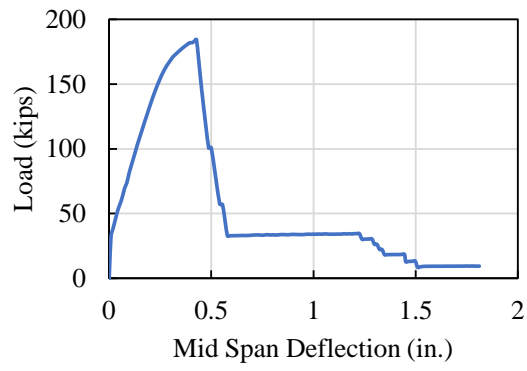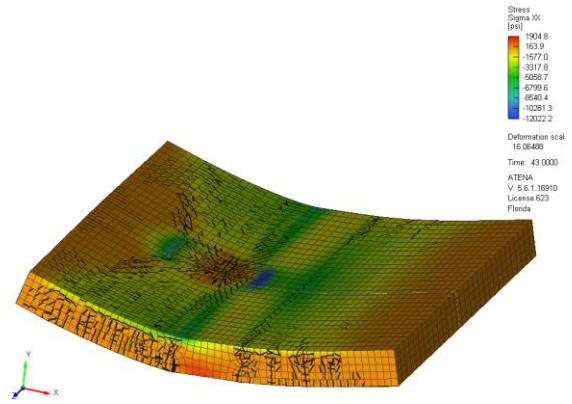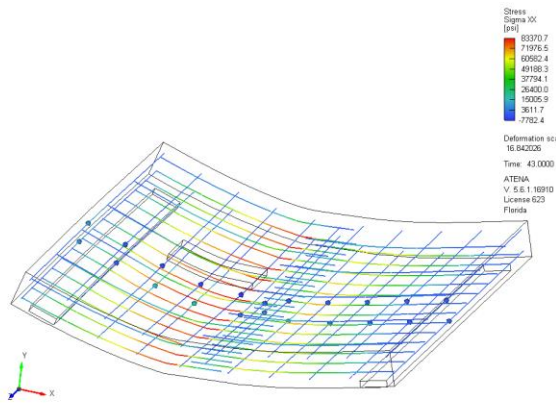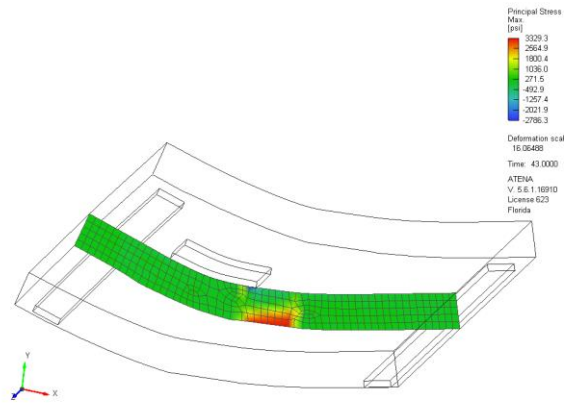
Figure B-7: Results for Model S3-C-UHPC; (a) load-deflection curve, (b) crack pattern of deck, (c) reinforcements stress and (d) Max. principal stress at joint
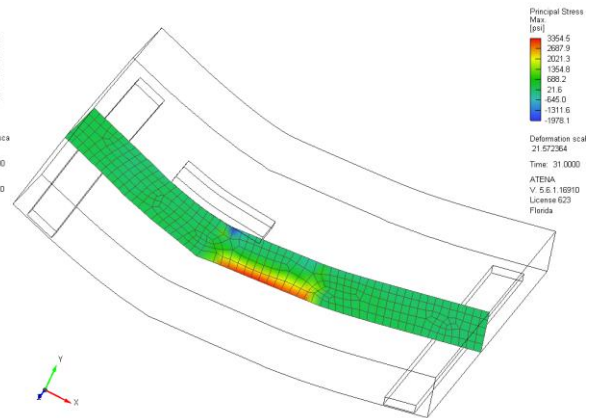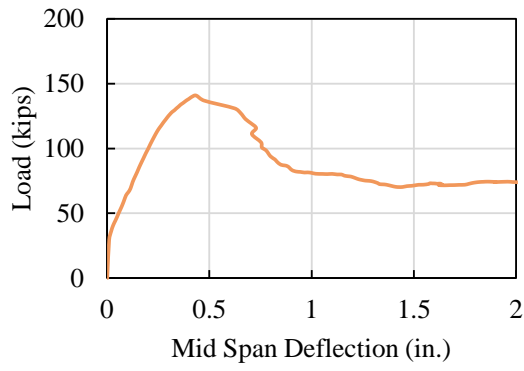
(a)

(b)

(c)

(d)
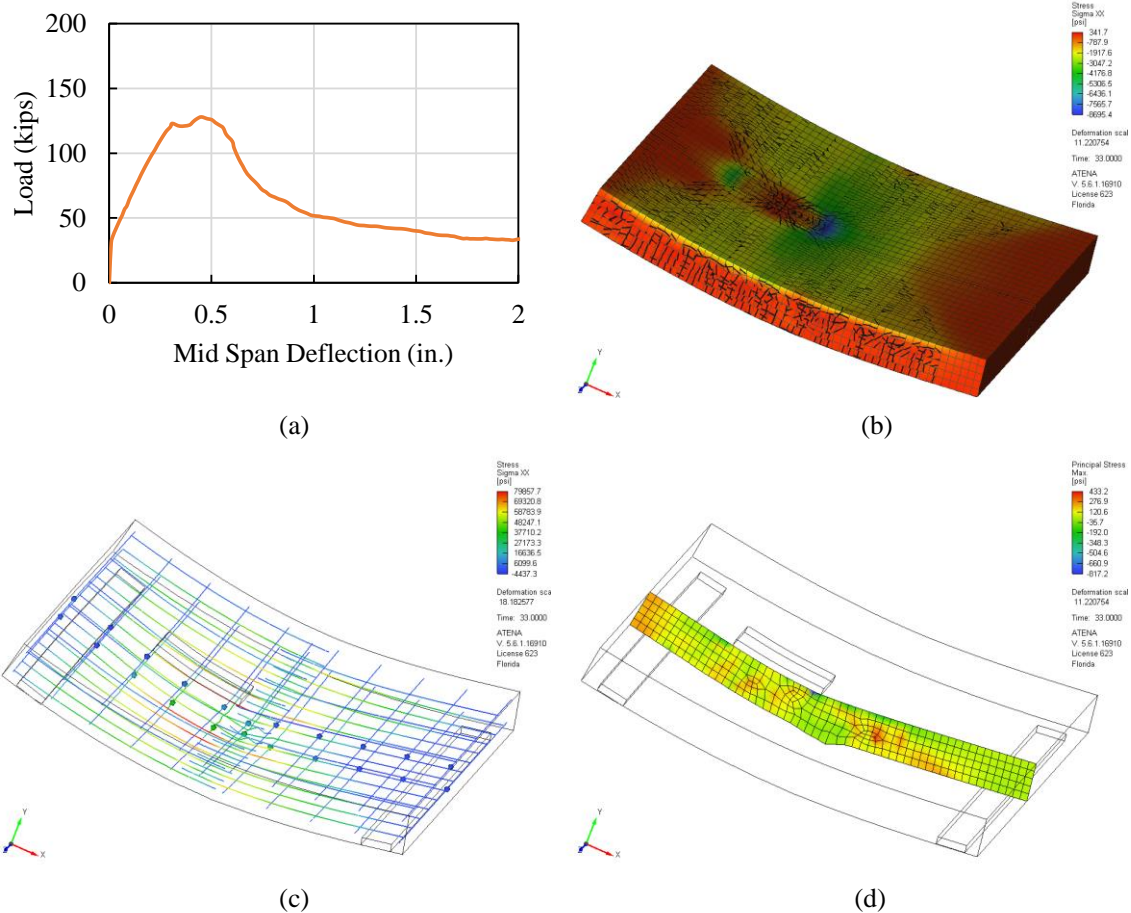
Figure B-8: Results for Model S3-CC; (a) load-deflection curve, (b) crack pattern of deck, (c) reinforcements stress and (d) Max. principal stress at joint

(a)

(b)

(c)

(d)
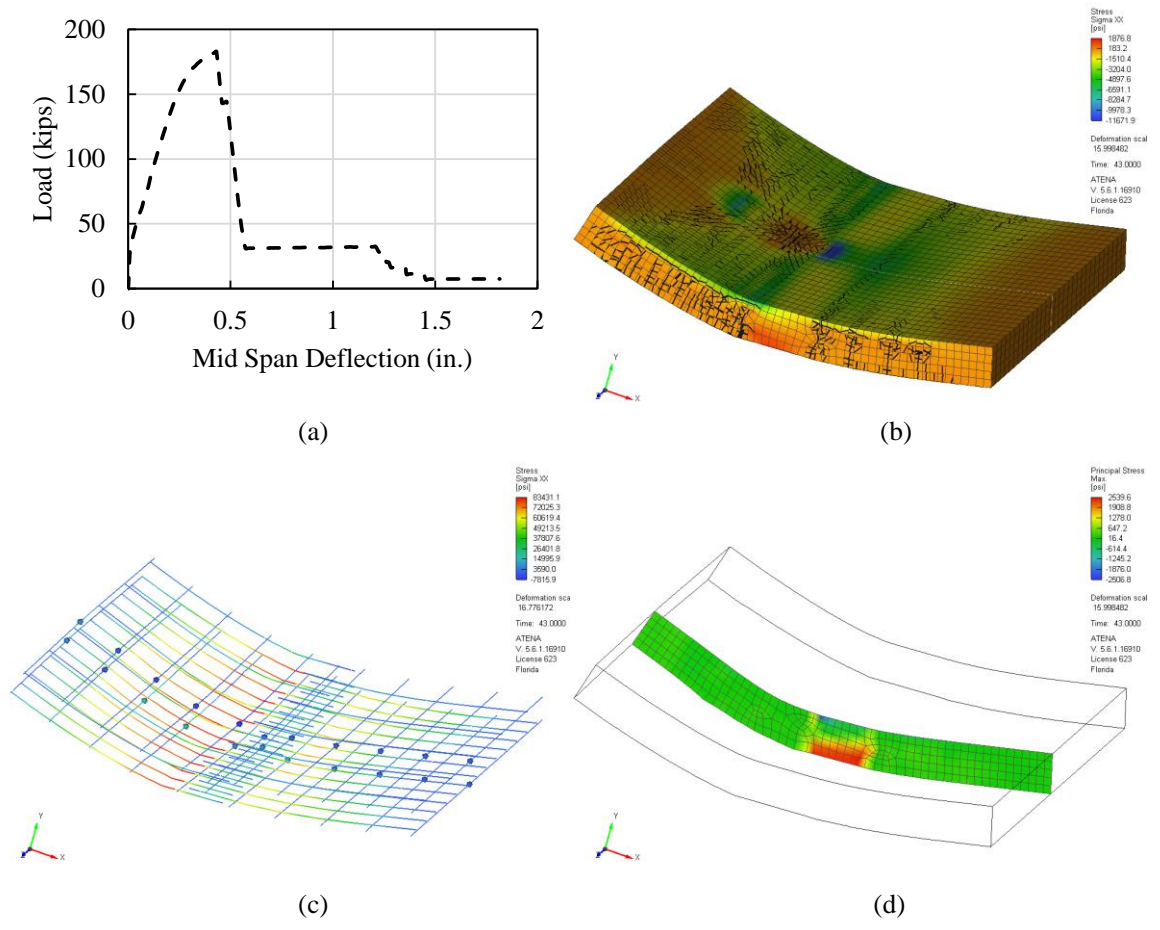
Figure B-9: Results for Model S3-N-UHPC; (a) load-deflection curve, (b) crack pattern of deck, (c) reinforcements stress and (d) Max. principal stress at joint
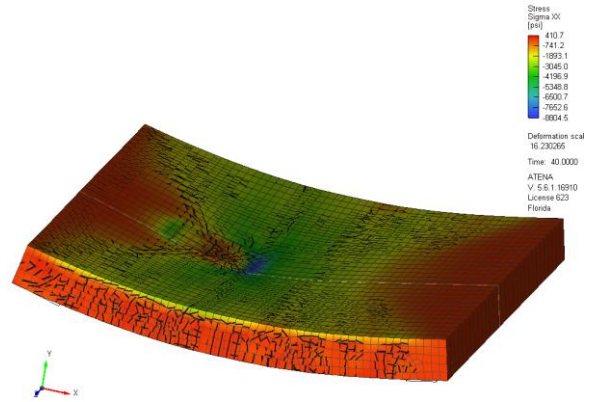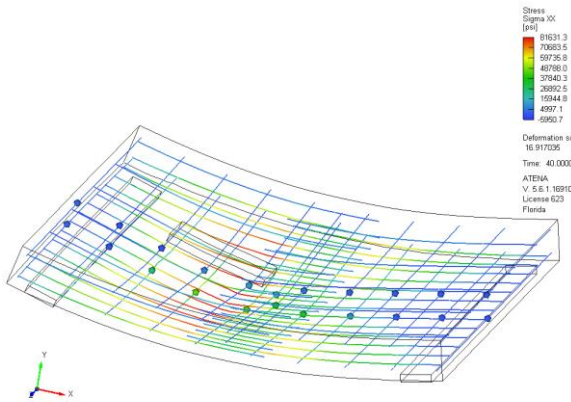
(a)

(b)

(c)

(d)
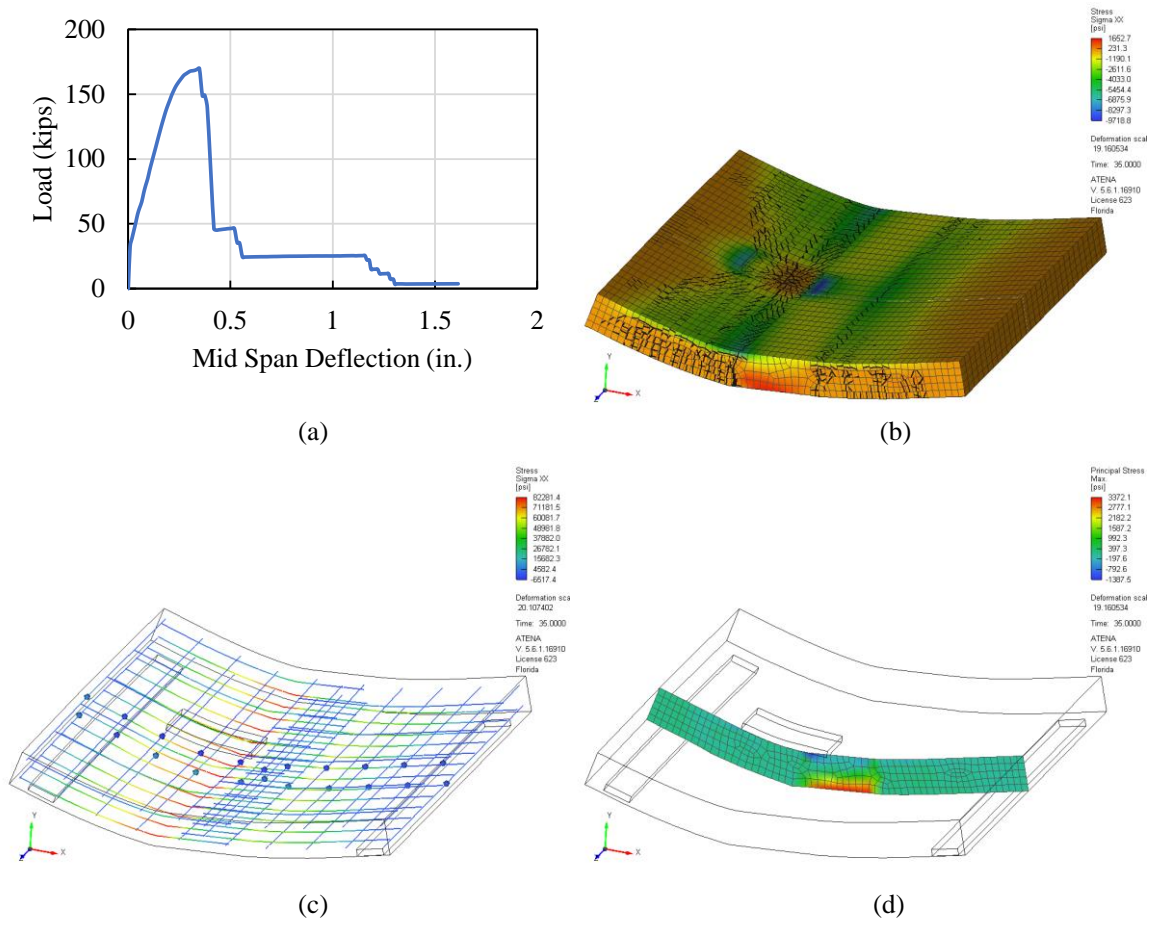
Figure B-10: Results for Model S4-C-UHPC; (a) load-deflection curve, (b) crack pattern of deck, (c) reinforcements stress and (d) Max. principal stress at joint

(a)

(b)

(c)

(d)

Figure B-11: Results for Model S4-CC; (a) load-deflection curve, (b) crack pattern of deck, (c) reinforcements stress and (d) Max. principal stress at joint

261

Figure B-12: Results for Model S4-N-UHPC; (a) load-deflection curve, (b) crack pattern of deck, (c) reinforcements stress and (d) Max. principal stress at joint
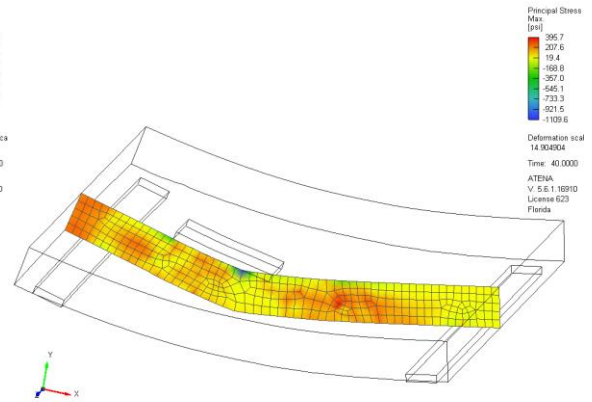
(a)

(b)

(c)

(d)

Figure B-13: Results for Model S5-C-UHPC; (a) load-deflection curve, (b) crack pattern of deck, (c) reinforcements stress and (d) Max. principal stress at joint

(a)

(b)

(c)

(d)

Figure B-14: Results for Model S5-CC; (a) load-deflection curve, (b) crack pattern of deck, (c) reinforcements stress and (d) Max. principal stress at joint
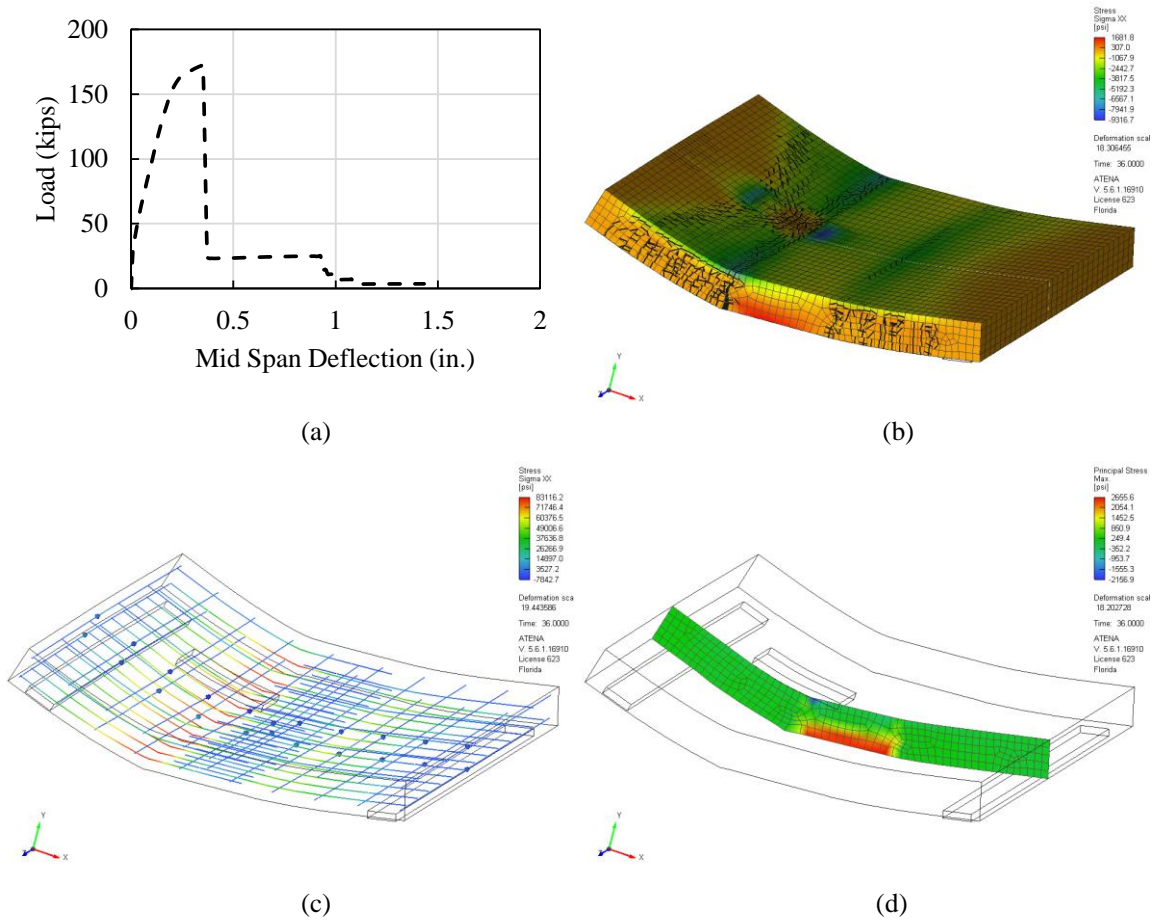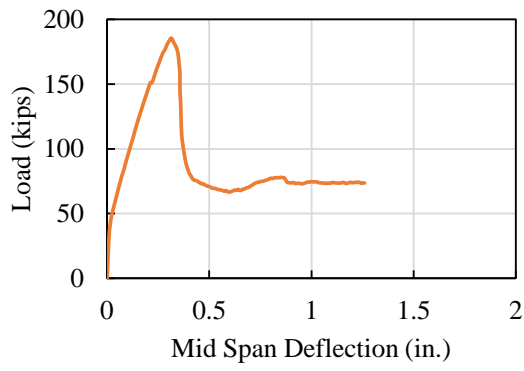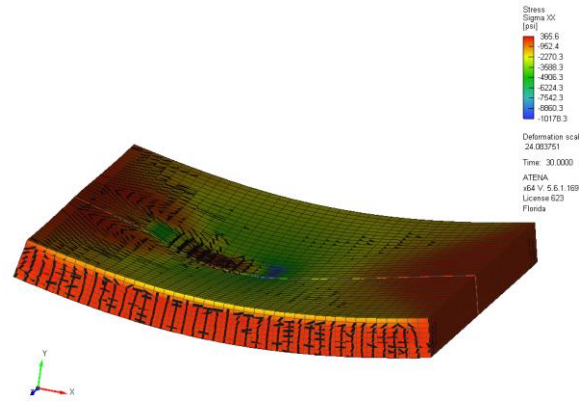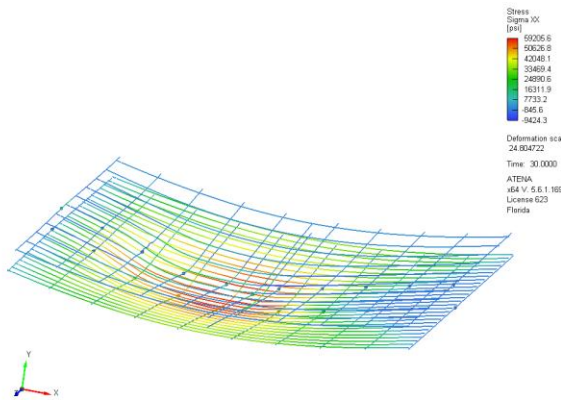

(a)

(b)

(c)

(d)

Figure B-15: Results for Model S5-N-UHPC; (a) load-deflection curve, (b) crack pattern of deck, (c) reinforcements stress and (d) Max. principal stress at joint
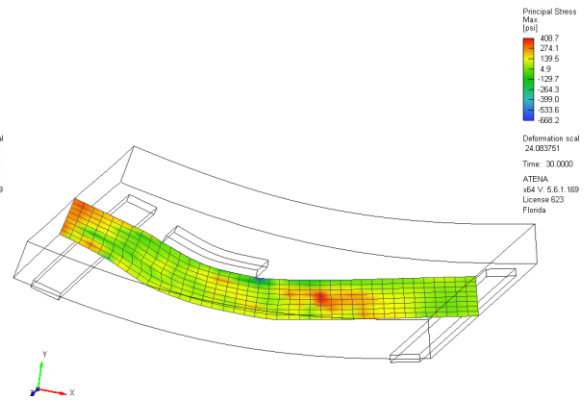
(a)

(b)

(c)

(d)

Figure B-16: Results for Model S0-CC; (a) load-deflection curve, (b) crack pattern of deck, (c) reinforcements stress and (d) Max. principal stress at joint

266

VITA

ESMAIL SHAHROKHINASAB

Born, Tehran, Iran

2005-2009	B.A., Civil Engineering
	Amirkabir University , Iran
2009-2012	M.S., Railway Track Engineering
	Iran University of Science and Technology, Iran
2018-2021	Research Assistant
	Florida International University, Florida
2020 -2021	Doctoral Candidate
	Florida International University, Florida

PUBLICATIONS AND PRESENTATIONS

- E. Shahrokhinasab, T. Looney, R. Floyd, and D. Garber (2021). *Effect of Fiber, Cement, and Aggregate Type on Mechanical Properties of UHPC," Civ. Eng. J., vol. 7, no. 8, pp. 1290–1309.*

- E. Shahrokhinasab and D. Garber (2021). *Long-term performance of full-depth precast concrete (FDPC) deck panels," Eng. Struct., vol. 244, p. 112738.*

- E.Shahrokhinasab, D.Garber, *"Performance Comparison of In-Service, Full-Depth Precast Concrete Deck Panels to Cast-in-Place Decks," Research Seminar, October 25, 2019*

- E.Shahrokhinasab, D.Garber, *"Performance Comparison of In-Service, Full-Depth Precast Concrete Deck Panels to Cast-in-Place Decks," ASCE SEI Structures Congress 2020, 685839 - Management, Inspection, and Rehabilitation of ABC Bridges,Location: Regency B, Orlando, FL, April 2019.*

- E.Shahrokhinasab, D.Garber, *"Performance Comparison of In-Service, Full-Depth Precast Concrete Deck Panels to Cast-in-Place Decks," 2019 International Accelerated Bridge Construction Conference, December 2019*

- E.Shahrokhinasab, D.Garber, *"Long-Term Performance of Full-Depth Precast Concrete Deck Panels," TRB 99th Annual Meeting-Location: Washington DC, January 2020.*

List of full publication can be found on:
https://scholar.google.com/citations?user=8EBLcjsAAAAJ&hl=en&oi=ao